The impact of wastewater effluent and enantiomers of venlafaxine on darters (*Etheostoma* spp.) in the Grand River

by

Louis Joseph Pfeifer

A thesis

presented to the University of Waterloo

in fulfillment of the

thesis requirement for the degree of

Doctor of Philosophy

in

Biology

Waterloo, Ontario, Canada, 2025

© Louis Joseph Pfeifer 2025

Examining Committee Membership

The following served on the Examining Committee for this thesis. The decision of the Examining Committee is by majority vote.

External Examiner	Dr. Kenneth Jeffries Associate Professor Department of Biology, University of Manitoba
Supervisor(s)	Dr. Paul Craig Associate Professor, Department of Biology
Internal Member	Dr. Andrew Doxey Associate Professor, Department of Biology
Internal-external Member	Dr. Maricor Arlos Assistant Professor, Civil and Environmental Engineering
Other Member(s)	Dr. Graham Scott Associate Professor, Department of Biology McMaster University

AUTHOR'S DECLARATION

This thesis consists of material all of which I authored or co-authored: see Statement of Contributions included in the thesis. This is a true copy of the thesis, including any required final revisions, as accepted by my examiners.

I understand that my thesis may be made electronically available to the public

Statement of Contributions

Louis Pfeifer conducted the experimental design, sample collection and analysis, data analysis, and manuscript writing.This research was conducted under the supervision of **Dr. Paul M. Craig**, who provided guidance on experimental design, manuscript editing, and funding.

Research presented in chapter 2:

Leslie Bragg developed analytical methods and conducted pharmaceutical and contaminant quantification in water samples.

Research presented in chapter 3 and 4:

Dr. Mark R. Servos contributed to the design methodology for the experimental tank design setup.

Abstract

Aquatic organisms, such as fishes, are in constant contact with various anthropogenic stressors present within their environments, including contaminants from wastewater treatment plant effluents (WWTPE). WWTPE represents a pervasive source of pharmaceutically active compounds (PhACs) in surface waters, with the serotonin and norepinephrine reuptake inhibitor venlafaxine (VEN), frequently detected at elevated concentrations in receiving waters worldwide. VEN is a chiral pharmaceutical administered as a racemic (50:50) mixture of R- and S-enantiomers, which exhibit distinct pharmacological activities and can be selectively degraded or enriched in effluent depending on treatment processes. However, little is known about the stereoselective toxicological effects of VEN in fish, particularly in the context of multi-contaminant WWTPE exposure.

This thesis investigates the systemic effects of WWTPE and enantiomer-specific VEN exposure on *Etheostoma* spp. (darters) using transcriptomic profiling, oxidative stress assays, and biochemical markers of cellular damage. Wild darters (rainbow, greenside, fantail, and johnny darter) were collected upstream and downstream of the Waterloo municipal WWTP outfall (Grand River, ON). Additionally, a laboratory-controlled VEN exposure was conducted using rainbow darters, where liver tissue was analysed for transcriptomic responses and brain tissue was assessed for oxidative stress markers. Findings reveal that WWTPE alters hepatic function and stress responses, with species-specific transcriptional responses. However, key biological pathways related to lipid metabolism, immune regulation, and mitochondrial function were consistently disrupted across species. Laboratory exposure to VEN demonstrated stereoselective effects, where R-VEN primarily influenced amino acid metabolism, vesicle trafficking, and immune pathways, while S-VEN affected chromatin remodelling, epigenetic regulation, and extracellular matrix organization. Despite some overlap in lipid metabolism and inflammatory pathways, few transcripts were shared between VEN-exposed fish and WWTPE-exposed wild populations, highlighting the complex interactions of multi-contaminant mixtures in effluent-exposed fish. In the brain, VEN exposure induced oxidative stress and cellular damage, as evidenced by increased superoxide dismutase (SOD) and glutathione peroxidase (GPX) activity, as well as elevated lipid peroxidation byproducts. S-VEN had a more rapid oxidative impact,

suggesting a higher potential for neurotoxicity, which may contribute to behavioural alterations in exposed fish.

Overall, this research contributes to the development of biomonitoring practices by identifying molecular markers and key biological pathways disrupted by WWTPE and VEN exposure. Findings support the refinement of Adverse Outcome Pathway (AOP) frameworks for pharmaceutical contaminants and provide high-quality transcriptomic reference data for use in high-throughput ecotoxicological monitoring. These results raise considerations for improving monitoring, regulation, and treatment strategies to better address the potential ecological impacts of effluent-derived pollutants in freshwater ecosystems.

Acknowledgements

This PhD has been an incredible and challenging experience and throughout it I have met and worked with many wonderful people who have helped along the way. First, I would like to thank my supervisor, Dr. Paul Craig, for his unwavering guidance, patience, and support throughout this journey. His insights and encouragement have shaped not only this dissertation, but also the way I think about science and approach research more broadly. He also helped keep me grounded when I could have easily spent years trying to interpret every last signal and pattern in the data. I would also like to thank the members of my committee, especially Dr. Andrew Doxey and Dr. Graham Scott. Their feedback and guidance during committee meetings helped shape the direction of this project in incredibly meaningful ways, and I truly appreciate their time and thoughtful engagement with my work.

This thesis was made possible through the collaborative efforts of many people, whose dedicated and unrelenting assistance was truly invaluable. I would like to thank Dr. Mark Servos and the entire Servos lab, particularly Leslie Bragg and Hadi Dhiyebi, whose help during fieldwork was essential in both the fish collection and data generation that underpin this thesis. Hadi, I can't thank you enough for helping me collect what was left of our caging experiment, when we were up to our waders in those treacherous November waters.

I am extremely grateful to all members of the Craig Lab, past and present, for their support throughout this journey. Whether it was working through experimental issues, engaging in scientific discussions, or simply offering motivation when it was most needed, I've deeply appreciated having such a thoughtful and generous group around me. Heather, thank you for making me feel so welcome when I was just starting out in the lab. Karyn, I really appreciated your calm presence and steady support along the way. Ivan, I always enjoyed our sci-fi chats—they were a welcome break and a reminder of the bigger picture. Sana, our lunches at the Grad House were a bright spot in many weeks. And Allison—yes, I still ride that bike to campus, though I'll admit it's a summer-only thing now. Working in the lab, going to trivia nights, travelling to conferences, and getting to know everyone are among my fondest memories of my time at this university.

Finally, I would like to express my deepest thanks to my parents for their sacrifice, encouragement, and unwavering support. Your reminders to have a nap once in a while were just as important as your pep talks. You've always pushed me to do my best and, more importantly, to believe in myself and my work.

Table of Contents

Examining Committee Membership ii
AUTHOR'S DECLARATION iii
Statement of Contributions iv
Abstract v
Acknowledgements vii
List of figures xiv
List of tables xviii
List of Abbreviations xix
Chapter 1 1
1.1 Municipal Waste Water Treatment Plant Effluent 2
1.2 Impacts of MWWTPE on Aquatic Ecosystems 3
1.3 Biological monitoring and management guidelines 4
1.4 Wastewater Treatment 6
1.5 Waterloo MWWTPE and The Grand River 7
1.6 Pharmaceuticals in MWWTP Effluent and Their Impact on Non-Target Organisms 8
1.9 Transcriptomics in Ecotoxicology 9
1.10 Darters 12
1.11 Objectives and hypotheses 12
Chapter 2 14
2.0 Introduction 15
2.0.1 CECs of concern 15

2.0.2 Using transcriptomic approaches on darters 16
2.0.3 Functional integration networking 17
2.0.4 Objectives and hypothesis 18
2.1 Materials and methods 18
2.1.1 Sample collection 18
2.1.2 Water quality parameters 21
2.1.3 RNA extraction, library preparation and sequencing 21
2.1.4 Sequence analysis 22
2.1.4.1 Sequence quality control and de novo assembly 22
2.1.4.2 Functional annotation and differential expression analysis 23
2.1.4.3 Phylogenetic Inference of Orthology 24
2.1.4.4 Gene ontology enrichment and pathway analysis 24
2.2 Results 25
2.2.1 Water quality parameters 25
2.2.2 RNA quality control and sequencing results 28
2.2.3 Transcriptome assembly and quality metrics 28
2.2.4 Differential gene expression analysis 31
2.2.5 Comparative Functional Annotation and Gene Ontology Analysis 35
2.2.6 Protein network analysis 43
2.4 Discussion 48
2.4.1 Water quality 48
2.4.2 Transcriptome Assembly 49
2.4.3 Annotation 50
2.4.4 Species comparisons of shared and unique pathways 51
2.4.4.1 Stress, Immune Response and Inflammatory Regulation 51

2.4.4.2 Lipid Metabolism and Cholesterol Homeostasis 53
2.4.4.3 Mitochondrial Function and Broader Metabolic Activity 55
2.4.4.4 Protein Homeostasis and Stress Responses 57
2.4.4.5 Cellular Communication and Neural Activity 60
2.4.4.6 Environmental and Pharmaceutical Impact 61
2.4.4.7 Divergence and Shared Adaptations 63
2.4.5 Unique identified pathways not captured by ontology enrichment 63
2.4.5.1 DNA Replication, Repair, and Transcriptional Regulation 63
2.4.5.2 Cytoskeletal and cellular remodelling 64
2.4.5.3 Up-Regulation of hemoglobin complex genes 65
2.4.6 Species specific orthogroups 65
2.5 Conclusion 66
Chapter 3 69
3.0 Introduction 70
3.0.1 Objectives and hypothesis 71
3.2 Materials and methods 71
3.2.1 Fish collection and handling 71
3.2.2 Venlafaxine exposure 72
3.2.3 RNA Processing and Sequencing 74
3.2.4 Transcriptome Assembly 74
3.2.5 Differential expression and functional annotation 75
3.2.6 Orthology Comparison 75
3.2.6.1 Retrospective Contaminant Identification Trough OrthoFinder 76
3.2.7 Gene Ontology Enrichment and Pathway Network Analysis 77
3.3 Results 77

3.3.1 RNA Integrity: Quality Control and Sequencing Analysis.....77
3.3.2 Functional Annotation and Differential expression.....80
3.3.3 Orthogroups.....85
3.3.4 Gene ontology annotation.....87
3.3.5 Gene ontology enrichment and networking.....87
3.3.6 Transcript networking.....92
3.4 Discussion.....93
3.4.1 Quality control, sequencing, and de novo assembly.....93
3.4.2 Annotation.....94
3.4.3 Stereoselective Effect of Venlafaxine on Rainbow Darter.....96
3.4.3.1 Neurological Signalling.....96
3.4.3.2 Metabolic Disruptions.....97
3.4.3.3 Immune and Inflammatory Modulation.....100
3.4.3.4 Cytoskeletal Dynamics and Vesicular Trafficking.....102
3.4.3.5 Transcriptional and Epigenetic Regulation.....104
3.4.3.6 Comparison with wild rainbow darter exposed to wastewater treatment plant effluent (WWTPE).....106
3.4.3.7 Conclusions.....107
Chapter 4.....109
4.0 Introduction.....110
4.0.1 Reactive oxygen species and defence mechanisms.....110
4.0.3 Contaminant induced oxidative stress.....112
4.0.1 Objectives and hypothesis.....114
4.2 Materials and methods.....114
4.2.1 Fish collection, handling and processing.....114

4.2.2 Enzymatic activity analysis 115
4.2.3 Quantification of cellular damage 117
4.2.5 Statistical analysis 117
4.3 Results 118
4.3.1 Antioxidant enzyme activity 118
4.3.2 Cellular damage 121
4.4 Discussion 123
4.4.1 Enzyme activity 123
4.4.2 Markers of cellular damage 126
4.5 Conclusions 129
Chapter 5 131
Conclusion - Synthesis and implications 131
5.1 Overview 132
5.2 Effects of WWTPE on darters (Etheostoma spp.) 132
5.3 Enantiomer-Specific effects of venlafaxine 136
5.4 Limitations 138
5.5 Management considerations and future perspectives 139
5.6 Conclusions 141
Bibliography 143
Appendix A 197
Appendix B 227

List of figures

Figure 1.1: Conceptual framework illustrating the relationship between biological scale, sensitivity, and ecological relevance in response to toxicant exposure. (A) Subcellular and cellular responses are highly sensitive to stressors (solid blue line) but have lower ecological relevance, whereas population- and ecosystem-level effects have high ecological relevance but are less sensitive to individual stressors (dashed red line) (Connon et al., 2019). (B) Hierarchical progression of biological responses to toxicant exposure, demonstrating causally linked events at multiple levels of biological organisation within the Adverse Outcome Pathway (AOP) framework (adapted from Ankley et al., 2010) 11

Figure 2.1: (A) Map of the Grand River Watershed, Ontario. (B) Sampling sites along the Grand River, Ontario, where darter species were collected in relation to the Waterloo WWTP outfall (WWTPO). Kiwanis (KIW, blue) represents the upstream collection site, while Economic Insurance Trailway (EIT, red) is the downstream site (Google Maps; Map data ©2024, CNES/ Airbus, Landsat, Copernicus, Maxar Technologies). (C) The four darter species (Etheostoma spp.) collected in this study. From top to bottom: rainbow darter (RBD), fantail darter (FTD), johnny darter (JD), and greenside darter (GSD). Illustrations sourced from online open-access repositories, originally published in A Biological Survey of the Oswego River System (State of New York, 1927). 20

Figure 2.2: Cumulative percentage of single copy orthologs identified for rainbow, fantail, johnny, and greenside darters through BUSCO analysis from four databases A) Eukaryota (255), B) Metazoa (954), C) Vertebrata (3354) and D) Actinopterygii (3640) was assessed against unigenes sequences from the assembled transcriptomes of four darter species. Orthologs are classified as complete single-copy (blue), duplicated (green), fragmented (yellow), or missing (red). 30

Figure 2.3: (A) Venn diagram illustrating the overlap of differentially expressed genes (log2FC < -1 or > 1; FDR < 0.05), among four darter species: rainbow darter (blue), fantail darter (yellow), johnny darter (green), and greenside darter (red), following exposure to MWWTP effluent. (B) Matrix plot showing the expression patterns of upregulated (blue; log2FC > 1), and downregulated (red; log2FC < -1) differentially expressed genes shared across species, highlighting conserved and divergent transcriptomic responses to effluent exposure. 34

Figure 2.4: (A) Venn diagram illustrating the number and percentage of orthogroups shared among rainbow (blue), fantail (yellow), johnny (green), and greenside darters (red). (B) Species tree constructed using single-copy orthogroups identified by OrthoFinder. The four darter species form a single clade within the subfamily Etheostomatinae (purple line), with two distinct groupings. The scale bar (0.01) indicates the number of substitutions per site. 35

Figure 2.5: Proportion of Level 2 Gene Ontology (GO) term classifications mapped to unigenes from the transcriptomes of four darter species: rainbow darter (blue), fantail darter (green), johnny darter (yellow), and greenside darter (red). GO terms are categorized into the three primary GO ontologies: (A) Biological Process, (B) Molecular Function, and (C) Cellular Component. Percentages represent the proportion of mapped unigenes assigned to each GO term.

37

Figure 2.6: Significantly enriched (FDR < 0.05) biological process gene ontologies identified from differentially expressed genes in (A) rainbow darter (Etheostoma caeruleum), (B) fantail darter (E. flabellare), (C) johnny darter (E. nigrum), and (D) greenside darter (E. blennioides). Enrichment analysis was performed using background sets of (A) 47,944, (B) 58,452, (C) 57,292, and (D) 62,204 unigenes, with 36, 239, 50, and 68 differentially expressed genes, respectively 41

Figure 2.7: Network maps illustrating relationships between enriched biological process gene ontologies (GO) for (A) rainbow darter (Etheostoma caeruleum), (B) fantail darter (E. flabellare), (C) johnny darter (E. nigrum), and (D) greenside darter (E. blennioides). Each node represents a significantly enriched GO term, with node size corresponding to the number of genes in each pathway. Edges indicate shared gene overlap, with thickness proportional to the percentage of overlapping genes. Node colour represents the significance level (FDR) of enrichment.....42

Figure 2.8: STRING-derived protein-protein interaction (PPI) network (p = 9.97e-8) for differentially expressed genes in liver of rainbow darter (Etheostoma caeruleum) exposed to WWTP effluent, illustrating four clusters of interacting transcripts. Dashed lines indicate edges between nodes that do not belong to the same MCL cluster. Node colour represents log fold change (log2FC), with larger nodes indicating higher degree centrality. Squares denote hub transcripts, while triangles indicate bottleneck transcripts. Edges are coloured according to MCL cluster membership, with thickness reflecting confidence in protein interactions.....43

Figure 2.9: STRING-derived protein-protein interaction (PPI) network (p = 1.0e-16) for differentially expressed genes in liver of fantail darter (Etheostoma flabellare) exposed to WWTP effluent, illustrating four clusters of interacting transcripts. Dashed lines indicate edges between nodes that do not belong to the same MCL cluster. Node colour represents log fold change (log2FC), with larger nodes indicating higher degree centrality. Squares denote hub transcripts, while triangles indicate bottleneck transcripts. Edges are coloured according to MCL cluster membership, with thickness reflecting confidence in protein interactions. Nodes outside the top four most connected clusters are omitted for visual clarity. 45

Figure 2.10: STRING-derived protein-protein interaction (PPI) networks for differentially expressed genes in the liver of (A) Johnny darter (Etheostoma nigrum; p = 5.61e-4) and (B) Greenside darter (E. blennioides; p = 2.19e-2) exposed to WWTP effluent. Edges are coloured by MCL cluster membership, and grey edges represent interactions outside these top four clusters. Edge thickness corresponding to interaction confidence scores, and dashed lines indicate interactions between nodes belonging to different MCL clusters. Node colour represents log fold change (log2FC), with larger nodes indicating higher degree centrality. Hub transcripts are denoted by squares, while triangles indicate bottleneck transcripts. 47

Figure 3.1: (A) Map of the Grand River Watershed illustrating fish collection site near Grand Valley, Southwestern Ontario (red), relative to Waterloo and previous sampling sites from Chapter 2 (orange) (Google Maps; Map data ©2024, CNES/Airbus, Landsat, Copernicus, Maxar Technologies). (B) Schematic of R- and S-venlafaxine (VEN) exposure demonstrating experimental design for one of three troughs. 73

Figure 3.2: Cumulative percentage of single-copy orthologs identified in rainbow darter transcriptomes using BUSCO analysis. Orthologs were assessed against unigene sequences from four databases: (A) Eukaryota (255), (B) Metazoa (954), (C) Vertebrata (3,354), and (D) Actinopterygii (3,640). Transcriptomes were derived from rainbow darters exposed to venlafaxine and their controls (Venlafaxine) and from a wild population collected upstream and downstream of the Waterloo MWWTP effluent outfall (Environment, Chapter 2). Orthologs are classified as complete single-copy (blue), duplicated (green), fragmented (yellow), or missing (red).....80

Figure 3.3: Heat map showing expression levels of 78 differentially expressed transcripts (log2FC < -1 or >1, FDR < 0.05, n = 6) in rainbow darter exposed to either R-venlafaxine (REN; green) or S-venlafaxine (SEN; blue), or control conditions (CON; red) for fourteen days. Expression values represent log2-transformed, median-centered FPKM. Yellow and purple intensities indicate transcript upregulation and downregulation, respectively. Dendrogram clustering on the X-axis reflects sample similarity, while clustering on the Y-axis groups transcripts with similar expression patterns.....82

Figure 3.4: Matrix plot illustrating conserved and divergent transcript expression of significantly differentially expressed genes (DEGs; log2FC < -1 or >1, FDR < 0.05) identified in R-venlafaxine (R-VEN), S-venlafaxine (S-VEN), between treatments (R/S-VEN) after 14 days of exposure, and effluent exposure (ENV-RBD, Chapter 2). DEGs are colour-coded based on log fold change (log2FC), with blue indicating upregulation and red indicating downregulation.....84

Figure 3.5: (A) Venn diagrams illustrating shared and unique orthogroups identified in rainbow darter exposed to venlafaxine (Rainbow-VEN/venlafaxine), rainbow darter (Rainbow-ENV/ Environment), fantail darter, greenside darter, and johnny darter based on OrthoFinder analysis after presumed parasite transcript removal from VEN-RBD. Numbers represent the count of orthogroups unique to or shared among species, with percentages indicating their relative proportion. The upper left Venn diagram compares orthogroups between venlafaxine-exposed and effluent exposed rainbow darters. (B) Phylogenetic tree of Percidae species based on OrthoFinder results. VEN-RBD represents the transcriptome of rainbow darters exposed to venlafaxine. Darter species are color-coded (Etheostoma caeruleum in blue, E. flabellare in yellow, E. blennioides in red, and E. nigrum in green) to distinguish among taxa. 86

Figure 3.6: (A) Significantly enriched (FDR < 0.05) biological process gene ontologies identified from differentially expressed genes in rainbow darter (Etheostoma caeruleum) to R-venlafaxine for fourteen days. Enrichment analysis was performed using background sets of 46,149 unigenes, with 26, differentially expressed genes. (B) Network map illustrating relationships between enriched biological process gene ontologies. Each node represents a significantly enriched GO term, with node size corresponding to the number of genes in each pathway. Edges indicate shared gene overlap, with thickness proportional to the percentage of overlapping genes. Node colour represents the significance level (FDR) of enrichment.....89

Figure 3.7: (A) Significantly enriched biological process gene ontologies (FDR < 0.05) from differentially expressed genes in rainbow darter (Etheostoma caeruleum) exposed to S-venlafaxine for 14 days. Enrichment analysis used a background set of 46,149 unigenes, with 25 differentially expressed genes. (B) Network map depicting relationships among enriched biological process GO terms. Node size reflects the number of associated genes, edge thickness

represents gene overlap percentage, and node colour indicates enrichment significance (FDR). .90

Figure 3.8: Significantly enriched gene ontologies (Fisher's exact P and weight W test, P < 0.05) identified in assembly-specific orthogroups from transcriptomes of rainbow darters (Etheostoma caeruleum) exposed to venlafaxine (VEN) and those collected upstream and downstream of the Waterloo municipal wastewater treatment plant outfall (ENV) (Chapter 2). The colour scale represents the -log10 P-value of enrichment. 91

Figure 3.9: STRING-derived interaction networks (p > 0.05) for differentially expressed genes in liver of rainbow darter (Etheostoma flabellare) exposed to (A) R-venlafaxine and (B) S-venlafaxine for fourteen days. Node colour represents log fold change (log2FC), with larger nodes indicating higher degree centrality. Edges are coloured according to subnetwork. 92

Figure 4.1: Flow diagram of reactive oxygen species (ROS) pathways, illustrating sources of ROS from stressors and enzymatic activity, including monoamine oxidase (MAO) and cytochrome P450 (CYP) enzymes. Antioxidant enzymes, superoxide dismutase (SOD), catalase (CAT), and glutathione peroxidase (GPX), detoxify ROS, leading to either oxidative damage or or stable byproducts. Adapted from Matés & Sánchez-Jiménez (1999), with additional context from Edmondson et al. (2009) and Veith & Moorthy (2018). 112

Figure 4.2: Activity of antioxidant enzymes in the cytosolic and mitochondrial fractions of brain tissue from rainbow darter (Etheostoma caeruleum) exposed to R- and S-venlafaxine for 1, 4, and 14 days (n = 6). (A, B) Superoxide dismutase (SOD) activity (units/mg protein) in the cytosolic (A) and mitochondrial (B) fractions. (C, D) Glutathione peroxidase (GPX) activity (μmol/min/mg protein) in the cytosolic (C) and mitochondrial (D) fractions. (E, F) Catalase (CAT) activity (μmol/min/mg protein) in the cytosolic (E) and mitochondrial (F) fractions. Data is presented as means ± SD, compared using a Two-way ANOVA and post-hoc Tukey test ($p < 0.05$, n = 6 per treatment per time-point. (A) Asterisks indicate significant differences between time points for a given treatment group (**$p < 0.01$, *$p < 0.001$) and lowercase letters indicate significant differences between treatment groups within each time point (Tukey HSD, $p < 0.05$). (B-F) Bars labeled with different letters (a, b, c) differ significantly (Tukey HSD, $p < 0.05$). Groups sharing a letter (e.g., 'ab') are not significantly different from either 'a' or 'b' groups. 120

Figure 4.3: Levels of malondialdehyde (MDA; μmol/mg protein) in brain tissue from rainbow darter exposed (Etheostoma caeruleum) to R- and S-venlafaxine for 1, 4, and 14 days. Data is presented as means ± SD, compared using a Two-way ANOVA and post-hoc Tukey test ($p < 0.05$, n = 6). Bars labeled with different letters (a, b, c) differ significantly (Tukey HSD, $p < 0.05$). Groups sharing a letter (e.g., "ab") are not significantly different from either "a" or "b" groups.....121

Figure 4.4: Levels of 8-hydroxy-2'-deoxyguanosine (8-OHdG; pg/8-OHdG/mg DNA) as in brain tissue from rainbow darter (Etheostoma caeruleum) exposed to R- and S-venlafaxine for 1, 4, and 14 days. Sampling days a grouped by treatment. Data is presented as means ± SD, compared using a Two-way ANOVA and post-hoc Tukey test ($p < 0.05$, n = 6). Bars labeled with different letters (a, b, c, d) differ significantly (Tukey HSD, $p < 0.05$). 122

Figure 5.1: Conceptual overview of the effects of wastewater effluent and venlafaxine exposure on aquatic organisms. This summary diagram illustrates the focus of this thesis and how it aligns with the Adverse Outcome Pathway (AOP) framework.....140

List of tables

Table 2.1:Water quality measurements at Grand River collection sites upstream (KIW) and downstream (EIT) of the Waterloo WWTP outfall in October 2020. Samples were collected from the near, centre, and far banks of the river, with EIT samples taken on the side of the effluent plume, and values are presented as means (n = 3 per site). Flow rate data were retrieved from Historical Hydrometric Data at monitoring stations located 15 km upstream of KIW and downstream of EIT (Government of Canada, 2022). 26

Table 2.2: Comparison of CEC concentrations detected at upstream (KIW) and downstream (EIT) collection sites in October 2020. At each site, three samples were collected from the near, center, and far banks of the river, or within the effluent plume at downstream sites. Values are presented as means (n = 3 per site). n.d. = not detected. Cell colour indicates relative concentration, with a gradient from green (low or undetected levels) to red (high concentrations). 27

Table 2.3: Summary of de novo transcriptome assembly and quality metrics for four darter species. Quality metrics, including raw and filtered read counts, total assembled bases, transcript and unigene counts, contig N50 values, and alignment statistics, are reported for rainbow darter (Etheostoma caeruleum), fantail darter (E. flabellare), johnny darter (E. nigrum), and greenside darter (E. blennioides) (n=12). Average self alignment is expressed as mean ± SD 29

Table 2.4: The number of differentially expressed genes (log2FC < -1, > 1; FDR < 0.05) in the liver of rainbow (Etheostoma caeruleum), fantail (E. flabellare), johnny (E. nigrum), and greenside darters (E. blennioides) following exposure to MWWTP effluent. The number of upregulated (Up; log2FC > 1) and downregulated (Down; log2FC < -1) genes, as well as the average log fold change (Avg. log2FC ± SD), are provided for each species. 32

Table 2.5: Log fold change (log2FC) of the top 5 most significant differentially expressed genes in liver of rainbow (Etheostoma caeruleum), fantail (E. flabellare), johnny (E. nigrum), and greenside darter (E. blennioides) following exposure to MWWTP effluent ranked by false discovery rate (FDR).....33

Table 3.1: Summary of de novo transcriptome assembly and quality metrics for rainbow darter (Etheostoma caeruleum) exposed to venlafaxine, including controls (n=12). Quality metrics, including raw and filtered read counts, total assembled bases, transcript and unigene counts, contig N50 values, and alignment statistics. Average self alignment is expressed as mean ± SD 79

Table 3.2: Total number of significantly differentially expressed genes (DEGs; log2FC < -1 or >1, FDR < 0.05) identified in R-venlafaxine (R-VEN), S-venlafaxine (S-VEN), and between treatments (R/S-VEN) after 14 days of exposure. DEGs are categorized as upregulated (Up) or downregulated (Down). Average log fold change (Avg. log2FC) is reported as mean ± SD.....81

List of Abbreviations

AOPs – Adverse outcome pathways
BOD – Biochemical Oxygen Demand
CAT – Catalase
CBZ – Carbamazepine
CECs – Contaminants of Emerging Concern
CYP – Cytochrome P450
CYTO – Cytosolic Fraction
DEGs – Differentially Expressed Genes
DCF – Diclofenac
EDC – Endocrine Disrupting Compounds
EEM – Environmental Effects Monitoring
EIT – Economical Insurance Trailway; immediately downstream of Waterloo WWTP
ENV-RBD – Rainbow darter exposed to effluent
FTD – Fantail darter (*Etheostoma flabellare*)
GPX – Glutathione Peroxidase
GSD – Greenside darter (*Etheostoma blennioides*)
GEO – Gene Expression Omnibus
HPLC – High-Performance Liquid Chromatography
HSPs – Heat Shock Proteins
JD – Johnny darter (*Etheostoma nigrum*)
KIW – Kiwanis; upstream of Waterloo WWTP
LC-MS/MS – Liquid Chromatography-Tandem Mass Spectrometry
LPO – Lipid Peroxidation
MDA – Malondialdehyde
NCBI – National Center for Biotechnology Information
NGS – Next-Generation Sequencing
NSAID – Non-Steroidal Anti-Inflammatory Drugs
ORF – Open reading frame
O-VEN – O-desmethylvenlafaxine
PFAS – Per- and Polyfluoroalkyl Substances
PhACs – Pharmaceutically active compounds
PPCPs – Pharmaceuticals and Personal Care Products
PUFAs – Polyunsaturated Fatty Acids
RBD – Rainbow darter (*Etheostoma caeruleum*)
RIN – RNA Integrity Number
ROS – Reactive Oxygen Species
R-VEN – R-enantiomer of venlafaxine
SNRI – Serotonin and Norepinephrine Reuptake Inhibitor
SOD – Superoxide Dismutase
STRING – Search Tool for the Retrieval of Interacting Genes/Proteins
S-VEN – S-enantiomer of venlafaxine
TCAG – The Center for Applied Genomics
TMM – Trimmed Mean of M-values

TSS – Total Suspended Solids
VEN – Venlafaxine
VEN-RBD – Rainbow darter exposed to venlafaxine
WWTP – Wastewater Treatment Plant

Chapter 1

Introduction

Researching aquatic contaminants and their impacts on aquatic species in Canada is vital to understanding and mitigating the complex challenges posed by municipal wastewater treatment plant effluent (MWWTPE). Wastewater effluents introduce a diverse array of contaminants, including nutrients, microplastics, and contaminants of emerging concern (CECs) such as pharmaceuticals and personal care products, many of which persist post-treatment (Grbić et al., 2020; Hodgson et al., 2020; Howell & Benoit, 2021; Lalonde & Garron 2021; Kaboré et al., 2022). These contaminants significantly affect aquatic ecosystems, causing physiological, reproductive, and behavioral changes in fish, which can cascade into population and community-level effects, including altered biodiversity and ecosystem structure (Saaristo et al.. 2018; McCallum et al., 2019; Gauthier & Vijayan, 2020; Hodgson et al., 2020; Lau et al., 2021; Mehdi et al., 2021; Mehdi et al., 2022). Incorporating genetic endpoints through next-generation sequencing (NGS) offers a powerful approach to identifying early signs of adverse outcome pathways (AOPs) (Brockmeier et al., 2017; Bajard et al., 2023). By detecting molecular changes at the transcriptomic level, NGS can provide sensitive indicators of sub-lethal stress and physiological disruptions before they manifest as population-level effects (Connon et al., 2018; Hook et al., 2018; Wang et al., 2020; Song et al., 2021). In Canada, ongoing efforts to monitor and regulate wastewater effluents, such as the Environmental Effects Monitoring (EEM) program and national standards under the Fisheries Act, highlight the importance of mitigating these impacts (Fisheries Act, 2019). However, the persistence of certain contaminants, coupled with challenges in biomonitoring and treatment efficacy, underscores the need for innovative approaches like NGS, enhanced wastewater management strategies, and stricter regulatory frameworks to protect aquatic ecosystems from long-term harm.

1.1 Municipal Waste Water Treatment Plant Effluent

In the context of MWWTPE, wastewater encompasses any water that exits a commercial or residential building via a drain, including outputs from toilets, bathtubs, sinks, dishwashers, or washing machines. These inflows introduce a variety of contaminants, each often requiring specific treatment mechanisms, making indiscriminate substitution of decontamination methods ineffective (Henze et al., 2002; Arvai et al., 2014; Mohamed et al., 2023; Solcova et al., 2024). To address these pollutants, municipalities typically implement a series of treatment steps targeting dissolved and suspended solids, organic matter, nutrients such as phosphorus and

nitrogen, pathogenic bacteria, viruses, metals, and microplastics (Arvai et al., 2014; Qiu et al., 2018; Gies et al., 2018). Despite these efforts, some contaminants persist in the treated effluent and are discharged into receiving waters through outfall pipes (Prajapati et al., 2021; Vaudreuil et al., 2022). This effluent can cause physical habitat disruption and significantly elevate winter thermal regimes in receiving waters, altering local ecosystems (Mehdi et al., 2021; Adams et al., 2023). Effluents with high biochemical oxygen demand (BOD), resulting from the oxidation of organic contaminants by aerobic bacteria, can reduce dissolved oxygen levels in the receiving environment, posing a threat to aquatic life (Henze et al., 2002; Arvai et al., 2014). Additionally, nutrients like phosphorus and nitrogen in the effluent can drive eutrophication, promoting excessive growth of micro- and macrophytes, which can lead to hypoxic or even anoxic conditions in the water (Preisner et al., 2020; Kelly et al., 2021).

.

Compounding these issues are contaminants of emerging concern (CECs), including pharmaceuticals, personal care products (PPCPs), endogenous and exogenous hormones, and illicit drugs, which are increasingly detected in WWTP effluent (Oulton et al., 2010; Yadav et al., 2017; Yazdan et al., 2022; Kuch et al., 2000). While their biochemical and physiological properties vary, CECs share common traits such as environmental persistence (Sinthuchai et al., 2016; Baker et al., 2022), toxicity to aquatic organisms like fish (Gros et al., 2010; Topić et al., 2023), and the potential to bioaccumulate and biomagnify within trophic systems (Muir et al., 2017; Gwenzi et al., 2022). These contaminants can disrupt growth, reproduction, and development in aquatic organisms, leading to changes at multiple levels of biological organization (Tyler et al., 1998; Mills and Chichester, 2005; Schoenfuss et al., 2020; Medkova et al., 2022). Understanding the impacts of these effluents is essential, as MWWTPE has been shown to induce direct and indirect changes in aquatic environments, threatening ecosystem health and biodiversity.

1.2 Impacts of MWWTPE on Aquatic Ecosystems

Within Canada the impact of WWTP effluent on aquatic systems and biota including fish is relatively well documented (Holeton et al. 2011; Tetreault et al., 2012; McCallum et al., 2019; Parekh & Marlatt, 2023; Nikel et al., 2023). Responses in fish include alterations in sex steroid hormones (Tetreault et al., 2011; Parekh & Marlatt, 2023) with histological evidence of intersex in male fish (Woodling et al., 2006; Tetreault et al., 2011; Bahamonde et al., 2015;

Niemuth, et al., 2015). Transformation in the weight of organs including gonads and liver, as well as changes in condition factor have been observed in fish exposed to effluent (Kilgour et al., 2005; Nikel et al., 2021; Gauvreau et al., 2022). Additionally, exposure to effluent may shift energy allocation and storage (Saravanan et al., 2011; Cazenave et al., 2014) and disrupt energetics and metabolism in fish by increasing metabolic demands and altering enzyme activities, reflecting the energetic costs of detoxification and coping with chronic contaminant exposure (Mehdi et al., 2018; Hodgson et al., 2020; Beghin et al., 2022; Ball et al., 2024). Exposure to effluent containing measurable levels of CECs has been linked to altered behaviours, including changes in courtship and reduced aggression in the context of territory acquisition and defense (McCallum et al., 2017; Swank et al., 2021). Physiological, endocrine, and behavioural changes, along with disruptions in energy storage, may contribute to population-level effects, such as shifts in sex ratios, reduced growth, decreased survival, and impaired reproductive success (Schoenfuss et al., 2020; Barreto et al., 2020; Ashrafi et al., 2021; Di Prinzio et al., 2024). At higher levels of biological organisation, these population-level effects can lead to community-wide responses, including shifts in species diversity and richness, changes in assemblage structure and trophic guilds, and an increased prevalence of pollution-tolerant species (Porter & Janz, 2003; Wirgin & Waldman, 2004; McCallum et al., 2019; Hoyer & Geheber, 2024

1.3 Biological monitoring and management guidelines

Due to the environmental implications of effluent on receiving waters, particular effort is placed into both improving the quality of effluents released into the environment, and the active monitoring of its impacts. However, given the complexity of WWTP effluent and its effects on many levels of biological organisation, standardization of biomonitoring programs has not yet been achieved. The Canadian government published the *Wastewater Systems Effluent Regulations* (WSER; SOR/2012-139) under the *Fisheries Act (*Government of Canada, 2024a), which sets national standards for MWWTPs, that receive at least 100 m^3 of influent a day. These regulations establish mandatory minimum effluent quality standards for BOD, suspended solids, chlorine, and ammonia (Holeton et al., 2011;Government of Canada, 2024a). While these standards have likely improved effluent quality, the adequacy of these targets for protecting aquatic receiving environments from contaminants including CEC is unclear due to the lack of a formal biological monitoring program.

Under the Canadian federal *Fisheries Act* (2019), the Canadian EEM program, sets guidelines for monitoring the effects of industrial effluent from pulp and paper mills, and mines on receiving waters (Walker, et al., 2002; Walker, et al., 2003; Government of Canada 2018; Government of Canada, 2024b). This is an effects-based program that monitors the impacts of industrial effluent on sentinel fish species between exposed and reference sites. This program focuses on surveying adult fish through measurements of abundance, age, length, sex, liver, gonad, and egg size, fecundity, and external appearance as indicators of the health of fish populations with regards to survival, energy use and storage (Walker, et al., 2002; Walker, et al., 2003; Environment Canada, 2010, 2012). In this program benthic macroinvertebrates are also monitored for abundance, and richness (Kilgour et al., 2005; Environment Canada, 2010, 2012). Within the EEM program, molecular endpoints and physiological variables such as liver enzyme activity, and sex steroid hormone levels are not incorporated, as it was not possible to meet requirements that define a magnitude of change that could be considered impactful for all species in all environments (Bahamonde et al., 2016). Although well documented, the complexity and variance of WWTP effluent composition and its effects on retaining waters makes the selection of appropriate biomonitoring endpoints difficult.

A framework similar to the EEM could be proposed for monitoring WWTP effluent. However, this concept is criticized due to limitations including a lack of viable reference sites, influences of natural variability, and genetic variability influencing species characteristics (Munkittrick et al., 2010). Surveying whole fish communities may be challenging, as only drastic declines in common species may be detectable. This raises concerns that detectable changes may only emerge once fish populations and entire ecosystems have already begun to shift. Limiting biomonitoring to proxy endpoints involving lower trophic levels such as individual sentinel species, rather than whole ecological guilds could help act as a warning for community level impacts (Kilgour et al. 2005; Colin et al., 2016; Ehrman, 2022). Ideally, more sensitive monitoring methods could be implemented; however, demonstrating higher-order ecological effects may remain challenging (Matono et al., 2012). Ongoing developments in the implementation of '-omics' approaches (transcriptomics, proteomics, metabolomics) within ecology propose a potential for sensitive large-scale environmental monitoring through the collection of data on molecular changes that occur at the cellular, tissue, and organismal level

(Bahamonde et al., 2016; Machuca-Sepúlveda, et al., 2023). Several hurdles remain in implementing -omics endpoints within a regulatory monitoring program. Specifically, standardization, consistency, natural variability, and the establishment of actionable thresholds must be rigorously defined to predict broader ecological transformations (Machuca-Sepúlveda, et al., 2023).

1.4 Wastewater Treatment

WWTPs operate at varying levels of treatment, influenced by the population they serve, with smaller facilities sometimes releasing raw sewage. However, they are generally designed to reduce a diverse array of contaminants from wastewater before its release into the environment (Holeton et al., 2011; Ehalt Macedo et al., 2022). MWWTPs are classified based on their level of treatment, which determines their contaminant removal efficiency (Lishman et al., 2006; Holeton et al., 2011). Preliminary treatment involves physical and mechanical processes (sedimentation, coagulation) to remove large debris, followed by primary treatment to eliminate suspended solids and organic matter through physical clarification or chemical processes (precipitation, flocculation) (George et al., 2003; Crini and Lichtfouse, 2018). This is followed by varying levels of secondary treatment. Secondary treatment may focus solely on BOD removal, however this phase can also include disinfection (chlorination, UV, ozone) (Collivignarelli et al., 2017) and the removal of nutrients such as phosphorus and nitrogen through biodegradation, filtration, and adsorption (Crini and Lichtfouse, 2018). In certain facilities, tertiary treatment is also employed, involving the removal of residual solids, secondary treatment byproducts, and nutrients, as well as disinfection through methods such as adsorption, ion exchange, ultrafiltration, and oxidation (George et al., 2003; Crini and Lichtfouse, 2018).

The various methods MWWTP operations employ influence the effectiveness of wastewater remediation and removal of contaminants including CECs. Compounds including carbamazepine, diclofenac, and venlafaxine are generally recalcitrant to removal by conventional wastewater treatment processes, resulting in their continued presence in treated effluent (Rúa-Gómez & Püttmann, 2012; Tran & Gin, 2017). In some instances enantiomeric enrichment of pseudo-persistent substances including chiral pharmaceuticals and their metabolites can occur (MacLeod & Wong, 2010; Ma et al., 2020). For example, the serotonin and norepinephrine

reuptake inhibitor (SNRI) venlafaxine (VEN), appears to undergo some stereoselective processes resulting in the preferential enrichment of one enantiomer (Kasprzyk-Hordern & Baker, 2012; Evans et al., 2015; Ma et al., 2020). Evidence suggests that treatment methods contribute to this enrichment, as activated sludge exhibits greater enrichment than trickling filters (Kasprzyk-Hordern & Baker, 2012). Furthermore, regardless of the treatment method, venlafaxine levels can be found to be higher in treated water than in raw water (Kasprzyk-Hordern & Baker, 2012). Demethylated metabolites may undergo transformation, and glucuronide conjugate metabolites may be enzymatically hydrolyzed during secondary treatment, both resulting in the regeneration of the parent compound (Calisto & Esteves, 2009; Lajeunesse et al., 2012; Bahlmann et al., 2014; Lindholm-Lehto et al., 2016). These findings highlight the need to optimize treatment strategies based on raw water composition and to integrate additional remediation methods for CECs and their derivatives.

1.5 Waterloo MWWTPE and The Grand River

The Grand River watershed, the largest in Southern Ontario, covers approximately 6965 km^2 and drains into the northern part of Lake Erie (Veale and Cooke, 2018). This watershed experiences significant anthropogenic pressures, with 71% of its area dedicated to agriculture, and a rapidly growing urban population exceeding 1 million people (Loomer & Cooke, 2011). The Grand River receives effluent from 30 MWWTPs, which differ in their level of treatment efficiency (Veale & Cooke, 2018). Among these, the Waterloo Wastewater Treatment Plant is one of the largest contributors of effluent to the Grand River, serving a population of over 151,945, including temporary university and college students. As of 2021, this plant had an average daily outflow of 41,430 m^3 (Region of Waterloo, 2022). The plant employs conventional secondary activated sludge treatment. However, historically, water quality downstream of its outfall has been impacted by elevated levels of un-ionized ammonia (Loomer & Cooke, 2011). Further concerns include the measurable presence of pharmaceuticals, personal care products, and endocrine-disrupting compounds in both the effluent and downstream waters, raising questions about the ecological impacts of these contaminants (Arlos et al., 2015).

Studies in the Grand River, primarily focusing on the rainbow darter (*Etheostoma caeruleum*), have linked poor water quality from the Waterloo and Kitchener MWWTP outfalls to adverse physiological and reproductive effects on wild fish, particularly males. These effects

include increased vitellogenin expression (Bahamonde et al,. 2015, Fuzzen et al., 2016), reduced steroid hormone production (Tetreault et al., 2011, Fuzzen et al., 2016) delayed sperm development (Fuzzen et al., 2016), and a high prevalence of severe intersex conditions (Tetreault et al., 2011, Bahamonde et al,. 2015, Fuzzen et al., 2016). Furthermore, fish abundance and diversity have declined downstream of these outfalls, accompanied by a shift in community composition, with darter species being replaced by tolerant-omnivorous fish including sunfish and suckers (Tetreault et al., 2013), suggesting significant ecological impacts. However, further research is needed to confirm these observations and rule out other contributing factors. Upgrades to the Waterloo MWWTP became fully operational in 2017-2018 with the addition of more efficient fine bubbler aeration tanks, and increased solid retention time (Region of Waterloo. 2007; Srikanthan, 2019; Nikel et al., 2023). These upgrades achieve near-complete year-round nitrification, significantly reducing effluent ammonia, BOD, total suspended solids (TSS), selected pharmaceuticals, and estrogenicity (Srikanthan, 2019; Nikel et al., 2023). Despite these upgrades, persistent, unregulated CECs such as VEN, carbamazepine (CBZ), and diclofenac (DCF) remained in effluent and were detected at ng/L concentrations in downstream waters (Srikanthan, 2019; Hodgson et al., 2020).

1.6 Pharmaceuticals in MWWTP Effluent and Their Impact on Non-Target Organisms

While pharmaceuticals improve human health and quality of life, unintended environmental consequences arise when they are released into waterways through WWTPE (Vaudreuil et al., 2022, 2024; Aladekoyi et al., 2024). Among these contaminants, pharmaceuticals classified as CECs pose significant risks to non-target aquatic organisms. Fish are particularly vulnerable to pharmaceutical exposure, which can disrupt endocrine processes (Fuzzen et al., 2016) and may negatively affect the hypothalamus-pituitary-interrenal (HPI) axis, as well as associated processes such as metabolism, immune function, and reproduction (Filby et al., 2007; Vijayan et al., 2010; Pottinger et al., 2013; Mehdi et al., 2018; Beghin et al., 2022). Many psychotropic pharmaceuticals interact with neurotransmitter systems in fish, leading to behavioral changes, disrupted reproductive traits, and altered metabolism (Melnyk-Lamont et al., 2014; Tan et al., 2020; Wiles et al., 2020; Aich et al., 2024). VEN is frequently detected downstream of WWTPE outfalls, and is known to affect fish by increasing cortisol production, and inducing maladaptive behavioural dysfunctions. These include reduced activity and predator

avoidance, impaired food-seeking behaviour, inhibited courtship, and increased post-copulatory aggression (Horst & Preskorn, 1998; Painter et al., 2009; Bisesi et al., 2014; Melnyk-Lamont et al., 2014; Parrott & Metcalfe, 2018; Thompson et al., 2020; Tang et al., 2022). While VEN-induced behavioral impairment is well-documented, its mechanisms cannot be fully explained by brain serotonergic modulation (Bisesi et al., 2014), suggesting potential peripheral effects or possibly reactive oxygen species (ROS) related neurotoxicity (Islas-Flores et al., 2013; Afifi et al., 2016; Ezeoyili et al., 2019). These individual-level effects raise concerns on how they could cascade into population-level consequences.

The removal efficiency of pharmaceuticals like VEN varies among WWTPs, with some compounds persisting post-treatment despite technological upgrades. In the Waterloo WWTP, VEN and its metabolite O-desmethylvenlafaxine (O-VEN) remain detectable downstream, posing chronic exposure risks due to their bioaccumulative nature (Srikanthan, 2019; Metcalfe et al., 2010; Arlos et al., 2015; Mehdi et al., 2018). Exposure to pharmaceuticals, including VEN, can induce cellular stress responses, particularly through the generation of reactive oxygen species (ROS) (Gomes et al., 2019; Maulvault et al., 2019; Ziegler et al., 2020). Under stress, ROS can induce lipid peroxidation by attacking polyunsaturated fatty acids (PUFAs) in cell membranes, creating lipid radicals that propagate chain reactions and produce toxic aldehydes like malondialdehyde (MDA). These toxic byproducts can damage proteins, DNA, and cell membranes (Sies & Cadenas, 1985; Marnett, 1999; Fritz & Petersen, 2013). Additionally, ROS can induce oxidative DNA damage, forming lesions such as 8-hydroxydeoxyguanosine (8-OHdG), which, if un-repaired, can contribute to genomic instability and mutagenesis (Kasai et al., 1986; Ock et al., 2012). Thus MDA and 8-OHdG, are valuable indicators of oxidative stress and ROS induced damage (Ito et al., 2019; Tugasworo et al., 2023). The persistence of pharmaceuticals like VEN in aquatic environments, coupled with their potential to induce oxidative damage, highlights the need for comprehensive assessments of their long-term ecological consequences.

1.9 Transcriptomics in Ecotoxicology

Transcriptomics is a highly informative tool for identifying adverse outcome pathways (AOPs) in ecotoxicology, as it provides a detailed snapshot of how organisms respond to environmental stressors at the molecular level (Brockmeier et al., 2017; Machuca-Sepúlveda et

al., 2023). By examining global gene expression patterns, transcriptomics enables the detection of early, sub-lethal changes that precede physiological, behavioral, or population-level effects (Albers et al., 2024; Escobar & Lampert et al., 2024; Evans et al., 2012; Jeffries et al., 2018; Shi et al., 2024). These molecular responses can reveal specific biological pathways and processes disrupted by contaminants, such as endocrine disruptors and pharmaceuticals, which might otherwise go undetected using traditional biomonitoring methods. Transcriptomic data also facilitate the identification of key molecular events within an AOP, bridging the gap between exposure to a stressor and adverse ecological outcomes (Ankley et al., 2010; Sørhus et al., 2017; Mahoney et al., 2024). Integrating transcriptomics with higher levels of biological organisation, such as cellular and tissue-level responses, aids in developing a more comprehensive effect-based assessment (Connon et al., 2019; Figure 1.1). This mechanistic understanding is crucial for improving the predictive accuracy of risk assessments, developing targeted biomarkers, and informing regulatory policies aimed at protecting aquatic ecosystems. Furthermore, transcriptomics enhances the ability to detect species-specific and conserved responses across taxa, allowing for more comprehensive and comparative studies of contaminant effects on diverse organisms (Barrett et al., 2021; Ellison et al., 2020; Marra et al., 2017; Sepp et al., 2024; Whitehead et al 2010).

Orthology analysis plays a critical role in *de novo* transcriptomic studies, particularly for non-model organisms, as it enables researchers to infer gene function in the absence of reference genomes and improves cross-species comparisons (Spurgeon et al., 2020: Mittal et al., 2023). Traditional annotation approaches relying on sequence similarity using reference databases such as UniProt may misclassify orthologs when transcripts from different species align to functionally divergent proteins, complicating unigene annotation (Bick et al., 2019; Deutekom et al., 2021). OrthoFinder addresses this limitation by clustering genes into orthogroups based on shared ancestry, utilizing phylogenetic inference rather than simple pairwise similarity (Emms & Kelly, 2019). This approach helps differentiate orthologs from paralogs and provides a more evolutionarily meaningful classification of genes. By applying orthology analysis to transcriptomics, researchers can gain deeper insights into evolutionary conservation and divergence of gene function, particularly in ecotoxicology, where molecular responses to pollutants need to be interpreted across non-model species. This integration deepens our understanding of how pollutants affect aquatic life at a molecular level and strengthens the predictive power of AOPs in ecotoxicological research.

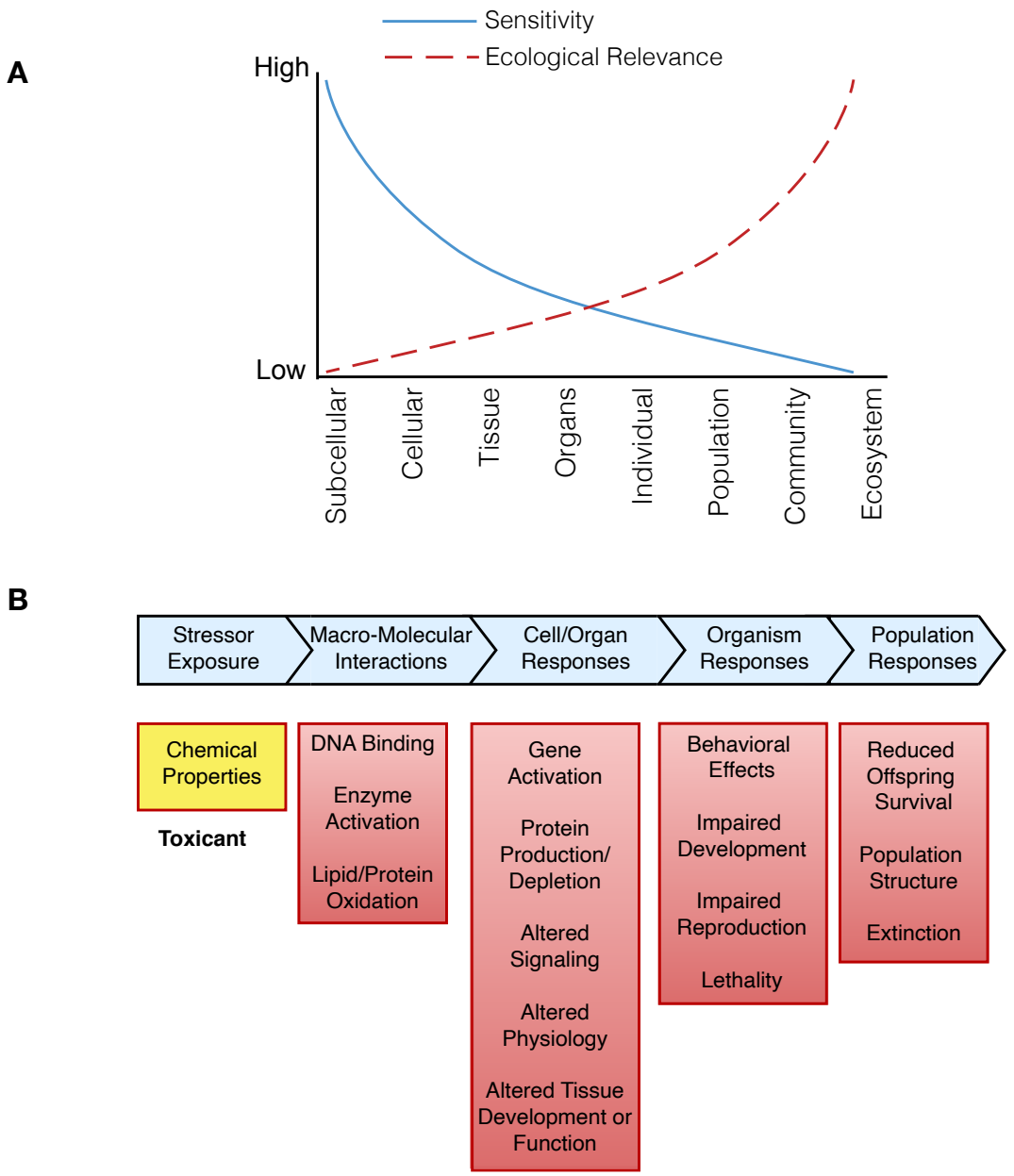


Figure 1.1: Conceptual framework illustrating the relationship between biological scale, sensitivity, and ecological relevance in response to toxicant exposure. (A) Subcellular and cellular responses are highly sensitive to stressors (solid blue line) but have lower ecological relevance, whereas population- and ecosystem-level effects have high ecological relevance but are less sensitive to individual stressors (dashed red line) (Connon et al., 2019). (B) Hierarchical progression of biological responses to toxicant exposure, demonstrating causally linked events at multiple levels of biological organisation within the Adverse Outcome Pathway (AOP) framework (adapted from Ankley et al., 2010)

1.10 Darters

Darters, belonging to the subfamily Etheostomatinae, represent one of the most diverse clades of freshwater fish in North America, comprising an estimated 250 species (Near et al., 2011). Darters exhibit sexual dimorphism, with substantial colour variation among species, and experience isolation driven by divergent sexual selection, which likely contributes to the diversification of this group (Mendelson, 2003; Moran et al., 2017; Moran & Fuller, 2018a, 2018b). Darters are often restricted to small streams with limited dispersal resulting in physical isolation. This separation influences allopatric speciation, acting as another driver of diversification within this clade (Near & Benard 2004, Hollingsworth & Near 2009). Moreover, hybridization is common in darters, as postzygotic barriers are relaxed between sympatric species (Bossu & Near, 2013; Moran et al., 2017, 2018, 2020). Given the multiple drivers of diversification in darters, this clade represents an example of species radiation with significant potential to elucidate the biotic and abiotic mechanisms influencing biological diversity.

Darters are frequently used in ecological studies to infer the effects of anthropogenic pollutants and habitat disruption across North America. Their high site fidelity allows for the study of chronic effects of point-source contaminants or localized environmental stressors while reducing confounding effects from fish migration or exposure to distant habitats (Mundahl & Ingersoll, 1983; Hicks & Servos, 2017). The effects of stressors such as WWTPE discharge on darter population size are well documented, identifying a pattern of population decline downstream from the discharge site (Hicks et al., 2017; Marjan et al., 2017; Mehdi et al., 2018). Despite these effects, some populations of the same species persist in polluted environments, suggesting intraspecific variation in stress tolerance.

1.11 Objectives and hypotheses

This thesis aims to investigate the molecular and oxidative stress responses to MWWTPE exposure in four darter species, a taxonomically diverse and environmentally sensitive group of freshwater fish. Using next generation transcriptome sequencing, this study characterizes species-specific and conserved molecular responses to effluent contamination. To further assess the role of pharmaceuticals in MWWTPE toxicity, this research evaluates the effects of VEN on various biological pathways in rainbow darter through transcriptomic analysis, providing a

comparative framework to MWWTPE exposure. Given VEN's neuroactive properties and the potential for oxidative stress, ROS production and markers of cellular damage were measured in brain tissue to assess physiological stress following exposure. Additionally, because VEN enantiomers can become enriched in receiving waters, this study examined the distinct effects of each VEN enantiomer on transcriptional regulation, ROS production, and oxidative damage, an aspect rarely explored in ecotoxicology. By evaluating the impact of effluent-associated contaminants on aquatic organisms at the genetic and cellular level, this study aimed to support the development of AOPs, inform biomonitoring practices, and contribute to the development of more effective environmental regulations. This thesis addressed these three main objectives with each presented as an individual chapter (Chapter 2-4). The broad hypotheses guiding these objectives are presented below:

1. Exposure to MWWTPE will induce distinct transcriptional responses across four darter species (*Etheostoma caeruleum, Etheostoma nigrum, Etheostoma flabellare, Etheostoma blennioides*), reflecting species-specific adaptations or susceptibilities to effluent, particularly in pathways related to endocrine disruption and metabolism.

2. Laboratory exposure of rainbow darter to each enantiomer of VEN will uncover differential gene expression profiles between enantiomers, which involve pathways similar to those affected by effluent exposure.

3. Exposure to VEN will increase ROS production and oxidative damage in the brains of rainbow darters, as indicated by ROS enzyme activity and biomarkers such as lipid peroxidation products and DNA damage markers, with each enantiomer exhibiting a different magnitude of effect

By addressing these hypotheses, the study will provide critical insights into the molecular mechanisms underlying contaminant impacts on aquatic species, offering novel biomarkers for ecotoxicological assessment and informing conservation efforts for freshwater ecosystems.

Chapter 2

Transcriptomic exploration on the effects of WWTPE on *Etheostoma* spp.

2.0 Introduction

The Grand River watershed in Southern Ontario, Canada, spans approximately 6,900 km^2 and supports over one million residents across multiple municipalities and two First Nations. The watershed is drained by the Grand River and four major tributaries (Nith, Speed, Eramosa, and Conestogo Rivers) and contains 30 wastewater treatment plants (WWTPs) with varying sewage treatment capacities, primarily serving urbanized areas (Tetreault et al., 2013; Srikanthan, 2019). Effluent from these plants frequently contains contaminants of emerging concern (CECs), including pharmaceuticals, personal care products (PPCPs), and endocrine-disrupting compounds (EDCs). These substances have been linked to sub-lethal effects in fish populations, such as growth reduction, reproductive impairments, feminization, and metabolic disruptions, particularly downstream of effluent discharge points (Bahamonde et al., 2015; Fuzzen et al., 2016; Mehdi et al., 2018; Hodgson et al., 2020).

In the past decade, major upgrades to the Kitchener-Waterloo WWTPs have led to significant improvements in effluent quality, reducing the presence of estrogenic compounds, nitrogenous substances, and some pharmaceuticals like ibuprofen and naproxen (Srikanthan, 2019; Nikel et al., 2023). However, other pharmaceuticals, such as the antidepressant venlafaxine (VEN) and anticonvulsant carbamazepine (CBZ), persist in the effluent, leading to detectable concentrations in surface waters (Srikanthan, 2019; Hodgson et al., 2020). These residual contaminants disrupt endocrine, neurological, and metabolic pathways in aquatic organisms, resulting in behavioral and physiological changes (Lange et al., 2009; Mennigen et al., 2011; Mehdi et al., 2018; Hodgson et al., 2020).

2.0.1 CECs of concern

VEN exposure has been particularly studied for its behavioral impacts. For instance, hybrid striped bass exposed to VEN (1–500 μg/L) exhibited increased predation times and reduced brain serotonin levels (Bisesi et al., 2014). Brown trout (*Salmo trutta*) exposed to 10 μg/L VEN showed decreased growth rates, slower reaction times, and altered anti-anxiety behaviors (Ziegler et al., 2021). Fathead minnow embryos and larvae exposed to environmentally relevant VEN concentrations (0.5–2 μg/L) displayed delayed predator avoidance responses, and developmental exposure to VEN caused reduced activity and hyperactivity under light and dark

conditions, respectively, due to serotonergic disruptions (Painter et al., 2009; Thompson and Vijayan, 2020; Thompson et al., 2017, 2021, 2022). Similarly, CBZ exposure in zebrafish at 10 μg/L resulted in reduced feeding times and reproductive issues (da Silva Santos et al., 2018).

CECs can bioaccumulate in aquatic organisms, with studies documenting the presence of antidepressants like fluoxetine, sertraline, and CBZ in the brain tissues of fish from U.S. streams and the Niagara River (Brooks et al., 2005; Schultz et al., 2010; Valdés et al., 2016; Arnnok et al., 2017). These findings underscore significant neurological impairments and behavioural disruptions in fish exposed to waterborne pharmaceuticals, potentially leading to population-level impacts. The persistent presence of antidepressants and other CECs in aquatic environments highlights the need for further research and improved treatment strategies to mitigate their ecological consequences (Brown et al., 2015; Perez et al., 2022).

2.0.2 Using transcriptomic approaches on darters

Transcriptomics is a valuable tool in ecotoxicology, offering detailed insights into how organisms respond to environmental stressors at the molecular level (Brinke et al., 2017; Head et al., 2024). By analyzing global gene expression patterns, transcriptomics detects early, sub-lethal changes that precede observable physiological, behavioral, or population-level effects (Clinton et al., 2021; Li et al., 2021; Liu et al., 2023; Semeniuk et al., 2022). This approach identifies disrupted biological pathways caused by contaminants like endocrine disruptors and pharmaceuticals, which traditional biomonitoring might overlook. By linking contaminant exposure to adverse ecological outcomes, transcriptomics improves risk assessment accuracy, aids biomarker development, and informs conservation policies. This process also reveals species-specific and conserved responses, enabling comparative studies across taxa and advancing understanding of biodiversity impacts (Bernal et al., 2020; Jones et al., 2020; Kavembe et al., 2015).

Darters (subfamily *Etheostomatinae*), comprising approximately 250 freshwater fish species in North America (Near et al. 2011), serve as ideal models for transcriptomic studies. Their sexual dimorphism and striking coloration are outcomes of divergent sexual selection, with traits such as male coloration playing roles in both male-male competition and behavioral isolation further driving their diversity (Mendelson 2003**;** Moran et al. 2017**;** Moran and Fuller

2018a**,** 2018b). Limited dispersal within isolated streams drives allopatric speciation, while hybrid zones illustrate that strong but incomplete reproductive barriers allow some gene flow between sympatric species (Near and Benard 2004**;** Hollingsworth and Near 2009; Bossu & Near 2013; Moran et al. 2017, 2018, 2020). Darters are frequently used in ecological studies to evaluate anthropogenic stressors like wastewater treatment plant effluent, which may reduce populations dynamics downstream (Hicks et al. 2017; Marjan et al. 2017; Mehdi et al. 2018). However, some populations persist in polluted environments, suggesting intraspecific stress tolerance. Integrating transcriptomics could reveal molecular mechanisms behind resilience, improving our understanding of contaminant impacts and guiding conservation efforts.

2.0.3 Functional integration networking

Transcript networking within a set of DEGs aids in identifying functionally related genes and understanding how molecular interactions contribute to broader biological processes. Hub transcripts represent highly connected central nodes in protein-protein interaction (PPI) networks, interacting with numerous other proteins (Vallabhajosyula et al., 2009; Vandereyken et al., 2018). Like a busy intersection in a traffic network, these proteins serve as key connectivity that integrate and regulate multiple pathways (Jin et al., 2007; Ota et al., 2016). Their high connectivity makes them critical for maintaining network integrity, and their interactions allow them to simultaneously influence various biological processes (He & Zhang, 2006). This makes them key nodes in terms of controlling or affecting overall cellular functions. Beyond connectivity, betweenness centrality is another key metric used to identify proteins that facilitate communication within the network by quantifying how often a protein lies on the shortest path between others (Zhang, 2009). Proteins with high betweenness but low connectivity, termed bottlenecks, act as crucial conduits for signal transduction, and their disruption can significantly impact cellular processes (Yu et al., 2007; Joy et al., 2005). The Markov Cluster Algorithm (MCL) is used to identify functional modules within the PPI network by clustering transcripts that are more densely connected to each other than to the rest of the network. These modules often represent protein groups involved in specific biological processes or pathways (Vallabhajosyula et al., 2009; Vandereyken et al., 2018.) By clustering DEGs into these functional modules, key pathways influenced by experimental conditions can be identified, providing a systems-level perspective on molecular interactions and their role in broader cellular functions.

2.0.4 Objectives and hypothesis

This study aims to investigate the molecular mechanisms underlying resilience and susceptibility to wastewater effluent exposure in four darter species—rainbow darters (*Etheostoma caeruleum*), fantail darters (*E. flabellare*), johnny darters (*E. nigrum*), and greenside darters (*E. blennioides*). By incorporating transcriptomic analyses, we seek to identify species-specific and shared gene expression responses to environmental stressors in the Grand River. These findings will enhance our understanding of contaminant impacts on aquatic ecosystems and inform conservation strategies for these and other vulnerable freshwater species. We hypothesized that transcriptomic approaches would reveal distinct differences in gene expression profiles among the four darter species, reflecting their varying levels of tolerance or susceptibility to wastewater effluent exposure. These differences are expected to highlight species-specific molecular pathways and mechanisms associated with resilience, providing insights into how closely related species respond to anthropogenic stressors in their environment. Transciptomic analysis is targeted at the liver, as it has a dynamic range of gene expression, and acts as a hub for systemic homeostasis, playing a pivotal roll in metabolic processes (Ni et al., 2022), detoxification and drug metabolism (Baron et al., 2017), protein synthesis (Arukwe and Goksøyr, 2003), and innate immune response (Wu et al., 2016). Thus the liver is expected to respond to environmental changes and would provide insight into molecular mechanisms underlying various physiological and pathological processes to help identify genes and pathways affected by environmental contaminants

2.1 Materials and methods

2.1.1 Sample collection

In November 2020, six adult male and female rainbow darters (*Etheostoma caeruleum*), fantail darters (*E. flabellare*), johnny darters (*E. nigrum*), and greenside darters (*E. blennioides*) were collected from two sites along the Grand River in southwestern Ontario, Canada: 4.5 km upstream of the Waterloo municipal wastewater treatment plant (MWWTP) at Kiwanis Park (KIW; 43°50′26″N, 80°47′57″W) and 600 m downstream at the Economic Insurance Trailway (EIT; 43°47′26″N, 80°47′41″W) (Figure 2.1). Fish were collected through

backpack electrofishing (Smith Root, LR-20, LR-24), held in aerated buckets filled with river water, and sampled within 3h post collection on site. Fish were measured for total length (±0.1 cm) and wet weight (±0.01 g), and the results of these collections were published by Gauvreau et al. (2022). Fish were then sacrificed through cervical dislocation, and dissected immediately to remove hepatic tissue which was flash-frozen in liquid nitrogen and stored at -80˚C for later RNA extraction. Those smaller than 4 cm were released as they were deemed immature. Animal handling and collection was approved by the Animal Care Committee at the University of Waterloo under AUPP#40318 and following the guidelines set by the Canadian Council of Animal Care.

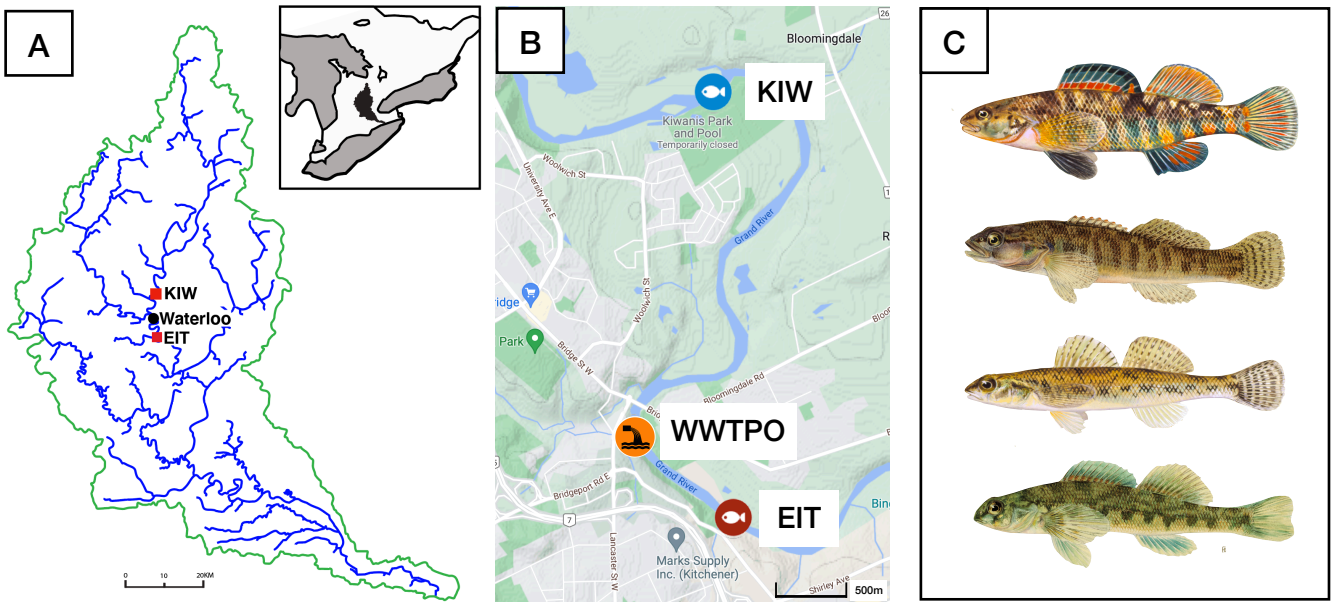


Figure 2.1: (A) Map of the Grand River Watershed, Ontario. (B) Sampling sites along the Grand River, Ontario, where darter species were collected in relation to the Waterloo WWTP outfall (WWTPO). Kiwanis (KIW, blue) represents the upstream collection site, while Economic Insurance Trailway (EIT, red) is the downstream site (Google Maps; Map data ©2024, CNES/ Airbus, Landsat, Copernicus, Maxar Technologies). (C) The four darter species (*Etheostoma* spp.) collected in this study. From top to bottom: rainbow darter (RBD), fantail darter (FTD), johnny darter (JD), and greenside darter (GSD). Illustrations sourced from online open-access repositories, originally published in *A Biological Survey of the Oswego River System* (State of New York, 1927).

2.1.2 Water quality parameters

On the day of fish collection, several river water quality parameters were measured at both EIT and KIW using a YSI Professional Plus multimeter (YSI Incorporated, OH, USA). These included conductivity (µS/cm), temperature(˚C), dissolved oxygen (mg/L), and pH. In addition, water samples were collected in triplicate at each site using 500 mL sterile amber glass jars, with samples taken from the near, center, and far bank of the river. Water samples were preserved in 1 g/L sodium azide and 50 mg/L ascorbic acid, then stored at 4°C until analysis. Liquid chromatography–tandem mass spectrometry (LC-MS/MS) was conducted using an Agilent 1200 High-Performance Liquid Chromatography system (Agilent Technologies, Santa Clara, CA) coupled to an Applied Biosystems 3200 QTRAP mass spectrometer (Thermo Fisher Scientific, Waltham, MA). The multi-residue analysis targeted a broad spectrum of contaminants, including NSAIDs, fibrates, antiepileptics, antibacterials, acetaminophen, the beta-blocker atenolol, the stimulant caffeine, SNRIs, selective serotonin reuptake inhibitors (SSRIs), antibiotics, statins, and the herbicide atrazine. These compounds were selected based on their documented presence in effluent-receiving waters (Kasprzyk-Hordern & Baker, 2012; Arlos et al., 2015; Koné et al., 2013; Khasawneh & Palaniandy, 2021).

2.1.3 RNA extraction, library preparation and sequencing

Total RNA was isolated though phenol-chloroform extraction using QIAzol (Qiagen; Hilden, Germany) following the standard manufacturer protocol. Briefly, liver tissue (20-30mg) was homogenized in 500µl of QIAzol, and nucleic acids were separated with 500µl of chloroform and fractioned through centrifugation. RNA was precipitated with isopropanol and eluted with 50µl of nuclease free water. RNA quality and concentration was measured using an RNA Pico chip on an Agilent 2200 Tapestation Bioanalyzer (Agilent Technologies; Santa Clara, CA). Samples with RNA integrity number (RIN) ≥ 8 were deemed to be of high quality suitable for sequencing. Normalized RNA samples were sent to The Center for Applied Genomics (TCAG, Toronto, Canada) for multiplex library production using an NEBNext Ultra II Directional RNA Library Prep Kit for Illumina (New England Bioscience; Ipswich, MA). Normalized libraries were pooled for sequencing performed as 150 bp, paired-end reads in a single lane of an S4 chip on a NovaSeq 6000 System (Illumina; San Diego, CA) producing no

less than 50 million reads per sample (2.4 billion reads total). All data generated has been uploaded to the NCBI GEO database repository (GSE292546)

2.1.4 Sequence analysis

This study utilized a comprehensive transcriptomic pipeline to evaluate gene expression and identify differentially expressed genes (DEGs) in darter species exposed to environmental stressors. The process involved sequence quality control, *de novo* transcriptome assembly, redundancy elimination, and differential expression analysis, employing a variety of bioinformatics tools.

2.1.4.1 Sequence quality control and *de novo* assembly

Raw paired-end reads were processed using Trimmomatic (v0.36) (Sliding Window: 5:20; leading/trailing threshold: 20) to remove sequences with low-quality bases (Q<20), trim adapters and low quality leading/trailing ends, and filter sequences shorter than 45 bp (Bolger et al., 2014). Quality assessments pre- and post-trimming were conducted using FastQC (v0.11.9), and aggregated then visualized via MultiQC (Ewels et al., 2016). Trimmed reads were assembled *de novo* with Trinity (v2.13.2) under default parameters (Haas et al., 2013), leveraging Google Cloud resources. Reads were mapped to their respective assemblies using Bowtie2 (v2.2.7) (Langmead & Salzberg, 2012) and quantified with RSEM (v1.3.1) (Li & Dewey, 2011). Metrics such as N50, E90N50, and full-length transcript representation were used to assess assembly completeness and contiguity. To explore relationships among sample replicates, principal component analysis (PCA) of the top 500 most variable transcripts was performed on $\log_2$-transformed transcript counts using the "PCA" function in the scikit-learn package in Python. Preliminary BUSCO analyses evaluated transcriptome completeness against Eukaryota, Metazoa, Vertebrata, and Actinopterygii single-copy ortholog databases (Simão et al., 2015). Functional annotations were generated by aligning transcripts to the UniProtKB/Swiss-Prot database using DIAMOND (BlastX) (v2.0.13) with a relaxed e-value (1e-6) to account for phylogenetic diversity. If two or more transcripts exhibited ≥80% similarity, only the longest transcript was retained to maintain a non-redundant set of unigenes.

2.1.4.2 Functional annotation and differential expression analysis

Open reading frames (ORFs) were predicted using TransDecoder (v5.5.0) to define coding regions with a minimum length of 100 peptides (Haas et al., 2013). Functional annotation of transcripts and ORFs were further refined with DIAMOND, using a more stringent e-value cutoff (1e-20). Any transcript showing greater than 50% similarity to viral, bacterial, or fungal genes were removed. Reads were mapped to predicted ORFs, and transcript abundances were normalized as fragments per kilobase per million reads (FPKM). DEGs were identified using edgeR (Robinson et al., 2010) after performing trimmed mean of M-values (TMM) scaling normalization (Robinson et al., 2010). DEGs were defined as genes with a fold change > 2 or < -2 and a false discovery rate (FDR) $\leq 5\%$ (Brauer et al., 2017; McCulloch et al., 2019; Sandoval-Castillo et al., 2020). DEGs were partitioned into hierarchical clusters based on similar expression patterns using a tree cutoff of 60% to assess sample clustering and identify potential biases in the dataset.

Transcriptomes were further annotated using Trinotate (v3.2.2) within the Trinity suite (Bryant et al., 2017). Predicted protein sequences (ORFs) were analysed with HMMER (v3.3.2) against the Pfam database to identify conserved domains. Signal peptides and transmembrane domains were predicted using SignalP v5.0 and tmHMM v2.0, respectively (Almagro et al., 2019; Krogh et al., 2001; Sonnhammer et al., 1998). RNAmmer v1.2 identified and removed any remaining rRNA transcripts (Lagesen et al., 2007). An SQLite database was created to map annotated features to unigenes, enabling gene ontology (GO) term assignment via Trinotate (v3.2.2) through homology and domain presence. Annotations and DEG heat maps were visualized using the TrinotateWeb interface facilitated by a lighttpd webserver. A final BUSCO analysis was completed to further confirm transcriptome completeness, and the reduction of duplicate single-copy orthologs. To address species-specific annotations in the UniProtKB/Swiss-Prot database, initial gene ID conversion was performed with DAVID (Huang et al., 2009; Sherman et al., 2021), using human ID equivalents. This step ensured cross-species comparability by normalizing annotations, when orthologous genes aligned to different model organisms. When Human equivalents were not available, the unique gene IDs were preserved. Shared DEGs across species were visualized with Venni (v2.1) (Oliveros, 2015).

2.1.4.3 Phylogenetic Inference of Orthology

Protein sequences of ORFs identified with TransDecoder were analysed using OrthoFinder (v2.5.5) to infer orthogroups and orthologs, providing insight into conserved and divergent gene expression across species. Orthogroup comparisons were visualized as Venn diagrams using Venni (v2.1) (Oliveros, 2015). To enhance phylogenetic resolution and orthogroup inference, proteomes from five additional Percidae species were incorporated: *Etheostoma cragini* (Arkansas darter; Taxonomy ID: 41792), *E. spectabile* (orangethroat darter; Taxonomy ID: 54343), *Perca flavescens* (yellow perch; Taxonomy ID: 8167), *P. fluviatilis* (European perch; Taxonomy ID: 8168), and *Sander lucioperca* (pikeperch; Taxonomy ID: 283035), obtained from the National Center for Biotechnology Information (NCBI). These taxa, representing the subfamilies Etheostomatinae, Percinae, and Luciopercinae, were included to improve tree resolution. The phylogenetic tree was generated using OrthoFinder results and visualized in Dendroscope (v3.0) (Huson & Scornavacca, 2012).

2.1.4.4 Gene ontology enrichment and pathway analysis

Gene Ontology (GO) terms were assigned using Trinotate (v3.2.2) by linking transcripts to Swiss-Prot annotations. GO enrichment analysis of DEGs was performed using GOseq (Young, 2010), which accounts for transcript length bias. Enriched and depleted GO categories (FDR ≤ 0.05) were identified by comparing DEGs to the transcriptome background, with significant enrichment indicating overrepresentation of a given category. GO term assignments for each unigene were compared across species transcriptomes to assess the congruence of term assignment as a metric of annotation completeness. Fold enrichment was calculated as the ratio of the percentage of DEGs assigned to a GO category to the percentage of background genes assigned to the same term. The most enriched GO terms were visualized in R as lollipop bar graphs, displaying gene counts, fold enrichment, and FDR values. GO terms were further analysed in Cytoscape (v3.9.1) (Lotia et al., 2013) to generate network maps of enriched categories, illustrating overlaps in GO assignment and functional relationships among DEGs. Additionally, GO analysis was conducted on assembly-specific transcripts identified by OrthoFinder, which were unique to individual species. Enrichment analysis for these transcripts was performed using topGO (v2.55) (Alexa & Rahnenfuhrer, 2023), which accounts for the hierarchical structure of GO terms. This analysis aimed to identify functional category

differences among species-specific transcript subsets, providing insight into unique functional traits.

Protein-protein interaction (PPI) networks were constructed using STRING (v11.5) (Szklarczyk et al., 2021), incorporating DEGs from each species to separately identify functionally interacting proteins with medium confidence (score ≥0.4). Interactions were inferred based on presumed orthologous functions in zebrafish (*Danio rerio*). The Markov Cluster Algorithm (MCL) (Van Dongen, 2008) with an inflation parameter of 2 was applied to group transcripts into broader functional clusters, excluding orphan nodes for clarity. The resulting networks, representing functionally interacting transcripts, were visualized in Cytoscape (v3.9.1) (Lotia et al., 2013). For this research, hub transcripts (high connectivity nodes) were defined with a floating cutoff, as nodes with a degree greater than or equal to the sum of the mean degree plus twice the standard deviation of the degree distribution (Dosztany et at., 2006; Rakshit et al., 2014), where degree implies the number of edges (links) connecting a hub.

$$\text{Hub threshold} = \text{mean degree} + (2 \times \text{SD})$$

The betweenness centrality scores of the nodes were organized in descending order, and those in the upper half were selected. From this group, nodes that had fewer connections than the threshold for hub nodes, but were linked to at least one hub were identified as bottlenecks (Rakshit et al., 2014)

2.2 Results

2.2.1 Water quality parameters

Water quality measurements in the Grand River are recorded in Table 2.1. Means were calculated from three measurements at each site (Table 2.1). In Fall 2020, downstream measurements at EIT showed increases in temperature (+1.2°C), conductivity (+162.27 µS/cm), and flow rate (+6.68 m^3/s) compared to the upstream reference site, KIW. Conversely, there was a decrease in dissolved oxygen (DO) by 0.9 mg/L and pH by 0.35 downstream compared to upstream. Moreover, water samples were analysed for 24 different contaminants at both sites relative to the Waterloo WWTP. Upstream of the WWTP, only 11 out of 24 contaminants screened for were detected

compared to 19 out of 24 detected downstream of the WWTP (Table 2.2). An increase can be observed for naproxen, diclofenac (DCF), desmethyl-VEN, VEN, CBZ, ibuprofen, triclosan, sulfamethoxazole, trimethoprim, and p-hydroxy atorvastatin at EIT compared to KIW. The most prevalent contaminants detected downstream were diclofenac (133.72 ng/L) and venlafaxine (153.58 ng/L). In contrast, there was a decrease observed for atrazine downstream (92.67ng/L) compared to upstream (120.03ng/L).

Table 2.1:Water quality measurements at Grand River collection sites upstream (KIW) and downstream (EIT) of the Waterloo WWTP outfall in October 2020. Samples were collected from the near, centre, and far banks of the river, with EIT samples taken on the side of the effluent plume, and values are presented as means (n = 3 per site). Flow rate data were retrieved from Historical Hydrometric Data at monitoring stations located 15 km upstream of KIW and downstream of EIT (Government of Canada, 2022).

Site	Water Temp (ºC)	DO (mg/L)	Flow (m^3/s)	Conductivity (µS/cm)	pH
KIW	7.1	11.7	7.92	335.7	8.50
EIT	8.3	10.8	14.6	497.97	8.15

Table 2.2: Comparison of CEC concentrations detected at upstream (KIW) and downstream (EIT) collection sites in October 2020. At each site, three samples were collected from the near, center, and far banks of the river, or within the effluent plume at downstream sites. Values are presented as means (n = 3 per site). n.d. = not detected. Cell colour indicates relative concentration, with a gradient from green (low or undetected levels) to red (high concentrations).

Classification	Pharmaceutical	KIW (ng/L)	EIT (ng/L)
NSAIDs	Naproxen	n.d.	15.48
	Diclofenac	27.53	133.72
	Ibuprofen	7.66	16.08
Fibrates	Gemfibrozil	n.d.	0.32
Antiepileptics	11,12-epoxide carbamazepine	0.32	1.51
	Carbamazepine	7.99	45.23
Antibacterials	Triclosan	n.d.	9.51
	Triclocarban	n.d.	n.d.
	Sulfamethoxazole	n.d.	1.15
	Sulfamethazine	5.28	31.99
	Trimethoprim	0.52	5.98
Pain relievers	Acetaminophen	n.d.	n.d.
Beta-blockers	Atenolol	n.d.	n.d.
Stimulant	Caffeine	16.17	25.11
SNRI	Desmethyl-venlafaxine	4.99	44.01
	Venlafaxine	11.33	153.58
SSRI	Fluoxetine	n.d.	4.55
	Norfluoxetine	n.d.	n.d.
Antibiotic	Lincomycin	3.72	2.44
	Monensin	n.d.	n.d.
Statins	p-hydroxy atorvastatin	n.d.	15.04
	o-hydroxy atorvastatin	n.d.	11.41
	Atorvastatin	n.d.	5.79
Herbicide	Atrazine	120.03	92.67

2.2.2 RNA quality control and sequencing results

RNA Integrity Numbers (RIN) of all samples averaged 9.94 ± 0.17, ensuring high-quality RNA for library preparation and sequencing (Table A1.1). Three samples (JK4, FE7, GK5) initially had inadequate coverage (35.9–47.7 million reads) and underwent a second sequencing run on a shared Illumina NovaSeq 6000 lane, which was concatenated with the respective initial run for downstream processing. The combined dataset yielded approximately 3.1 billion paired-end reads, with rainbow darters (*Etheostoma caeruleum*), fantail darters (*E. flabellare*), johnny darters (*E. nigrum*), and greenside darters (*E. blennioides*) contributing 836 million, 721 million, 793 million, and 755 million reads, respectively. Reads per sample ranged from 50–73 million for single-lane runs and 63–86 million for concatenated dual runs. Mean sequence quality (Phred scores) remained high (34–38), with negligible base N content (<0.001%), except for JK4, which exhibited 0.06% N content near base 72. Post-trimming, 96.8–97.0% of reads survived, with 98% of sequences retaining lengths between 147–150 bp (Table A1.1). Quality control using FastQC and MultiQC confirmed adapter removal and sequence integrity. Duplicate reads were high (70.7–80.6%) but less than 1% of overrepresented sequences were detected.

2.2.3 Transcriptome assembly and quality metrics

Trinity assembles genes and their corresponding transcripts by first generating contigs from RNA-Seq reads, clustering these contigs into putative gene groups, and then reconstructing isoforms to represent distinct transcripts associated with each gene. Transcriptome assembly statistics for all four darter species are summarized in Table 2.3. Trinity assembled 560,377–654,641 contigs, corresponding to 362,394–445,800 Trinity genes. N50 values ranged from 1,733–1,985 bp, median contig lengths were 391–437 bp, and average lengths were 850.61–955.37 bp. E90N50 values ranged from 2,446–2,556 bp, representing the N50 of the most highly expressed genes comprising 90% of expression data (Figure A1.1) . The percentage of reads that aligned back to their respective assemblies ranged between 85.46% and 89.2%. Between 134,331 and 150,523 Trinity genes remained after more stringent filtering with DIAMOND, removing unwanted viral, bacterial, and fungal sequences. After isolating only the top non-redundant hits, 56,528, 64,925, 58,152, and 65,595 unigenes were identified for rainbow, fantail,

johnny, and greenside darters, respectively. Of these, 19,427, 20,376, 19,912, and 21,454 unigenes containing ORFs were annotated for rainbow, fantail, johnny, and greenside darters, respectively (Table 2.3). BUSCO analysis revealed high transcriptome completeness, recovering 78–82.4% of eukaryotic orthologues, 77.3–81.8% of metazoan orthologues, 70–73.9% of vertebrate orthologues, and 68.5–70.7% of actinopterygii orthologues as complete. Additionally, 16.9–21.2% of orthologues were classified as putative paralogs, while fragmented or missing orthologues accounted for 0.5–12%, depending on the dataset (Figure 2.2). These metrics confirm the high quality of transcriptome assemblies for all darter species (Simão et al., 2015).

Table 2.3: Summary of *de novo* transcriptome assembly and quality metrics for four darter species. Quality metrics, including raw and filtered read counts, total assembled bases, transcript and unigene counts, contig N50 values, and alignment statistics, are reported for rainbow darter (*Etheostoma caeruleum*), fantail darter (*E. flabellare*), johnny darter (*E. nigrum*), and greenside darter (*E. blennioides*) (n=12). Average self alignment is expressed as mean ± SD

	Rainbow Darter (12)	Fantail Darter (12)	Johnny Darter (12)	Greenside Darter (12)
Raw read pairs	836,244,028	721,085,970	793,276,446	755,286,159
Retained filtered read pairs	811,011,633	698,049,073	769,540,579	731,772,152
Assembled bases (bp)	539,201,692	556,842,250	535,366,433	563,395,246
Transcripts	575,924	654,641	560,377	598,053
Trinity genes	384,271	445,800	362,394	401,838
Trinity genes with ORFs	**144,021**	**150,297**	**144,486**	**154,639**
Unigenes	56,528	64,925	58,152	65,595
Contig N50 (bp)	1,913	1,733	1,985	1,915
E90N50 (bp)	2,519	2,552	2,556	2,446
Median contig length (bp)	432	391	435	437
Average contig length (bp)	936.24	850.61	955.37	942.05
Avg. read mapping (±SD) (%)	89.2 (±0.34)	87.33 (±1.49)	88.71 (±0.38)	88.17 (±0.65)
ORF genes annotated	19,427	20,376	19,912	21,454

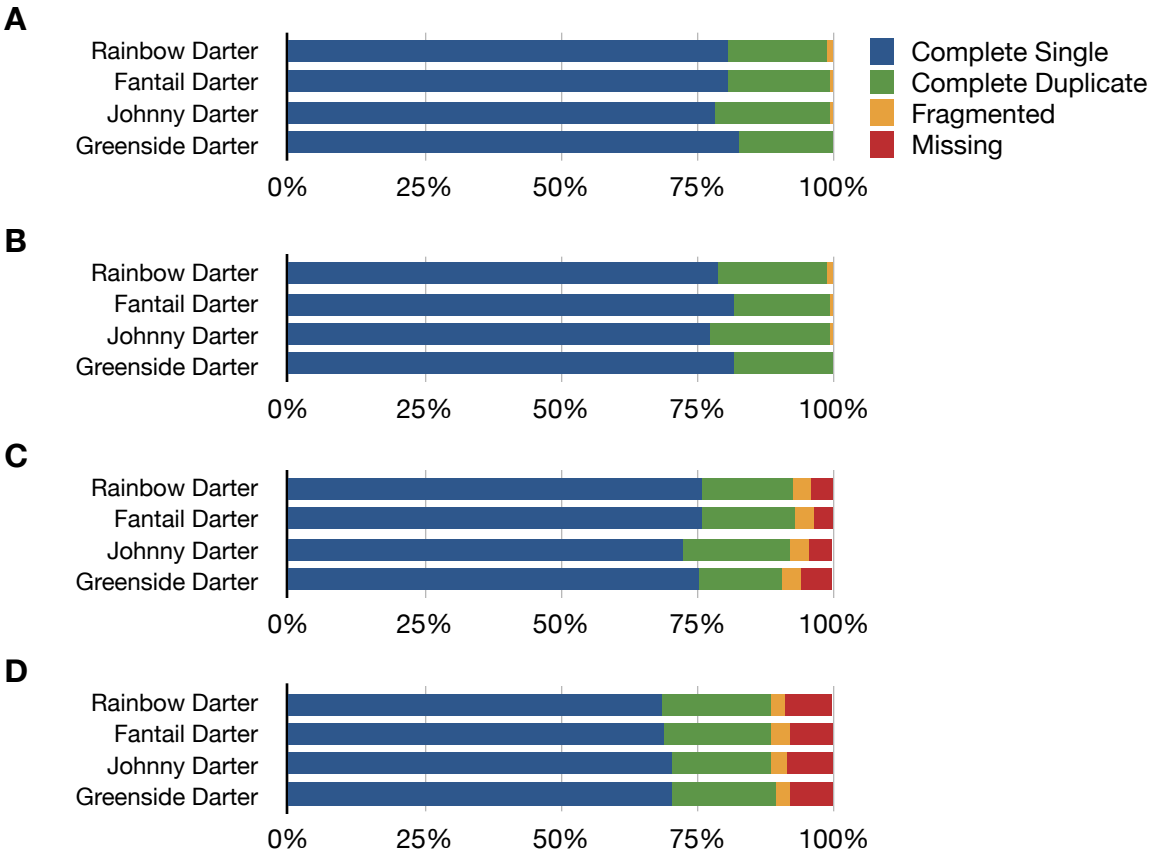


Figure 2.2: Cumulative percentage of single copy orthologs identified for rainbow, fantail, johnny, and greenside darters through BUSCO analysis from four databases A) Eukaryota (255), B) Metazoa (954), C) Vertebrata (3354) and D) Actinopterygii (3640) was assessed against unigenes sequences from the assembled transcriptomes of four darter species. Orthologs are classified as complete single-copy (blue), duplicated (green), fragmented (yellow), or missing (red)**.**

2.2.4 Differential gene expression analysis

Functional annotation and differential gene expression analyses provided significant insights into the transcriptional response of darters to WWTP effluent exposure. Differential expression analysis identified 36 DEGs in rainbow darters, 239 in fantail darters, 50 in johnny darters, and 68 in greenside darters, with unique patterns of upregulation and downregulation (Figure 2.3). The average log fold expression of DEGs varied among species, with values ranging from -0.47 ± 2.06 in Fantail Darter to 6.62 ± 2.1 in Rainbow Darter (Table 2.4). Heatmaps and volcano plots illustrating DEG expression patterns are provided in Appendix A (Figures A1.2–A1.4), along with a complete list of differentially expressed genes (Table A1.2).

Rainbow darters demonstrated significant downregulation of *nlrp12* and *rnf180,* along with other downregulated genes such as *cenpa, nlrp1,* and *smcr8a*. The highest positive change in expression was observed for *dipk1b*, with additional upregulated genes including *hk1*, *lpl*, and *cdh2*, and *ldlr*. In fantail darters, c*3* was the most significantly upregulated gene, with *per2* and *rxraa* also showing substantial positive fold changes. However, most DEGs in fantail darters were downregulated, including the mitochondrial gene *mt-nd2* and heat shock proteins *hsp90aa1* and *hsp90ab1*. In johnny darters, *cfhr2* exhibited the most significant upregulation, followed by *nherf1* and *mt-co3*. Additional highly expressed DEGs included *hexa* and the mitochondrial genes *mt-co1 and mt-cyb*. Conversely, significant downregulation was observed in the complement genes *c7* and c*3*. Greenside darters demonstrated significant upregulation of *nlrp3* and *lce*, while *kptn*, *c1s*, and *top2b* were significantly downregulated. While no DEGs were shared among all four species, greenside darters exhibited the greatest number of shared DEGs with the other species (Figure 2.3). Specifically, greenside darters shared the downregulation of *nlrp12* and *smcr8a* with rainbow darters, the upregulation of *klf13* with johnny darters, and the downregulation of *hspa8* and *stab2* with fantail darters. Divergence was also observed, with opposing expression patterns of *bhmt*, *gpi*, and *tp53inp2* in greenside and fantail darters. Additionally, johnny and fantail darters demonstrated opposing expression of *c*3 (Figure 2.3).

Table 2.4: The number of differentially expressed genes (log2FC < -1, > 1; FDR < 0.05) in the liver of rainbow (*Etheostoma caeruleum*), fantail (*E. flabellare*), johnny (*E. nigrum*), and greenside darters (*E. blennioides*) following exposure to MWWTP effluent. The number of upregulated (Up; log2FC > 1) and downregulated (Down; log2FC < -1) genes, as well as the average log fold change (Avg. log2FC ± SD), are provided for each species.

Species	DEGs	Up	Down	Avg. log2FC
Rainbow	36	26	10	6.62 ± 2.1
Fantail	239	49	190	-0.47 ± 2.06
Johnny	50	34	16	0.97 ± 5.23
Greenside	68	40	28	0.22 ± 3.1

Table 2.5: Log fold change (log2FC) of the top 5 most significant differentially expressed genes in liver of rainbow (*Etheostoma caeruleum*), fantail (*E. flabellare*), johnny (*E. nigrum*), and greenside darter (*E. blennioides*) following exposure to MWWTP effluent ranked by false discovery rate (FDR).

Species	Significant DEGs	log2FC	FDR	Gene Name
Rainbow Darter	*nlrp12*	-10.12	2.88e-13	NLR Family Pyrin Domain Containing 12
	h1	9.47	2.75e-06	Hexokinase 1
	b3gnt9	10.44	2.03e-06	UDP-GlcNAc:Beta-3-Glycosyltransferase 9
	cdh2	8.68	3.10e-06	Cadherin 2 (N-Cadherin)
	ZG7_XENLA	10.44	4.63e-05	Gastrula zinc finger protein
Fantail Darter	*c3*	8.59	8.40e-07	Complement Component 3
	srebf2	-1.42	4.69e-05	Sterol Regulatory Element-Binding Transcription Factor 2
	cyp51	-1.17	2.89e-04	Cytochrome P450 Family 24 Subfamily A Member 1
	cyp3a40	-1.79	3.65e-04	Cytochrome P450 Family 3 Subfamily A Member 40
	cry1	-1.18	5.33e-04	Cryptochrome Circadian Regulator 1
Johnny Darter	*cfhr2*	8.79	7.44e-08	Complement Factor H-Related 2
	nherf1	2.27	8.48e-07	Na^+/H^+ Exchanger Regulatory Factor 1
	mt-co3	5.10	1.31e-06	Mitochondrial Cytochrome C Oxidase III
	mt-cyb	5.89	2.15e-05	Mitochondrial Cytochrome B
	tpt1	9.86	2.26e-05	Translationally Controlled Tumour Protein 1
Greenside Darter	*ZG57_XENLA*	9.39	1.73e-04	Gastrula zinc finger protein XlCGF57.1
	orai1	1.62	1.77e-04	ORAI Calcium Release-Activated Calcium Modulator 1
	card9	1.46	5.12e-04	Caspase Recruitment Domain Family Member 9
	ctsl	1.22	5.12e-04	Cathepsin L
	pnat10	1.46	5.12e-04	N-acetyltransferase, pineal gland isozyme NAT-10

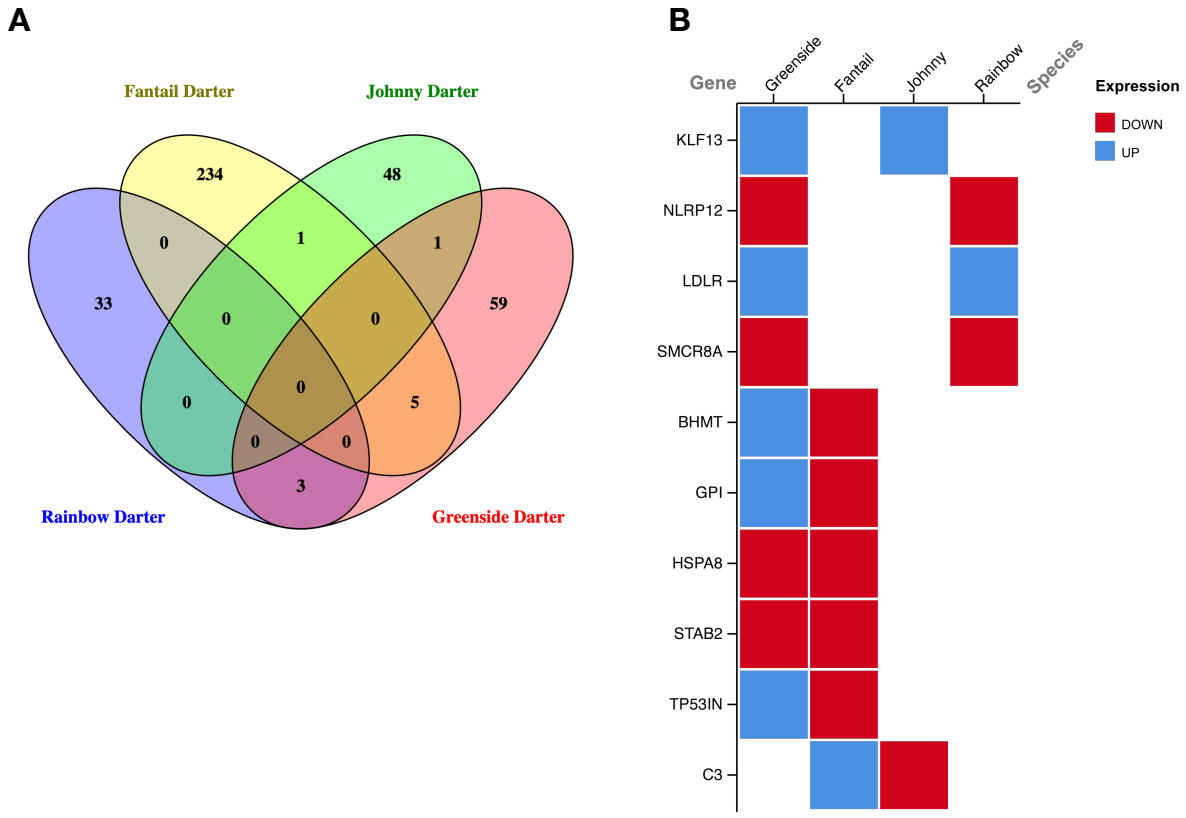


Figure 2.3: (A) Venn diagram illustrating the overlap of differentially expressed genes (log2FC < -1 or > 1; FDR < 0.05), among four darter species: rainbow darter (blue), fantail darter (yellow), johnny darter (green), and greenside darter (red), following exposure to MWWTP effluent. (B) Matrix plot showing the expression patterns of upregulated (blue; log2FC > 1), and downregulated (red; log2FC < -1) differentially expressed genes shared across species, highlighting conserved and divergent transcriptomic responses to effluent exposure.

2.2.5 Comparative Functional Annotation and Gene Ontology Analysis

Functional annotation and Gene Ontology (GO) analysis of transcriptomes across the four darter species provided insights into both shared and species-specific responses to effluent exposure. A total of 245,200 unigenes were assigned to 33,657 orthogroups, with 30,658 orthogroups represented in at least one darter species. Shared orthogroups among all four species accounted for approximately 40% (12,469), indicating substantial overlap across assemblies. Additionally, 63% of orthogroups were present in at least three species, and 89% were shared with at least one other species (Figure 2.4). Unique orthogroups were limited, comprising only 2.1–3.3% of the total orthogroups per species, representing 978–1,579 transcripts. The species tree, constructed using single-copy orthogroups generated by OrthoFinder, with Sander lucioperca as an outgroup, demonstrated a clear separation between subfamilies (Figure 2.4). Species within the subfamily Etheostomatinae, including the four darter species analysed in this study, formed a single clade with two distinct groupings.

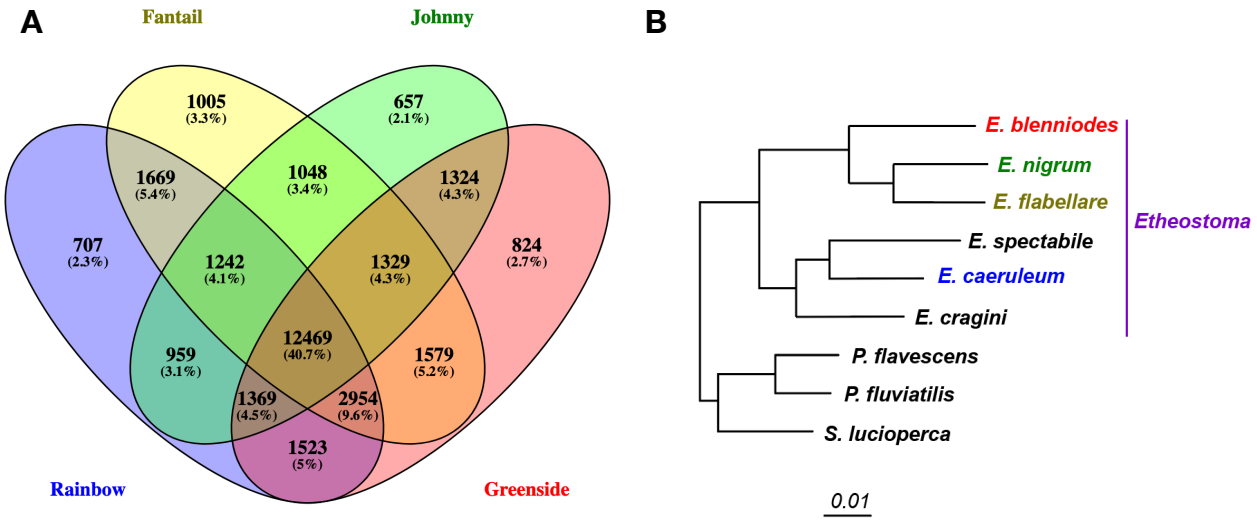


Figure 2.4: (A) Venn diagram illustrating the number and percentage of orthogroups shared among rainbow (blue), fantail (yellow), johnny (green), and greenside darters (red). (B) Species tree constructed using single-copy orthogroups identified by OrthoFinder. The four darter species form a single clade within the subfamily *Etheostomatinae* (purple line), with two distinct groupings. The scale bar (0.01) indicates the number of substitutions per site.

Following the GOseq pipeline, a wide range of Gene Ontology (GO) terms were identified for each assembly, with minimal variation in both the number and distribution of terms across species (Figure A1.5). Level 2 GO term classifications demonstrated a high degree of congruence in proportions and distribution across species (Figure 2.5), indicating consistency in annotated functional categories. The most frequently assigned GO terms under Biological Process included "cellular processes" (GO:0009987; 18.6–18.7%), “biological regulation” (GO:0065007; 14.8–15.7%), and "metabolic processes” (GO:0008152; 11.8–12.1%). Within Molecular Function, “binding” (GO:0005488; 52.0–52.6%), “catalytic activity” (GO:0003824; 22.6–23.9%), and “transcription regulator activity” (GO:0140110; 5.7–6.8%) were the most prevalent. Finally, for Cellular Component, the most frequently assigned terms were cell (GO:0005623; 32.4–33.1%), “organelle” (GO:0043226; 27.5–28.0%), and "macromolecular complex" (GO:0032991; 11.8–12.3%).

Gene ontology enrichment analysis using topGO revealed distinct functional profiles in species-specific orthogroups among the four darter species (Table A1.3). Rainbow darters exhibited significant enrichment in terms related to neural signalling, cell adhesion, and ion channel activity, while greenside darters showed significant enrichment in terms related to structural integrity, extracellular matrix organization, apoptotic processes, and the cellular component lamellipodium (GO:0030027). Greenside darters demonstrated the highest number of enriched terms and shared the most enriched terms with other species, sharing seven of the sixteen total enriched terms with other species. Fantail darters demonstrated enrichment in terms involving transport and cellular organization, as well as muscle system processes (GO:0003012). Johnny darters had fewer enriched terms, primarily focused on vesicular transport and organelle organization. Shared terms, such as protein binding (GO:0005515), were enriched across all four species, and multicellular organism development (GO:0007275) was shared among all but Johnny Darter.

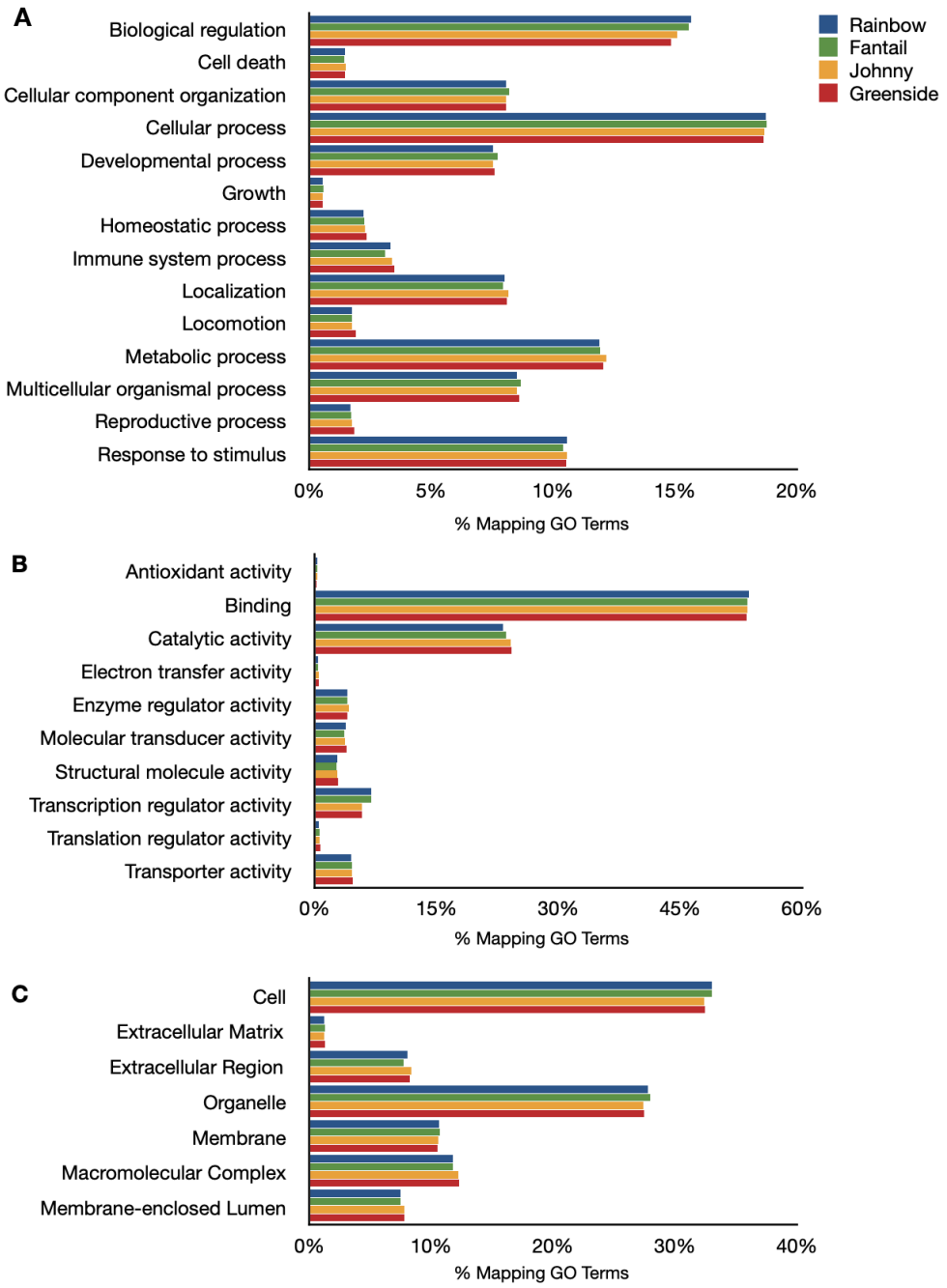


Figure 2.5: Proportion of Level 2 Gene Ontology (GO) term classifications mapped to unigenes from the transcriptomes of four darter species: rainbow darter (blue), fantail darter (green), johnny darter (yellow), and greenside darter (red). GO terms are categorized into the three primary GO ontologies: (A) Biological Process, (B) Molecular Function, and (C) Cellular Component. Percentages represent the proportion of mapped unigenes assigned to each GO term.

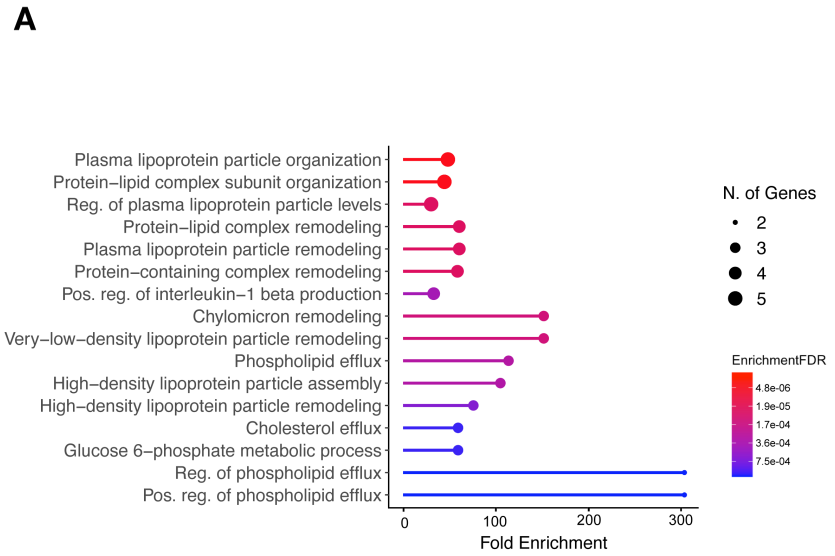
Enriched GO terms revealed key functional categories overrepresented among DEGs in each species (Table A1.3). In rainbow darters, significantly enriched biological processes were primarily associated with lipoprotein particle regulation, remodelling, and lipid transport. The most significantly enriched terms included plasma lipoprotein particle organization (GO:0071827; FDR = 4.79e-6) and protein-lipid complex subunit organization (GO:0071825; FDR = 4.06e-6), which were also linked to the highest number of DEGs. Clustering of enriched ontologies formed a single network of lipid-associated terms, represented by the parent categories protein–lipid complex subunit organization and regulation of plasma lipoprotein particle levels (GO:0097006; FDR = 1.85e-5). Additionally, lipid transport processes such as phospholipid efflux (GO:0033700; FDR = 8.60e-4) and cholesterol efflux (GO:0033344; FDR = 3.82e-4) were integrated into this network. Outside this primary network, two isolated nodes emerged: positive regulation of interleukin-1 beta production (GO:0032731; FDR = 9.81e-5) and glucose 6-phosphate metabolic process (GO:0051156; FDR = 8.47e-4), suggesting distinct functional pathways unrelated to lipid metabolism.

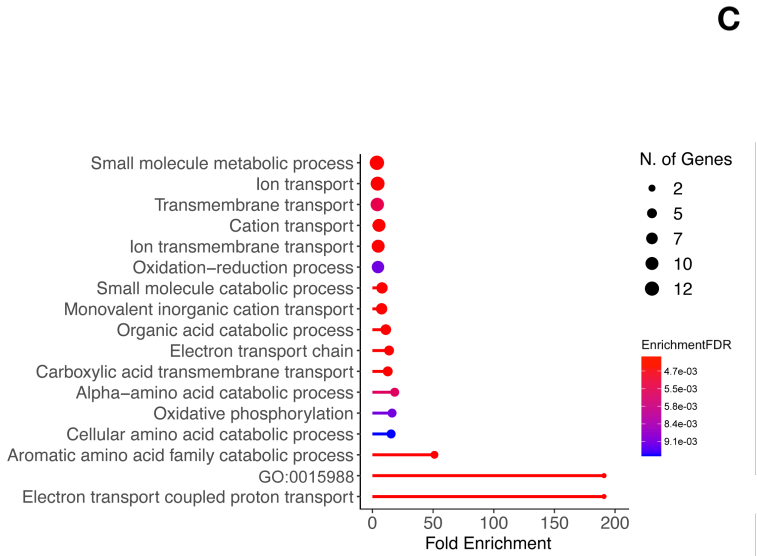
DEGs in fantail darters were primarily enriched in metabolic and catabolic processes, immune system functions, and cellular localization, with several terms exhibiting both high gene counts and significant enrichment. Metabolic and catabolic processes represented the most significantly enriched categories, including small molecule metabolic process (GO:0044281; FDR = 1.50e-8) and protein catabolic process (GO:0030163; FDR = 3.45e-8). The terms with the most assigned DEGs were associated with catabolic process (GO:0009056; FDR = 1.75e-8), immune system process (GO:0002376; FDR = 1.63e-7), and gene expression (GO:0010467; FDR = 2.66e-7). Network mapping of enriched GO terms revealed a less cohesive structure compared to other species, characterized by three distinct clusters and three isolated nodes. The first cluster encompassed a hierarchy of catabolic processes, including cellular catabolic process and protein catabolic process. The second was represented by immune related terms like immune system process and interspecies interaction between organisms (GO:0044419; FDR=1.13e-7). The third cluster involved nitrogen metabolism and biosynthesis, including amide metabolic process (GO:0043603) as well as gene expression (GO:0010467). The three isolated nodes represented distinct biological functions: mitochondrion organization (GO:0007005; FDR= 1.37e-6), establishment of localization in cell (GO:0051649; FDR= 1.69e-6), and small molecule metabolic process.

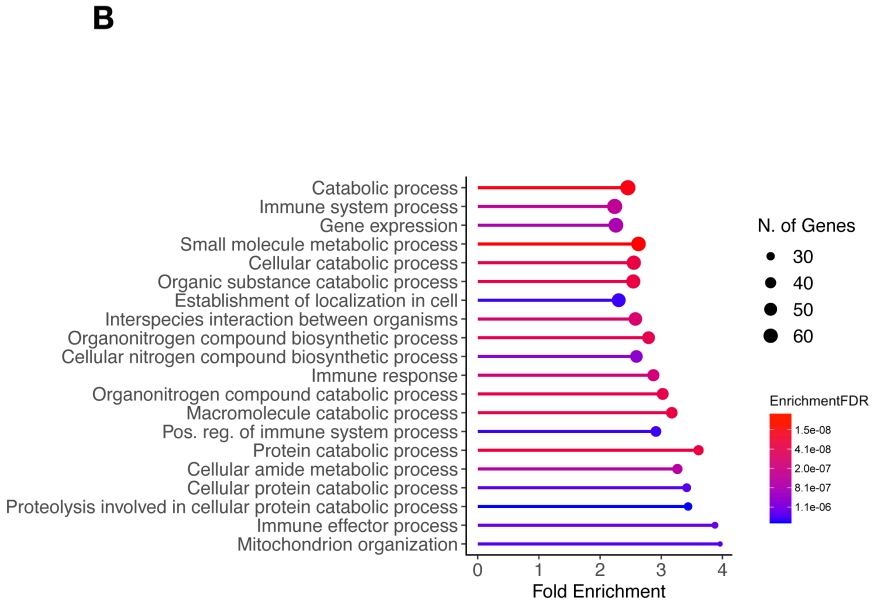
Several biological processes were significantly enriched among the DEGs identified in johnny darter, primarily involving metabolism, catabolism, transport, and redox processes. Notably, some of the most significantly enriched ontologies, also had the highest number of DEGs assigned, which included *small molecule metabolic process* (GO:0044281; FDR=3.74e-03), *ion transport* (GO:0006811; FDR=3.62e-03), and *transmembrane transport* (GO:0055085; FDR=4.70e-3). Network analysis revealed a single comprehensive network encompassing all enriched ontologies, grouped by functional similarity. These groups included terms related to ion and transmembrane transport and catabolic processes involving organic and amino acids. These clusters were interconnected through terms involving redox reactions and energy generation mechanisms including *oxidative phosphorylation* (GO:0006119; FDR= 9.1e-3) and *electron transport chain* (GO:0022900; FDR= 4.34e-03).

Significantly enriched GO terms among the greenside darter DEGs were primarily involved in immune system regulation, inflammatory responses, signal transduction, and phosphorylation. The most enriched terms included *negative regulation of interleukin-1 production* (GO:0032692; FDR=6.34e-3), *regulation of immune system process* (GO:0002682; FDR=6.73e-3), while processes with the most assigned DEGs included *interspecies interaction between organisms* (GO:0044419; FDR=2.06e-2), and *regulation of response to stress* (GO:0080134; FDR=1.76e-2). These GO terms clustered into a single integrated network centred on immune and inflammatory pathways, particularly negative regulation of interleukin production and NF-κB signalling. Additionally, broader processes related to phosphorylation and metabolic regulation were interconnected within this network. Two outlier terms were identified as isolated nodes: regulation of keratinocyte differentiation (GO:0045616; FDR=3.72e-2) and lipid homeostasis (GO:0055088; FDR=2.92e-2).

The overlap in GO enrichment between species was notably limited, however some shared patterns was observed. Specifically, the GO term small molecule metabolic process was identified as a common feature between fantail darter and johnny darter, and the term interspecies interaction between organisms was enriched in both fantail darter and greenside darter.


A
Plasma lipoprotein particle organization
Protein–lipid complex subunit organization
Reg. of plasma lipoprotein particle levels
Protein–lipid complex remodeling
Plasma lipoprotein particle remodeling
Protein–containing complex remodeling
Pos. reg. of interleukin–1 beta production
Chylomicron remodeling
Very–low–density lipoprotein particle remodeling
Phospholipid efflux
High–density lipoprotein particle assembly
High–density lipoprotein particle remodeling
Cholesterol efflux
Glucose 6–phosphate metabolic process
Reg. of phospholipid efflux
Pos. reg. of phospholipid efflux
0
100
200
300
Fold Enrichment
N. of Genes
2
3
4
5
EnrichmentFDR
4.8e-06
1.9e-05
1.7e-04
3.6e-04
7.5e-04


C
Small molecule metabolic process
Ion transport
Transmembrane transport
Cation transport
Ion transmembrane transport
Oxidation–reduction process
Small molecule catabolic process
Monovalent inorganic cation transport
Organic acid catabolic process
Electron transport chain
Carboxylic acid transmembrane transport
Alpha–amino acid catabolic process
Oxidative phosphorylation
Cellular amino acid catabolic process
Aromatic amino acid family catabolic process
GO:0015988
Electron transport coupled proton transport
0
50
100
150
200
Fold Enrichment
N. of Genes
2
5
7
10
12
EnrichmentFDR
4.7e-03
5.5e-03
5.8e-03
8.4e-03
9.1e-03


B
Catabolic process
Immune system process
Gene expression
Small molecule metabolic process
Cellular catabolic process
Organic substance catabolic process
Establishment of localization in cell
Interspecies interaction between organisms
Organonitrogen compound biosynthetic process
Cellular nitrogen compound biosynthetic process
Immune response
Organonitrogen compound catabolic process
Macromolecule catabolic process
Pos. reg. of immune system process
Protein catabolic process
Cellular amide metabolic process
Cellular protein catabolic process
Proteolysis involved in cellular protein catabolic process
Immune effector process
Mitochondrion organization
0
1
2
3
4
Fold Enrichment
N. of Genes
30
40
50
60
EnrichmentFDR
1.5e-08
4.1e-08
2.0e-07
8.1e-07
1.1e-06

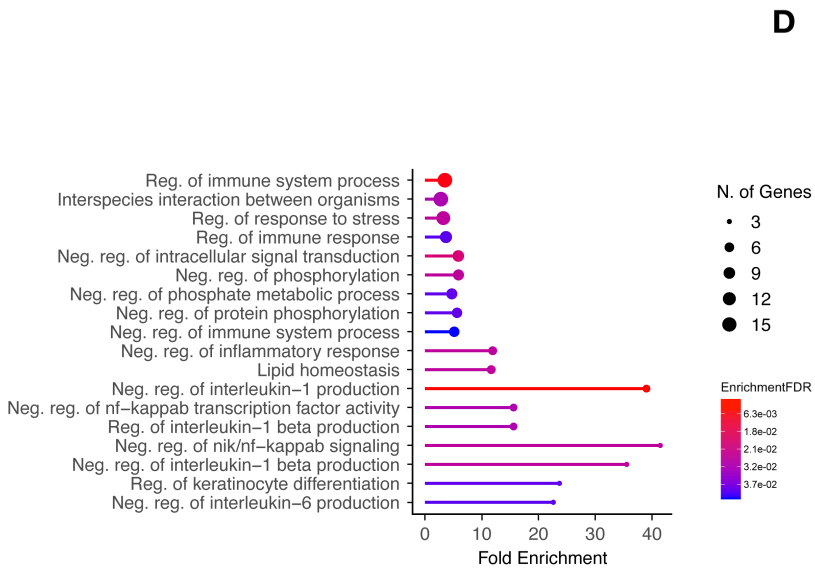

D
Reg. of immune system process
Interspecies interaction between organisms
Reg. of response to stress
Reg. of immune response
Neg. reg. of intracellular signal transduction
Neg. reg. of phosphorylation
Neg. reg. of phosphate metabolic process
Neg. reg. of protein phosphorylation
Neg. reg. of immune system process
Neg. reg. of inflammatory response
Lipid homeostasis
Neg. reg. of interleukin–1 production
Neg. reg. of nf–kappab transcription factor activity
Reg. of interleukin–1 beta production
Neg. reg. of nik/nf–kappab signaling
Neg. reg. of interleukin–1 beta production
Reg. of keratinocyte differentiation
Neg. reg. of interleukin–6 production
0
10
20
30
40
Fold Enrichment
N. of Genes
3
6
9
12
15
EnrichmentFDR
6.3e-03
1.8e-02
2.1e-02
3.2e-02
3.7e-02

Figure 2.6: Significantly enriched (FDR < 0.05) biological process gene ontologies identified from differentially expressed genes in (A) rainbow darter (*Etheostoma caeruleum*), (B) fantail darter (*E. flabellare*), (C) johnny darter (*E. nigrum*), and (D) greenside darter (*E. blennioides*). Enrichment analysis was performed using background sets of (A) 47,944, (B) 58,452, (C) 57,292, and (D) 62,204 unigenes, with 36, 239, 50, and 68 differentially expressed genes, respectively

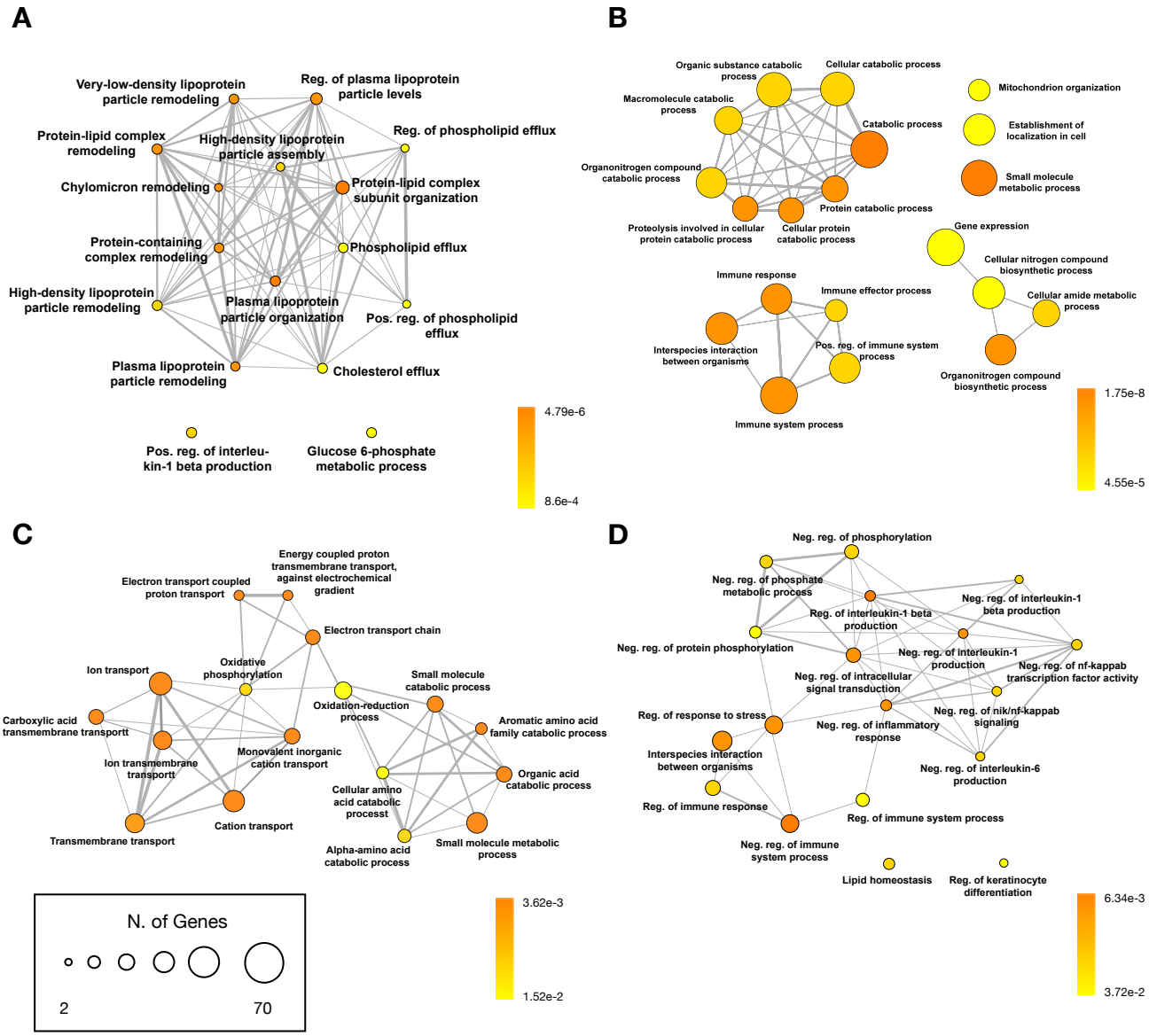


Figure 2.7: Network maps illustrating relationships between enriched biological process gene ontologies (GO) for (A) rainbow darter (*Etheostoma caeruleum*), (B) fantail darter (*E. flabellare*), (C) johnny darter (*E. nigrum*), and (D) greenside darter (*E. blennioides*). Each node represents a significantly enriched GO term, with node size corresponding to the number of genes in each pathway. Edges indicate shared gene overlap, with thickness proportional to the percentage of overlapping genes. Node colour represents the significance level (FDR) of enrichment.

2.2.6 Protein network analysis

The transcripts interaction network for rainbow darters consisted of four clusters, with an average node degree of 1.64, a clustering coefficient of 0.461, and significant PPI enrichment (p = 9.97e-8; Table A1.5). The largest cluster, indicated by green edges, included hub transcript *apoe*, with *lpl* as a bottleneck. This cluster encompassed all genes associated with enriched GO terms related to plasma lipoprotein assembly, remodelling, clearance, regulation, and cholesterol metabolism. Apart from *apoe* and *apoa4*, all genes in this cluster were upregulated. The yellow cluster, featuring *gck* as a bottleneck, contained three upregulated genes contributing to the enriched GO term glucose 6-phosphate metabolic process (GO:0051156). Additionally, a dyad cluster, indicated by red edges, contained two upregulated genes associated with the enriched GO term positive regulation of interleukin-1 beta production (GO:0032731) (Figure 2.8; Table A1.6).

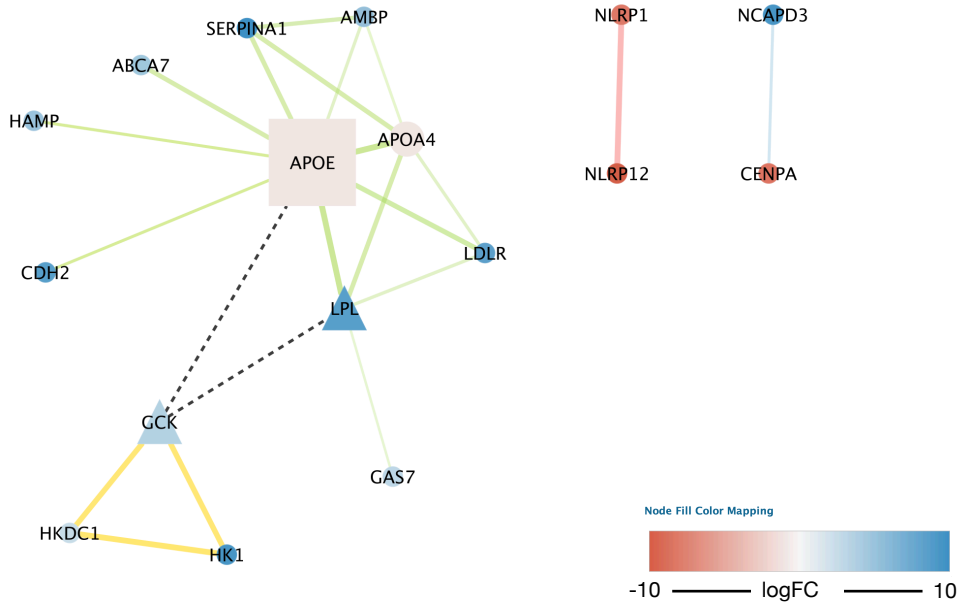


Figure 2.8: STRING-derived protein-protein interaction (PPI) network (p = 9.97e-8) for differentially expressed genes in liver of rainbow darter (*Etheostoma caeruleum*) exposed to WWTP effluent, illustrating four clusters of interacting transcripts. Dashed lines indicate edges between nodes that do not belong to the same MCL cluster. Node colour represents log fold change (log2FC), with larger nodes indicating higher degree centrality. Squares denote hub transcripts, while triangles indicate bottleneck transcripts. Edges are coloured according to MCL cluster membership, with thickness reflecting confidence in protein interactions.

A transcript network of 30 clusters was constructed from fantail darter DEGs, with an average node degree of 6.99, a clustering coefficient of 0.43, and highly significant PPI enrichment (p = 1.0e-16; Table A1.5). Overall, most DEGs were downregulated, indicating a general suppression of gene expression across the identified clusters. The largest cluster with green edges consisting of 60 nodes, featured highly connected hub proteins, including *hsp90aa1, hsp90ab,* and *hspa8*. DEGs within this cluster were significantly enriched in catabolic processes, particularly protein catabolic processes (GO:0030163). However, these genes also contributed to less connected enriched GO terms, including: response to stress (GO:0006950), mitochondrion organization (GO:0007005), organonitrogen compound biosynthetic process (GO:1901566) and small molecule metabolic process (GO:0044281). The second most connected cluster with yellow edges contained 15 nodes primarily involved in RNA processing, including the hub *eftud2*. The third sub-network with red edges was associated with small molecule and cellular amide metabolic processes, while the fourth cluster with blue edges comprised DEGs exclusively linked to small molecule metabolism (Figure 2.9; Table A1.6)

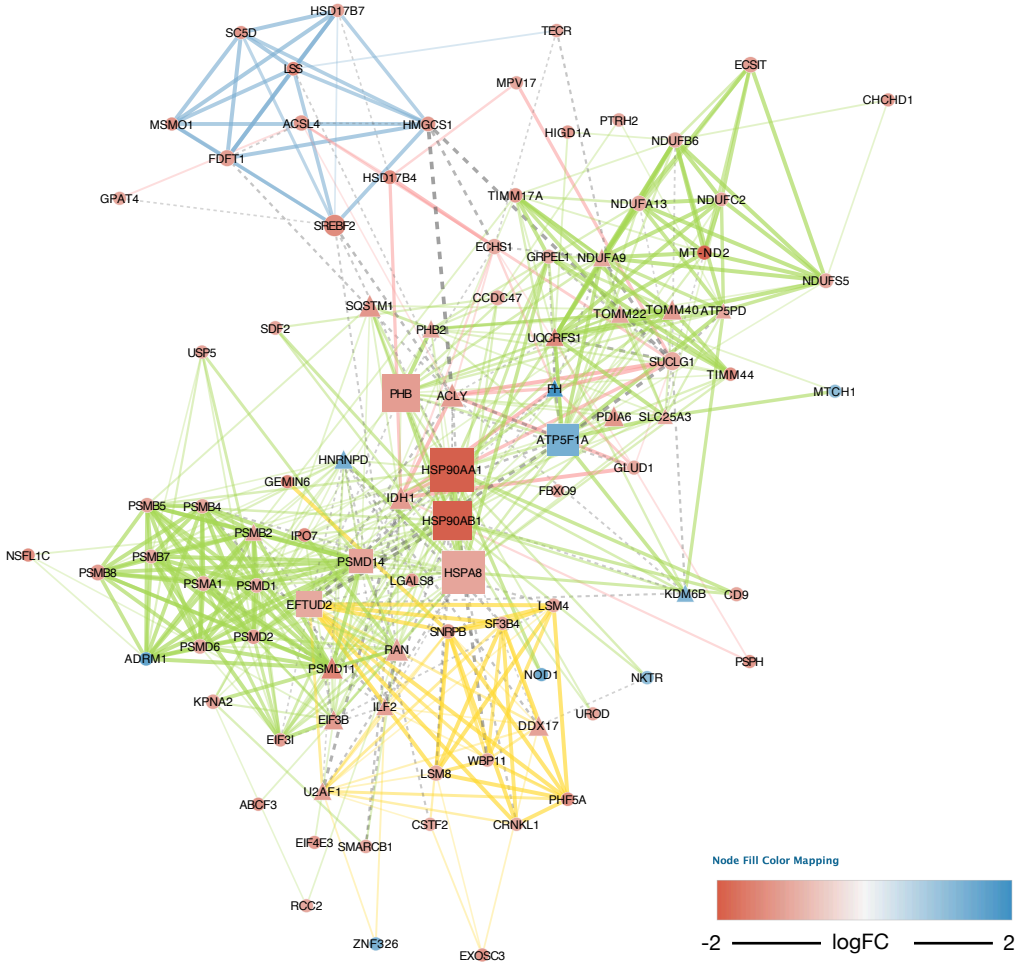


Figure 2.9: STRING-derived protein-protein interaction (PPI) network (p = 1.0e-16) for differentially expressed genes in liver of fantail darter (*Etheostoma flabellare*) exposed to WWTP effluent, illustrating four clusters of interacting transcripts. Dashed lines indicate edges between nodes that do not belong to the same MCL cluster. Node colour represents log fold change (log2FC), with larger nodes indicating higher degree centrality. Squares denote hub transcripts, while triangles indicate bottleneck transcripts. Edges are coloured according to MCL cluster membership, with thickness reflecting confidence in protein interactions. Nodes outside the top four most connected clusters are omitted for visual clarity.

The STRING network for johnny darters had an average node degree of 1.06, an average local clustering coefficient of 0.45, and significant PPI enrichment (p = 5.61e-4; Table A1.5). MCL clustering identified eight sub-clusters, including three distinct networks and four isolated dyads. The largest network with green edges, consisting of five upregulated DEGs, included the hub proteins *mt-co3* and *mt-atp6*, associated with mitochondrial function and respiratory chain

complexes. This cluster contributed to the enriched GO terms: Ion transport (GO:0006811), Electron transport chain (GO:0022900), and Oxidative phosphorylation (GO:0006119). The second most connected network with yellow edges contained the downregulated hub protein C3, while the third network with red edges comprised additional downregulated DEGs that did not significantly contribute to GO term enrichment. The fourth cluster, centred on the bottleneck protein *il4i1*, integrated into the primary network, with all DEGs upregulated and linked to amino acid catabolism GO terms (Figure 2.10; Figure A1.6).

The PPI network for greenside darters comprised 30 transcripts, with an average node degree of 1.12, an average local clustering coefficient of 0.255, and PPI enrichment (p = 2.19e-2; Table A1.5). Nine distinct clusters and one isolated dyad were identified. A majority of DEGs across clusters contributed to the enrichment of the biological process regulation of response to stress (GO:0080134). The most highly connected cluster with green edges was centred around the hub proteins *myc, crebbp,* and *hspa8,* containing DEGs associated with response to stress and immune regulation, contributing to the enriched GO term regulation of immune response (GO:0050776). The second cluster with yellow edges, centred on the bottleneck protein *nlrp3*, comprised DEGs involved in the negative regulation of inflammatory and immune responses. The third cluster, marked by blue edges, contained DEGs linked to the enriched ontology term lipid homeostasis (GO:0055088)(Figure 2.10; Figure A1.6). The fourth cluster (red) contained DEGs responsible for oxygen transport and glycolysis.

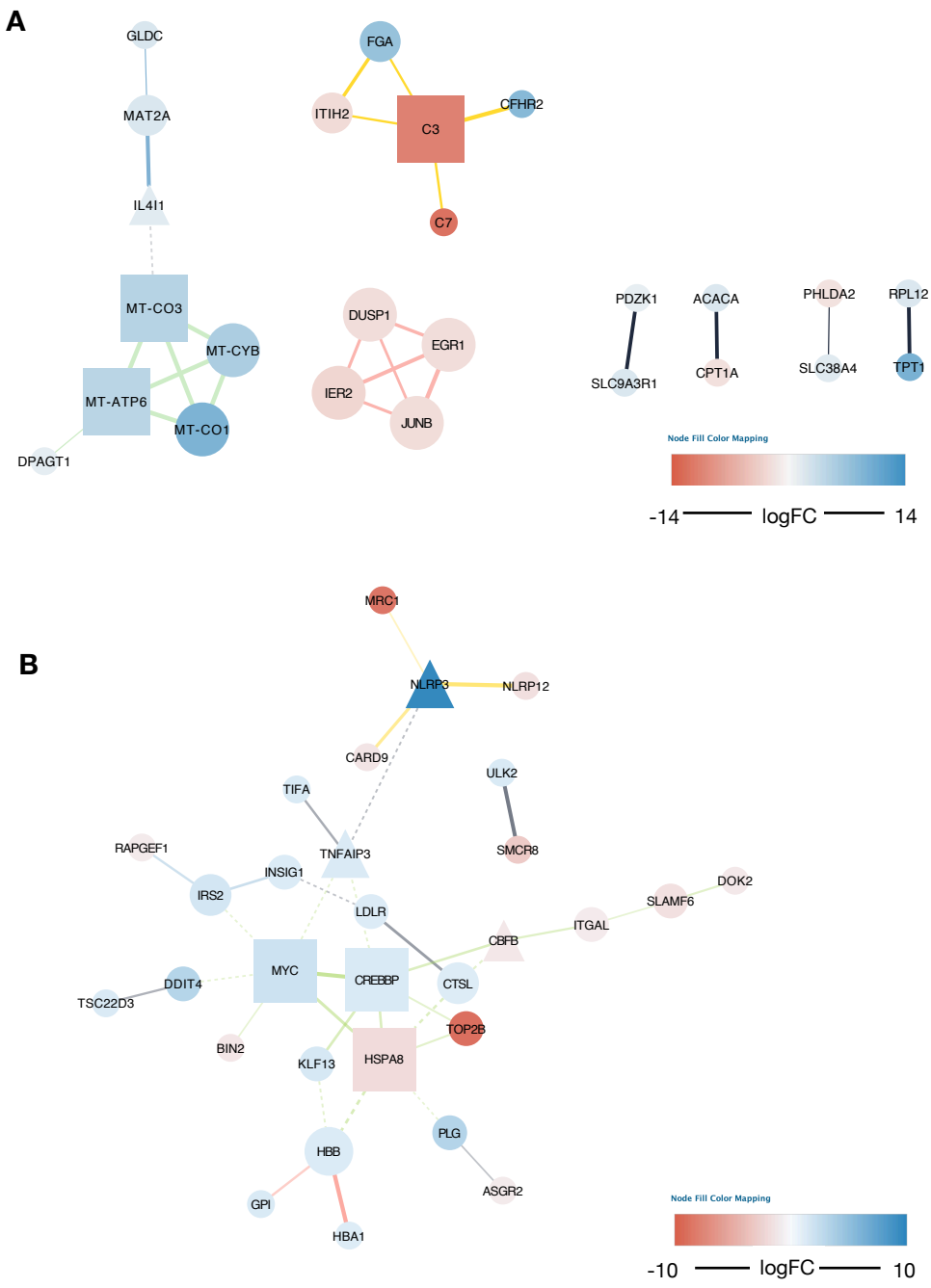


Figure 2.10: STRING-derived protein-protein interaction (PPI) networks for differentially expressed genes in the liver of (A) Johnny darter (*Etheostoma nigrum*; p = 5.61e-4) and (B) Greenside darter (*E. blennioides*; p = 2.19e-2) exposed to WWTP effluent. Edges are coloured by MCL cluster membership, and grey edges represent interactions outside these top four clusters. Edge thickness corresponding to interaction confidence scores, and dashed lines indicate interactions between nodes belonging to different MCL clusters. Node colour represents log fold change (log2FC), with larger nodes indicating higher degree centrality. Hub transcripts are denoted by squares, while triangles indicate bottleneck transcripts.

2.4 Discussion

The present study examined the transcriptional responses of rainbow darters (*E. caeruleum*), fantail darters (*E. flabellare*), johnny darters (*E. nigrum*), and greenside darters (*E. blennioides*) to wastewater treatment plant effluent exposure. Utilizing high-quality RNA sequencing, transcriptome assembly, annotation, differential gene expression analysis, gene ontology (GO) enrichment and protein-protein interaction (PPI) network visualization, the study revealed shared and species-specific transcriptome alterations. These highlighted significant modulation in immune regulation, metabolism, mitochondrial function, lipid transport, and stress response pathways. Functional annotation and GO enrichment emphasized distinct and overlapping biological processes affected by effluent exposure, while PPI network analysis identified key proteins potentially driving these responses. These findings elucidate the mechanisms underpinning darters' adaptive and stress responses to environmental contaminants, thereby advancing our understanding of the ecological impacts of wastewater effluents on aquatic organisms.

2.4.1 Water quality

In Fall 2020, water samples downstream of the Waterloo WWTP revealed high concentrations of pharmaceuticals, with venlafaxine (VEN) and diclofenac (DCF) being the most abundant contaminants, followed by atrazine and carbamazepine (CBZ) (Table 2.2). Atrazine was the highest upstream contaminant, while most other measured contaminants were undetectable, or much lower than their downstream counterparts. These findings align with a Fall 2015 study in the Niagara River, where similar contaminants were detected (Arnnok et al., 2017). Similar elevations of pharmaceuticals, such as VEN, were also reported by Metcalfe et al. (2010) in the Grand River, highlighting that the introduction of pharmaceuticals by WWTPs remains a persistent issue in this watershed. Pharmaceuticals such as ibuprofen, fluoxetine, VEN, CBZ, naproxen, and DCF have been detected in fish tissues (brain, liver, gonads) at concentrations ranging from 0.11 to 12.95 ng/g (Brooks et al., 2005; Arnnok et al., 2017; McCallum et al., 2017). Arnnok et al. (2017) observed SSRIs in fish tissues at up to 17 ng/g of sertraline, 0.2–40 ng/g of norfluoxetine, and up to 57 ng/g of VEN, highlighting significant

bioaccumulation and potential ecological impacts of wastewater contaminants on the darter species collected downstream of WWTPs. These findings illustrate the ongoing challenge of pharmaceutical contamination in aquatic environments downstream of WWTPs and raise concerns about their ecological implications for sensitive species.

2.4.2 Transcriptome Assembly

The quality and depth of sequencing data critically influence transcriptome assembly, as transcript coverage varies with RNA abundance, particularly for lowly expressed transcripts (Wang et al., 2011; Tarazona et al., 2011; Sims et al., 2014). While sequencing depth requirements depend on the biological question, a depth of 20–150 million paired-end reads (75–150 bp) is typically sufficient for identifying differentially expressed genes (DEGs) (Liu et al., 2014), with higher depths enabling capture of nearly full-length transcripts (Grabherr et al., 2011; Francis et al., 2013). In this study, sequencing depths of 50–96 million paired-end reads per sample, and 698–811 million paired-end reads per transcriptome (Table 2.3; Table A1.1), exceed commonly accepted standards, providing high coverage and supporting comprehensive transcriptome characterization.

Alignment rates to the assembled transcriptomes ranged from 85.46% to 89.2%, falling within the expected 70–90% range (Conesa et al., 2016), validating assembly quality and providing confidence in downstream analyses (Table 2.3). A single sample from the fantail darter (*FE7*) exhibited a lower alignment rate (68%) potentially due to initially insufficient sequencing depth and subsequent resequencing (Table A1.1). Although this may introduce batch effects or technical variations, FE7 did not deviate significantly in hierarchical clustering and sample correlation (Figure A1.2; Figure A1.3). Assembly statistics, including N50 values of 1,733–1,985 bp and E90N50 values of 2,446–2,556 bp (Table 2.3; Figure A1.1), confirmed the robustness of the assemblies, with transcripts sufficient to capture protein-coding regions (Tiessen et al., 2012). The identification of 56,528–65,595 unigenes compares favourably with other *de novo* teleost transcriptomes (Table 2.3). For instance, Gates et al. (2017) reported 67,938 unigenes in Australian rainbow fish (*Melanotaenia splendida tatei*), while Sandoval-Castillo et al. (2020) found 34,815 unigenes in *Melanotaenia* species. Comparatively, Chen et al. (2017) identified 83,834 non-redundant transcripts across multiple tissues in Eurasian perch (*Perca fluviatilis*), highlighting the breadth of transcriptome diversity across different species and tissue types.

BUSCO scores revealed high recovery rates of single-copy orthologs (68.5–82.4%), indicating transcriptome completeness (Figure 2.2). However, 16.9–21.2% of BUSCOs were identified as duplicates, which is unexpected given that BUSCOs typically evolve under single-copy control (Waterhouse et al., 2011). These duplications may reflect heterozygosity and allelic variations, consistent with observed genetic diversity in rainbow darters (Oliveira et al., 2021). Although 0.5–12% of genes were fragmented or missing, this is common in transcriptomic data due to isoform variability and is comparable to other assemblies (Carruthers et al., 2018; Bertel-Sevilla 2020; Sandoval-Castillo et al., 2020; Luo et al., 2022; Pomianowski et al., 2021; Marisaldi et al., 2021). The robust assembly metrics, high BUSCO completeness, and extensive unigene counts collectively emphasize the quality and comprehensiveness of these liver tissue transcriptomes, making them well-suited for downstream differential expression and functional analyses.

2.4.3 Annotation

Functional annotation of darter transcriptomes revealed that 13–14% of trinity genes matched unique proteins in the UniProtKB/Swiss-Prot database with at least 80% identity, yielding 19,427–21,454 annotated unigenes with ORFs (Table 2.3). This is consistent with *de novo* teleost assemblies reporting 18,313 to 34,192 annotated unigenes (Sun et al., 2019; Richards et al., 2018; Sandoval-Castillo, 2020; Martínez−Burguete et al., 2021).

Orthogroup inference via OrthoFinder revealed that that approximately 40% of orthogroups are shared across the four darters, while over 60% were shared by at least three species (Figure 2.4). This concordance is expected given their evolutionary relatedness (Thomas et al., 2011), and the phylogenetic tree constructed using single copy orthologs compares well with established taxonomy (Thomas et al., 2011; Daniel et al, 2018). Although species-specific orthogroups were limited (657–1005), these transcripts may reflect functional diversity linked to specific environmental adaptations or physiological demands, or may represent lowly expressed transcripts not captured in the other darter transcriptomes. These findings align with other *de novo* studies that have investigated orthogroups among both closely and more distantly related teleosts (Carruthers et al., 2018; Marisaldi et al., 2021).

Gene ontology assignments for all annotated transcripts revealed a diverse array of GO terms in each assembly, demonstrating comprehensive representation with minimal variation in

root ontologies and level 2 terms. High uniformity in GO profiles aligns with prior studies reporting stable GO term distributions across multiple species and phyla (Carruthers et al., 2018; Elmer et al., 2010; Riesgo et al., 2012), further validating the accuracy of the assemblies and their annotations. Additionally, assembly-specific transcripts exhibited greater differences in the proportion and variety of GO terms compared to the complete dataset, which were effectively characterized through GO enrichment analysis.

2.4.4 Species comparisons of shared and unique pathways

To compare and contrast the transcriptomic responses of rainbow (RBD), fantail (FTD), johnny (JD), and greenside (GSD) darters to wastewater treatment plant effluent (WWTPE), their differentially expressed genes (DEGs), enriched pathways, and modulated biological processes were examined. This analysis revealed both common and species-specific adaptations to effluent. These findings provide insights into conserved mechanisms for coping with environmental stressors and highlight potential unique molecular mechanisms or physiological adaptations in response to wastewater effluent exposure.

2.4.4.1 Stress, Immune Response and Inflammatory Regulation

All four darter species showed evidence of immune system dysregulation, including alterations in pattern recognition receptors, complement components, cytokine signalling, and inflammation-regulating protease inhibitors. Fantail darter downstream of the WWTPE outfall exhibited the highest number of DEGs with significant enrichment of immune system processes (Figure 2.6). Notably, networked transcripts within the complement cascade (*c1qbp, c1qc, c1qb, c3, c8b*) were predominantly downregulated, except for *c3*, which emerged as one of the most upregulated transcripts. The complement system acts as a key component of innate immunity, responsible for marking pathogens for clearance and the activation of downstream immune components (Ricklin et al., 2010). This observed pattern suggests atypical regulation of the classical complement pathway, potentially leading to incomplete activation. Modulation of cytokine signalling pathways (*ifi44, ifit1, trim25, stat1, stat3, tnfsf14*) was also evident, implicating processes of both pathogen detection, antiviral defenses and inflammatory regulation (Xu et al., 2015). Transcript networking in Johnny Darter (Figure 2.10) highlighted modulation of the complement system (*c3, c7, cfhr2*), as well as inflammation-associated tissue repair

processes (*fga, itih2*). These findings suggest a potential restraint in complement activity (Holland & Lambris, 2002; Eberhardt et al., 2013) along with evidence of inflammatory dysregulation and altered repair processes (Davalos & Akassoglou, 2012).

In rainbow darters, the significant downregulation of pattern recognition receptors (*nlrp12, nlrp1*) indicated a modulation in inflammatory singling, while the compensatory upreulation of the protease inhibitors *serpina1 and ambp* suggest a protective mechanism towards excessive inflammation and oxidative damage (Kono et al., 2003; Li et al., 2022; Su et al., 2017). This is further supported by enrichment of transcripts (Figure 2.6) involved in positive regulation of interleukin-1 beta (IL-1β), a key pro-inflammatory cytokine crucial in fish innate immunity (Kono et al., 2003).

Greenside darters most prominently showed significant modulation of stress and immune response pathways (Figutre 2.6), with *myc* and *crebbp* acting as hub transcripts in interaction networks (Figure 2.10). These hubs are transcriptional regulators that can be activated during cellular stress and infection (Matt, 2002; Nie et al., 2012; Wei et al., 2019). Transcripts within this network (*tifa, card9, nlrp3, slamf6, itgal*) influence innate immune activation including inflammasome assembly, and immune cell recruitment (Lin et al., 2016; Peng et al., 2024; Li et al., 2020; Chang, 2023; Sameshima et al., 2012). Other networked transcripts (*tnfaip3, tsc22d3, nlrp12, nlrc3*), function in the negative regulation of NF-κB and IL-1 signalling pathways, responsible for dampening of immune and inflammatory responses, helping to moderate excessive inflammation and maintain immune homeostasis (Vogel et al., 1996; Mérour et al., 2019; Morimoto et al., 2021; Chang et al., 2021). Varied expressional changes within these transcripts suggest a complex interplay between immune activation and attenuation. Such varied expression profiles could represent adaptive immunomodulation under effluent exposure or could indicate pathological dysregulation.

Stress can activate the hypothalamus-pituitary-interrenal (HPI) axis, leading to the release of neuroendocrine factors, such as cortisol (Nardocci et al., 2014). These factors can stimulate the innate immune response including the mobilization of leukocytes, and the complement cascade. However, chronic stress generally suppresses immune functions, in part as a protective mechanism to prevent tissue damage from excessive inflammation (Nardocci et al., 2014), and in part due to the reallocation of energy to cope with the stressor (Wendelaar Bonga, 1997; Tort,

2011). Consequently, fish may exhibit both acute immune activation and, over time, a suppressed immune capacity. This depression of immune processes increases susceptibility to infections and reduces overall fitness (Ndong et al., 2007; Small & Bilodeau, 2007; Mauri et al., 2011). Consistent with previous studies on fish exposed to MWWTPE, our findings highlight the immunomodulatory effects of such contaminants (Salo et al., 2007; Hébert et al., 2008; Arstikaitis et al., 2014). Overall, the transcriptomic signatures observed in darters suggest a complex interplay of stress responses, immune pathway modulation, and inflammation regulation. While some transcriptional changes may be adaptive, chronic dysregulation of these pathways could compromise immune function, increasing vulnerability to disease and ultimately reducing fitness under environmental stressors (Wendelaar Bonga, 1997). Future research should investigate how these transcriptomic alterations could translate into functional immune deficits and potential long-term ecological impacts on darter populations.

2.4.4.2 Lipid Metabolism and Cholesterol Homeostasis

Effluent exposure led to significant disruptions in metabolic and energy production pathways across the four darter species. Although species-specific differences in gene expression patterns were observed, commonalities emerged in the modulation of lipid metabolism and cholesterol homeostasis suggesting a shared adaptive response to WWTPE.

In response to effluent exposure, rainbow darters exhibited significant modulation of lipid metabolism, as highlighted by transcript networking analyses (Figure 2.8) and GO enrichment (Figure 2.6). Specifically, genes responsible for lipid and cholesterol transport (*apoe, apoa4, abca7, arf4*) and utilization (*ldlr, lpl*) via lipoproteins and chylomicrons were affected. Lipoproteins are complexes composed of apolipoproteins (*apoe, apoa4*) and lipids, including cholesterol and triglycerides, that facilitate lipid trafficking throughout the body via the circulatory system (Stan, et al., 2003; Wang et al., 2014; Giannisis et al., 2022). These lipoprotein-associated lipids are made available for utilization and storage through the coordinated actions of enzymes such as lipoprotein lipase (Lpl) and low-density lipoprotein receptor (Ldlr) (Weil et al., 2013; Yan et al., 2015; Van De Sluis et al., 2017). The modulation of these transcripts suggests an adjustment in lipid efflux and utilization pathways, potentially reflecting a rebalancing of cholesterol and lipid metabolism in response to effluent.

Greenside darters demonstrated significant disruptions in lipid homeostatic processes (Figure 2.6), particularly affecting cholesterol metabolism and energy production pathways. Elevated expression of *soat1, ldlr,* and *insig1* suggests increased cholesterol uptake (*ldlr*), enhanced storage via esterification (*soat1*), and feedback inhibition of cholesterol biosynthesis (*insig1*) (Lin et al., 1999; Go & Mani, 2012; Yang et al., 2002). In parallel, the upregulation of *pnpla2*, involved in triglyceride mobilization, could reflect increased lipolysis and potentially energy production through β-oxidation (Zimmermann et al., 2004; Schweiger et al., 2006). Furthermore, the upregulation of *soat1* may serve as an adaptive mechanism, potentially esterifying lipid-soluble xenobiotic compounds to mitigate cellular stress (Dodds, 1995; Lindqvist et al., 2014).

Transcript networking in fantail darter (Figure 2.9) highlighted distinct modulation of lipid metabolism and cholesterol biosynthesis contributing to the GO enrichment of small molecule metabolic processes (Figure 2.6). The third sub-network with red edges was composed of downregulated DEGs involved in fatty acid biosynthesis (*acly, acsl4, gpat4*) and β-oxidation (*hsd17b4, echs1, acsl4*), which generate fatty acyl-CoA esters for energy production via the Krebs cycle (De Launoit & Adamski, 1999; Chypre et al., 2012; Kuwata et al, 2019). The fourth sub-network, marked by blue edges, involved downregulated DEGs which encode enzymes that catalyze sequential steps in sterol biosynthesis through the mevalonate pathway. For instance, Hmgcs1 synthesizes HMG-CoA, a key precursor further processed by enzymes in this network, including Lss, Sc5d, and Msmo1, to produce cholesterol and other sterols (Hernandez et al., 2019; Song et al., 2023; Jiang et al., 2010; Xin et al., 2019). The transcription factor Srebf2 regulates the expression of these genes, controlling cholesterol and lipid biosynthesis (Madison, 2016). This profile suggests a coordinated downregulation of fatty acid metabolism, β-oxidation, and sterol biosynthesis, reflecting a reduced capacity for lipid and energy metabolism.

Johnny darters exhibited a less pronounced response in lipid metabolism pathways compared to other species. However, transcript networking identified the opposing expression of *acaca* and *cpt1a*, along with the upregulation of *fads6*, suggesting a metabolic shift favouring lipid biosynthesis and energy storage (Liu et al., 2023; Zhang et al., 2023; Dong et al., 2024).

Lipids are the primary energy source for most fish (Watanabe, 1982), and lipid metabolism is essential for maintaining energy balance, cholesterol homeostasis, and physiological processes, particularly in the liver (Tocher, 2003; Kondo et al., 2005). Disruptions in these pathways suggest potential metabolic consequences of effluent exposure, leading to shifts in energy allocation and lipid regulation. Environmental contaminants, including PFAS, PPCPs, insecticides, and WWTPE, have been shown to alter lipid metabolism in fish (Sarma et al., 2015; Hamid et al., 2021; Sun, 2023). These disruptions are often linked to energy reallocation, oxidative stress, and lipid peroxidation (Dépatie et al., 2020; Gonçalves et al., 2021). Lipid-regulating pharmaceuticals, such as fibrates and statins present in WWTPE, may further lower plasma cholesterol and triglyceride levels while modulating genes involved in lipid metabolism and cholesterol regulation (Teles et al., 2016; Blonç et al., 2023). Statins detected downstream (Table 2.2) inhibit HMG-CoA reductase activity, a key enzyme in cholesterol biosynthesis, which may explain the downregulation of cholesterol synthesis observed in fantail darters (Sharpe & Brown, 2013). Since cholesterol is a precursor for steroid hormones, reduced cholesterol metabolism could impair hormone production, potentially affecting stress responses, reproduction, and growth (Jiang et al., 2010; Maxfield & Tabas, 2005), thereby potentially affecting population dynamics. Lipid metabolism responses varied across species. Rainbow and greenside darters exhibited increased expression in lipid transport and utilization pathways, whereas johnny darters showed enhanced lipid biosynthesis and energy storage. In contrast, fantail darters demonstrate suppression of fatty acid biosynthesis, β-oxidation, and sterol synthesis. Collectively, these findings indicate that liver lipid metabolism, central to energy homeostasis and detoxification, is highly sensitive to contaminants in effluent. The observed transcriptomic shifts suggest a broad reallocation of metabolic resources that may negatively impact growth and reproduction.

2.4.4.3 Mitochondrial Function and Broader Metabolic Activity

In response to effluent exposure, transcripts involved in the construction and function of the electron transport chain (ETC), crucial for cellular respiration and ATP production through oxidative phosphorylation (Vercellino & Sazanov, 2022), were differentially expressed in both fantail and johnny darters. Fantail darters showed extensive modulation of transcripts related to

mitochondrial organisation (Figure 2.6), particularly those responsible for ETC construction and function. This included several components of Complexes I, III, and V (Gusdon et al., 2007; Mimaki et al., 2012; Bottani et al., 2017), along with essential transport and assembly factors. For instance, the chaperone Grpel1 facilitates the folding and assembly of Complex I subunits (Konovalova et al., 2018), and the carrier protein Slc25a3 transports inorganic phosphate into mitochondria for ATP synthesis (Baseler et al., 2012). All transcripts associated with these processes were downregulated except *atp5f1a*, a hub transcript (Figure 2.9) encoding a subunit of ATP synthase (Complex V) involved in ATP production (Chouhan et al., 2023). In contrast, transcripts involved in the construction and function of ETC Complexes III, IV, and V were upregulated in johnny darter. This upregulation was evident through GO enrichment of electron transport chain and oxidative phosphorylation processes (Figure 2.6), as well as transcript network analyses identifying *mt-co3 and mt-atp6* as hub transcripts (Figure 2.10).

Pharmaceuticals and personal care products can modulate mitochondrial function and content (Yeh et al., 2017). For example, antibiotics that inhibit bacterial protein synthesis may also target mitochondrial ribosomes (Moullan, 2015), while NSAIDs like diclofenac can generate reactive metabolites that interfere with mitochondrial oxidative phosphorylation and ATP synthesis (Syed et al., 2016). Additionally, a variety of other environmental contaminants including PAHs, heavy metals, pesticides, and CEC's may similarly disrupt mitochondrial function, linked to the induction of oxidative stress (Garceau et al., 2010; Lushchak, 2016; Yeh et al., 2017; Kozal et al., 2023). Oxidative stress can damage mitochondrial DNA and proteins, reducing ETC efficiency and increasing ROS production (Shokolenko et al., 2009; Roubicek et al., 2017). This can create a detrimental feedback loop, further exacerbating oxidative damage and impairing cellular energy metabolism (Kozal et al., 2023; Otsuka & Matsui, 2023). The observed downregulation of mitochondrial transcripts in fantail darters suggests reduced ATP synthesis capacity, and is consistent with CEC-induced mitochondrial impairment, conceivably as a means to reduce the rate of ROS production. This dysfunction may contribute to proton leakage, mitochondrial dysregulation, reduced mitochondrial content, and oxidative damage (Chandel, 2010). Conversely, johnny darters exhibit a potential compensatory response to sustain mitochondrial function under effluent exposure. If the upregulation of mitochondrial electron transport chain (ETC) transcripts reflects increased mitochondrial activity, it may also result in higher electron leakage and ROS production, thereby exacerbating oxidative stress. Similar

effects have been observed in Chinook salmon exposed to a mixture of CECs representative of WWTPE (Yeh et al., 2017).

Aside from energy production through oxidative phosphorylation, glucose metabolic processes were also affected. Effluent exposure influenced glycolytic pathways in rainbow darters evidenced by GO enrichment of Glucose-6-phosphate metabolic process (Figure 2.6) and a small cluster (Figure 2.8) of upregulated transcripts (*gck, hk1, hkdc1*). These DEGs encode enzymes that catalyze the phosphorylation of glucose into glucose-6-phosphate to initiate glycolysis, a critical step in energy production, storage, and biosynthetic reactions (Irwin et al., 2008; Polakof et al., 2009; Ludvik et al., 2016). While stress and cortisol release typically promote glucose availability to peripheral organs and tissue over use in the liver, contaminants present in effluents may disrupt these tightly regulated processes (Zhao et al., 2018). Additionally, both fantail and greenside darters exhibited divergent modulation of *gpi* (Figure 2.4), which encodes glucose-6-phosphate isomerase, a key enzyme involved in glycolysis and gluconeogenesis (Achari et al., 1981). Overall, in response to effluent exposure, contrasting transcriptional responses across darter species highlight a diverse disruption of mitochondrial and glucose metabolic processes.

2.4.4.4 Protein Homeostasis and Stress Responses

Effluent exposure elicited species-specific disruptions in cellular stress responses, proteostasis, and mitochondrial integrity, with notable impacts on protein homeostasis and degradation pathways. WWTPE exposure significantly disrupted proteolysis and protein catabolic processes in fantail darters, as evidenced by GO enrichment (Figure 2.6) and the widespread downregulation of *hsp90* and *hsc70* family genes, proteasome components, and mitochondrial protein translocases. This suppression suggests a diminished capacity for protein folding, degradation, and mitochondrial import, potentially exacerbating proteotoxic stress. Heat shock proteins (HSPs) such as *hs90aa1, hsp90ab1,* and *hspa8* emerged as prominent hubs with high degree and betweenness centrality in transcript network analyses (Figure 2.9), underscoring their roles in various biological processes. HSPs are essential for regulating protein synthesis by assisting in the folding, stabilization, and degradation of diverse client proteins, including signalling molecules (Haase & Fitze, 2016). This regulatory function is critical for maintaining protein quality control, ensuring proper signalling pathway function, **a**nd enabling cellular stress responses by preserving protein conformations (Pearl & Prodromou, 2000; Liu et al., 2012b;

Haase & Fitze, 2016). Additionally, several transcripts such as *psmd14*, which contribute to the structural formation and function of the 26S proteasome complex, were significantly affected, as evidenced by a highly interconnected subcluster within the transcript network (Figure 2.9). The proteasome plays a crucial role in degrading ubiquitinated proteins, thereby maintaining protein homeostasis by removing damaged or misfolded proteins (Byrne et al., 2010).

While the stress response in fish is typically characterized by the upregulation of heat shock proteins (HSPs) (Jeyachandran et al., 2023), exposure to pharmaceuticals may impede this adaptive mechanism. For instance, ibuprofen significantly suppressed heat shock-induced hsp70 protein expression in the liver and gill of trout (Gravel et al., 2007). Similarly, chronic venlafaxine exposure attenuated the heat shock response in the gill tissue of zebrafish (Weber et al., 2023). Thus, pharmaceuticals present down steam of the WWTP effluent outfall may be inducing this response. The downregulation of HSPs indicates a diminished capacity for managing misfiled proteins and responding to cellular stress, potentially impairing cellular functions and increasing susceptibility to additional stressors. Oxidative damage can disrupt protein conformation and integrity (Haynes 2004; Pamplona, 2008), increasing the burden on the already compromised protein quality control systems. When considered alongside the downregulation of proteasome components, these findings suggest that the proteasomal degradation pathway may be compromised. This impairment could lead to the accumulation of damaged or mis-folded proteins, disruption of protein homeostasis (Hipp et al., 2019), and and potentially increased susceptibility to environmental stressors and oxidative damage.

Disruption of mitochondrial integrity in fantail darters was evident, highlighted by the downregulation of the hub transcript *phb1* and bottleneck transcript *phb*2 (Figure 2.9). These transcripts encode prohibitin, a multifunctional protein that protects against stress-induced damage by stabilizing mitochondrial proteins as a chaperone (Signorile et al., 2019). In mammals, the downregulation of PHBs has been shown to impair mitochondrial complex I activity, resulting in increased ROS production (Liu et al., 2012). Furthermore, mitochondrial protein handling appears compromised, as genes encoding key components of mitochondrial translocase complexes including *tomm22, tomm40* (TOM complex) and *timm44, timm17a* (TIM complex, were dysregulated. These complexes facilitate the trafficking of cytosolic proteins into mitochondria, and their silencing can disrupt mitochondrial protein import, resulting in impaired ATP production, increased ROS levels, mitochondrial depolarization, and hepatocyte

degeneration (Ma et al., 2023; Wu et al., 2017). Beyond mitochondrial dysfunction, transcripts such as *ccdc47* and *pdia6* exhibited dysregulation, affecting endoplasmic reticulum (ER) protein translocation and quality control mechanisms (Chitwood et al., 2020; Bai et al., 2019). The ER plays a crucial role in regulating apoptosis via redox state modulation and apoptotic protein interactions (Trostchansky & Alarcon, 2023). Collectively, the downregulation of these proteins suggests a broader impact on proteostasis and dysfunction of stress response mechanisms in fantail darters. These effects, along with the downregulation of ETC components, indicate a broad impact of WWTPE exposure on mitochondrial function in fantail darters.

Gene Ontology enrichment analysis revealed significant alterations in stress response regulation in greenside darters (figure 2.6). While *hspa8* was downregulated, consistent with observations in fantail darters, a cohort of stress-responsive genes including *ddit4* and *ulk2* were upreguated. In response to stressors such as hypoxia, DNA damage, and oxidative stress, Ddit4 actively inhibits the mTORC1 pathway, thereby restricting protein synthesis to support DNA repair and autophagy before cell division (Pastor et al., 2017; Britto et al., 2018). Similarly, *Ulk2*, a key regulator of autophagy induction, facilitates the clearance of damaged organelles and proteins during stress conditions such as starvation and cellular damage (Demeter et al., 2020). Conversely, Smcr8a which helps maintain autophagy and lysosomal activity, was down regulated (Liu et al., 2022). This gene was similarly down regulated in rainbow darters exposed to effluent. Rainbow darters displayed efforts to manage oxidative stress through upregulation of antioxidant and cytoprotective genes like *ambp*, while downregulation of autophagy-related genes such as *smcr8a* suggested a compromised capacity for cellular repair. Collectively, these findings suggest that while greenside and rainbow darters activate stress response pathways to address immediate environmental challenges, the modulation of autophagy-related genes like *smcr8a* may dysregulate long-term cellular homeostasis and repair.

In johnny darters, immediate early response pathways were modulated, highlighted by a tightly interconnected cluster (Figure 2.9) of four downregulated transcripts: *dusp1, egr1, ier2,* and *junb*, which are involved in swift cellular response to stress (Shan et al., 2019; Chung et al., 1998; Cargnello & Roux, 2011). These genes are regulated by or directly participate in MAPK signalling pathways, which orchestrate various cellular processes including growth, differentiation, apoptosis, and inflammation by transmitting extracellular signals through a

cascade of kinase activations (Wei et al., 2020). This response is typically rapidly induced by various stressors, including oxidative stress, DNA damage, and infection, enabling cells to regulate downstream targets and adapt to environmental challenges (Ueda et al., 2019; Kyjacova et al., 2021). As these genes represent early response factors, their expression may be reduced under chronic stress via negative feedback self-regulation, potentially serving to prevent overactivation and subsequent cellular damage (Stamp et al., 1999). These expression patterns suggest that effluent exposure may dysregulate certain cellular stress response pathways in johnny darters, which could make the fish more vulnerable to environmental protuberances and diseases.

2.4.4.5 Cellular Communication and Neural Activity

Neural activity and cellular communication pathways displayed species-specific responses to effluent exposure. In rainbow darters, the significant downregulation of *rnf180* and *cacng4* suggests disruptions in serotonergic and noradrenergic signalling (Kabayama et al., 2013; Moriya et al., 2015) as well as in calcium signalling (Black, 2003; You et al., 2023). In contrast, the three other darter species (greenside, johnny, and fantail) showed modulation in distinct genes more closely associated with neural growth, differentiation, and development. For instance, *dscam* was modulated in greenside darters, while *trak1* was altered in johnny darters; both genes are implicated in neuronal development and contribute directly to neuronal function by maintaining the integrity of axons and synapses (Stephenson, 2014; Yeh et al., 2012). Similarly, fantail darters exhibited changes in genes such as *btbd3* and *dpysl2,* which play critical roles in ensuring proper neuronal connectivity and adaptability through dendritic growth and axon navigation (Matsui et al., 2013; Martins−de−Souza et al., 2015).

Pharmaceuticals present in WWTPE can alter neurotransmitter concentrations, behaviour, and nervous system development in fish (McCallum et al., 2017; David et al., 2018; Li et al., 2018). Therefore, the observed modulation of neuronal signalling and development in these darter species may be influenced by pharmaceutical compounds found downstream. For example, RING finger proteins such as *rnf180* are modulated by the serotonergic system, which governs emotional and social behaviours (Kabayama et al., 2013). Chronic citalopram treatment in medaka has been shown to modulate RING finger protein expression, highlighting the potential susceptibility of these genes to antidepressants. Additionally, *cacng4 and dscam* are

modulated by the antidepressants vortioxetine and fluoxetine, respectively, in mouse models (Guidi et al., 2013; Waller et al., 2017). Hormonal and neuronal signals tightly regulate glucose, lipid, and amino acid metabolism in the liver (Rui, 2014). Consequently, effluent-driven alterations in neuronal signalling pathways could contribute to the dysregulation of metabolic processes documented in this study. Moreover, some of these neuronal genes may have additional roles in peripheral tissues beyond the nervous system. For example, *shootin1 (SHTN1)*, which was downregulated in greenside darters, is typically involved in neuronal development and axon outgrowth; however, an isoform (*shootin1b*) has been identified in peripheral non-neuronal cells and is implicated in cytoskeleton organisation (Higashiguchi et al., 2016). The species-specific changes observed in genes related to neurotransmission, neuronal development, and synaptic integrity suggest that effluent exposure may differentially impact fish populations, highlighting the need for further mechanistic studies. Understanding how pharmaceutical contaminants alter peripheral neural pathways in wild populations is essential for evaluating ecological risk and implementing effective wastewater treatment and environmental management strategies.

2.4.4.6 Environmental and Pharmaceutical Impact

The transcriptomic analysis across all four darter species revealed evidence of exposure to xenobiotic pharmaceuticals and contaminants present in WWTPE, with species-specific responses. Alongside this, effluent exposure appears to modulate xenobiotic metabolism in rainbow and fantail darters, as indicated by the differential expression of cytochrome P450 genes *cyp2k1 and cyp3a40*, respectively. Both Cyp3a40 and Cyp2k1 play significant roles in hepatic detoxification by metabolizing a variety of endogenous and exogenous compounds, including steroids and xenobiotics (Korzekwa et al., 1993; Kashiwada et al., 2005). Upregulation of *cyp2k1* in rainbow darters suggests an increased need to detoxify xenobiotics, whereas downregulation of *cyp3a40* in fantail darters potentially indicates a diminished capacity for xenobiotic biotransformation. Pharmaceuticals including fluoxetine, diazepam, and diclofenac can inhibit the cytochrome P450 system in fish (Thibaut et al., 2006; Christen et al., 2010; Pihlaja et al., 2024), which may be influencing this downregulation. Consequently, impaired detoxification processes can exacerbate pollutant toxicity and promote bioaccumulation. Variations in biotransformation capacity influence resilience in polluted habitats, with species possessing

lower detoxification capabilities potentially accumulating higher chemical burdens, diminishing fitness, and ultimately affecting biodiversity (Franco et al., 2025).

In johnny darters, the organic anion transporter Slco1a2, which mediates the influx of hormones, statins, antibiotics, antidepressants, and other endogenous and exogenous molecules, was downregulated (Cvetkovic et al., 1999; Hagenbuch & Gui, 2008). Conversely, other solute carriers including *slc38a4, slc13a5, slc25a38b, and slc9a3r1* were upregulated, contributing to the enriched GO term transmembrane transport (figure 2.6). These expression changes indicate an adjustment to reduce contaminant uptake while maintaining or enhancing the transport of amino acids, nucleotides, ions, and metabolites under effluent-induced stress (Palmieri, 2013; Schiöth et al., 2013; Fernandez-Fuente et al., 2023). Overall, these findings highlight the complexity of effluent-driven alterations in xenobiotic metabolism and transporter function within darter species.

2.4.4.7 Divergence and Shared Adaptations

All four darter species exhibited shared transcriptomic responses to WWTPE exposure, including metabolic dysregulation, immune modulation, and oxidative stress, as reflected in enriched gene ontology terms related to inflammation, lipid metabolism, and mitochondrial function. Despite these commonalities, species-specific differences emerged. Rainbow darters showed pronounced effects on lipid transport, inflammatory pathways, and glycolysis, while johnny darters exhibited altered mitochondrial electron transport chain activity, lipid peroxidation, and suppression of early response gene expression. Greenside darters experienced significant disruptions in cholesterol and immune homeostasis, potentially reflecting sensitivity to lipid-regulating pharmaceuticals. In contrast, fantail darters uniquely demonstrated extensive downregulation of ETC components, protein handling, and endomembrane protein transport, suggesting distinct compensatory mechanisms. These findings highlight both conserved and species-specific strategies for coping with environmental contaminants.

2.4.5 Unique identified pathways not captured by ontology enrichment

2.4.5.1 DNA Replication, Repair, and Transcriptional Regulation

WWTPE and PPCPs have been implicated in genotoxicity and the disruption of DNA damage repair mechanisms in fish, potentially inducing compensatory transcriptional responses to mitigate genomic stress (Liney et al., 2006, Notch & Mayer, 2009, Wilhelm et al., 2018). In response to effluent greenside darters exhibited significant modulation of genes involved in DNA replication, repair, and transcriptional regulation (Figure 2.9). Notably, the upregulation of *donson* and *ddit4*, which facilitates accurate DNA replication and repair highlight an adaptive mechanism aimed at mitigating DNA damage (Ding et al., 2021; Cvetkovic et al., 2023). Conversely, the downregulation of *top2b*, responsible for managing DNA topology during replication and transcription, suggests potential limitations in DNA maintenance (Cowell et al., 2023). Additionally, the modulation of transcription factors and regulators such as t*p53inp2, csrnp1, klf13,* and *tfcp2*, which are implicated in cell proliferation, apoptosis, and autophagy (Outram et al., 2008; Feijóo et al., 2009; Nowak & Iovanna, 2009; Kotarba et al., 2018), suggests a possible suppression of proliferative pathways alongside enhanced autophagic processes.

Collectively, these transcriptional changes suggest a shift toward prioritizing DNA integrity and cellular survival by balancing damage mitigation with the controlled regulation of cell growth and death. Furthermore, some of these transcripts were differentially expressed in other darter species, with *klf13* also upregulated in Johnny darters and *tp53inp2* down regulated in fantail darters. However apart from early response genes previously discussed, johnny darters demonstrated limited modulation of genes relevant to DNA replication, repair, or transcriptional regulation

In fantail darters, numerous DEGs enriched the gene expression GO term (Figure 2.6), encompassing transcription factors and regulators central to the biological processes investigated in this present study. For instance, *rxraa* (RXRα) regulates the expression of Cytochrome P450 (CYP) enzymes, particularly CYP3A4 (Lehmann et al., 1998; Kliewer et al., 2002), while *stat1* and *stat3*, control the transcription of genes vital to immune responses (Au-Yeung et al., 2013). Additionally, many transcripts within this enriched ontology are involved in RNA metabolism, as represented by the second cluster with yellow edges in the transcriptional network (Figure 2.9). Genes within this enriched ontology also play roles in epigenetic modifications, including DNA methylation, histone acetylation, and chromatin condensation rather than repair. In rainbow darters, alterations in histone modification and chromosomal structure were suggested by the transcriptional networking of significantly modulated genes *cenpa* and *ncapd3* (Figure 2.9). The expression patterns of these genes imply regulatory adjustments that may support chromosomal stability and modulate cell division and differentiation processes (Cech et al., 2015; Khan et al., 2019). Together, these transcriptional changes across darter species suggest a regulatory response to effluent exposure, highlighting the interplay between DNA repair, and chromatin dynamics.

2.4.5.2 Cytoskeletal and cellular remodelling

Cytoskeletal remodelling is essential for liver function, facilitating cellular movement, shape maintenance, and intracellular transport as an adaptive response to environmental changes (Fletcher & Mullins, 2010). However, chronic effluent exposure appears to disrupt these processes in greenside darters. Oxidative stress can initiate cytoskeletal remodelling both as a regulatory response and as a consequence of cellular damage (Weng et al., 2007; Balta et al., 2021). The significant downregulation of *kptn, shtn1*, and *cyth2* suggests impaired actin polymerization and reduced cytoskeletal stability, which could compromise cell adhesion and

intracellular trafficking (Frank et al., 1998; Bearer & Abraham, 1999; Higashiguchi et al., 2016). Concurrently, the upregulation of *ssh2* enhances cofilin-mediated actin depolymerization and turnover, indicating a shift from a stable cytoskeletal structure to a more dynamic or disassembled state (Moon & Drubin 1995; Niwa et al., 2002). Additionally, the upregulation of plasminogen (*plg*) implies increased plasmin activity, which is involved in liver regeneration and the prevention of fibrosis through ECM degradation and tissue remodelling (Chana et al., 2019; Huang et al., 2021). These transcriptional alterations may reflect a compensatory response to cellular stress, wherein the liver activates regenerative pathways to mitigate damage. Collectively, these findings highlight a potential vulnerability of cytoskeletal integrity in greenside darters under prolonged effluent exposure.

2.4.5.3 Up-Regulation of hemoglobin complex genes

Upregulated expression of *hba* and *hbb* (Figure 2.9), genes encoding hemoglobin (Hb) subunits, suggests a potential adaptive response to oxidative stress in the liver of greenside darters downstream of the effluent outfall. In teleosts, hemoglobin expression can be influenced by hypoxia, ammonia, and high pCO_2, as well as physiological stressors like infection and oxidative stress, though these responses are species- and tissue-specific (Xu et al., 2021; Kang et al., 2022; Wang et al., 2023). Although Hb is typically expressed at low levels in liver tissue (Wang et al. 2023), Hb expression in the liver may contribute to redox balance by scavenging ROS through peroxidases-like activity (Widmer et al., 2010; Liu et al, 2011). Unlike true peroxidases however, Hb undergoes self-inflicted damage during this process (Alayash & Wilson, 2022), which may influence gene expression modulation though replenishment of lost Hb. Whether this response is primarily driven by oxidative stress, hypoxia, or other factors remains unclear, but it aligns with indications of environmental stress downstream of the effluent and may represent an adaptive strategy in greenside darters.

2.4.6 Species specific orthogroups

Comparative analysis of species-specific orthogroups in rainbow, fantail, johnny, and greenside darters revealed both shared and unique enriched ontologies, potentially representing novel isoforms, lowly expressed transcripts, or condition-specific responses (Figure 2.4; Table A1.3). In rainbow darter, enrichment for neuronal processes, cell junction and adhesion suggests

involvement in intrahepatic nerve innervation and neural maintenance (Tsuneki & Ichihara, 1981; Esteban et al., 1998; Miller et al., 2021). In teleost fish, the liver is innervated by nerve fibres analogous to the mammalian autonomic nervous system, which help regulate energy balance and metabolism (Blanco et al., 2020; Miller & Goessling, 2024). Elevated concentrations of the neuroactive SNRI venlafaxine downstream may disproportionately affect this species if it is especially sensitive to neuronal perturbations. Fantail darter specific orthogroups were enriched for terms related to membrane dynamics, cellular transport, and the endomembrane system, which facilitates in the metabolism, synthesis, and transport of lipids and proteins, as well as the detoxification of exogenous contaminants (Levine 2004, De Caroli et al., 2020). Enrichment of muscle system processes may reflect increased locomotive demands unique to this species, which prefer slow to moderately moving waters (Eakins, 2024). If these fish were subjected to suboptimal, faster-moving waters during collection, it might triggered higher expression of muscle-related genes to cope with enhanced physical demands. Meanwhile, johnny darter orthogroups were enriched for terms associated with intracellular trafficking, extracellular vesicle-mediated transport, and membrane organisation, suggesting a functional emphasis on cell-to-cell communication and structural maintenance (van Niel et al., 2022). Finally, greenside darter orthogroups were enriched for terms for neurone projection, cell periphery, and multicellular development parallels ontologies in rainbow and fantail darters, although driven by distinct transcripts. Enrichment for terms associated with cell adhesion, ECM remodelling, and apoptotic regulation suggests additional roles in tissue integrity and liver regeneration (Merino-Casallo et al., 2022). Notably, processes involving ECM organisation and cellular remodelling are uniquely represented among the DEGs identified in this species.

2.5 Conclusion

In this study, a transcriptomic analysis of four darter species provided critical insights into the molecular and cellular mechanisms by which these fishes respond to WWTPE exposure. Water quality assessments revealed elevated pharmaceutical concentrations downstream, including VEN and DCF, which align with previous findings of pharmaceutical presence in WWTPE-impacted aquatic environments (Arlos et al., 2015). However, atrazine was higher in the upstream sampling sites (Table 2.2). Atrazine is a pervasive herbicide that has been linked to endocrine disruption and reproductive effects in fish, including altered hormone levels, impaired

gametogenesis, and feminization of males (Solomon et al., 1996). Thus, the presence of this herbicide may be a confounding factor in this work, potentially influencing the observed gene expression patterns. Nevertheless, the nearly universal modulation of immune response, lipid metabolism, mitochondrial function, oxidative stress management, and detoxification pathways indicates common environmental pressures imposed by WWTPE across species.

Variations in mitochondrial resilience, detoxification capacity, and specific metabolic adjustments highlight species-specific vulnerabilities and adaptive strategies. Rainbow darters exhibited significant alterations in lipid metabolism, characterized by lipid utilization and storage mechanisms, along with modulation of inflammatory pathways. ETC components were not differentially expressed; however, glycolytic pathways were upregulated, suggesting a compensatory enhancement of glycolysis. This species demonstrated increased expression of antioxidant defences and a potential elevated capacity for xenobiotic detoxification, mediated by the upregulation of *cyp2k1*. Fantail darters exhibited possible impairments in mitochondrial function, evidenced by reduced expression of ETC and mitochondrial support genes, which may adversely affected energy production and ROS defence. Diminished capacity for protein management appears to be extensive, and may lead to increased proteotoxic stress. Additionally, lipid synthesis and cholesterol production process appear to be suppressed. Unlike rainbow darters, fantail darters may have a decreased detoxification capacity due to the downregulation of *cyp3a40*, which could facilitate the bioaccumulation of contaminants. Johnny darters demonstrated an upregulation of ETC components, suggesting compensatory mechanisms to meet elevated energy demands induced by effluent exposure. Despite this, effluent may compromise fatty acid oxidation. Additionally, johnny darters exhibited a diminished expression of early stress response genes, presumably resulting from chronic stress exposure, which may increase their vulnerability to environmental stressors. Transporter expression may be adjusted to manage contaminant uptake, indicating an adaptive response to reduce xenobiotic influx. Greenside darters exhibited significant modulation in cholesterol uptake and energy production, alongside a complex interplay between immune activation and attenuation. Mitochondrial activity was minimally affected, however protein quality control and autophagy processes appear to be affected, albeit to a lesser extent compared to fantail darters. Upregulated hemoglobin complex genes may be associated with elevated ROS, while unique pathways in DNA repair and ECM remodelling correlate with adaptive repair mechanisms. These results enhance our understanding of how ecologically sensitive, non-model fish species manage emerging pollutants

in WWTPE. Moreover, they propose targeted molecular pathways for ecological monitoring and highlight the importance of including multiple fish species in ecotoxicological studies, as species-specific responses reveal that fish do not respond uniformly to effluent exposure

Chapter 3

Transcriptional effects of acute and sub-chronic venlafaxine enantiomer exposure on rainbow darter (*Etheostoma caeruleum*), in comparison to environmental effluent exposure

3.0 Introduction

Analyzing the effects of wastewater treatment plant effluent (WWTPE) presents significant challenges as it contains a complex mixture of pollutants, which can vary greatly over time and between sources (Metcalfe et al., 2010, Kot-Wasik et al., 2016, McCann, 2016). This complexity impedes the identification of individual contaminants and hinders the understanding of their specific effects. Additionally, environmental assessments of wastewater effluent are often complicated by confounding factors such as temperature fluctuations, variable flow rates, seasonal changes in water chemistry, solar radiation, and daylight variation (Metcalfe et al., 2010; Kot-Wasik et al., 2016; Rodriguez-Mozaz et al., 2020). These factors, combined with the presence of multiple interacting substances, obscure the relationships between specific pollutants and their impacts, complicating the development of accurate and effective mitigation strategies (Metcalfe et al., 2010). While quantitative techniques like liquid chromatography-mass spectrometry (LC-MS) can identify contaminants and elucidate potential impact drivers, targeted studies on individual pollutants are essential for accurately determining their distinct effects.

As discussed in Chapter Two, venlafaxine (VEN) is identified as one of the most prevalent pharmaceutically active compounds (PhACs) downstream of the Waterloo Municipal MWWTPE outfall (Table 2.2). This observation is consistent with broader findings across North America, where elevated levels of VEN are commonly detected in receiving water (Schultz et al., 2010, Writer et al., 2013, Koné et al., 2013). VEN is serotonin and norepinephrine reuptake inhibitor, administered as a racemic 50:50 mixture of the R- and S-enantiomer. Each enantiomer demonstrates varying capacities to inhibit serotonin and norepinephrine reuptake (Hancu et al., 2021), bioaccumulate in fish (Jin et al., 2023), and undergo wastewater remediation (Barbara, 2012; Li et al., 2013; Ma et al., 2020). VEN exposure has been implicated in various adverse effects, including maladaptive behaviour (Tang et al., 2022), endocrine disruption affecting growth (Thompson & Vijayan, 2021), altered brain serotonin levels (Bisesi et al., 2014), impaired reproductive capabilities (Galus et al., 2013), and oxidative damage (Alves et al., 2023). However, few studies have investigates the individual effects of the the R- and S-enantiomers in fish, particularly in the context of systemic impacts rather than targeted markers of stress (Qu et al., 2019, Ribeiro et al., 2022). Addressing this gap is critical to understanding the stereoselective effects of VEN in aquatic organisms and their potential contributions to functional dysregulation in wild populations.

3.0.1 Objectives and hypothesis

This study aims to elucidate the distinct effects of R- and S-enantiomers of VEN on hepatic gene expression in rainbow darters (*Etheostoma caeruleum*). By analyzing each enantiomer independently, this research seeks to clarify their roles in mediating biological responses in an environmentally relevant context. We hypothesize that exposure to environmentally relevant concentrations of VEN will induce hepatic transcriptomic perturbations similar to those observed in effluent-exposed populations, with each enantiomer eliciting distinct transcriptional responses. These differences are anticipated to elucidate enantiomer-specific mechanisms of VEN toxicity and their contributions to hepatic functional dysregulation. The rainbow darter was selected as a model species due to its role as a sentinel fish in Southern Ontario, with well-established populations in the Grand River (Hicks & Servos, 2017). Rainbow darters have demonstrated sensitivity to effluent exposure and are well-suited for controlled laboratory research, as evidenced by their extensive use in captive studies (Fuzzen et al., 2016; Oliveira et al., 2021; Borowiec et al., 2024). Whole transcriptome sequencing and differential gene expression analysis were performed on hepatic tissue to maintain consistency with Chapter 2. These findings will help clarify how VEN exposure contributes to functional dysregulation patterns observed in WWTPE-exposed wild populations.

3.2 Materials and methods

3.2.1 Fish collection and handling

In October 2022, adult male rainbow darters (RBD) were collected from the Grand River near Grand Valley, Southwestern Ontario(43°56'32.6"N 80°19'32.8"W), through backpack electrofishing (Smith Root, LR-20, LR-24) (Figure 3.1). The collection site was selected due to its greater distance from the Waterloo WWTPE outfall, minimizing potential contaminant exposure. Additionally, its accessibility facilitated effective sampling. Fish were transported alive in aerated water tanks to the Waterloo Aquatic Threats in Environmental Research (WATER) facility at the University of Waterloo, Ontario, where they were acclimated in individual 10 L acrylic tanks in an Aquatic Habitats (AHAB) unit. The system was maintained at 18 °C comparable to the Grand River temperature at the time of collection. Water was replaced at a rate of 10% per day, and fish were maintained under a 12-hour light/dark cycle. Fish were fed to

satiation twice daily with San Francisco Bay Brand frozen bloodworms (Newark, USA), with feeding sustained both before and throughout the exposure period. PVC housing structures were incorporated into each tank to enhance habitat complexity, offering fish both shelter and resting surfaces. Prior to experimentation, fish underwent a two-week acclimation period in the laboratory to facilitate contaminant depuration.

3.2.2 Venlafaxine exposure

Fish were transferred to 12 L glass aquaria within a large water trough containing nine aerated aquaria, with six fish per tank (Figure 3.1). The same handling and feeding practices were followed as described in section 3.2.1. Each experimental tank was maintained at 18 °C through a continuous cold-water current generated by a chiller and two air pumps placed within a surrounding circulating water trough. Non-transparent dividers were placed between experimental tanks to prevent visual and physical interactions between fish in adjacent tanks. Fish were acclimated to the experimental tanks for three days prior to exposure and were fed once daily throughout the study. Tanks were assigned to one of three treatment groups: control, R-Venlafaxine (R-VEN), or S-Venlafaxine (S-VEN). The R-VEN and S-VEN treatment groups were exposed to 1 μg/L of the respective enantiomer of venlafaxine (Millipore- Sigma-Aldrich) which was maintained to replacement levels following 10% water replacement 1 hour after feeding. The control tanks did not receive VEN treatment. Water samples were collected to ensure a consistent concentration of venlafaxine exposure 1 hour after VEN replacement. Samples were preserved (1 g/L sodium azide; 50 mg/L ascorbic acid) in 125 mL amber glass bottles and stored at -20 °C until further extraction and analysis through LC-MS/MS using an Agilent 1200 HPLC (Mississauga, Canada) coupled to an Applied Biosystems 3200 QTRAPmass spectrometer (ABSciex, Concord, Canada). To establish a pre-exposure baseline, fish (n=6) from a randomly selected tank per trough were sacrificed, and liver tissues were flash-frozen in liquid nitrogen and stored at -80°C for later RNA extraction. Liver tissue (n=6) was sampled post-exposure on days one, four, and fourteen, and similarly preserved for analysis. Due to experimental constraints, only samples from the control, and day fourteen exposure were processed for library preparation and used in the differential expression analysis. Animal handling and collection was approved by the Animal Care Committee at the University of

Waterloo under AUPP#40318 and following the guidelines set by the Canadian Council of Animal Care. control

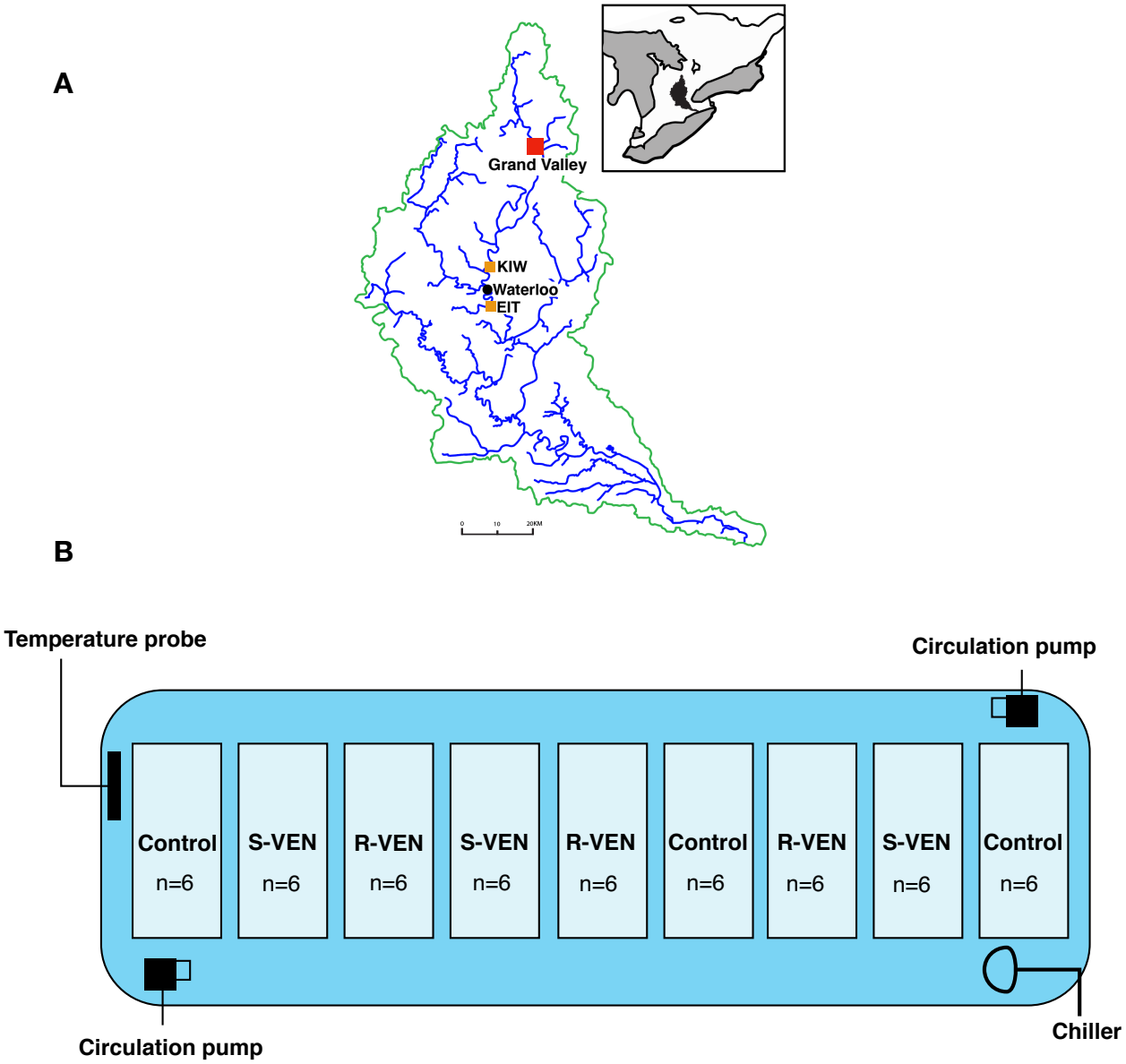


Figure 3.1: (A) Map of the Grand River Watershed illustrating fish collection site near Grand Valley, Southwestern Ontario (red), relative to Waterloo and previous sampling sites from Chapter 2 (orange) (Google Maps; Map data ©2024, CNES/Airbus, Landsat, Copernicus, Maxar Technologies). (B) Schematic of R- and S-venlafaxine (VEN) exposure demonstrating experimental design for one of three troughs.

3.2.3 RNA Processing and Sequencing

The processing of fish tissue was conducted following the protocols established in Chapter 2 (Section 2.2.4). To isolate RNA, liver tissue was processed using a phenol-chloroform extraction with QIAzol (Qiagen; Hilden, Germany), as per the manufacturer's protocol by Qiagen. This involved homogenizing the tissue, separating nucleic acids with chloroform, and precipitating RNA with isopropanol. RNA quality was assessed using an Agilent 2200 Tapestation (Agilent Technologies; Santa Clara, CA), with samples achieving a RIN of at least 8, deemed to be of high quality. These samples were sent to The Center for Applied Genomics (TCAG, Toronto, Canada) for library preparation and sequencing. The NEBNext Ultra II Directional RNA Library Prep Kit was used for multiplex library preparation, and sequencing was performed on an Illumina NovaSeq 6000 System with an S4 chip (Illumina; San Diego, CA), generating over 50 million 150bp paired-end reads per sample.

3.2.4 Transcriptome Assembly

Quality control and *de novo* assembly of RNA-Seq data from Control (n=6), R-Ven (n=6), and S-Ven (n=6) Day 14 exposure groups was conducted to construct a single rainbow darter transcriptome. For this, raw paired-end reads were first processed using Trimmomatic (v0.36) (Bolger et al. 2014) to remove low-quality sequences and adapters, with subsequent quality assessments performed using FastQC (v0.11.9) and MultiQC (v1.13) (Andrews, 2010; Ewels et al, 2016). High-quality reads were assembled *de novo* using Trinity (v2.13.2) (Haas et al., 2013) on servers provided by Google Cloud (Google LLC, 2023), with the assembly performed using default parameters. Reads were aligned to the assembly using Bowtie2 (v2.2.7) (Langmead and Salzberg, 2012), and gene-level abundance was estimated using RSEM (v1.3.1) normalized as fragments per kilobase of transcript per million mapped reads (FPKM) (Li and Dewey, 2011). To assess transcriptional variation among sample replicates, principal component analysis (PCA) was performed on $\log_2$-transformed transcript counts for the top 500 most variable transcripts with the scikit-learn library in Python. Assembly quality was assessed using metrics such as N50, E90N50, and contig length, while completeness was evaluated using BUSCO comparing single-copy orthologs against multiple databases (Eukaryota, Metazoa, Vertebrata, Actinopterygii). Initial annotation was performed with DIAMOND (v2.0.13)

(Buchfink et al., 2021) using BLASTx against UniProtKB/Swiss-Prot (e-value ≤ 1×10^{-6}), retaining only the longest sequence for alignments with >80% identity to reduce redundancy.

3.2.5 Differential expression and functional annotation

Following Chapter 2 protocols (2.2.5.2), candidate coding domain sequences were extracted from the VEN-exposed rainbow darter transcriptome using TransDecoder v5.5.0 by identifying open reading frames (ORFs) of at least 100 peptides. Transcripts were then re-annotated using DIAMOND v2.0.13 against the UniProtKB/Swiss-Prot database with a more strict e-value cutoff of 1e-20 and a single target hit, ensuring high-quality non redundant sequence identification (unigenes). Transcripts with >50% similarity to viral, bacterial, parasitic, or fungal genes were removed to maintain dataset integrity. As described in the previous section (3.2.3), transcriptome coverage and completeness were initially assessed through sample sequence to transcriptome mapping and abundance estimation through Bowtie2 (v 2.2.7) and RSEM (v1.3.1) respectively (Li, Dewey, 2011; Langmead, Salzberg, 2012). This process also serves as the preliminary step for differential expression analysis. Gene-level abundance was quantified using the trinity read contig clusters as a gene proxy. Differential expression analysis was performed using edgeR in Bioconductor (v3.14) with TMM normalization, identifying DEGs with a minimum fold change of two and an FDR < 0.05 (Robinson et al., 2010). Hierarchical clustering with a cutoff at 60% further validated sample integrity, serving as a check for sample preparation errors or other potential experimental biases. Additional annotation was conducted using Trinotate v3.2.2 (Bryant et al., 2017), which integrated domain predictions from HMMER (v2.0), SignalP (v5.0), tmHMM (v2.0), and rRNA detection via RNAmmer (v1.2) into an SQLite database, with visualization supported by TrinotateWeb (Almagro et al., 2019; Krogh et al., 2001; Sonnhammer et al., 1998; Lagesen et al., 2007). Finally, gene IDs for DEGs were standardized using DAVID (Sherman et al., 2021; Huang et al., 2009), and overlapping DEGs between exposure groups were visualized as a matrix plot.

3.2.6 Orthology Comparison

Unigenes containing ORFs were analysed using OrthoFinder v2.5.5 (Emms & Kelly, 2019) to assign them to established orthogroups form Chapter 2. These orthogroups incorporated proteomes from five related Percidae species: *Etheostoma cragini* (Arkansas darter; Taxonomy ID: 41792), *E. spectabile* (orangethroat darter; Taxonomy ID: 54343), *Perca flavescens* (yellow

perch; Taxonomy ID: 8167), *P. fluviatilis* (European perch; Taxonomy ID: 8168), and *Sander lucioperca* (pikeperch; Taxonomy ID: 283035), sourced from NCBI, alongside transcriptomes from rainbow, fantail, johnny, and greenside darters described in the previous chapter. The analysis identified conserved and divergent ortholog expression patterns across species, reduced redundant gene identifier assignments, flagged orthologs absent in the UniProt database, and highlighted unique expression profiles in venlafaxine-exposed rainbow darter. Orthogroups were visualized using InteractiVenn (Heberle et al., 2015) to generate Venn diagrams comparing orthogroups from transcriptomes assembled from venlafaxine-exposed rainbow darters (VEN-RBD), environmental effluent-exposed rainbow darters (ENV-RBD), and from fantail, johnny, and greenside darters. A phylogenetic tree was constructed using Orthofinder results and visualized in Dendroscope (v3.0) (Huson & Scornavacca, 2012).

3.2.6.1 Retrospective Contaminant Identification Trough OrthoFinder

OrthoFinder analysis revealed an unexpected abundance of assembly-specific orthogroups in the VEN-RBD transcriptome. To investigate this, transcripts within these orthogroups were aligned to the NCBI non-redundant database using DIAMOND v 2.0.13 BLASTx (e-value ≤1e-20) (Schoch et al., 2020; Sayers et al, 2022). Sequences exhibiting higher sequence identity to parasitic Platyhelminthes taxa (e.g., Nematoda, *Heterobilharzia* spp.) or Cnidaria (e.g. *Paramuricea* sp.) than Teleostei, were identified and presumed to originate from undetected infections in wild-caught specimens. Instead of immediately excising these potentially spurious sequences, based on sequence similarity alone, other factors such as biological relevance and phylogenetic inference needed to be considered. Therefore *Heterobilharzia americana* (txid39320), was added to the initial run of OrthoFinder, as this pipeline already employs tools like the multiple sequence alignment program MAFFT, and FastTree to more confidently defined orthology compared to sequence similarity alone. A subset of sequences was curated from orthogroups assigned exclusively to the VEN-RBD assembly and *H. americana* proteome. The corresponding sequences from these groups were then aligned with DIAMOND v 2.0.13 BLASTx against Teleostei (txid32443), *Heterobilharzia americana* (txid39320), and Cnidaria (txid6073). Queries showing ≥85% identity with an e-value ≤1e-60 to *Heterobilharzia americana* (txid39320) or the taxa Cnidaria (txid6073) and less than 50% identity (e-value >1e-20) to any teleost (taxid:32443) conformed this contamination. The pipeline outlined in section 3.2.4 was then subsequently re-executed after removal of transcripts

showing 50% or higher similarity to Platyhelminthes and Cnidaria. The filtered dataset was re-analysed with OrthoFinder to confirm resolution of anomalous orthogroups, conferring the integrity of our refined assembly.

3.2.7 Gene Ontology Enrichment and Pathway Network Analysis

Gene Ontology (GO) terms were assigned using Trinotate (v 3.2.2) through transcript homology to the Swiss-Prot database and assigned corresponding GO terms from TrEMBL/SwissProt. GO enrichment analysis was conducted on DEGs using GOseq (Young, 2010), with a threshold FDR of 0.05. The most significant GO categories, based on FDR and sorted by the number of genes assigned, were visualized in a lollipop bar graph for each treatment in R (v4.2.1; R Core Team, 2022). Additionally, DEGs and GO assignments were imported into Cytoscape (v3.9.1) (Lotia et al., 2013) to visualize shared DEGs across enriched GO categories. To assess transcriptome completeness, GO term assignments were compared between the VEN-RBD transcriptome and the transcriptome assembled from the liver of rainbow darter collected from the Grand River in Chapter 2 (ENV-RBD). To assess whether significant functional differences existed between VEN-RBD and ENV-RBD assembly-specific transcripts, a separate GO enrichment analysis was conducted using topGO v2.55 (Alexa & Rahnenfuhrer, 2023) within the Bioconductor framework (v3.14; Gentleman et al., 2004). The analysis employed Fisher's exact test and the weight01 algorithm, which incorporates the topology of GO term hierarchies to adjust for dependencies between terms. Additionally, protein-protein interaction networks were generated via STRING (Szklarczyk et al., 2021) linking transcripts based on functional interactions reported for humans with presumed orthologous functions in *Danio rerio* (medium confidence score: 0.4). Networks were clustered using the Markov Cluster Algorithm (MCL; inflation=2) to identify functionally related transcript groups, and orphan nodes were removed for clarity.

3.3 Results

3.3.1 RNA Integrity: Quality Control and Sequencing Analysis

The RNA samples exhibited high integrity, with a mean RIN of 9.23±1.08; all samples exceeded a RIN of 8 except for S14C3 (S-VEN exposure group), which had a RIN of 6.1 (Table

A2.1). Sequencing generated approximately 1.11 billion paired-end reads, each displaying consistent mean Phred scores (34–38) across their full lengths and a per-base N content below 0.001%. All data generated has been uploaded to the NCBI GEO database repository (GSE292719). After quality control, including trimming and adapter removal, an average of 89.78±0.39% of reads were retained, maintaining lengths between 147 and 150bp (Table A2.1).. FastQC analysis, aggregated via MultiQC, confirmed the complete removal of adapter sequences and the preservation of read integrity Duplicate read estimates remained similar before (79.2–83.4%) and after trimming (78.7–82.8%), with less than 1% of reads classified as overrepresented. *De novo* assembly using Trinity produced 459,492 contigs (transcripts) corresponding to 302,933 Trinity "genes". The assembly achieved a contig N50 of 2,092bp, with median and average contig lengths of 448bp and 991.81bp, respectively (Table 3.1). The E90N50 statistic was 2,519bp, indicating that the transcripts representing 90% of the total normalized expression had an N50 of 2,519bp (Figure A2.1). An initial evaluation of the assembly revealed an average sequence self-alignment of 89.7±0.35%. BUSCO searches of eukaryota, metazoa, vertebrata, and actinopterygii with these unigenes revealed that between 65.2-73.7% were recovered completely, with 24.7-26.3% duplicates, 0%-2.4% fragmented, and 0%-7.5% missing (Figure 3.2). These metrics were graphically compared with the BUSCO results from the ENV-RBD transcriptome (Chapter 2).

Table 3.1: Summary of *de novo* transcriptome assembly and quality metrics for rainbow darter (*Etheostoma caeruleum*) exposed to venlafaxine, including controls (n=12). Quality metrics, including raw and filtered read counts, total assembled bases, transcript and unigene counts, contig N50 values, and alignment statistics. Average self alignment is expressed as mean ± SD

	VEN Exposed Rainbow Darter (18)
Raw read pairs	1,114,764,007
Retained filtered read pairs	1,074,603,403
Assembled bases (bp)	455,730,968
Transcripts	459,492
Trinity “Genes"	302,933
Trinity "Genes" with ORFs	129,744
Uni-genes	47,083
Contig N50 (bp)	2,092
E90N50 (bp)	2,519
Median contig length (bp)	448
Average contig length (bp)	991.81
Avg. self alignment (%) (StDev)	89.7% (±0.35%)
ORF genes annotated	15,948

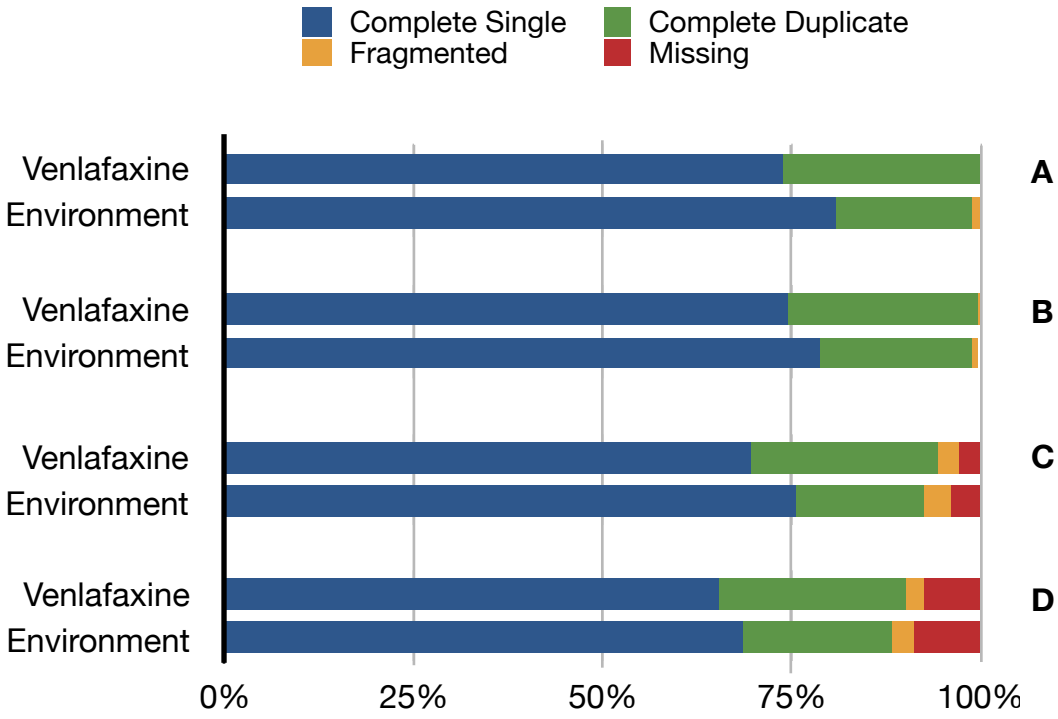


Figure 3.2: Cumulative percentage of single-copy orthologs identified in rainbow darter transcriptomes using BUSCO analysis. Orthologs were assessed against unigene sequences from four databases: (A) Eukaryota (255), (B) Metazoa (954), (C) Vertebrata (3,354), and (D) Actinopterygii (3,640). Transcriptomes were derived from rainbow darters exposed to venlafaxine and their controls (Venlafaxine) and from a wild population collected upstream and downstream of the Waterloo MWWTP effluent outfall (Environment, Chapter 2). Orthologs are classified as complete single-copy (blue), duplicated (green), fragmented (yellow), or missing (red).

3.3.2 Functional Annotation and Differential expression

TransDecoder, identified candidate coding regions in 129,744 of the 302,933 Trinity 'genes'. Following alignment of the trinity 'genes' and ORF-containing subset against the UniprotKB/Swiss-Prot database, 112,756 (37%) trinity 'genes' were annotated, and 93,362 (72%) of the 129,744 trinity 'genes' with ORFs were annotated. Following the exclusion of viral, bacterial, parasitic, and fungal transcripts and retention of only the top non-redundant alignments, 47,083 unigenes were retained. Of these, 22,079 were robustly annotated under stringent alignment criteria, with 15,948 representing unique protein-coding genes containing ORFs (Table 3.1)

Differential expression analysis identified 26 DEGs in the R-VEN group, with ten genes upregulated and 16 downregulated, and 25 DEGs in the S-VEN group, including 17 upregulated and eight downregulated (Table 3.2; Figure A2.3). A direct comparison of the R-VEN and S-VEN groups revealed 33DEGs, among which 17 exhibited positive log-fold changes, indicating higher expression in the R-VEN group, while 16 displayed negative log-fold changes, reflecting elevated expression in the S-VEN group (Table 3.2). A comprehensive list of annotated DEGs is provided in Appendix B (Table A2.2).

Table 3.2: Total number of significantly differentially expressed genes (DEGs; log2FC < -1 or >1, FDR < 0.05) identified in R-venlafaxine (R-VEN), S-venlafaxine (S-VEN), and between treatments (R/S-VEN) after 14 days of exposure. DEGs are categorized as upregulated (Up) or downregulated (Down). Average log fold change (Avg. log2FC) is reported as mean ± SD.

Exposure	Total	Up	Down	Avg. log2FC
R-VEN	26	10	16	-1.22 ± 8.84
S-VEN	25	17	8	2.461 ± 8.77
R/S-VEN	33	17	16	0.261 ± 9.06

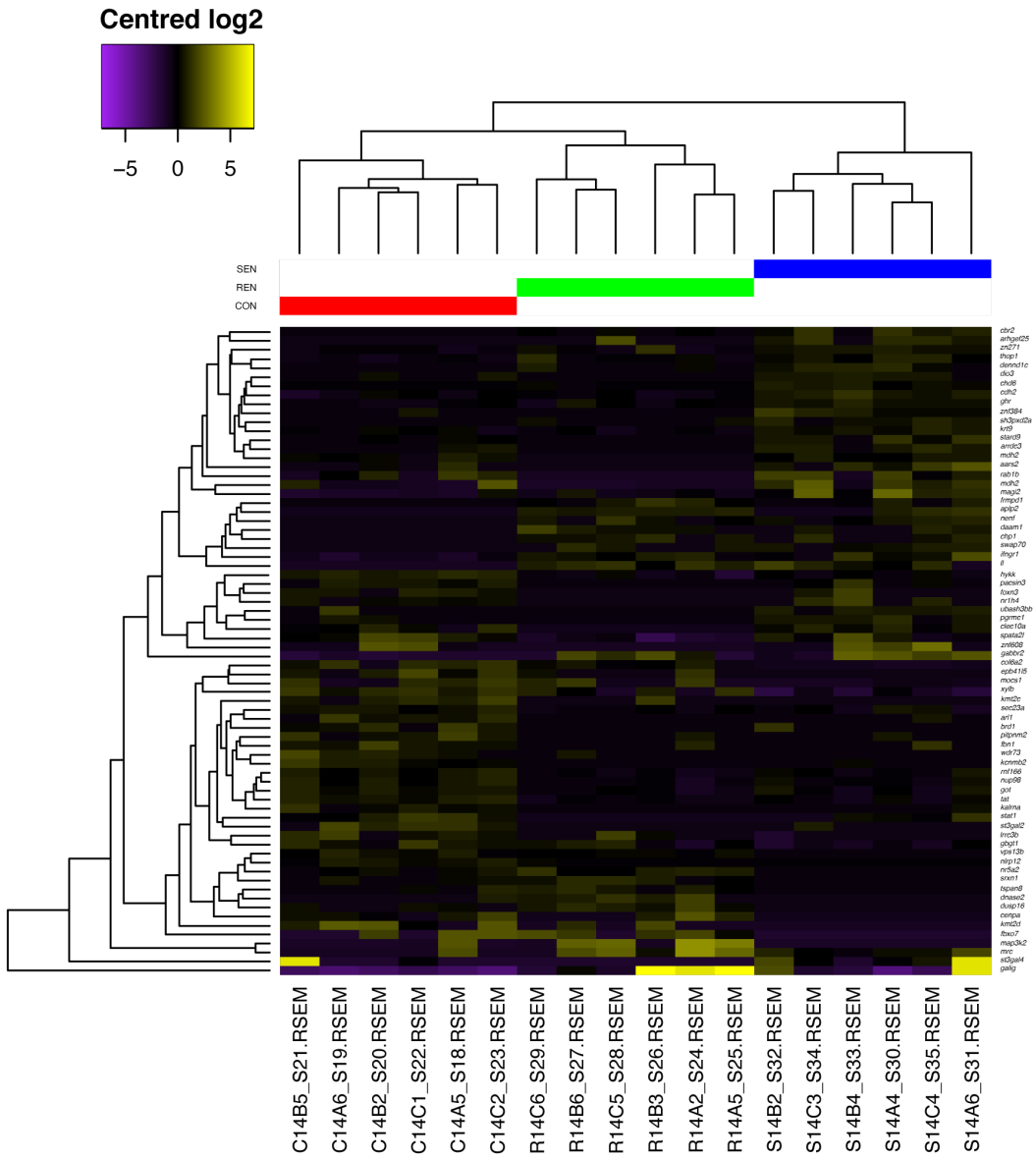


Figure 3.3: Heat map showing expression levels of 78 differentially expressed transcripts (log2FC < -1 or >1, FDR < 0.05, n = 6) in rainbow darter exposed to either R-venlafaxine (REN; green) or S-venlafaxine (SEN; blue), or control conditions (CON; red) for fourteen days. Expression values represent log2-transformed, median-centered FPKM. Yellow and purple intensities indicate transcript upregulation and downregulation, respectively. Dendrogram clustering on the X-axis reflects sample similarity, while clustering on the Y-axis groups transcripts with similar expression patterns

Differential gene expression analysis revealed distinct transcriptional profiles among treatment groups (Figure 3.3). In the R-VEN treatment group, presumed orthologs of *gabbr2*, Ladderlectin (*ll*), and *aplp2* were the most upregulated relative to controls, whereas *st3gal2* and *stat1* were substantially downregulated. Additional DEGs, including *kalrna*, *mrc2*, and *foxn3*, exhibited some of the most significant differential expression. Compared to S-VEN, R-VEN showed significant upregulation of *srxn1* while s*lc35b1* had the highest overall expression in this comparison. Moreover, *foxn3, pacsin3,* and *ifngr1* were similarly modulated in both R-VEN relative to control and S-VEN (Figure 3.4). In the S-VEN group, a presumed ortholog of *znf608* displayed the highest and most significant differential expression, while *kmt2d* and *kmt2c* were notably down regulated. Compared to ENV-RBD, *cenpa* was downregulated in S-VEN, while *cdh2* was upregulated. *nlrp12* exhibited lower expression in S-VEN and was also downregulated in ENV-RBD. Additionally, *gabbr2* and *ll* were upregulated in both R-VEN and S-VEN.

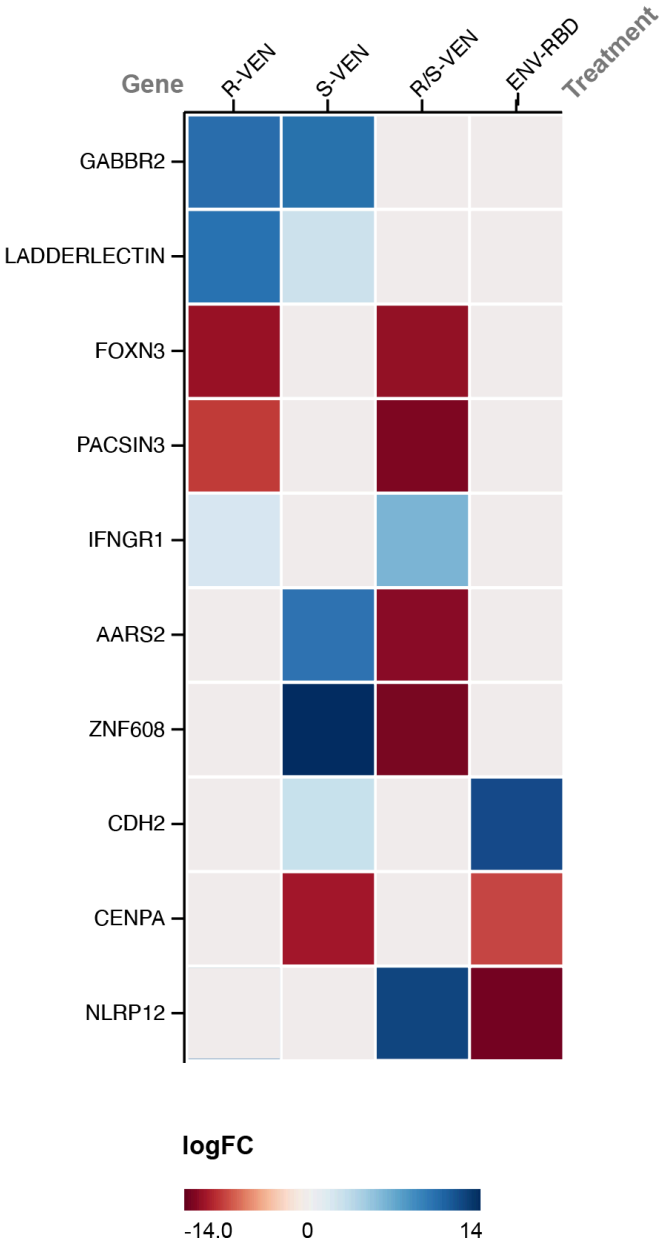


Figure 3.4: Matrix plot illustrating conserved and divergent transcript expression of significantly differentially expressed genes (DEGs; log2FC < -1 or >1, FDR < 0.05) identified in R-venlafaxine (R-VEN), S-venlafaxine (S-VEN), between treatments (R/S-VEN) after 14 days of exposure, and effluent exposure (ENV-RBD, Chapter 2). DEGs are colour-coded based on log fold change (log2FC), with blue indicating upregulation and red indicating downregulation.

3.3.3 Orthogroups

During the initial orthogroup assignment, VEN-RBD exhibited a high degree of divergence (7.2%) compared to the other assemblies, with the resulting phylogenetic tree positioning VEN-RBD as the earliest−diverging branch within the Etheostomatinae clade (Figure A2.4). Subsequent alignment of the assembly-specific orthogroups (ASOs) to the NCBI non-redundant protein database revealed high homology to sequences from Platyhelminthes (e.g., *Heterobilharzia americana*) and Cnidaria (e.g., *Paramuricea clavata*), suggesting that some ASOs may have arisen from a parasitic infection in the fish samples (Schoch et al., 2020). Integration of *H. americana* into the preliminary OrthoFinder dataset and the single-copy orthogroup tree positioned *H. americana* within the ingroup, sharing a common node with VEN-RBD. Notably, nearly 30% of the initially defined VEN-RBD ASOs were exclusively shared with *H. americana*. These sequences exhibited greater than 86% identity (e-value < 1e-150) to *H. americana*, with the next closest matches found in *P. clavata*, whereas their best matches to any teleost species showed less than 50% homology (e-value > 1e-20).

Following the exclusion of transcripts exhibiting ≥50% similarity to Platyhelminthes and Cnidaria, 2,392 transcripts were removed, resulting in 264,114 unigenes categorized into 32,362 orthogroups. Approximately 91.4% of unigenes were assigned to an orthogroup, with 34% (11,173 orthogroups) shared across all four species, indicating substantial overlap among assemblies. Additionally, 66% of orthogroups were shared between VEN-RBD and ENV-RBD (Figure 3.4). Unique orthogroups were limited, accounting for 1–2.3% of total orthogroups per species (314–736 transcripts) and exhibited greater homology to teleosts than to other taxa. The species tree, based on single-copy orthogroups generated by OrthoFinder, clearly delineated subfamily separations (Figure 3.5). Within Etheostomatinae, species formed a single clade with two distinct groupings, with VEN-RBD and *Etheostoma caeruleum* (ENV-RBD) sharing a common node and forming a well-supported subclade.

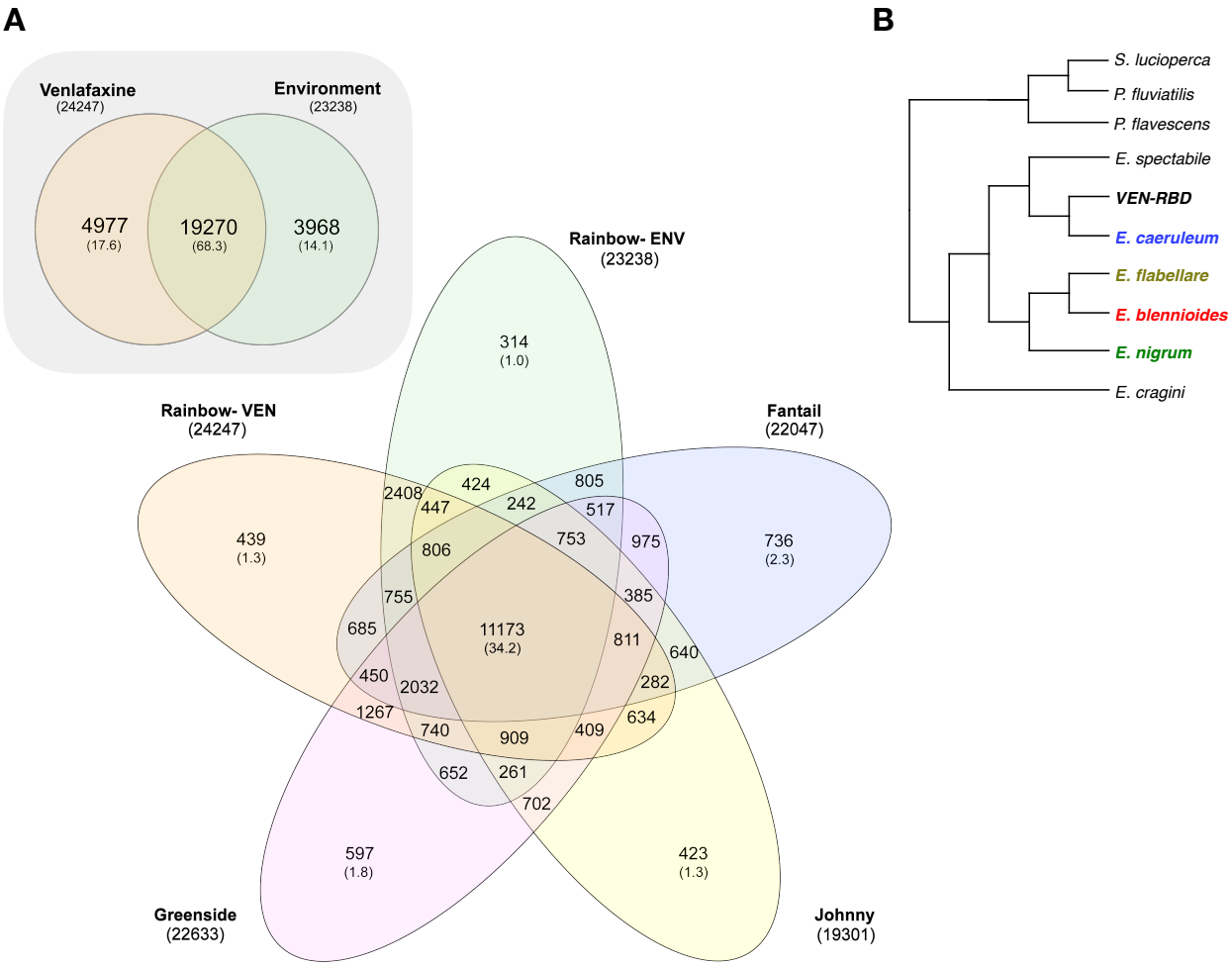


Figure 3.5: (A) Venn diagrams illustrating shared and unique orthogroups identified in rainbow darter exposed to venlafaxine (Rainbow-VEN/venlafaxine), rainbow darter (Rainbow-ENV/ Environment), fantail darter, greenside darter, and johnny darter based on OrthoFinder analysis after presumed parasite transcript removal from VEN-RBD. Numbers represent the count of orthogroups unique to or shared among species, with percentages indicating their relative proportion. The upper left Venn diagram compares orthogroups between venlafaxine-exposed and effluent exposed rainbow darters. (B) Phylogenetic tree of Percidae species based on OrthoFinder results. VEN-RBD represents the transcriptome of rainbow darters exposed to venlafaxine. Darter species are color-coded (*Etheostoma caeruleum* in blue, *E. flabellare* in yellow, *E. blennioides* in red, and *E. nigrum* in green) to distinguish among taxa.

3.3.4 Gene ontology annotation

Following the GOseq pipeline, a wide range of GO terms for each assembly were identified, with little variation in the number and assortment of GO terms under each domain compared between VEN-RBD and ENV-RBD (Figure A2.5). Transcripts from each assembly grouped based on level two gene ontology terms also demonstrated a high degree of congruence in proportions and distribution across assemblies and assembly specific orthogroups (Figure A2.6). While the overall distribution of terms remained consistent between transcriptomes, some divergence was observed in VEN-RBD-specific sequences, including a higher relative representation of terms such as Developmental Process (BP; GO:0032501), Multicellular Organismal Process (BP; GO:0032501), Binding (MF; GO:0005488), Plasma Membrane (CC; GO:0005886), and Transporter Activity (MF; GO:0005215). In contrast, terms such as Cellular Process (BP; GO:0009987), Metabolic Process (BP; GO:0008152), and Catalytic Activity (MF; GO:0003824) were less frequently assigned. However, this divergence was limited, ranging from 1% to 3.7% compared to ENV-RBD. Additionally, ENV-RBD-specific unigenes exhibited a higher relative assignment of the term Structural Molecule Activity (MF; GO:0005198) by 2.7%.

3.3.5 Gene ontology enrichment and networking

Differentially expressed genes in the R-VEN exposure group exhibited enriched GO terms (FDR<0.05) across several functional categories (Table A2.4). Amino acid metabolism and catabolism were notably overrepresented, as evidenced by significant enrichment in amino acid metabolic and catabolic process, including glutamate metabolic process (GO:0006536) (Figure 3.6). Phospholipid biosynthetic processes were also also enriched. Furthermore, enriched GO terms related to cellular process regulation were identified, notably including the positive regulation of cation transmembrane transport (GO:1904064) and modulation of the interferon-gamma response. Finally, enrichment was observed in terms associated with stress response and cell differentiation regulation, such as response to immobilization stress (GO:0035902) and positive regulation of erythrocyte differentiation (GO:0045648). These enrichments were primarily driven by a small subset of transcripts annotated as *nr1h4, got1, tat, hykk, chp1, ifngr1,* and *stat1*. Network mapping of enriched GO terms illustrates the functional relationships and gene overlap among ontologies, revealing a prominent cluster of interconnected terms related to metabolic, catabolic, biosynthetic, and transport processes (Figure 3.6). A distinct peripheral

offshoot consists of two interferon-gamma-related terms, indicating a specialized functional module separate from the core metabolic network.

A small subset of DEGs in the S-VEN treatment group primarily accounted for GO enrichment. Enriched biological categories (FDR < 0.05) included developmental and cellular structural processes integral to neural tissue patterning (Figure 3.7). Additionally, terms related to calcium ion transport regulation and nerve growth factor signalling were enriched. Biosynthetic processes were represented by the enrichment of lipid and prostaglandin biosynthetic pathways, while monocarboxylic acid metabolism (GO:0032787) indicated broader organic compound metabolic activity. These enrichments were primarily driven by transcripts annotated as ***e****pb41l5, magi2, xylb, cbr1, pitpnm2,* aars2 and *sestd1*. Ontology networking revealed two distinct functional sub-networks (Figure 3.7). One sub-network comprised ontologies associated with developmental, morphogenetic, and neuronal processes. The other involved two clusters, comprised of lipid biosynthetic processes and organic acid metabolic processes linked together by monocarboxylic acid metabolic process. Notably, the R/S-VEN DEGs as a whole did not exhibit significant functional enrichment, nor was enrichment observed when the upregulated R- or S-VEN DEGs from this group were analysed as an individual subgroup using topGO.

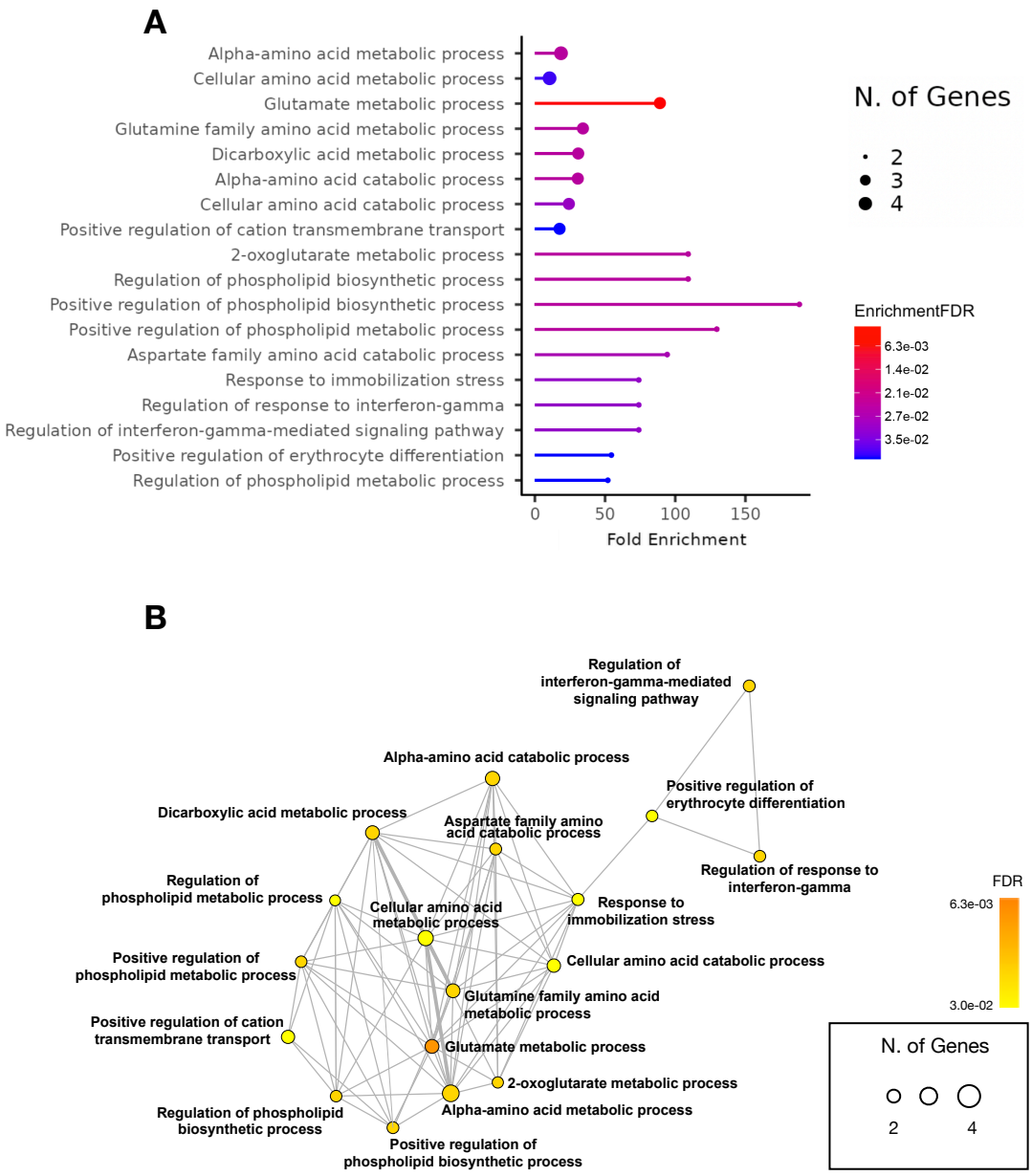


Figure 3.6: (A) Significantly enriched (FDR < 0.05) biological process gene ontologies identified from differentially expressed genes in rainbow darter (*Etheostoma caeruleum*) to R-venlafaxine for fourteen days. Enrichment analysis was performed using background sets of 46,149 unigenes, with 26, differentially expressed genes. (B) Network map illustrating relationships between enriched biological process gene ontologies. Each node represents a significantly enriched GO term, with node size corresponding to the number of genes in each pathway. Edges indicate shared gene overlap, with thickness proportional to the percentage of overlapping genes. Node colour represents the significance level (FDR) of enrichment.

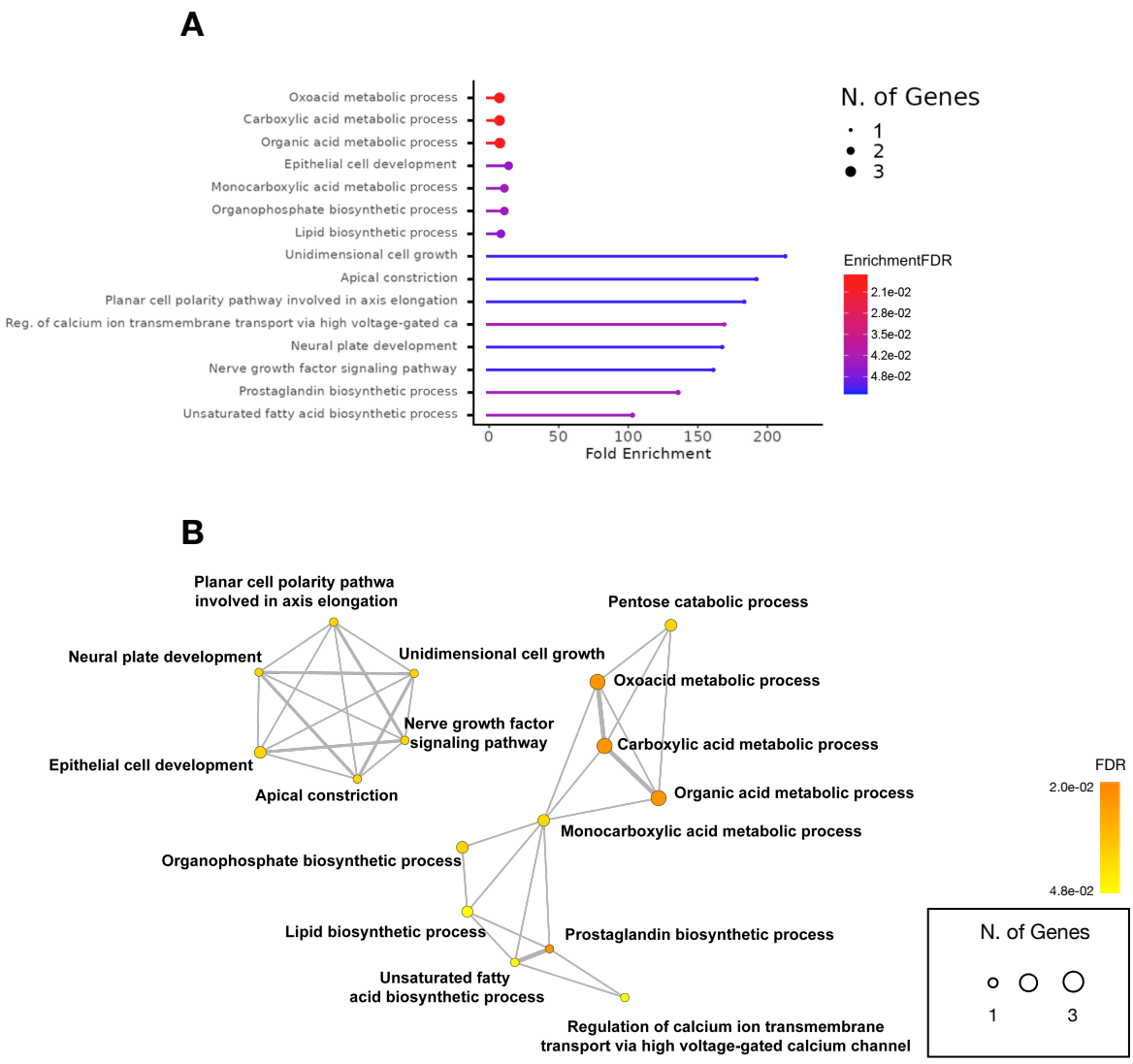


Figure 3.7: (A) Significantly enriched biological process gene ontologies (FDR < 0.05) from differentially expressed genes in rainbow darter (*Etheostoma caeruleum*) exposed to S-venlafaxine for 14 days. Enrichment analysis used a background set of 46,149 unigenes, with 25 differentially expressed genes. (B) Network map depicting relationships among enriched biological process GO terms. Node size reflects the number of associated genes, edge thickness represents gene overlap percentage, and node colour indicates enrichment significance (FDR).

Gene ontology enrichment on unigenes assigned to assembly-specific orthogroups in topGO identified several enriched ontologies (p-value < 0.05) between groups (Figure 3.8). In VEN-RBD unigenes, enriched ontologies associated with neural function and ion transport such as nervous system processes, cation channels, and voltage gated channel activity (GO:0022832) were enriched. Additionally, categories encompassed cellular signalling and regulatory mechanisms, including pathways involved in intracellular communication, membrane-associated processes, enzymatic lipid modification, and GPTase activity, were also enriched. In ENV-RBD assembly-specific transcripts, enriched ontologies related to cytoskeletal organisation and extracellular dynamics were identified, including vesicle transport (GO:0030050), myosin complex (GO:0016459), and cell cortex (GO:0005938). Additionally, enriched categories related to contractile and motor functions were identified, including those involved in microfilament motor activity (GO:0000146) and muscle structural integrity.

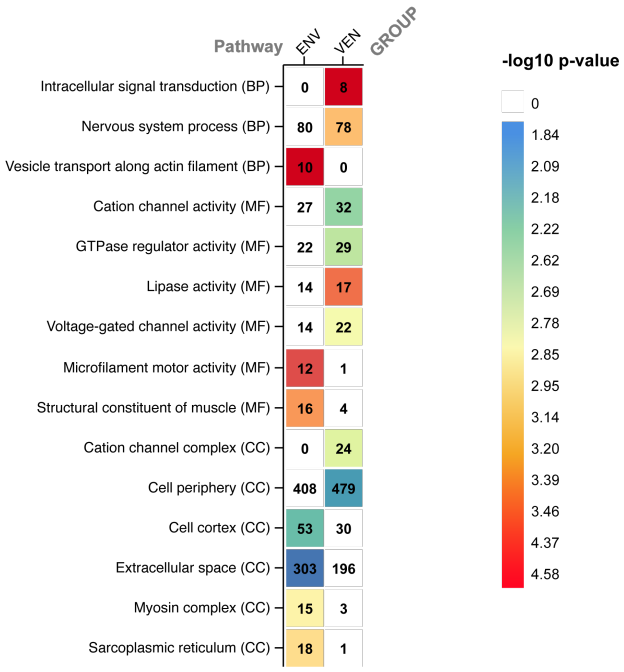


Figure 3.8: Significantly enriched gene ontologies (Fisher's exact *P* and weight *W* test, $P < 0.05$) identified in assembly-specific orthogroups from transcriptomes of rainbow darters (*Etheostoma caeruleum*) exposed to venlafaxine (VEN) and those collected upstream and downstream of the Waterloo municipal wastewater treatment plant outfall (ENV) (Chapter 2). The colour scale represents the -$\log_{10}$ *P*-value of enrichment.

3.3.6 Transcript networking

Protein-protein interaction (PPI) analysis of differentially expressed transcripts from the R-VEN treatment revealed a sparse network consisting of three dyads, indicating limited connectivity among transcripts and a non-significant PPI enrichment ($p = 0.104$). The identified dyads—*aplp2–nup98*, *got1–tat*, and *ifngr1–stat1*—exhibited distinct expression patterns. Similarly, the PPI network constructed from S-VEN treatment DEGs incorporated additional transcripts not fully captured by GO enrichment, including *thop1*, *chd6*, *kmt2c*, and *kmt2d*, but did not reach the significance threshold ($p = 0.175$). A distinct open dyad linked *cdh2* and *nenf*, both of which were upregulated. Given the overall sparsity of these networks, MCL clustering was deemed unnecessary, and no central hubs or bottlenecks were identified.

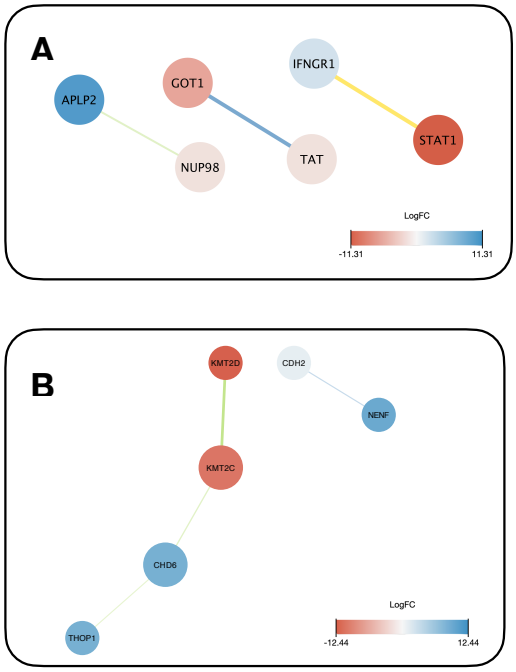


Figure 3.9: STRING-derived interaction networks ($p > 0.05$) for differentially expressed genes in liver of rainbow darter (*Etheostoma flabellare*) exposed to (A) R-venlafaxine and (B) S-venlafaxine for fourteen days. Node colour represents log fold change (log2FC), with larger nodes indicating higher degree centrality. Edges are coloured according to subnetwork.

3.4 Discussion

This study aimed to elucidate the stereoselective effects of the R- and S-enantiomers of venlafaxine (VEN) on the hepatic transcriptome of the rainbow darter (*Etheostoma caeruleum*). Fish were exposed to environmentally relevant concentrations of each enantiomer to assess whether VEN contributes to the transcriptomic alterations observed in wild populations exposed to wastewater treatment plant effluent (WWTPE), as detailed in Chapter 2. Using *de novo* sequencing, differential gene expression analysis, and gene ontology enrichment, VEN enantiomers were found to induce complex, stereoselective changes in hepatic gene expression. Both enantiomers modulated genes related to neural signalling, metabolism, immune function, and cytoskeletal dynamics, yet each elicited a distinct transcriptional signature. Notably, the consistent upregulation of *gabbr2* across treatments suggests a shared influence on GABAergic signalling, hinting at broader systemic implications. Although some similar genes were affected by both VEN and WWTPE exposures, the limited overlap in transcriptomic responses indicates that while VEN may contribute to gene expression perturbations in wild populations, other effluent constituents likely also play significant roles. These findings underscore the importance of considering stereoselectivity in ecotoxicological assessments when evaluating the impacts of chiral contaminants.

3.4.1 Quality control, sequencing, and *de novo* assembly

The high RIN scores observed across most samples confirmed that the RNA samples were of sufficient quality for robust downstream analyses. The lower RIN score observed in the S14C3 sample did not appear to significantly affect sequencing or assembly quality, as indicated by alignment metrics (90.06%), sample correlation matrix heatmaps (Figure A2.2), and PCA (Figure A2.7). Consistent Phred scores above 34 and low N content further corroborate the reliability of the sequencing data. The average alignment of reads to the assembled transcriptome (89.7%) was well within the expected range (Conesa et al., 2016). BUSCO analysis demonstrated that the assembled transcriptome captured a substantial portion of the expected single copy orthologs for Eukaryota, Metazoa, Vertebrata, and Actinopterygii. Despite some duplication (24.7–26.3%), fragmentation (0–2.4%), and missing genes (0-7.5%), these metrics are comparable to those reported in *de novo* assemblies of non-model organisms and represent an improvement over the ENV-RBD assembly (Pomianowski et al., 2021; Marisaldi et al., 2021).

The assembled VEN-RBD transcriptome was generated using a greater number of paired-end reads than the ENV-RBD transcriptome, potently resulting in greater capture of full-length and lowly expressed transcripts (Grabherr et al., 2011; Sims et al., 2014). This may have contributed to improved completeness in core gene sets (BUSCOs) by reducing fragmentation and missing orthologs (Figure 3.2). Additionally, the VEN-RBD assembly exhibited a higher contig N50, as well as greater average and median contig lengths, with transcripts sufficient to capture protein-coding regions (Tiessen et al., 2012). Notably, despite the higher number of reads used, the VEN-RBD assembly produced fewer unigenes than the ENV-RBD assembly. This may reflect a more diverse gene expression profile in ENV-RBD driven by dynamic environmental factors absent in controlled laboratory conditions. Furthermore, the reduced number of unigenes could be attributed to parasitic infections that were initially captured during sequencing and assembly but were subsequently removed through transcript filtering. Nevertheless, the construction of 47,083 unigenes remains comparable to other *de novo* teleost transcriptomes (Sandoval-Castillo et al., 2020)**.** This high-quality sequencing and transcriptome completeness support the reliability of the differential expression results and subsequent functional interpretations.

3.4.2 Annotation

Of the total unigene set, 34% (15,948 unigenes) were successfully annotated with predicted open reading frames. This annotation rate is consistent with other de novo teleost transcriptome assemblies; for example, Ning et al. (2024) identified 14,383 annotated transcripts out of 30,560 unigenes in *Perccottus glenii*. Orthogroup analysis identified an unexpectedly high number of sequences unique to the VEN-RBD assembly. BLASTx alignment against the NCBI nr database (Schoch et al., 2020) demonstrated that many of these sequences shared high homology with genes from *Heterobilharzia americana*, a trematode parasite, and various Cnidaria species. For detailed background on these parasites, and the rationale behind identifying them as contaminants, see Appendix B. To investigate this further, *H. americana* was incorporated into the orthogroup analysis. This revealed that 30% of the sequences originally unique to the VEN-RBD assembly were exclusively shared with *H. americana,* and erroneously suggested that VEN-RBD orthologs were more evolutionarily similar to *H. americana* than ENV-RBD. Moreover, presumed spurious transcripts exhibited greater homology to Cnidaria and Platyhelminthes then to other teleosts, strongly suggesting a parasitic origin. Notably, *H. americana* showed limited homology to transcripts from effluent exposed rainbow, fantail,

johnny, and greenside darters, highlighting this contamination as a specific issue in the VEN-RBD assembly. These findings bring to light a key methodological challenge that, while seemingly uncommon in fish transcriptomics, is pervasive across transcriptome and genome sequencing methodologies. Contaminants have been identified even in complete model organism genomes within public databases (Steinegger & Salzberg, 2020; Lupo et al., 2021), emphasizing the necessity of rigorous contaminant exclusion strategies. This work highlights the importance of identifying and removing foreign contaminants, particularly parasitic transcripts, rather than solely focusing on bacterial, fungal, and viral genes. The significance of this approach is further supported by recent advancements in developing more stringent methods for spurious transcript exclusion (Alvarez & Landsman, 2024).

In response, the post-assembly annotation filtering was revised to remove transcripts with greater than 50% similarity to Cnidaria and Platyhelminthes, along with those aligning to bacterial, viral, and fungal sequences. This additional filtering eliminated 2,392 transcripts from the unigene set, resulting in the refined dataset presented herein. Orthogroup inference using OrthoFinder indicated that approximately 34% of orthogroups were shared among the four darter species and VEN-RBD, while over 68% were shared between VEN-RBD and ENV-RBD. Although assembly-specific orthogroups were limited, the divergence between these assemblies may reflect differences in environmental influences, laboratory exposure, temporal fluctuations in gene regulation, and the presence of lowly expressed transcripts. These findings are consistent with other de novo studies investigating orthogroups among closely related teleosts (Carruthers et al., 2018), and the resulting phylogenetic tree aligns with established taxonomies (Near et al., 2011).

Comparison of GO annotations between the VEN-RBD and ENV-RBD transcriptomes revealed a consistent distribution of level 2 GO terms across the three primary domains: Biological Process, Molecular Function, and Cellular Component. This uniformity aligns with previous findings in teleost transcriptomes and supports the completeness and broad functional coverage of the VEN-RBD transcriptome, as no apparent functional bias was detected (Salem et al., 2015). Minor differences in the proportion and diversity of level 2 ontologies were observed in assembly-specific transcripts, which were effectively characterized through GO enrichment analysis.

3.4.3 Stereoselective Effect of Venlafaxine on Rainbow Darter

Pharmaceuticals such as venlafaxine (VEN) are increasingly detected in aquatic environments due to incomplete removal during wastewater treatment (Metcalfe et al., 2010; Schultz et al., 2010). Venlafaxine is clinically administered as a racemic mixture of R- and S-enantiomers, each with distinct pharmacokinetic and pharmacodynamic profiles in mammals (Otton et al., 1996; Gaynor & Teal, 2012). Consequently, questions arise as to whether these stereoselective actions lead to divergent effects on aquatic vertebrates exposed to the compound in surface waters. To compare the effect of exposure to the R- and S-enantiomers of venlafaxine (VEN) of rainbow darters, we analysed differentially expressed genes (DEGs), enriched pathways, and affected biological processes. The results demonstrate that exposure to both enantiomers induces stereoselective alterations in hepatic gene expression. Differential expression and pathway analysis revealed both enantiomers modulating genes associated with neural signalling, metabolism, immune function, and cytoskeletal dynamics. However, each enantiomer elicited a distinct transcriptional signature. These findings provide insights into the stereoselective mechanisms underlying VEN exposure and highlight potential disruptions in biological pathways resulting from pharmaceutical contaminants in wastewater effluent.

3.4.3.1 Neurological Signalling

Exposure to either R- or S-VEN led to the altered expression of genes associated with neuronal function. Most notably, both VEN exposures led to significant upregulation of *gabbr2*, encoding the gamma-aminobutyric acid (GABA)-B receptor subunit 2. *Gabbr2* pairs with *Gabbr1* to form functional heterodimeric receptors that, upon GABA binding, typically exert inhibitory effects through G-protein-coupled signalling (Kaupmann et al., 1997). Although the liver is not traditionally viewed as a major site of neurotransmitter action, GABAergic signalling components do exist in peripheral tissues, including teleost liver (Minuk et al., 1992; Macqueen & Johnston, 2009). In mammals, peripheral GABAergic signalling can modulate the autonomic nervous system, particularly through the vagus nerve, influencing diverse hepatic functions, including glucose clearance, hepatocyte membrane potential, lipid accumulation and metabolism (Geisler et al., 2023; Kim & Yoon, 2023). Beyond these metabolic roles, GABA also possesses tissue growth regulatory properties, playing a protective role in response to toxic hepatic injury by preventing apoptosis and supporting liver regeneration and repair (Minuk et al., 1992; Wang

et al., 2017; Hata et al., 2019). In fish, the conservation of receptor subunits and transporters similarly suggests that GABA may influence metabolic homeostasis, tissue repair, and immune responses in extra-neural tissues (Macqueen & Johnston, 2009; Cocco et al., 2009; Biggs et al., 2013). The consistent upregulation of *gabbr2* across both R- and S-VEN treatments suggests that venlafaxine, irrespective of enantiomer, may influence GABAergic signalling in the liver. In rodent models, venlafaxine alters excitatory/inhibitory balance by modulating perineuronal nets around parvalbumin-positive GABAergic interneurons in the brain (Coutens et al., 2022), which can impact inhibitory tone. Given that Gabab receptors regulate serotonin and dopamine release, it is plausible that venlafaxine exposure influences GABA receptor expression as a secondary effect (Fatemi et al., 2017). The upregulation of *gabbr2* in both R- and S-VEN treatments may reflect a compensatory response to this disruption seeking to restore or enhance inhibitory tone, though further research is needed to determine whether local GABA availability in the liver is directly affected by venlafaxine exposure.

While both enantiomers influenced *gabbr2* expression, each modulated a distinct set of genes associated with synaptic function and neural development. GO enrichment analysis of S-VEN differentially expressed transcripts (Figure 3.7) identified genes such as *magi2, arhgef25, and nenf*, which contribute to neuronal differentiation and the maintenance of synaptic structural integrity (Hirao et al., 1998; Wood et al., 1998; Byerly et al., 2013). Similarly, R-VEN modulated the expression of *kcnmb2, aplp2, st3gal2 and kalrn*, each of which has well-established roles in synaptic function and plasticity (Hartmann et al., 2007; Mandela et al., 2012; Wallner et al., 1999; Bentrop et al., 2001). In certain teleost species, blood vessels and biliary structures receive some degree of autonomic innervation (Tsuneki & Ichihara, 1981; Esteban et al., 1998; Miller et al., 2021), and thus VEN may be influencing this gene expression through autonomic neuromodulation. However, given the broader functional roles of these genes in processes such as cell adhesion, ion channel regulation, and tissue repair, their differential expression in hepatic tissue may reflect more generalized cellular responses.

3.4.3.2 Metabolic Disruptions

Venlafaxine exposure impacted multiple metabolic pathways, with notable effects on lipid, carbohydrate, and amino acid metabolism. R-VEN exposure disrupted metabolic regulation, particularly affecting phospholipid and amino acid metabolism (Figure 3.6). This was

exemplified by the downregulation of *nr1h4* (FXR) which is responsible for regulating bile acid synthesis and transport, lipid metabolism, and exerting anti-inflammatory effects in the liver (Claudel et al., 2005; Ma et al., 2006; Jiao et al., 2015). Lower expression could compromise bile acid secretion and predispose the liver to cholestasis or inflammatory stress (Fiorucci et al., 2010; Han et al., 2018). R-VEN also downregulated *foxn3* relative to both control and S-VEN treatment (Figure 3.4), which acts as a transcriptional repressor of gluconeogenic genes. Reduced expression of *foxn3* might shift the liver toward increased glucose utilization or altered gluconeogenic capacity (Scot**t** et al., 2005; Karanth et al., 2016; Karanth et al., 2019)**,** potentially compounding bile acid dysregulation.

Moreover, genes integral to amino acid catabolism were suppressed in R-VEN treatments. These include *got1* (glutamic-oxaloacetic transaminase 1), *tat* (tyrosine aminotransferase), and *hykk* (hydroxylysine kinase). The enzymes Got1 and Tat participate in transamination and nitrogen balance, and their downregulation can hamper the malate-aspartate shuttle, disrupt redox equilibrium, and promote accumulation of amino acids (Safer, 1975; Subramanya et al., 2023). In particular, inhibited *got1* and *tat* activity can heighten oxidative stress through altered NADH/NAD^+ ratios and excess tyrosine, each linked to ROS production, inhibited ROS scavenger activity, and lipid peroxidation in model organisms (Sgaravatti et al., 2009; Macêdo et al., 2013; De Prá et al., 2014; Abrego et al., 2017; Ipson et al., 2019). The net effect is a potential synergy of metabolic and oxidative stress, exposing rainbow darters to hepatic injury if they cannot mitigate these disruptions. Additionally, *nr1h4* (Fxr) also plays a regulatory role in amino acid metabolism, and may influence the expression of *got1* and *hykk* (Massafra et al., 2017) suggesting down regulation of *nr1h4* may underlie the observed expressional changes in these transcripts.

S-VEN exposure disrupted metabolic processes involved in the synthesis and metabolism of organic acids, lipids, and related compounds (Figure 3.7). Notably, *cbr1* was significantly upregulated by S-VEN. This gene encodes and enzyme that detoxifies various reactive carbonyl compounds, including certain xenobiotics, and lipid peroxidation byproducts such as 4-HNE and MDA, which accumulate under oxidative stress (Forrest & Gonzalez, 2000; Ellis 2007; Hoffmann et al., 2007). The reduction of these lipid peroxidation products can mitigate oxidative damage and generate bioactive intermediates that activate the NF-ϰB inflammatory pathway (Rotondo et al., 2016). Venlafaxine and its primary metabolites do not appear to possess

reducible carbonyl groups (Santos et al., 2020), suggesting that the observed upregulation of *cbr1* is not the result of direct detoxification of S-VEN. Instead, this induction may reflect an adaptive response to oxidative stress, as a means to mitigate cellular damage. Concurrent downregulation of *pitpnm2*, a mediator of phosphatidylinositol and phosphatidylcholine membrane trafficking (Allen-Baume et al., 2002; Cockcroft, 2012), suggests compromised lipid transport. This perturbation may disrupt lipoprotein assembly, secretion, and membrane turnover. Further supporting altered lipid homeostasis, diminished *xylb* (xylulokinase) expression points to dysfunctions in pentose and fructose metabolism, as well as pathways critical for modulating lipid biosynthesis (Bunker et al., 2015). In contrast, upregualtion of *aars2* (mitochondrial alanyl-tRNA synthetase), which ensures fidelity in mitochondrial translation, suggests an elevated requirement for mitochondrial protein synthesis and quality control (Kaiser et al., 2020; Mao et al., 2024). Overall, these transcriptional shifts indicate a regulatory response to S-VEN exposure, characterized by oxidative stress adaptation, disruptions in lipid handling, and potential compensatory mechanisms to maintain mitochondrial function and metabolic equilibrium.

R-VEN appears to exert a broader impact on metabolic regulation, influencing lipid, glucose, and amino acid metabolism, which could contribute to metabolic dysregulation and oxidative stress. This is further exemplified by the differential transcriptional modulation observed between enantiomers. The higher expression of *mocs1* and *nr5a2* in R-VEN relative to S-VEN treatment suggests a stereoselective shift in amino acid metabolism and dysregulation of bile acid synthesis and secretion (Goodwin et al., 2000; Kožich et al., 2022). A metabolomic study by Santos et al. (2023) similarly found downregulation of amino acid metabolism, including tyrosine, in the liver of *Argyrosomus regius* (merger) following VEN exposure, potentially due to a combination of disrupted serotonin and noradrenergic signalling, monoamine biosynthesis, oxidative stress, and metabolic compensation. In humans, VEN treatment has been linked to cholestatic liver injury in individuals with impaired xenobiotic metabolism due to a CYP2D6 polymorphism (Stadlmann et al., 2012). Cholestasis is characterized by disruptions in bile acid homeostasis and impaired bile flow through the biliary system (Stadlmann et al., 2012; Gijbels et al., 2019). Pharmaceutical agents can induce cholestasis via mechanisms that disrupt hepatic transporter function, alter bile canaliculi dynamics, and/or compromise cellular structure and the subcellular localization of hepatic proteins (Gijbels et al., 2019). This disruption can lead to altered amino acid transaminase activity and inflammation as the liver responds to bile acid

accumulation (Desmet, 1995; Lee, 2003; Stadlmann et al., 2012; Gijbels et al., 2019). The transcriptional response observed in rainbow darter exposed to R-VEN resembles these effects of impaired VEN metabolism in humans. Teleosts lack a clear CYP2D6 homolog and are not thought to efficiently metabolize VEN (Uno et al., 2012, Connors et al., 2013), raising the possibility that R-VEN exposure may similarly promote cholestatic liver injury in rainbow darters. Together, these findings suggest that VEN exposure perturbs key hepatic metabolic pathways in a stereoselective manner, with R-VEN exerting broader effects on lipid and amino acid metabolism, potentially predisposing fish to metabolic dysregulation, oxidative stress, and bile acid disturbances. However, S-VEN appears to elicit a more targeted response, primarily engaging adaptive mechanisms to oxidative stress and mitochondrial function, while potentially disrupting lipid transport and carbohydrate metabolism.

3.4.3.3 Immune and Inflammatory Modulation

R-VEN treatment displayed more pronounced modulation of immune-related genes, spanning both innate and adaptive systems. For instance, R-VEN altered components of the IFN-γ signalling axis, as evidenced by the enrichment of IFN-γ regulatory pathways (Figure 3.6) and the modulation of the interferon-gamma receptor *ifngr1,* as well as *stat1,* a transcription factor activated downstream of Ifngr1 (Darnell et al., 1994; Pestka et al., 1997; Zou & Secombes, 2011). The opposing regulation of these genes could contribute to partial or dysregulated IFN-γ signalling, potentially impairing the transcription of IFN-γ-responsive genes and altering macrophage activation or inflammatory resolution (Grayfer & Belosevic, 2009; Zou & Secombes, 2011). R-VEN additionally affected the expression of *map3k2* and *spata2l,* which have opposing influences on the MAPK signalling cascade, a key regulator of stress responses, proliferation, and inflammation (Shinohara et al., 2009; Zhang et al., 2022). Upregulation of *map3k2* may enhance NF-ϰB-mediated pro-inflammatory signalling, while downregulation of *spata2l* could attenuate negative feedback regulation. Additionally, *dusp16*, which encodes a negative regulator of MAPK signalling activation, as well as *ifngr1* were upregulated in R-VEN relative to S-VEN. Together, these changes suggest that R-VEN may modulate pro-inflammatory activity to a greater extent that S-VEN treatment.

R-VEN treatment further affected innate immune modulation through the upregulation of transcripts encoding lectins (*ll, ntc*) and the mannose receptor *mrc2*. These genes encode lectins that act as pattern recognition receptors, facilitating pathogen detection, agglutination, immune activation, and inflammatory responses (Russell et al., 2008; Lopes-Ferreira et al., 2011; Lv et al., 2016). In teleosts, Mrc2 contributes to immune defence, beyond its role in mediating collagen uptake and tissue remodelling by recognizing pathogen-associated molecular patterns, facilitating pathogen clearance, and potentially modulating inflammatory responses during infections (Zheng et al., 2015; Dong et al., 2016). Upregulation of these transcripts suggests that R-VEN may heighten innate immune detection. However, downregulation of *rnf166*, an E3 ubiquitin ligase important in antiviral signalling and autophagy, suggests some facets of innate immunity might be impaired (Chen et al., 2015). Together, the modulation of immune components demonstrates that R-VEN exerts a complex, potentially unbalanced, immune influence, amplifying certain pro-inflammatory or detection pathways while dampening others.

Compared to R-VEN, S-VEN induced a more limited set of differentially expressed immune-related genes. However, S-VEN treatment led to the upregulation of *thop1*, *ll*, and the immune-associated scaffolding protein Swap70 (Pearce et al., 2011). Upregulation of *thop1* may influence peptide-based immune signalling by modulating antigen processing for MHC class I presentation to cytotoxic T cells (Neves et al., 2023). However, *thop1* also degrades a variety of peptides, including neuropeptides, and has been implicated in the regulation of energy metabolism (Ferro et al., 2020). While genes encoding pathogen recognition lectins were upregulated in R-VEN, *clec10a*, a pattern recognition receptor lectin-encoding gene, was more highly expressed in S-VEN. These findings suggest that venlafaxine exposure modulates lectin transcription regardless of enantiomer.

Elevated serotonin and norepinephrine can modulate immune response through receptor-mediated signalling. Serotonin can modulate cytokine release and cell communication via 5-HT receptors on immune cells, though effects vary contextually (Khan & Deschaux, 1997; Duffy & Zelikoff, 2008). Norepinephrine influences macrophages and Kupffer cells via β-adrenergic receptors, modulating cytokine production as part of a sympathetic neuroimmune crosstalk (Elenkov et al., 2000; Miksa et al., 2009). VEN, when administered as a racemic mixture both in vitro and in vivo models, has been shown to regulate the expression of both pro- and anti-inflammatory cytokines via this neuroimmune interplay**,** potentially promoting an anti-

inflammatory state (Vollmar et al., 2008; Chen et al., 2018). In the present study, the more pronounced effects of R-VEN on immune-related transcript expression may be attributable to its higher affinity for serotonin and norepinephrine reuptake inhibition, thereby potentially amplifying neuroimmune signalling (Burnett & Dinan, 1998). Chronic perturbation of this balance due to R-VEN exposure may contribute to a state of immune dysregulation, potentially increasing susceptibility to infections, autoimmune reactivity, and hepatic inflammation (Voican et al., 2014; Dai et al., 2023; Larivuo et al., 2023).

3.4.3.4 Cytoskeletal Dynamics and Vesicular Trafficking

Modifications in the expression of genes related to cytoskeletal architecture and cellular organisation within hepatic cells was evident following both R-VEN and S-VEN exposures. In the R-VEN treatment, this dysregulation is reflected by the downregulation of vesicle formation and transport genes, including *arl1, sec23a,* and *pacsin3*. Arl1 maintains Golgi integrity and regulates vesicle trafficking between the Golgi and endosomal compartments, while Sec23a is a core component of the COPII complex, facilitating ER-to-Golgi vesicle formation (Lu et al., 2001; Khoriaty et al., 2018). Pacsin3 orchestrates membrane remodelling and endocytosis, linking cytoskeletal elements to curvature-sensing domains (Sumoy et al., 2001; Dumont & Lehtonen, 2022). Additionally, R-VEN exposure also induced the expression of genes involved in cytoskeletal organisation and cellular signalling, such as *daam1***,** which regulates actin filament assembly through non-canonical Wnt signalling, playing a role in polarized cell growth and cytokinesis (Lu et al., 2007; Ang et al., 2010). The reduced expression of vesicular transport genes, including *rab1b* and *pacsin3,* in R-VEN relative to S-VEN further suggests that the R-enantiomer may have a greater disruptive impact on cellular trafficking mechanisms (Plutner et al., 1991). Such dysregulation may impair intracellular trafficking and disrupt efficient protein processing. In addition, R-VEN may more strongly limit the sialylation of glycolipids and glycoproteins, as indicated by the lower expression of *st3gal2* relative to the control and *st3gal4* relative to S-VEN (Kitagawa & Paulson, 1994; Kim et al., 1996). Reduced activity of these sialyltransferases could disrupt Golgi-mediated post-translational glycosylation, potentially impairing proteins essential for cellular communication and receptor function (Harduin-Lepers et al., 2001; Varki, 2017). Overall, these transcriptional changes could result in the accumulation of misfolded proteins in the ER, activation of ER stress pathways, and compromised secretion of

essential proteins, including enzymes and lipoproteins that are critical for hepatic detoxification and metabolism (Jackson & McNiven, 2020)

In response to S-VEN treatment, key pathways involved in cell growth, adhesion, cytoskeletal dynamics, and ECM remodelling were significantly altered, suggesting an adaptive remodelling response. The opposing expression of genes such as *magi2***,** which encodes a scaffolding protein critical for establishing and stabilizing cell–cell junctions, and *epb41l5*, encoding an actin-binding factor known to destabilize adherens junctions, may serve to preserve cadherin-based adhesion and thereby reduce cell migration and ECM remodelling. However, the modulation of *sh3pxd2a* (Tks5) and *col6a2* suggests an adaptive remodelling of tissue. Increased matrix stiffness characteristic of liver fibrosis can stimulate *sh3pxd2a* driven podosome formation, contributing to ECM remodelling and potentially influencing fibrosis development (Juin et al., 2013). Additionally, the upregulation of *arhgef25* may promote cytoskeletal remodelling, altered cell adhesion, and tissue restructuring (Guo et al., 2003; Van Unen et al., 2016). In this context, the downregulation of *col6a2*, which encodes a structural component of type VI collagen in the ECM (Chu et al., 1989), further highlights disruptions in ECM integrity, which may help to facilitate remodelling processes. This remodelling potential is further supported by the upregulation of *cdh2* (N-cadherin), which, unlike E-cadherin, affords greater plasticity to cell–cell adhesion, thereby maintaining structural cohesion during dynamic remodelling processes (Zeisberg & Neilson, 2009; Alimperti & Andreadis, 2015). The stereoselective influence of S-VEN on actin cytoskeletal dynamics is further evidenced by the higher relative expression of *dennd1c*, which regulates actin remodelling and cell morphology (Marat et al., 2012), compared to R-VEN. This aligns with the upregulation of other guanine nucleotide exchange factors (GEFs), including *swap70 and arhgef25*, in S-VEN relative to control.

The transcriptional response observed following S-VEN treatment could result from elevated ROS production. ROS can act as regulators of cell adhesion, influencing integrin signalling pathways and the phosphorylation of α-catenin within cadherin complexes (van Wetering et al., 2002; Chiarugi et al., 2003; Hurd et al., 2012). Both Cdh2 and Magi2 engage β-catenin, which subsequently binds to α-catenin within cadherin structures (Alimperti & Andreadis, 2015; Nagashima et al., 2015). Sh3pxd2a directly interact with integrins, while, Epb41l5 plays a regulatory role in both cadherin-mediated and integrin-mediated adhesion

processes (Hirano et al., 2008; Murphy & Courtneidge, 2011). Thus, the modulation of genes involved in cell adhesion, cytoskeletal dynamics, and cellular movement, by S-VEN treatment is potentially stimulated through ROS-dependent mechanisms.

The modulation of genes involved in vesicle formation, transport, and cytoskeletal dynamics indicate molecular responses that could compromise liver function. Similar systemic effects have been observed in other studies, such as the disruption of epididymal structure and function in male rats due to VEN-induced cytoskeletal disorganization, and modulation of intracellular endosomal vesicles (da Silva et al., 2023). VEN has also been shown to influence cell proliferation via β-catenin activation in the hippocampus (Mostany et al., 2008) and to promote the expression of proteins associated with cellular growth and differentiation while downregulating those linked to cytoskeletal stability in human pluripotent cells (Doh et al., 2015) Our findings extend this understanding by demonstrating enantioselective effects of R-VEN and S-VEN on cytoskeletal architecture and vesicular trafficking in hepatic cells of rainbow darters. This suggests that even at relatively low doses, chronic VEN exposure may alter hepatic cellular processes, with potential implications for liver function.

3.4.3.5 Transcriptional and Epigenetic Regulation

One of the most distinguishing differences in the effect of S-VEN on rainbow daters is the significant modulation of transcription factors and chromatin modifiers. Notably, two zinc finger family genes, znf608 and znf271, were upregulated, with znf608 demonstrating the most significant increase in expression in this treatment group. Znf608 has been implicated in various biological contexts, including transcriptional repression via histone modification, cell migration, immune cell maturation, and developmental regulation (Williams et al., 2012; Reed et al., 2013; van den Berg et al., 2017). Similarly, Znf271, although less characterized, contains a KRAB domain and zinc finger motifs, suggesting a role in transcriptional regulation (Abrink et al., 1995; Tune et al., 2002). Simultaneously, *kmt2c and kmt2d*, two lysine methyltransferases responsible for histone H3K4 methylation, were among the most downregulated genes. These enzymes activate enhancers crucial for cell-specific gene expression and their suppression might stifle the expression of genes involved in cell growth or tissue repair (Heintzman et al., 2009; Duo et al., 2013; Lee et al., 2013; Dawkins et al., 2016; Lavery et al., 2020; Seehawer et al.,

2024). Supporting this, S-VEN downregulated *cenpa and wdr73*, possibly limits cell proliferation or division. Cenpa is a centromere-specific histone H3 variant essential for kinetochore assembly and accurate chromosome segregation during cell division (Cech & Peichel, 2015), while *wdr73* encodes a microtubule-associated protein that interacts with cell cycle proteins including tubulins to maintain cell architecture and survival (Colin et al., 2014; Cech & Peichel, 2015). In contrast, chd6, a chromatin-remodelling factor stabilized during oxidative stress, was upregulated. Chd6 typically relieves chromatin compaction at sites of ocxadative DNA damage, enhancing repair (Lutz et al., 2006; Moore et al., 2019; Kargapolova et al., 2021). Collectively, S-VEN affects the expression of the genes responsible for regulating the epigenetic and transcriptional landscape in rainbow daters, which may have implications on cellular proliferation to prioritize DNA integrity and enhance stress resilience.

R-VEN induced the downregulation of chromatin remodelling factors such as Brd1, which promotes chromatin remodelling and transcriptional activation (Mishima et al., 2011). However, rather than broadly reprogramming epigenetic regulation, R-VEN primarily modulated transcriptional regulators associated with immune and metabolic pathways. These findings reveal distinct enantiomer-specific transcriptional regulation, with S-VEN exerting a broader effect on chromatin regulation and epigenetic modifiers. Antidepressants have been shown to modulate epigenetic mechanisms, including chromatin remodelling, alterations in DNA methylation, histone post-translational modifications, and the regulation of miRNA expression (Inserra et al., 2024). These mechanism can be influenced by neuronal activity-driven chromatin remodelling, serotonin receptor signalling, and direct interactions with DNA or chromatin-modifying complexes (Inserra et al., 2024). Evidence has been provided to suggest that VEN affects epigenetic regulation in the brain by inhibiting histone deacetylase activity, specifically HDAC5 and HDAC6, thereby enhancing histone acetylation and upregulating genes critical for neurotransmitter synthesis (Qiao et al., 2019; El-Saiy et al., 2022). The evidence presented in this study supports a role for VEN in epigenetic regulation, suggesting that S-VEN may exert systemic effects on epigenetic processes in the liver.

3.4.3.6 Comparison with wild rainbow darter exposed to wastewater treatment plant effluent (WWTPE)

It is essential to place these laboratory findings on VEN exposure in a broader ecological context. In chapter two, we outlined how WWTPE effluent exposure affected multiple pathways in rainbow darter related to lipid metabolism, glycolysis, oxidative stress responses, detoxification, immune modulation, and inflammatory signalling. With VEN occurring at the highest concentration near the effluent plume we presumed that some of these observed effects may be influenced by high VEN exposure. VEN treatment broadly influenced similar metabolic, immune, and inflammatory pathways in a stereospecific manner. However, the specific processes within these pathways differed between lab and environmental exposures, and few transcripts were consistently modulated between effluent exposure and VEN treatment. Interestingly, cytochrome P450 activation was not observed following VEN exposure, despite *cyp2k1* upregulation in effluent-exposed RBD. This suggests that VEN alone may not be the primary driver of CYP induction in effluent-exposed fish and that xenobiotic metabolism remains largely unresponsive to either VEN enantiomer at the transcriptional level. A lack of significant metabolic activation could impair VEN clearance, potentially promoting bioaccumulation (Burkina et al., 2015).

Among the few genes similarly regulated between exposures were *cenpa* and *cdh2,* both of which were comparably modulated in the S-VEN treatment group. Cenpa is responsible for ensuring centromere integrity, and its downregulation may reflect inhibited cell proliferation or genomic instability(Mahlke & Nechemia-Arbely et al., 2020). CDH2 helps maintain robust but somewhat plastic cell–cell adhesions, and upregulation might reflect an effort to sustain tissue architecture during ECM remodelling or under adverse conditions (Mahlke & Nechemia-Arbely, 2020; Wu et al., 2024). Additionally, *nlrp12*, an anti-inflammatory factor, was significantly downregulated in effluent-exposed fish, and showed a reduction in expression the S-VEN treatment relative to R-VEN. These parallels suggest that the S-enantiomer may partially contribute to the immune and chromosome structure gene expression patterns observed in wild rainbow darters; however, the overall effluent mixture undoubtedly exerts broader, polypharmacological effects that extend beyond single-enantiomer influences.

Assembly specific transcripts in VEN-RBD were enriched for neuronal functions, including nervous system processes and voltage-gated channel activity, potentially as response to chronic exposure to the neuroactive pharmaceutical VEN. In contrast, ENV-RBD shows greater expression of genes related to cytoskeletal and muscle-related functions, which may reflect adaptations to a more active, free-flowing river environment or roles in intracellular transport and structural maintenance. The ENV-RBD group also exhibited significant modulation of more transcripts compared to either S-VEN or R-VEN treatments alone. This is unsurprising, as effluent is a complex mixture containing multiple potentially perturbing compounds, likely leading to a broader and more varied response in fish exposed to this pollutant. Nevertheless, the observed modulation of immune and metabolic pathways after R- and S-VEN treatments still demonstrates concerning disruptions, which could have physiological implications.

3.4.3.7 Conclusions

Our transcriptomic analysis of rainbow darter liver demonstrates overlapping and stereoselective effects of venlafaxine. Most notably, both enantiomers consistently upregulated *gabbr2* expression, implicating a common impact on GABAergic signalling that may serve as a compensatory response to neurotransmitter imbalances. While both enantiomers influenced pathways related to metabolism, immunity, and cytoskeletal regulation, each triggered distinct patterns of gene expression. R-VEN disrupted expression of transcripts involved in lipid, amino acid, and bile acid metabolism suggesting potential for cholestatic injury and altered redox balance, characteristic of poor VEN clearance. R-VEN further more broadly modulated immune responses by altering both IFN−γ pathway components, and lectins implicated in immune sensing. R-VEN treatment suppressed expression of key regulators of vesicular trafficking and cytoskeletal dynamics, which could compromise intracellular transport, a process essential for proper liver function.

In contrast, the effects of S-VEN treatment were more targeted, modulating transcriptional regulators, epigenetic modifiers, and chromosome maintenance, which may hinder cellular progression and proliferation. Additionally, S-VEN induced changes indicative of adaptive remodelling in cell adhesion and extracellular matrix dynamics, suggesting a compensatory response to preserve tissue integrity under stress. Interestingly, while R-VEN induced transcriptional changes that could affect redox balance and attenuate ROS scavenger

expression, genes involved in the direct response to lipid peroxidation and oxidative DNA damage were exclusively upregulated following S-VEN treatment. Measuring the levels of ROS or biomarkers of cellular damage could provide further insight into whether the potential effects of R-VEN on redox balance are actively promoting oxidative stress, or whether the upregulated genes in S-VEN reflect an adaptive response to ROS that is sufficient to counteract oxidative damage. While both VEN and effluent exposure modulated biological processes such as lipid metabolism and immune function, the specific mechanisms affected within these pathways differed. Only a few transcripts, including *cenpa, cdh2,* and *nlrp12*, were consistently modulated, potentially linking S-VEN exposure to the effects observed in effluent exposed RBD.

Collectively, the findings of this study suggest that both R- and S-enantiomers have the potential to disrupt liver function through distinct mechanisms. The stereoselective divergence in hepatic responses not only enhances our understanding of venlafaxine's extra-neural effects but also highlights the need to consider enantiomer-specific actions in the context of environmental risk assessment. Ultimately, while venlafaxine is but one of many psychoactive pharmaceuticals entering aquatic systems, the hepatic responses documented here in RBD underscore broader implications for how teleost fishes contend with pharmaceutical pollution. By disentangling stereoselective effects, we deepen our mechanistic understanding and foster a more nuanced approach to environmental monitoring, conservation, and the management of water resources in the face of escalating pharmaceutical load.

Chapter 4

Modulation of antioxidant enzyme activity, and markers of cellular damage in the brain of rainbow darter (*Etheostoma caeruleum*) exposed to venlafaxine

4.0 Introduction

Venlafaxine (VEN) has been measured at elevated concentrations in wastewater treatment plant effluent (WWTPE) worldwide (Schultz et al., 2010; Schlüsener et al., 2015; Huerta et al., 2018; Chen et al., 2022), including the Grand River in Ontario, Canada (Metcalfe et al., 2010), as further substantiated by the present study. In fish, VEN bioaccumulates (Arnnok et al., 2017; Duarte et al., 2023) and exposure has been implicated in several adverse effects, including alter energy metabolism (Best et al., 2014; Mehdi et al., 2019; Thompson et al., 2022), disrupt monoamine levels (Melnyk-Lamont et al., 2014), and maladaptive behavioral changes, at environmentally relevant concentrations (Tang et al., 2022). Additionally, oxidative stress evidenced by increased ROS generation in muscle, gill, liver, and brain, have been observed in fish following varying concentrations of VEN exposure (Maulvault et al., 2019; Qu et al., 2019, Ziegler et al., 2020, Ribeiro et al., 2022, Alves et al., 2023).

4.0.1 Reactive oxygen species and defence mechanisms

ROS are characterized by an array of highly reactive oxygen containing molecules (Bandyopadhyay, 1999). Most of the ROS present in cells are produced within the mitochondria as natural by-products of aerobic respiration, and can play an integral role in cell signalling and adaptation (Finkel & Holbrook, 2000; Ray et al., 2012; Sena & Chandel 2012). Incomplete oxygen reduction at Complex I and III leads to leakage of electrons, forming superoxide (O_2-) (Ott et al., 2007). Physiological stress may elevate energy demand, increasing oxygen consumption and ATP production in mitochondria, accelerating electron flow through the electron transport chain (ETC), elevating superoxide generation. However, it is unclear whether higher aerobic respiration actually alters *in vivo* ROS levels (Salin et al., 2015; Zhang & Wong, 2021). Other endogenous sources of ROS can originate from enzymatic activity like the oxidative deamination of neurotransmitters such as dopamine and serotonin, through monoamine oxidase (MAO) producing their corresponding aldehydes, ammonia, and hydrogen peroxide (Pizzinat et al., 1999; Edmondson et al., 2009). Other enzymes such as cytochrome P450 monooxygenases use NADPH and oxygen to metabolize various substrates including drugs, fatty acids, and steroids and uncoupling of this reaction can also produce ROS in the form of superoxide (Veith & Moorthy 2018).

As a primary antioxidant defence mechanism (Figure 4.1), superoxide can undergo dismutation by superoxide dismutase (SOD), resulting in the production hydrogen peroxide (H_2O_2) which can be further reduced to water by catalase (CAT) and glutathione peroxidase (GPX), preventing the formation of highly reactive hydroxyl radicals (OH) (Matés & Sánchez-Jiménez 1999). Antioxidant enzymes are distributed throughout the cell, but their compartmentalization within organelles influences their local effectiveness, substrate accessibility, and ability to neutralize oxidative stress within specific microenvironments (Kaludercic et al., 2014; Benáková et al., 2021). Cytosolic SOD (SOD1) is the predominant form of the enzyme in most tissues and cells, accounting for the majority of cellular SOD activity; however, mitochondria also possess their own isoform of SOD (SOD2) (Murphy, 2009; Fukui and Zhu, 2010). Although catalase is primarily only present in peroxisomes, CAT activity is likely present at low levels the mitochondria (Du et al., 2016; Benáková et al., 2021). Oxidative stress arises when ROS generation exceeds antioxidant defence and repair mechanisms, leading to oxidative damage (Chowdhury et al., 2020; Juan et al., 2021). This damage can alter membrane properties, disrupt enzyme activities, impair protein synthesis, and compromise DNA and lipid integrity, leading to mitochondrial dysfunction, cellular damage, and apoptosis (Echtay et al., 2002; Zorov et al., 2014; Ahmadian et al., 2016; Juan et al., 2021). Lipid peroxidation produces reactive aldehydes such as malondialdehyde (MDA) that can further compromise membrane fluidity, permeability, and various cellular functions. Lipid peroxidation intermediates can propagate oxidative chain reactions, leading to further ROS generation and subsequent damage to proteins, DNA, and cell membranes (Sies & Cadenas, 1985; Marnett, 1999; Fritz & Petersen, 2013; Su et al., 2019). GPX activity, particularly that of GPX4, helps mitigate this cascading cellular damage by reducing lipid hydroperoxides to their corresponding alcohols, thereby preventing further propagation of lipid peroxidation (Gaschler & Stockwell, 2017). DNA oxidation can induce base modifications, such as the formation of 8-OHdG, which, if left unrepaired, can contribute to genomic instability and mutagenesis (Kasai et al., 1986; Ock et al., 2012). ROS are also implicated in neuromodulation and have been associated with mood disorders, including depression and bipolar disorder (Bhatt et al., 2020; Correia et al., 2023). Increased oxidative stress has been observed in individuals with depression, and certain antidepressants, including monoamine oxidase inhibitors (MAOIs) and fluoxetine, may exert therapeutic effects, in part, by reducing ROS production in the mammalian brain (Bortolato et al., 2008; Caiaffo et al., 2016; Correia et al., 2023). Furthermore, emerging evidence suggests that oxidative stress is a critical factor in cognitive aging and neurodegenerative diseases such as

Alzheimer's, Parkinson's, and Huntington's disease (Moreira et al., 2005; Zhao et al., 2013; Xiao et al., 2022).

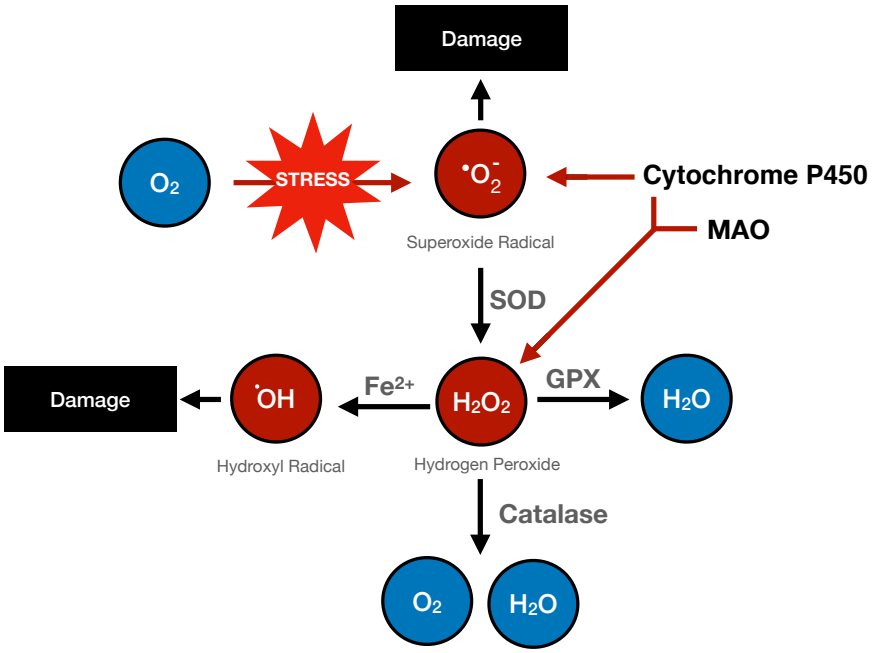


Figure 4.1: Flow diagram of reactive oxygen species (ROS) pathways, illustrating sources of ROS from stressors and enzymatic activity, including monoamine oxidase (MAO) and cytochrome P450 (CYP) enzymes. Antioxidant enzymes, superoxide dismutase (SOD), catalase (CAT), and glutathione peroxidase (GPX), detoxify ROS, leading to either oxidative damage or or stable byproducts. Adapted from Matés & Sánchez-Jiménez (1999), with additional context from Edmondson et al. (2009) and Veith & Moorthy (2018).

4.0.3 Contaminant induced oxidative stress

Environmental contaminants, such as pesticides, heavy metals, polycyclic aromatic hydrocarbons (PAHs), and contaminants of emerging concern (CECs), serve as exogenous sources of reactive oxygen species (ROS). These contaminants can promote oxidative stress either by directly generating ROS, disrupting mitochondrial function, or inducing ETC uncoupling (Garceau et al., 2010; Lushchak, 2016; Yeh et al., 2017; Kozal et al., 2023). Thus,

ROS are commonly used as a biomarker of contaminant-induced stress. Given the role of ROS in both neuromodulation and neurodegeneration, oxidative stress raises concerns regarding the neurotoxic potential of pharmaceuticals capable of inducing ROS in fish exposed to WWTPE. Supporting this concern, Bisognin et al. (2020) demonstrated that exposure to pharmaceutical-laden effluent induced oxidative stress in fish brains and inhibited acetylcholinesterase activity in muscle tissue, suggesting potential neurotoxicity of pharmaceutical contaminants. Similarly, exposure to environmentally relevant concentrations of fluoxetine induced oxidative stress and inhibited acetylcholinesterase activity in the brain of zebrafish, resulting in neurotoxic effects and anxiety-like behaviors (Orozco-Hernández et al., 2022). These studies highlight the contrasting and potentially contradictory effects of antidepressant exposure on neural ROS production in fish compared to mammals, which may be neurotoxic.

The brain is among the most metabolically active organs in fish (Phrompanya et al., 2021; Soengas & Aldegunde, 2002). This high metabolic rate, coupled with elevated polyunsaturated fatty acid (PUFA) content, makes the brain particularly susceptible to oxidative damage, as PUFAs are prone to peroxidation (Hong et al., 2014). Consequently, the brain is highly vulnerable to ROS-induced damage, which can contribute to neurodegeneration and potential behavioural alterations (Islas-Flores et al., 2013; Afifi et al., 2016; Ezeoyili et al., 2019). While VEN-induced behavioural impairment is well-documented (Parrott & Metcalfe, 2018; Maulvault et al., 2019; Thompson & Vijayan, 2020; Salahinejad et al., 2022; Thompson et al., 2022), the underlying mechanisms may not be fully explained by brain serotonergic modulation alone. Other factors, such as hormone regulation and gene modulation, may also contribute (Bisesi et al., 2014). Behavioural changes have also been shown to persist following VEN exposure, suggesting residual effects on brain chemistry or other physiological systems (Bisesi et al., 2014). Delayed behavioural recovery may be partially attributed to ROS-induced oxidative damage affecting neuronal function or neurotransmitter systems. Although VEN exposure appears to induce ROS production in fish, few studies have examined markers of cellular damage in the brain, and even fewer have assessed these effects in relation to individual VEN enantiomers (Qu et al., 2019; Ribeiro et al., 2022; Alves et al., 2023). This distinction is particularly important because wastewater treatment methods can stereoselectivity remediate VEN, leading to the enrichment of a specific enantiomer in receiving waters (Evans et al., 2017; Ma et al., 2020). In an ecological context, VEN-induced oxidative stress, and behavioural disruptions, may negatively affect individual fitness and reproduction, with potential adverse

population-level consequences (Fuiman et al., 2005; Farrell et al., 2008, Brodin et al., 2014; Saaristo et al., 2018; Candolin et al., 2019).

4.0.1 Objectives and hypothesis

This study aims to assess the antioxidant stress response of rainbow darters (*Etheostoma caeruleum*) to environmentally relevant concentrations of each enantiomer of venlafaxine, by using ROS scavenging enzyme activity as a proxy for ROS generation. To determine if cellular damage is present following exposure, markers of oxidative damage including products of lipid peroxidation (MDA), and DNA damage (8-OHdG) will also be investigated. We hypothesize that exposure to VEN will increase ROS production and oxidative damage in the brain of rainbow darters, with each enantiomer exhibiting a different magnitude of effect. Assessing enzyme activity separately in cytosolic and mitochondrial fractions may help clarify the extent of mitochondrial-specific oxidative stress, and the efficiency of ROS detoxification within each compartment. Rainbow darter (RBD) were chosen for this study due to their relative abundance in the Grand River, Southern Ontario (Hicks & Servos, 2017), their suitability for laboratory studies (Borowiec et al., 2024), and their demonstrated sensitivity to Waterloo WWTPE, including effects on antioxidant enzyme activity in brain tissue (Gauvreau et al., 2022). These findings will help clarify how VEN exposure contributes to neural ROS production observed in WWTPE-exposed wild populations and will enhance our understanding of the stereoselective effects of VEN, particularly in relation to oxidative stress, neurotoxicity, and potential behavioral consequences in aquatic organisms.

4.2 Materials and methods

4.2.1 Fish collection, handling and processing

Tissue samples for enzymatic activity assays and cellular damage quantification were collected from the same cohort of the R-venlafaxine (R-VEN) and S-venlafaxine (S-VEN) exposure trial described in Chapter 3. Briefly, adult male rainbow darters (*Etheostoma caeruleum*) were collected via backpack electrofishing (Smith Root, LR-20, LR-24) from the Grand River near Grand Valley, Southwestern Ontario (43°56'32.6"N 80°19'32.8"W). Captured

fish were transported in aerated water tanks to the Waterloo Aquatic Threats in Environmental Research (WATER) facility at the University of Waterloo, Ontario.

Upon arrival, fish were transferred into 10 L acrylic tanks within an Aquatic Habitats (AHAB) unit and acclimated at 18°C under a 12-hour light/dark cycle for two weeks to facilitate contaminant depuration. Fish were fed twice daily to satiation with San Francisco Bay Brand frozen bloodworms (Newark, USA). Following depuration, fish were transferred to 12 L glass aquaria housed within three large water trough. Each experimental tank contained at least six fish, randomly assigned to Control, S-VEN, or R-VEN treatment groups. A total of nine tanks per trough were used (n=162). Fish were further acclimated to the experimental tanks for three days prior to exposure and were fed once daily throughout the study. The R-VEN and S-VEN groups were exposed to 1 μg/L of the respective venlafaxine enantiomer (Millipore-Sigma Aldrich), which was maintained through 10% water replacement 1 hour after feeding. VEN was not administered to control tanks. Water samples were collected 1 hour post-replacement to confirm venlafaxine concentrations via Liquid Chromatography-Tandem Mass Spectrometry (LC-MS/MS), using an Agilent 1200 HPLC (Mississauga, Canada) coupled to an Applied Biosystems 3200 QTRAP mass spectrometer (ABSciex, Concord, Canada).

Tissue samples were collected at Day 1, Day 4, and Day 14 to assess time-dependent effects. On each sampling day, 18 randomly selected fish from each treatment and Control were euthanized via cervical dislocation. Whole brain tissue was immediately excised, flash-frozen in liquid nitrogen, and stored at -80°C. The Day 14 fish whose liver tissues were analysed for differential gene expression in Chapter 3 are the same individuals used for the biochemical assays described in this chapter. All animal handling and tissue collection procedures were approved by the Animal Care Committee at the University of Waterloo under AUPP#40318, following the guidelines established by the Canadian Council of Animal Care.

4.2.2 Enzymatic activity analysis

Prior to homogenization, brain tissue was rinsed in phosphate-buffered saline (PBS, pH 7.4) to remove residual red blood cells. Tissue (n = 6) was then homogenized using an OMNI tissue homogenizer (Omni International, GA, USA) in a cold buffer solution (20 mM HEPES, 1 mM EGTA, 210 mM mannitol, 70 mM sucrose, pH 7.2) at a 10:1 buffer-to-tissue ratio.

Mitochondrial isolation was performed via differential centrifugation, consisting of two sequential steps: an initial centrifugation at 1,500 × g for 5 minutes to pellet cellular debris, followed by a second centrifugation at 10,000 × g for 15 minutes to isolate mitochondria, both conducted at 4°C. Cytosolic and mitochondrial fractions were evaluated for enzymatic antioxidant activities. Glutathione peroxidase (GPX) activity was measured with the Glutathione Peroxidase Assay Kit (Item No. 703102) from Cayman Chemical (MI, USA). Superoxide dismutase (SOD) activity was assessed using the Superoxide Dismutase Assay Kit (Item No. 706002) provided by the same manufacturer, both used in accordance with manufacturer's protocol. Assays were performed in duplicate on 96-well microplates, and absorbance readings were obtained through spectrophotometry on a Spectramax 190 spectrophotometer (Molecular Devices, CA, USA) which was operated with SoftMax Pro v6.4 software.

GPX activity was measured by change in absorbance (340 nm) over time relative to the background, and expressed as nanomoles per minute per milliliter (nmol/min/mL). Results were normalized to total protein content (mg) and buffer dilution volume, yielding final activity values in micromoles per minute per milligram of protein (μmol/min/mg). Protein content was quantified using the Bicinchoninic Acid (BCA) assay (Sigma-Aldrich, MO, USA) and bovine serum albumin (BSA) as a standard, with absorbance measured at 562 nm. SOD activity was measured in duplicate (450nm), normalized against a reference standard, and reported as SOD units/ml. This value was then adjusted for buffer dilution and protein concentration, with a final activity expressed as units per milligram per millilitre (units/mg/mL). Catalase (CAT) activity was measured in duplicate following methods (Claiborne, 1985) modified by *Craig et al., 2007*. Briefly, 10 μL of each fractioned homogenate was added to a reaction buffer (20 mM potassium phosphate, pH 7.0) in a 96-well UV-transparent plate. The reaction of CAT was initiated by adding10 μL of 800 mM stock H2O2, to a final concentration of 40mM, and the resulting decomposition of hydrogen peroxide was monitored by measuring the change in absorbance (240 nm) over time. CAT activity was calculated using the extinction coefficient of 43.6 $M^{-1}cm^{-1}$, adjusted for path length, and expressed as the amount of enzyme required to decompose 1.0 μM of hydrogen peroxide per minute. The final values were normalized to protein concentration and buffer dilution and reported as μmol/min/mg protein.

4.2.3 Quantification of cellular damage

Lipid peroxidation in brain tissue (n=6) was assayed using a commercial colorimetric lipid peroxidation (MDA) assay Kit (ab233471) (Abcam Limited, Cambridge, United Kingdom), following manufacturer's protocol. Brain samples (n=6, >20mg) were first washed with ice-cold PBS, then homogenized using an OMNI tissue homogenizer (Omni International, GA, USA) in 20 mM sodium phosphate buffer (pH 3.2) containing 0.5% Triton X-100. The homogenates were then centrifuged at 2,500 rpm for 5 minutes at 4°C. Lipid peroxidation (LPO) levels were measured in duplicate by directly quantifying malondialdehyde (MDA) in the supernatant at an absorbance of 695 nm using a Spectramax 190 spectrophotometer (Molecular Devices, CA, USA). MDA concentrations were determined against a standard curve of known values, adjusted for buffer dilution, normalized to protein concentration, and expressed as μM/mg protein.

DNA damage was quantified using a DNA oxidative damage ELISA kit (501130, Cayman Chemical, MI, USA), which detects 8-hydroxy-2′-deoxyguanosine (8-OHdG). Brain samples (n=6, >20mg) were homogenized in 5 μL of homogenization buffer (0.1 M phosphate buffer, pH 7.4, 1 mM EDTA) per mg of tissue and centrifuged at 2,500 rpm for 10 minutes at 4°C. DNA was extracted using a DNeasy Blood & Tissue DNA Extraction Kit (QIAGEN, Aarhus, Denmark) according to the manufacturer's protocol, then quantified using a Qubit fluorometer with the dsDNA HS Assay Kit (Thermo Fisher, MA, USA). Single-stranded DNA and RNA were enzymatically hydrolyzed into individual nucleotides using P1 nuclease. Subsequently, 1 unit of alkaline phosphatase was added per 100 μg of DNA, and the mixture was incubated at 37°C for 30 minutes, followed by heat inactivation at 100°C for 10 minutes. The sample was then immediately placed on ice before being assayed using the ELISA kit, in accordance with manufacturer's protocol. Absorbance was measured at 420 nm and corrected for non-specific binding. 8-OHdG concentrations (pg/mL) were calculated using a four-parameter logistic fit standard curve, normalized to DNA mass, and expressed as pg 8-OHdG/mg DNA.

4.2.5 Statistical analysis

Statistical analyses were performed using Python (Python Software Foundation, version 3.7). Data were imported and processed using the pandas library (McKinney, 2010). The

statistical model was constructed using the ordinary least squares (OLS) method from the statsmodels library (Seabold & Perktold, 2010). A two-way analysis of variance (ANOVA) was conducted, assessing the effects of treatment, time, and their interaction on the response variable. Post-hoc comparisons between treatment groups at different time points were performed using the Tukey HSD test. The results of the ANOVA and Tukey HSD test were examined to assess both main effects and interaction effects. Prior to statistical testing, data normality was assessed using the Shapiro-Wilk test, while homogeneity of variances was evaluated using Levene's test. If the assumptions of normality or homogeneity of variance were violated, data transformations (logarithmic base 10 or square root) were applied. Statistical significance was determined using an alpha (α) threshold of 0.05, with p-values less than α considered statistically significant.

4.3 Results

4.3.1 Antioxidant enzyme activity

In the cytosolic fraction, a two-way ANOVA revealed that SOD activity was significantly affected by treatment ($F_{2,45} = 35.35$, $p < 0.001$) and time ($F_{2,45} = 13.18$, $p < 0.001$). Post hoc Tukey HSD analysis confirmed a significant increase in SOD activity in both R-VEN and S-VEN treatments compared to the Control ($p < 0.001$); however, no significant difference was observed between R-VEN and S-VEN treatments ($p = 0.2208$). SOD activity significantly increased from Day 1 to Day 4 ($p = 0.0188$) and remained elevated through Day 14 without further significant change ($p = 0.9$). By Day 14, SOD activity in R-VEN and S-VEN treatments was 4.9-fold and 5.6-fold higher than in the Control, respectively ($p < 0.001$). In the mitochondrial fraction, there was a significant interaction effect between treatment and time ($F_{4,45} = 10.37$, $p < 0.001$). A Tukey post-hoc test revealed that SOD activity was significantly higher in the S-VEN treatment at Day four by 2.8-fold ($p = 0.0305$), and this increase persisted through Day 14, reaching a 3.08-fold change compared to Control ($p < 0.001$). By Day 14, R-VEN treatment resulted in a 2.9-fold higher SOD activity compared to Control ($p < 0.001$). At this time point, there was no significant difference between S-VEN and R-VEN treatments.

GPX activity was significantly affected by treatment in both the cytosolic ($F_{2,45} = 49.10$, $p < 0.0001$) and mitochondrial ($F_{2,45} = 40.17$, $p < 0.0001$) fractions. A post-hoc Tukey HSD test revealed that in the cytosolic fraction, GPX activity was significantly higher in the R-VEN

treatment by 2.47 fold ($p < 0.001$), however activity in the S-VEN treatment was also significantly higher than the Control by 4.51 fold ($p < 0.001$) and was higher than R-VEN treatment ($p < 0.001$). In the mitochondrial fraction there was also a significant increase in GPX activity following R-VEN treatment by 4.23 fold ($p < 0.01$), and S-VEN treatment by 5.07 fold ($p < 0.01$). However, no significant difference in GPX activity was observed between treatments, and similarly no significant time-dependent differences were detected.

A significant interaction effect between treatment and time was observed for both cytosolic ($F_{4,45} = 3.82$, $p = 0.009$) and mitochondrial ($F_{4,45} = 3.02$, $p = 0.027$) relative CAT activity. Post-hoc Tukey HSD tests showed that in the cytosolic fraction, S-VEN exhibited significantly higher relative CAT activity compared to both Control (2.9-fold, $p < 0.001$) and R-VEN (2.7-fold, $p < 0.001$) at day one, with S-VEN also showing increase in activity at Day 14 compared Control (1.7-fold, $p < 0.001$) and R-VEN (2.23-fold, $p<0.001$). In contrast, Control and R-VEN showed no significant differences across time points. In the mitochondrial fraction, relative CAT activity was significantly higher in the S-VEN treatment group at Day 14 compared to both R-VEN (2.5-fold, $p < 0.001$) and Control (2.3-fold, $p < 0.001$). However, there was no significant difference in activity between treatments on Day 1 or Day 4. There was also no significant change in S-VEN activity over time, although S-VEN at Day 14 narrowly missed statistical significance when compared to Day 1 ($p = 0.051$).

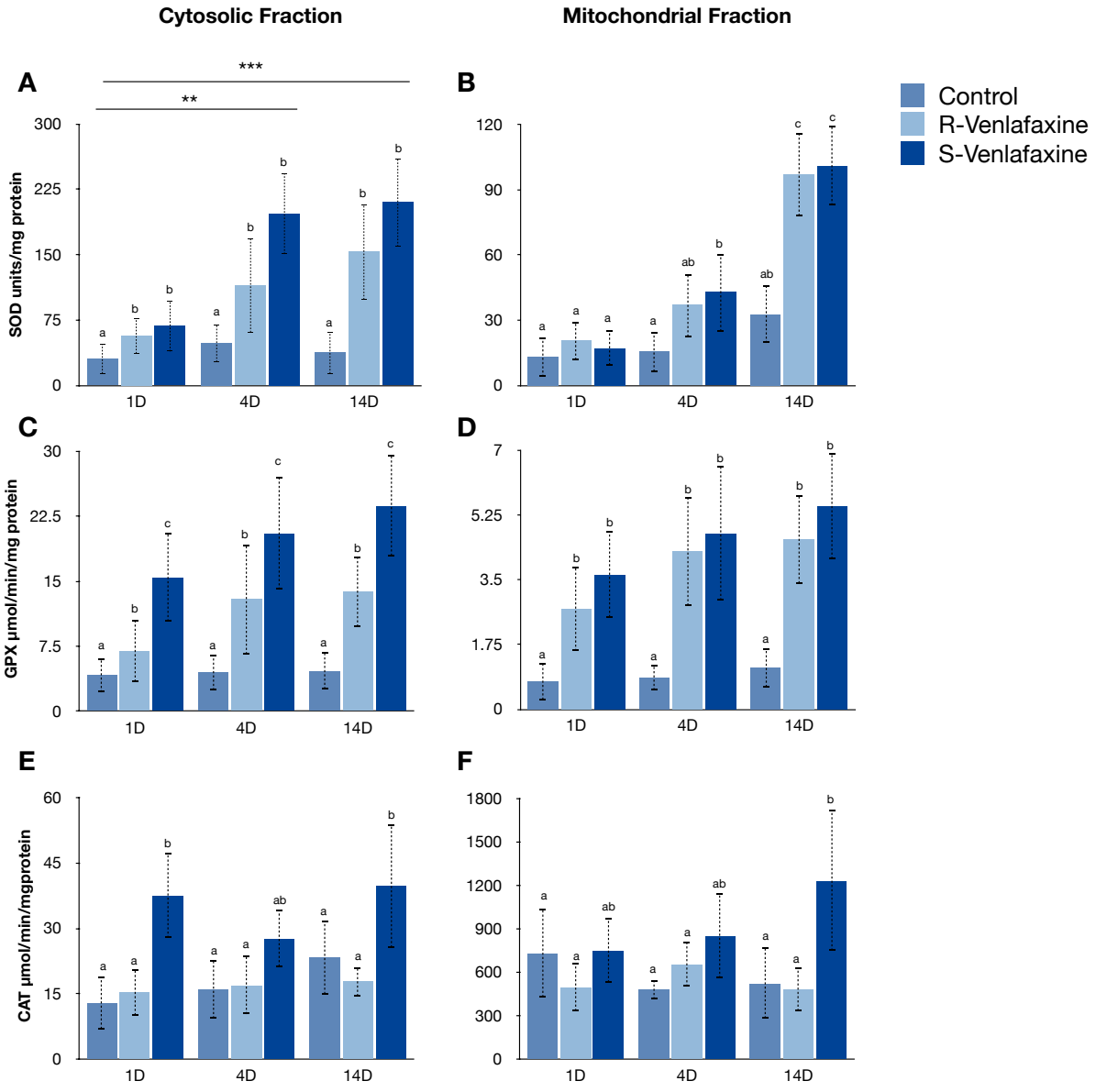


Figure 4.2: Activity of antioxidant enzymes in the cytosolic and mitochondrial fractions of brain tissue from rainbow darter (*Etheostoma caeruleum*) exposed to R- and S-venlafaxine for 1, 4, and 14 days (n = 6). (A, B) Superoxide dismutase (SOD) activity (units/mg protein) in the cytosolic (A) and mitochondrial (B) fractions. (C, D) Glutathione peroxidase (GPX) activity (µmol/min/mg protein) in the cytosolic (C) and mitochondrial (D) fractions. (E, F) Catalase (CAT) activity (µmol/min/mg protein) in the cytosolic (E) and mitochondrial (F) fractions. Data is presented as means ± SD, compared using a Two-way ANOVA and post-hoc Tukey test ($p < 0.05$, n = 6 per treatment per time-point. (A) Asterisks indicate significant differences between time points for a given treatment group (**$p < 0.01$, *$p < 0.001$) and lowercase letters indicate significant differences between treatment groups within each time point (Tukey HSD, $p < 0.05$).

(B-F) Bars labeled with different letters (a, b, c) differ significantly (Tukey HSD, $p < 0.05$). Groups sharing a letter (e.g., 'ab') are not significantly different from either 'a' or 'b' groups.

4.3.2 Cellular damage

A two-way ANOVA revealed a significant interaction effect between VEN treatment and time on MDA concentrations ($F_{4,45} = 4.77$, $p = 0.003$). Post hoc analysis indicated that S-VEN treatment led to a significant increase in MDA levels across all time points compared to the Control group. Specifically, MDA concentrations were elevated 5.8-fold at day one ($p < 0.0001$), 12.7-fold at day four ($p < 0.001$), and 2.9-fold at Day 14 ($p = 0.001$), with no significant difference between day four and Day 14 ($p > 0.05$), suggesting a steady-state response. S-VEN also induced significantly higher MDA concentrations than R-VEN on day four ($p < 0.001$). In contrast, R-VEN treatment exhibited a delayed response, with MDA levels significantly increasing by 4.2-fold on day four ($p < 0.001$) and further rising to 2.7-fold above Control levels by Day 14, at which point concentrations were comparable to those observed in the S-VEN group ($p > 0.05$). Additionally, MDA concentrations increased over time in the Control group, with a significant rise between day four and day fourteen ($p < 0.001$).

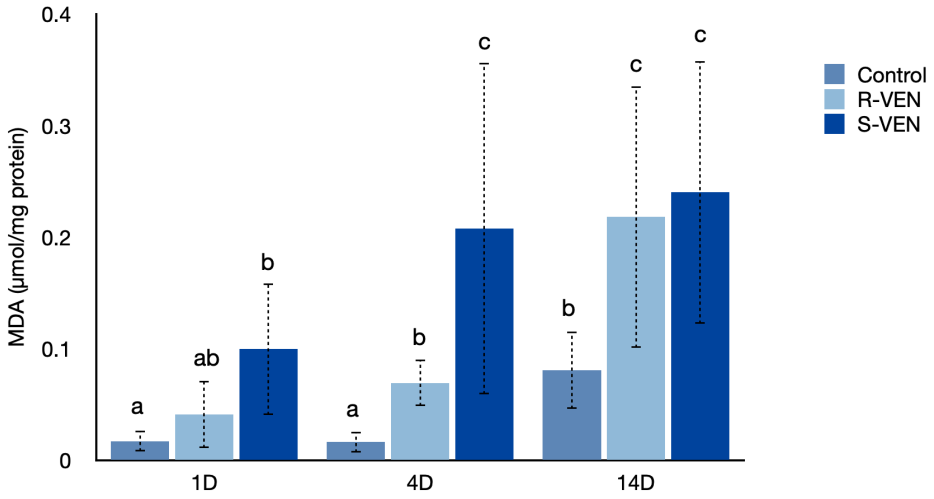


Figure 4.3: Levels of malondialdehyde (MDA; µmol/mg protein) in brain tissue from rainbow darter exposed (*Etheostoma caeruleum*) to R- and S-venlafaxine for 1, 4, and 14 days. Data is presented as means ± SD, compared using a Two-way ANOVA and post-hoc Tukey test ($p < 0.05$, $n = 6$). Bars labeled with different letters (a, b, c) differ significantly (Tukey HSD, $p < 0.05$). Groups sharing a letter (e.g., "ab") are not significantly different from either "a" or "b" groups.

DNA damage was quantified by measuring the concentration of 8-hydroxy-2'-deoxyguanosine (8-OHdG), a primary oxidized derivative of deoxyguanosine and a key marker of oxidative DNA damage. A two-way ANOVA revealed a significant interaction between time and treatment ($F_{4,45} = 11.48$, $p < 0.001$). Post-hoc analysis indicated that at Day 4, 8-OHdG concentrations in S-VEN-exposed fish were significantly elevated, increasing 2.2-fold relative to the Control group ($p < 0.001$) and 2.5-fold relative to R-VEN-exposed fish ($p < 0.001$). Within the S-VEN treatment, 8-OHdG concentrations at Day 14 were 2.5-fold higher than at Day 1 ($p = 0.001$) and 3.1-fold higher than at Day 14 ($p = 0.001$), suggesting a transient peak in oxidative DNA damage. In contrast, at Day 1, 8-OHdG concentrations in S-VEN-exposed fish were significantly lower than in the Control group, decreasing 0.53-fold ($p = 0.031$). By Day 14, levels remained lower, with a 0.51-fold reduction relative to Controls ($p = 0.044$). Similarly, at Day 14, 8-OHdG concentrations in R-VEN-exposed fish were significantly lower than in Control, decreasing by 0.40-fold ($p = 0.031$).

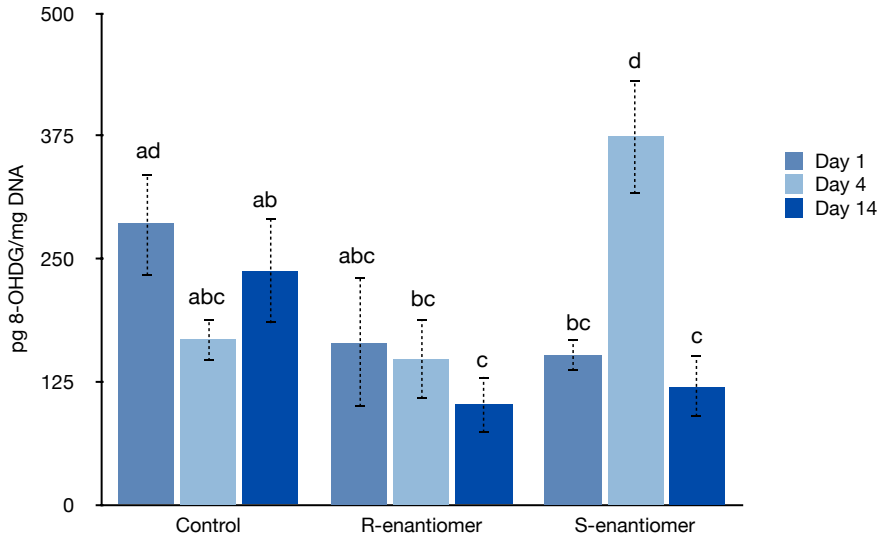


Figure 4.4: Levels of 8-hydroxy-2'-deoxyguanosine (8-OHdG; pg/8-OHdG/mg DNA) as in brain tissue from rainbow darter (*Etheostoma caeruleum*) exposed to R- and S-venlafaxine for 1, 4, and 14 days. Sampling days a grouped by treatment. Data is presented as means ± SD, compared using a Two-way ANOVA and post-hoc Tukey test ($p < 0.05$, $n = 6$). Bars labeled with different letters (a, b, c, d) differ significantly (Tukey HSD, $p < 0.05$).

4.4 Discussion

This study investigated the differential effects of R-venlafaxine (R-VEN) and S-venlafaxine (S-VEN) on antioxidant enzyme activities within cytosolic and mitochondrial fractions of brain tissue over fourteen days. The observed increases in superoxide dismutase (SOD), glutathione peroxidase (GPX), and catalase (CAT) activities suggest a compensatory antioxidant response to venlafaxine-induced oxidative stress. To evaluate cellular damage, 8-hydroxy-2'-deoxyguanosine (8-OHdG) and malondialdehyde (MDA) levels, which reflect oxidative DNA damage and lipid peroxidation respectively, were measured. While venlafaxine exposure induced lipid peroxidation, the enhanced ROS-scavenging activity appeared to mitigate DNA damage. Notably, the temporal patterns of enzyme activity and lipid peroxidation revealed enantiomer-specific differences, with S-VEN eliciting a more pronounced and rapid response compared to R-VEN. These findings emphasize the importance of stereochemical considerations in assessing the oxidative impact of pharmaceutical exposure in fish.

4.4.1 Enzyme activity

Both enantiomers significantly increased SOD activity in the cytosolic fraction at all measured time points, with a notable elevation as early as Day 1. Activity continued to rise through Day 4 and remained elevated through Day 14. The absence of a significant difference between R-VEN and S-VEN suggests that both enantiomers induce SOD1 activity to a similar extent. In the mitochondrial fraction, VEN exposure led to a delayed increase in SOD2 activity, with both enantiomers showing significant elevations by Day 14. However, S-VEN induced this increase earlier, with activity rising significantly by Day 4, indicating a more rapid mitochondrial response compared to R-VEN. The observed increases in SOD1 and SOD2 activity following VEN exposure are consistent with a cellular response to elevated superoxide levels, suggesting that VEN may induce superoxide production in both cytosolic and mitochondrial compartments (Fridovich, 1981; Buettner, 2011).

GPX activity also increased significantly following both R-VEN and S-VEN treatments at all time points. In the cytosolic fraction, S-VEN elicited a higher response, nearly doubling the activity observed with R-VEN. In contrast, mitochondrial GPX activity increased similarly with both enantiomers, with no significant difference between treatments. The consistent elevation of

GPX activity suggests a rapid and sustained antioxidant response. While S-VEN may stereoselectively enhance cytosolic GPX activity, both enantiomers contributed to its increased activity. These findings indicate that VEN exposure, regardless of enantiomer, may elevate hydrogen peroxide and potentially lipid hydroperoxides (Little et al., 1970). The sustained increase of GPX activity suggests persistent oxidative stress, necessitating continuous antioxidant compensation.

S-VEN treatment significantly increased cytosolic CAT activity compared to both the control and R-VEN treatment, with the greatest elevations observed at Day 1 and Day 14. Meanwhile, mitochondrial CAT activity following S-VEN exposure exhibited a delayed response, increasing significantly only at Day 14. In contrast, R-VEN did not significantly alter CAT activity in either cellular compartment throughout the time course. This pattern suggests that S-VEN exposure may increase cytosolic peroxide production, with higher mitochondrial peroxide formation occurring later in response to prolonged exposure (Dringen & Hamprecht, 1997). Elevated GPX activity within the mitochondrial fraction beginning at Day 1 following S-VEN treatment may effectively neutralize peroxide production, potentially keeping peroxide concentrations sufficiently low to prevent additional induction of CAT beyond its baseline activity (Baud et al., 2004). Similarly, if R-VEN induces lower peroxide production that remains within the neutralizing capacity of GPX or baseline CAT activity in either fraction, additional activation of CAT may be unnecessary. In contrast, the delayed increase in mitochondrial CAT activity following prolonged S-VEN exposure suggests that peroxide accumulation eventually surpasses the neutralizing capability of GPX and baseline CAT, necessitating enhanced CAT activity to manage elevated peroxide levels (Baud et al., 2004).

The observed increase in antioxidant enzyme activity strongly suggests that VEN exposure induces ROS production, potentially arising from cytochrome P450 (CYP) enzyme activity, mitochondrial dysfunction, alterations in energy metabolism, or a combination of these pathways. In mammals, VEN is primarily metabolized by CYP2D6 and CYP3A4, producing O-desmethylvenlafaxine (ODV) and N-desmethylvenlafaxine (NDV) (Otton et al., 1996; Fogelman et al., 1999). Both of these CYP isoforms can generate superoxide and hydrogen peroxide when their catalytic cycles become partially uncoupled, with CYP3A4 in particular exhibiting higher uncoupling due to its flexible active site (Veith & Moorthy, 2018; Albertolle & Guengerich, 2018). In fish, few direct orthologs to mammalian CYP2D6 exist; instead, they rely on a

combination of less-characterized CYP isoforms that primarily perform N-demethylation of VEN (Santos et al., 2020; Jin et al., 2023). This process can be inefficient, and excessive uncoupling of CYP metabolism can promote direct hydrogen peroxide formation (Veith & Moorthy, 2018). Moreover, the enzyme CYP2E1, known in mammals to be relatively prone to electron leakage, has also been implicated in VEN-induced oxidative stress and cytotoxicity (Ahmadian et al., 2016). When CYP2E1 activity is high, superoxide and hydrogen peroxide generation increase substantially, thereby challenging antioxidant defences. In contrast, inhibition of CYP2D6 also exasperated ROS generation and cytotoxicity, likely due to increased VEN accumulation (Ahmadian et al., 2016). Although the exact contribution of CYP2E1-like enzymes to VEN metabolism is unclear in fish, similar activity could further heighten ROS generation. Thus, inefficient metabolism likely creates a twofold stress: (i) excessive ROS leakage from CYP-catalyzed reactions and (ii) increased VEN accumulation that could disrupt other cellular processes, including mitochondrial function. Additionally, poor CYP metabolism likely contributes to the bioaccumulation of VEN, as incomplete metabolism prolongs its residence time and elevates local concentrations in tissues, including the brain (Arnnok et al., 2017; Santos et al., 2020). This bioaccumulation may also explain why GPX, SOD and CAT activity increases over time, as cellular VEN concentration magnify.

In the brain, VEN may alter mitochondrial function, potentially through its modulation of serotonergic and noradrenergic neurotransmission, which enhances postsynaptic activity. However, this effect could also result from transcriptional and biochemical alterations in energy metabolism (Kalman et al., 2005; Scaini et al., 2011; Brivio et al., 2023; Gardea-Resendez et al., 2023). While increased mitochondrial respiration may lead to elevated ROS production, there is limited evidence of direct mitochondrial dysregulation *in vitro* in the brains of fish exposed to VEN (Robichaud et al., 2024). Given the potential for VEN to influence mitochondrial activity through both neurotransmission and metabolic pathways, further research is needed to elucidate its role in mitochondrial function and ROS dynamics, particularly in non-mammalian models.

These results align with and are further supported by existing research, which has documented similar antioxidant enzyme modulations following venlafaxine exposure. In rat liver, VEN treatment was followed by ROS production, and glutathione depletion (Ahmadian et al., 2016). Acute 30-minute exposure of zebrafish to venlafaxine caused dose-dependent effects in brain tissue, including enhanced antioxidant enzyme activities (SOD, GST) at 150 mg/L

concentrations (Alves et al., 2023). Following chronic racemic VEN exposure Ziegler et al. (2020) demonstrated an increase in SOD activity in brown trout larvae (10µg/L), and Mehdi et al. (2019) found no effect on CAT activity in zebrafish muscle (1µg/L). The few studies that have specifically analysed stereoselective effects of VEN exposure are somewhat inconsistent. Loach (*Misgurnus anguillicaudatus*) exposed to either VEN enantiomer (500 µg/L) for four days exhibited increased SOD in the liver, with the R-VEN enantiomer inducing a greater increase (Qu et al., 2019). In whole zebrafish embryos, exposure to R-VEN decreased SOD activity compared to S-VEN, while S-VEN reduced CAT activity and increased GPX activity relative to R-VEN and racemic venlafaxine in a concentration-dependent manner (0.3–3µg/L) (Ribeiro et al., 2022). The differential responses to each enantiomer observed between studies highlight the complexity of the impact of VEN on fish, suggesting that factors such as concentration, exposure duration, developmental stage, tissue type, and potentially species-specific differences may influence VEN's overall impact. Additionally VEN can modulate epigenetic regulation of SOD, GPX, and CAT, and has demonstrated an induction of both CAT promoter methlyation and reduced mRNA expression (Wigner et al., 2020). Thus, beyond direct oxidative stress modulation, VEN may exert longer-term effects on antioxidant capacity through epigenetic mechanisms, further complicating the interpretation of antioxidant responses across different exposure conditions. Assessing markers of oxidative damage, such as lipid peroxidation and DNA oxidation, alongside antioxidant enzyme activity, provides a more comprehensive understanding of the cellular consequences of VEN exposure.

4.4.2 Markers of cellular damage

In this present study MDA levels were quantified in brain tissue following R and S-VEN exposure, as a proxy for lipid peroxidation. MDA levels increased over time in all groups, including the control, potentially due to inherent stress occurring during the experiment in a lab setting (Barton, 2002). Treatment with S-VEN resulted in a significant increase in MDA levels compared to the control group. This increase was more rapid, and sustained between acute and longer term exposure. Although the R-VEN treatment also showed an increase in MDA levels, this increase was not significant until Day 4, and did not reach similar concentrations as S-VEN treatment until Day 14. The elevated MDA due to longer term R- and S-VEN treatment are indicative of ROS-induced lipid peroxidation in the brain (Sies & Cadenas, 1985; Marnett, 1999; Fritz & Petersen, 2013). Despite increased GPX and SOD activity, antioxidant defences were

insufficient to mitigate oxidative damage, suggesting that ROS production exceeded the scavenging capacity of these enzymes (Ahmadian et al., 2016). Moreover, S-VEN appears to have a more rapid induction of lipid peroxidation than R-VEN despite relatively higher activity of GPX and CAT in the cytosol.

The observed increase in MDA is supported by a recent study in zebrafish, which reported similar elevations in brain tissue MDA levels following VEN administration, alongside anxiolytic-like behaviors and markers indicative of neuroendocrine disruption (Alves et al., 2023). Likewise, Maulvault et al. (2019) also demonstrated elevated lipid peroxidation in the brain of meagre (*Argyrosomus regius*) following VEN exposure. In rat liver, VEN exposure resulted in lipid peroxidation followed by loss of lysosmal membrane integrity, mitochondrial membrane potential collapse, and cell death (Ahmadian et al., 2016). Elevated lipid peroxidation in the brain is particularly concerning due to its dual impact. Beyond the initial disruption of membrane architecture, fluidity, and permeability caused by direct ROS assault (Bhattacharjee, 2014), the resulting byproducts are both highly reactive and neurotoxic. These byproducts disrupt ion channels, signal transduction pathways, and microtubules (Mattson, 1998; Keller & Mattson, 1998; Montine, 2002), triggering cascades of neurodegenerative processes that can ultimately lead to cell death (Keller & Mattson, 1998). Such processes have been linked to several neurodegenerative conditions in mammals (Peña-Bautista et al., 2019; Angelova et al., 2021) and elevated MDA has also been associated with a range of psychiatric and behavioral disorders (Joshi & Praticò, 2014). If lipid peroxidation due to VEN exposure in this present study was substantial enough to induce such neurodegeneration, it may partially explain some of the maladaptive behavioral changes observed in fishes exposed to VEN, which cannot always be fully explained by alterations in brain serotonin levels alone (Bisesi et al., 2014). Prenatal exposure to VEN in mice has been associated with increased ROS production, neurodegeneration, and long-term behavioral impairments (Singh et al., 2015). These findings are potentially relevant for fish populations, as externally fertilized eggs and newly hatched fry may be exposed to environmental VEN, which could disrupt early developmental processes. The current findings demonstrate the neurotoxic potential of VEN, highlighting its ability to induce oxidative stress and lipid peroxidation that can disrupt critical cellular structures and functions. However, given the context-specific nature of these effects, it is difficult to draw definitive conclusions about neurotoxicity based on MDA levels alone. Therefore, future work should

include immunohistochemistry and histological examinations to assess and confirm cellular damage (Montine, 2002; Singh et al., 2015).

DNA damage was assessed by measuring the levels of 8-OHdG, a marker of DNA oxidation, which changed differently over time depending on the treatment received. Specifically, on Day 4, fish treated with the S-VEN showed significantly higher 8-OHdG compared to the control group and fish treated with R-VEN. While the R-VEN treatment and control did show a decrease in 8-OHdG over time, these changes were not significant. However, by Day 14, both R-VEN and S-VEN treatment exhibited significantly lower 8-OHdG levels compared to the control group on the same day. This suggests that longer term exposure to VEN, regardless of enantiomer may have a protective effect against DNA damage in brain tissue. This protective effect is potentially due to the increased activity of ROS. Conversely the transient increase at Day 4 in the S-VEN treatment may be due to elevated oxidative damage, that is later mitigated by scavengers and repaired over time. A similar decrease in 8-OHdG levels following VEN treatment has been reported in the mouse hippocampus, likely as a result of increased ROS scavengers (Abdel-Wahab & Salama, 2011). However, DNA damage measured using the comet assay showed elevated DNA damage in mouse brains following treatment with VEN (Madrigal-Bujaidar et al., 2021). This discrepancy may be due to differences in DNA damage quantification methods, as the 8-OHdG ELISA assay used in the present study specifically measures ROS-induced DNA oxidation but does not account for DNA adduct formation caused by reactive aldehydes generated during lipid peroxidation (Gentile et al., 2017). The limited availability of literature demonstrating the influence of VEN exposure on oxidative DNA damage in fish brains specifically, highlights a gap in our current knowledge that this work begins to address.

The observed stereoselective activity of VEN may be attributed to the distinct pharmacological profiles of its enantiomers, with R-VEN inhibiting both norepinephrine and serotonin reuptake, whereas S-VEN inhibits only the serotonin reuptake (Hancu et al., 2021). These differences may influence fish behaviour in distinct ways (Ribeiro et al., 2022) and could also contribute to stereospecific modulation of mitochondrial function (Scaini et al., 2011; Gardea-Resendez et al., 2023), as well as monoamine accumulation followed by MAO-mediated oxidation and ROS production (Edmondson, 2009). Further, enantio-specific ROS production may arise from the differential metabolism of each enantiomer, as fish exhibit a metabolic preference for S-VEN, although this preference may be species-specific (Qu et al., 2019; Jin et

al., 2023), leading to stereoselective and tissue-specific bioaccumulation (Santos et al., 2020; Jin et al., 2023). Moreover, such metabolic preferences could lead to the formation of different metabolites with varying capacities to inhibit serotonin and norepinephrine reuptake, potentially resulting in differential physiological or behavioral effects (Hancu et al., 2021). However, such conclusions on metabolic capacity cannot be made without directly measuring VEN and its metabolites in the studied tissue. Future work should quantify these values to further elucidate the mechanisms underlying these stereoselective effects.

4.5 Conclusions

The results of this study suggest that both R-VEN and S-VEN enantiomers increase antioxidant enzyme activity at environmentally relevant concentrations, which may induce cellular damage. This was demonstrated through elevated SOD and GPX activity, in both cytosolic and mitochondrial fractions of RBD brain tissue following 14 Day exposure. Despite similar effects on SOD activity between enantiomers, S-VEN has a greater influence on GPX activity in the cytosol and CAT activity increased across both cellular compartments, although only after longer exposure. The increase in MDA levels, particularly more rapidly with S-VEN treatment, indicates that the antioxidant responses observed are insufficient to fully counteract VEN-induced oxidative stress and lipid peroxidation. This demonstrates that S-VEN may have a more detrimental impact on RBD populations exposed to this enantiomer even for shorter periods, as elevated MDA in the brain may be a sign of neurotoxicity. Oxidative DNA damage was not readily observed, and may even be protected against following chronic VEN treatment. These findings highlight the value of assessing both proxies for oxidative stress and cellular damage when assessing the oxidative effects of pharmaceuticals present in WWTPE. Additionally, the stereoselectivity observed demonstrates the importance of evaluating individual enantiomers rather than racemic mixtures when assessing the environmental and physiological impacts of VEN and other chiral pharmaceuticals, especially considering the potential for enantiomer enrichment in effluent. Without direct measurement of VEN metabolites in fish tissues, linking stereospecific ROS production to enantiomeric metabolism or bioaccumulation remains speculative. Future research should focus on elucidating the precise metabolic pathways involved in VEN detoxification, quantifying VEN and its metabolites within tissues, and

employing comprehensive cellular damage assessments to better understand the long-term implications of VEN exposure on aquatic organisms.

Chapter 5

Conclusion - Synthesis and implications

5.1 Overview

This thesis aimed to investigate the systemic effects of wastewater treatment plant effluent (WWTPE) and venlafaxine (VEN) exposure on *Etheostoma* spp., using transcriptomic and biochemical analyses to infer molecular, physiological, and organismal responses. To achieve these objectives, a combination of field-based and laboratory-controlled experiments was conducted, employing RNA sequencing, differential expression analysis, gene ontology enrichment, and biochemical assays to assess oxidative stress and cellular damage. Findings from this thesis provide insight into how WWTPE exposure alters hepatic function and stress responses in freshwater fish and highlight the enantiomer-specific impacts of VEN exposure at environmentally relevant concentrations. These results contribute to a deeper understanding of the ecological effects associated with pharmaceutical contaminants in aquatic environments.

5.2 Effects of WWTPE on darters (*Etheostoma* spp.)

The detection of elevated pharmaceutical concentrations downstream of the Waterloo WWTP, including venlafaxine, diclofenac, and carbamazepine, emphasize the persistent and pervasive nature of effluent-driven pollution in this watershed. These findings contribute to a growing body of evidence that pharmaceutical contamination is not a localized concern but a global environmental issue, with wastewater effluent serving as a significant vector for biologically active compounds in freshwater systems worldwide (Metcalfe et al., 2010; Schultz et al., 2010; Schlüsener et al., 2015; Huerta et al., 2018; Chen et al., 2022; Wilkinson et al., 2022). The widespread presence of pharmaceuticals in surface waters has raised concerns about their potential to compromise the health of aquatic organisms (Wilkinson et al., 2022).

Transcriptomic analysis of darter liver revealed significant shifts in immune-related pathways, most notably complement, cytokine, and inflammasome signalling, indicating that WWTPE contaminants may invoke an atypical, and potentially maladaptive, inflammatory state. Energy metabolism and lipid homeostasis were also broadly disrupted, with species-specific differences in cholesterol regulation, fatty acid oxidation, and sterol biosynthesis pathways. The consistent disruption of immune and inflammatory signalling, alongside lipid metabolic dysregulation, underscores these processes as hallmarks of effluent-induced physiological stress. This is supported by previous studies that have observed immunomodulatory effects and lipid

metabolism dysregulation in response to the complex mixture of contaminants present in WWTPE (Salo et al., 2007; Hébert et al., 2008; Arstikaitis et al., 2014; Sarma et al., 2015; Hamid et al., 2021; Sun, 2023). However, while these findings highlight that similar biological pathways were disrupted across species, the specific transcriptomic responses recruited within these processes were distinct, reflecting species-specific sensitivities and adaptive strategies.

Greenside darters exhibited the most uniquely affected biological pathways, particularly those related to hemoglobin, cytoskeletal remodelling, and DNA repair and replication. However, they also shared the highest number of DEGs with other species, suggesting a mix of species-specific and conserved molecular responses. Moreover, while some species like fantail darters showed an apparent suppression of mitochondrial activity and protein homeostasis pathways, others like johnny darters upregulated electron transport chain components, suggesting contrasting strategies for coping with the same contaminant-induced stress. This diversity of responses not only deepens our understanding of species-level responses and adaptive strategies but also highlights caution in assuming uniform effects of contaminants across related taxa.

The transcriptomic responses observed in darters down stream of the Waterloo WWTP outfall align with known pharmacological effects of various PhACs in fish. Statins and fibrates, for example, disrupt cholesterol biosynthesis and fatty acid metabolism, while NSAIDs can interfere with inflammatory signalling and immune regulation (Hoeger et al., 2005; Blonç et al., 2023). Antidepressants such as venlafaxine modulate serotonergic signalling and neuroendocrine function, leading to systemic effects in fish. These include alterations in glucose metabolism and utilization, as well as amino acid and fatty acid metabolism (Best et al., 2014; Mehdi et al., 2019; Costa et al., 2021; Santos et al., 2023). Detoxification pathways involving CYP-mediated metabolism is indicative of drug detoxification processes (Corcoran et al., 2012; Uno et al., 2012; Burkina et al., 2015). These pharmaceuticals may also exert additive, synergistic, or antagonistic effects, leading to complex physiological outcomes in a manner that complicates the interpretation of individual drug responses (Celander, 2011; Matthee et al., 2023). Despite the challenge of isolating the effects of individual pharmaceuticals in mixed exposures, this study provides evidence that effluent-associated pharmaceuticals drive both shared and species-specific transcriptional responses, potentially leading to metabolic trade-offs, altered stress axis regulation, and impaired organismal fitness.

The similarity in affected pathways between darters also suggests physiological stress, which can activate the hypothalamus-pituitary-interrenal (HPI) axis, triggering the release of neuroendocrine factors like cortisol. While cortisol may initially enhance immune function, chronic exposure can lead to immune suppression (Nardocci et al., 2014). This immunosuppression is partly a consequence of energy reallocation to cope with prolonged stressors and to prevent excessive inflammation, a process well-documented in teleost fish (Wendelaar Bonga, 1997; Tort, 2011). Chronic dysregulation of immune processes may increase susceptibility to infections and ultimately reduce individual fitness (Mauri et al., 2011; Small & Bilodeau, 2007; Ndong et al., 2007). Cortisol also mobilizes energy stores by regulating metabolic pathways, including promoting lipolysis to release free fatty acids and glycerol for energy production in fish (Wendelaar Bonga, 1997; Mommsen et al., 1999; Schreck & Tort, 2016). Additionally, alterations in lipid metabolism may reflect energy reallocation in response to oxidative stress and lipid peroxidation, as cells prioritize fatty acid oxidation or membrane repair (Dépatie et al., 2020; Gonçalves et al., 2021). If these metabolic transcriptional adaptations observed in this study are maintained at the organismal level in natural populations, they may alter energy allocation toward life history traits such as growth, reproduction, and survival (Pankhurst & Van Der Kraak, 1997; Van Weerd & Komen, 1998; Zera & Harshman, 2001; Canosa & Bertucci, 2023). Chronic exposure to effluent-induced stressors may therefore contribute to alterations in key fitness-related traits in exposed populations.

Although it is challenging to determine species susceptibility to WWTPE based on transcriptomic data alone, fantail darters exhibited the highest number of DEGs and widespread transcriptional suppression of critical biological functions rather than adaptive adjustments. These fish demonstrated extensive downregulation of pathways involved in complement system function, fatty acid oxidation, cholesterol metabolism, and mitochondrial protein handling, indicating compromised metabolic and immune function. In contrast to johnny and rainbow darters, which exhibited potentially adaptive metabolic shifts, fantail darters showed broad dysregulation of ATP synthesis and oxidative phosphorylation pathways, further suggesting mitochondrial dysfunction and impaired energy production. Additionally, the extensive downregulation of protein-handling processes, including the proteasome and heat shock proteins (HSPs), is particularly concerning, as it indicates a reduced ability for protein maintenance and cellular stress recovery. This diminished capacity to manage proteotoxic stress may limit their ability to cope with environmental challenges, making them more vulnerable to effluent exposure

(Feder & Hofmann, 1999; Pirkkala et al., 2000; Shang & Taylor, 2011). Further, the downregulation of CYP-mediated xenobiotic metabolism suggests a reduced capacity to detoxify contaminants and process pharmaceutical pollutants present in WWTPE, potentially limiting resilience in polluted habitats (Franco et al., 2025). Together, these findings suggest that fantail darters may be particularly susceptible to effluent exposure, with a physiological response profile characterized by broad metabolic and immune suppression rather than compensatory adaptation.

While fantail darters exhibited widespread ETC pathway suppression, the upregulation of mitochondrial respiratory pathways in johnny darters suggests a compensatory response to sustain ATP production under effluent exposure, potentially due to increased metabolic demands observed in fish following WWTPE exposure (Du et al., 2019). A study by Gauvreau et al. (2022), conducted at the same downstream site and sampling period as this study, found that condition factor indices varied among rainbow, fantail, and greenside darters across seasons. However, downstream johnny darters consistently exhibited shorter body lengths and significantly lower Fulton's condition factors compared to their upstream counterparts, suggesting reduced physiological condition within this population. These indices serve as proxies for individual health and vigor, reflecting an organism's capacity to allocate energy toward essential processes such as growth and maintenance (Bolger & Connolly, 1989; Hendry et al., 1999). This pattern is consistent with the observed upregulation of mitochondrial respiratory pathways in johnny darters, which may reflect a compensatory mechanism to sustain ATP production under effluent-induced stress (Du et al., 2019). Increased metabolic activity may impose energetic trade-offs, diverting resources from growth and potentially contributing to reduced condition in downstream populations. However, the direct relationship between mitochondrial activity and growth remains speculative and is likely influenced by broader metabolic factors, including lipid metabolism (Allen et al., 2016; Quéméneur et al., 2022; Canosa et al., 2023).

Overall, the results of this work indicate that wastewater effluent from the Waterloo MWWTP, comprising a complex mixture of biologically active pharmaceuticals, elicits significant species-specific transcriptomic alterations in darter populations. Although similar biological pathways are affected across taxa, the divergent responses observed suggest variable sensitivities and adaptive strategies, which may translate into differential fitness and reproductive success. Over time, such species-specific responses could alter population dynamics in favour of

taxa better equipped to mitigate chronic contaminant stress, with potential ramifications for aquatic community structure. Consequently, this study highlights the critical need for enhanced wastewater management practices and demonstrates caution in assuming uniform effects of contaminants across closely related taxa.

5.3 Enantiomer-Specific effects of venlafaxine

This thesis set out to elucidate the stereoselective effects of the R- and S-enantiomers of VEN on rainbow darter and compare these enantiomer-specific responses with those elicited by environmental effluent exposure. Some transcriptional changes were shared, including the consistent upregulation of *gabbr2* and *ll*, implicating VEN exposure in the disruption of GABAergic signalling and innate immune response in the liver. However, the two enantiomers elicited distinct transcriptional signatures. R-VEN exerted broader transcriptional effects on lipid, amino acid, and bile acid metabolism, as well as vesicular trafficking and immune signalling. Collectively, these findings suggest that R-VEN exposure may generally affect liver metabolic function, potentially contributing to cholestatic injury and oxidative stress**.** In contrast, S-VEN exposure induced upregulation of genes involved in epigenetic regulation, lipid and DNA damage response, and cellular remodelling. These changes may reflect adaptive repair mechanisms due to cellular oxidative damage induced by S-VEN exposure, which could signify disruptions to normal cell proliferation and tissue homeostasis. The distinct hepatic effects of each enantiomer may be linked to VEN metabolism. Previous studies indicate a preference for S-VEN metabolism in fish (Qu et al., 2019; Santos et al., 2020; Jin et al., 2023) which may produce ROS through inefficient CYP-mediated detoxification. Additionally, these differences may be influenced by the greater affinity of R-VEN for serotonergic and noradrenergic reuptake inhibition. Norepinephrine signalling plays a role in regulating glycogenolysis and gluconeogenesis in fish (Danulat & Mommsen, 1990; Tocher, 2003), and sustained elevation of norepinephrine potentially depresses hepatocellular transport capacity (Wang et al., 2000). Thus sustained peripheral norepinephrine signalling may be influencing the observed affected pathways in vesicular transport.

Despite similarities in the biological pathways affected by VEN enantiomers and effluent exposure, particularly in lipid and energy metabolism, immune modulation, and cell adhesion, the specific mechanisms and transcripts involved were not identical. Only a small subset of genes

exhibited parallel expression changes in both S-VEN-exposed and effluent-exposed Rainbow Darters, indicating that VEN contributes to, but does not fully account for, the broader hepatic transcriptomic disturbances observed in wild fish from effluent-impacted sites. Furthermore, the distinct set of differentially expressed transcripts modulated by effluent exposure underscores the complexity of wastewater mixtures, highlighting the interactions of multiple contaminants beyond VEN in driving hepatic responses in situ.

This thesis also provides evidence that chronic exposure to environmentally relevant concentrations of VEN disrupts redox homeostasis in the brain of rainbow darters, eliciting a persistent and stereospecific oxidative stress response. Both enantiomers significantly increased SOD, and GPX antioxidant enzyme activities. However, S-VEN consistently induced stronger or earlier oxidative responses than R-VEN, exemplified by elevated GPX and CAT activity in the cytosol and higher levels of lipid peroxidation at earlier time points. These findings underscore the heightened sensitivity of teleost brain tissue to oxidative insults and highlight the differential capacity of VEN enantiomers in eliciting ROS-related damage. Although increased antioxidant enzyme activity suggests a compensatory response to excess ROS, the marked rise in MDA concentrations reveals that these defenses can be overwhelmed, particularly under prolonged VEN exposure. Moreover, 8-OHdG results indicate that oxidative DNA damage is temporally dynamic, reflecting an interplay between ROS generation, repair mechanisms, and the protective capacity of antioxidant responses. The increase in lipid peroxidation and transient DNA damage following S-VEN exposure may be systemic, as the transcriptional response in the liver following S-VEN was characterized by the upregulation of lipid aldehyde detoxification and chromatin remodelling pathways (Ellis 2007; Moore et al., 2019).

Taken together, these findings demonstrate that venlafaxine modulates liver gene expression and induces oxidative stress in rainbow darters through both shared and stereoselective mechanisms. Such insights advocate for a chiral-focused approach in pharmaceutical risk assessment and underscore the need for integrated, multifaceted investigations into complex environmental mixtures. While VEN clearly contributes to hepatic transcriptomic changes, these results emphasize that no single pharmaceutical can fully account for the broad metabolic disruptions observed in WWTPE-exposed wild fish. The greater oxidative impact of S-VEN highlights the importance of assessing not only VEN but also enantiomer-specific environmental toxicology in effluent-dominated waterways. The precise

molecular mechanisms underlying VEN-induced oxidative stress remain unresolved. Future studies should explore direct interactions between VEN and mitochondrial pathways, as well as its impact on neurotransmitter regulation.

5.4 Limitations

This study provides valuable insight into the chronic effects of WWTPE on *Etheostoma* spp. and the sub-chronic exposure of VEN on rainbow darter; however, some factors may limit broader interpretation. While transcriptomic analysis revealed significant changes, it remains uncertain whether these translate into functional protein-level disruptions, as mRNA abundance does not always correlate with protein expression or enzymatic activity (Feder & Walser, 2005). Additionally, transcriptional changes observed in this thesis represent only a snapshot of cellular and molecular functions within a single tissue, which could be influenced by temporal fluctuations in cellular activity. Nevertheless, transcriptomics is widely recognized as an early and sensitive indicator of emerging sublethal physiological disruption, often preceding detectable organismal effects (Evans & Hofmann, 2012; Oomen & Hutchings, 2017; Wang et al., 2020; Reinwald et al., 2022; Escobar & Lampert, 2024). This is especially valuable in monitoring environmental protuberance, with gene expression changes closely aligning with organismal fitness and stress thresholds (Evans & Hofmann, 2012; Oomen & Hutchings, 2017). Future studies integrating transcriptomics with proteomics or metabolomics would provide a more comprehensive understanding of the physiological consequences of effluent and VEN exposure (Haider et al., 2013; Shi et al., 2024).

The laboratory exposure to VEN was conducted in a single species, limiting confident extrapolation to other fish, as highlighted by the species variability observed in WWTPE-exposed fish. Moreover, fish in natural environments are exposed to complex pollutant mixtures, introducing multi-stressor interactions that were not fully captured in this lab study. Expanding sampling to multiple tissues and species and including additional pharmaceuticals, such as diclofenac and carbamazepine, could enhance the connection between pharmaceuticals and WWTPE exposure (Reinwald et al., 2022). However, such expansions would likely require alternative methodologies, such as microarrays, to remain cost-effective given the sequencing demands of multi-tissue, multi-contaminant and multi-timepoint studies. Now that high-quality, relatively complete transcriptomes for these non-model species have been established, chip-based technology presents a feasible approach for more comprehensive targeted pharmaceutical

studies, and long-term transcriptional monitoring in effluent-exposed fish. Future research should incorporate longer exposure durations, multiple sampling points, behavioural assessments, and expanded '-omics' approaches to further elucidate the biochemical, physiological, and ecological implications of WWTPE and VEN exposure.

5.5 Management considerations and future perspectives

This research enabled the detection of early, sub-lethal molecular disruptions that may serve as early warning indicators before physiological, behavioural, or population-level effects manifest. These transcriptomic and cellular responses revealed biological pathways and processes disrupted by WWTPE and VEN, which might otherwise go undetected using traditional biomonitoring methods such as morphological condition assessments or tissue analysis. The data presented in this thesis could contribute to the development of an Adverse Outcome Pathway (AOP), by highlighting potential key events (KEs) that link molecular initiating events (MIEs) to adverse biological effects (Ankley et al., 2010). A schematic illustrating the focus of this work and how it aligns with the AOP framework is provided in Figure 5.1. AOPs span multiple levels of biological organisation, from molecular and cellular responses, to whole-organism physiology and population dynamics, and are used to improve risk assessment by providing mechanistic insights into how contaminants induce toxic effects (Ankley et al., 2010). Efforts to develop AOPs for complex chemical mixture exposure are ongoing, including Van Der Oost et al. (2020), who proposed an AOP for fish in urban waterways, though many of these frameworks remain incomplete. Transcriptomic data can serve as a strong foundation for defining MIEs and KEs, offering a set of biomarkers suitable for toxicity testing and hazard identification (Vinken, 2019; Bakker et al., 2023). Thus, the research presented in the present study can contribute to AOP refinement for aquatic pollutant exposure of WWTPE and VEN. Although speculative, a potential AOP for VEN exposure in fish may begin with MIEs such as interaction with serotonergic and noradrenergic transporters and impaired CYP-mediated metabolism and clearance, leading to the accumulation of VEN and its metabolites. These molecular disruptions could initiate a cascade of KEs, including dysregulated neurotransmission, disrupted lipid metabolism, ROS production, stimulation of antioxidant enzyme activity, lipid peroxidation, inflammatory responses, and neurotoxicity. These molecular and cellular perturbations could culminate in AOs such as metabolic dysregulation, maladaptive behaviours, and reduced reproductive success.

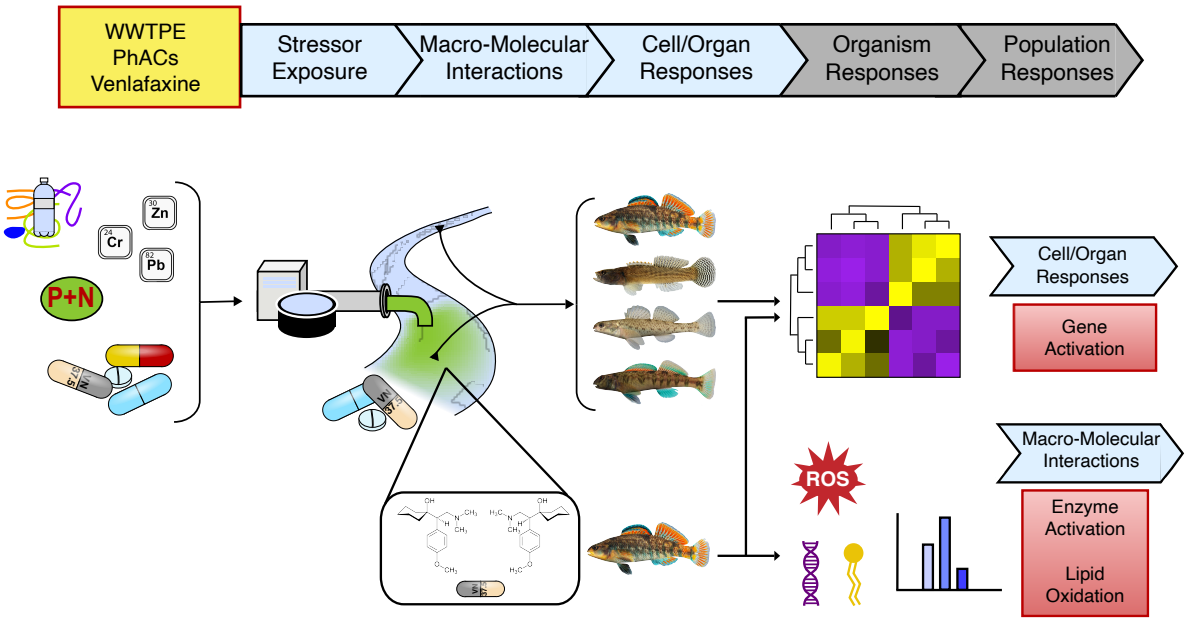


Figure 5.1: Conceptual overview of the effects of wastewater effluent and venlafaxine exposure on aquatic organisms. This summary diagram illustrates the focus of this thesis and how it aligns with the Adverse Outcome Pathway (AOP) framework.

One of the salient findings of this work lies in the divergent transcriptional responses observed among species closely related phylogenetically and occupying similar ecological niches. This interspecific variability highlights the importance of examining multiple species to capture the breadth of molecular adaptations that can occur under anthropogenic stress. Thus, this work promotes the use of multi-species monitoring to offer a more nuanced understanding of how environmental stressors can manifest across taxa. Additionally, the data suggest that chronic, multi-contaminant exposures can lead to nuanced regulatory shifts, such as reduced expression of heat shock proteins and compromised proteasomal activity, that deviate from the canonical acute-stress responses. These perturbations may leave fish populations more vulnerable to further stressors and raise concerns about disease susceptibility, growth, reproductive success, and population-level impacts.

With global pharmaceutical consumption steadily increasing, the release of PACs into surface waters is expected to rise unless WWT technologies are improved (González et al., 2021; Etit et al., 2024). Eliminating these contaminants remains a major challenge, particularly for chiral pharmaceuticals, which exhibit enantioselective degradation patterns (Dogan et al., 2020). Several treatment technologies, including granular activated carbon filtration, advanced oxidation processes, and constructed wetlands, are being explored as potential solutions (Zhou et al., 2018; Angeles et al., 2020; Eniola et al., 2022; Kisielius et al., 2023). However, economic feasibility varies, as large-scale implementation costs can be prohibitively high depending on treatment scale and infrastructure availability (Kårelid et al., 2017; Ozgun et al., 2021; Zagklis et al., 2022). Optimizing cost-effective wastewater management strategies while ensuring the efficient removal of pharmaceutical contaminants remains as a research priority.

By highlighting the sublethal biological effects of WWTP effluent and VEN exposure, this work demonstrates the value of transcriptomics within an ecological framework as a sensitive tool for large-scale environmental monitoring. Our findings also emphasize that environmental regulators and policymakers should account for pharmaceutical pollution, including enantiomer-specific monitoring, to better assess ecological risks. Currently, pharmaceuticals remain largely unaddressed within established Environmental Effects Monitoring (EEM) practices under the Canadian federal Fisheries Act (2019). Future research should build upon these findings by investigating population-level consequences of pharmaceutical exposure and evaluating interactive effects of multiple contaminants, including mixture toxicity and cumulative risk assessments. Addressing these knowledge gaps is critical for informing science-based environmental management policies and ensuring the long-term sustainability of freshwater ecosystems amid increasing anthropogenic stressors.

5.6 Conclusions

This thesis advances our understanding of how WWTPE and pharmaceutical contaminants, particularly the enantiomers of VEN, affect freshwater fish at different biological scales. By integrating high-quality *de novo* transcriptomic analyses, enzymatic activity assays, and cellular damage markers, this research uncovered molecular pathways and responses indicative of environmental and cellular perturbation. The multi-species approach revealed pronounced interspecies variability, even among closely related species, underscoring the

importance of broad taxonomic coverage in ecotoxicological assessments. Our finding that VEN enantiomers elicit distinct toxicological profiles highlights the importance of accounting for stereoselective toxicity when assessing environmental risks. This work also contributes to the future development and refinement of AOP frameworks in mixed contaminant WWTPE, and VEN exposure. Finally, the provision of high-quality transcriptomes for four commonly studied fish species establishes a foundation for more targeted and high-throughput ecotoxicological evaluations, ultimately advancing conservation and management strategies for aquatic ecosystems.

Bibliography

Abdel-Wahab, B. A., & Salama, R. H. (2011). Venlafaxine protects against stress-induced oxidative DNA damage in hippocampus during antidepressant testing in mice. *Pharmacology Biochemistry and Behavior*, *100*(1), 59-65.

Abrego, J., Gunda, V., Vernucci, E., Shukla, S. K., King, R. J., Dasgupta, A., ... & Singh, P. K. (2017). GOT1-mediated anaplerotic glutamine metabolism regulates chronic acidosis stress in pancreatic cancer cells. *Cancer letters*, *400*, 37-46.

Åbrink, M., Aveskogh, M., & Hellman, L. (1995). Isolation of cDNA clones for 42 different Krüppel-related zinc finger proteins expressed in the human monoblast cell line U-937. *DNA and cell biology*, *14*(2), 125-136.

Achari, A., Marshall, S. E., Muirhead, H., Palmieri, R. H., & Noltmann, E. A. (1981). Glucose-6-phosphate isomerase. *Philosophical Transactions of the Royal Society of London. B, Biological Sciences*, *293*(1063), 145-157.

Afifi, M., Saddick, S., & Zinada, O. A. A. (2016). Toxicity of silver nanoparticles on the brain of Oreochromis niloticus and Tilapia zillii. *Saudi journal of biological sciences*, *23*(6), 754-760.

Ahmadian, E., Babaei, H., Nayebi, A. M., Eftekhari, A., & Eghbal, M. A. (2016). Venlafaxine-induced cytotoxicity towards isolated rat hepatocytes involves oxidative stress and mitochondrial/lysosomal dysfunction. *Advanced Pharmaceutical Bulletin*, *6*(4), 521.

Aich, U., Polverino, G., Yazdan Parast, F., Melo, G. C., Tan, H., Howells, J., ... & Wong, B. B. (2024). Long−term effects of widespread pharmaceutical pollution on trade−offs between behavioural, life−history and reproductive traits in fish. *Journal of Animal Ecology*.

Aladekoyi, O., Siddiqui, S., Hania, P., Hamza, R., & Gilbride, K. (2024). Accumulation of antibiotics in the environment: Have appropriate measures been taken to protect Canadian human and ecological health?. *Ecotoxicology and Environmental Safety*, *280*, 116513.

Alayash, A. I., & Wilson, M. T. (2022). Hemoglobin can Act as a (Pseudo)-Peroxidase in Vivo. What is the Evidence?. *Frontiers in Molecular Biosciences*, *9*, 910795.

Albers, J. L., Ivan, L. N., Clark, B. W., Nacci, D. E., Klingler, R. H., Thrash, A., ... & Murphy, C. A. (2024). Impacts on Atlantic Killifish from Neurotoxicants: Genes, Behavior, and Population-Relevant Outcomes. *Environmental Science & Technology*, *58*(39), 17235-17246.

Albertolle, M. E., & Guengerich, F. P. (2018). The relationships between cytochromes P450 and H2O2: Production, reaction, and inhibition. *Journal of inorganic biochemistry*, *186*, 228-234.

Alimperti, S., & Andreadis, S. T. (2015). CDH2 and CDH11 act as regulators of stem cell fate decisions. *Stem cell research*, *14*(3), 270-282.

Allen-Baume, V., Ségui, B., & Cockcroft, S. (2002). Current thoughts on the phosphatidylinositol transfer protein family. *FEBS letters*, *531*(1), 74-80.

Allen, D., Rosenfeld, J., & Richards, J. (2016). Physiological basis of metabolic trade-offs between growth and performance among different strains of rainbow trout. *Canadian Journal of Fisheries and Aquatic Sciences*, *73*(10), 1493-1506.

Alvarez, R. V., & Landsman, D. (2024). GTax: improving de novo transcriptome assembly by removing foreign RNA contamination. *Genome Biology*, *25*(1), 12.

Alves, C., Tamagno, W. A., Pompermaier, A., Vanin, A. P., & Barcellos, L. J. G. (2023). Neurotoxicological effects of venlafaxine on Caenorhabditis elegans and Danio rerio. *Comparative Biochemistry and Physiology Part C: Toxicology & Pharmacology*, *271*, 109658.

Ang, S. F., Zhao, Z. S., Lim, L., & Manser, E. (2010). DAAM1 is a formin required for centrosome re-orientation during cell migration. *PloS one*, *5*(9), e13064.

Angeles, L. F., Mullen, R. A., Huang, I. J., Wilson, C., Khunjar, W., Sirotkin, H. I., ... & Aga, D. S. (2020). Assessing pharmaceutical removal and reduction in toxicity provided by advanced wastewater treatment systems. *Environmental Science: Water*

Angelova, P. R., Esteras, N., & Abramov, A. Y. (2021). Mitochondria and lipid peroxidation in the mechanism of neurodegeneration: Finding ways for prevention. *Medicinal Research Reviews*, *41*(2), 770-784.

Ankley, G. T., Bennett, R. S., Erickson, R. J., Hoff, D. J., Hornung, M. W., Johnson, R. D., ... & Villeneuve, D. L. (2010). Adverse outcome pathways: a conceptual framework to support ecotoxicology research and risk assessment. *Environmental toxicology and chemistry*, *29*(3), 730-741.

Arlos, M. J., Bragg, L. M., Parker, W. J., & Servos, M. R. (2015). Distribution of selected antiandrogens and pharmaceuticals in a highly impacted watershed. *Water research*, *72*, 40-50.

Arnnok, P., Singh, R. R., Burakham, R., Pérez-Fuentetaja, A., & Aga, D. S. (2017). Selective uptake and bioaccumulation of antidepressants in fish from effluent-impacted Niagara River. *Environmental science & technology*, *51*(18), 10652-10662.

Arstikaitis, J., Gagné, F., & Cyr, D. G. (2014). Exposure of fathead minnows to municipal wastewater effluent affects intracellular signaling pathways in the liver. *Comparative Biochemistry and Physiology Part C: Toxicology & Pharmacology*, *164*, 1-10.

Arvai, A., Klecka, G., Jasim, S., Melcer, H., & Laitta, M. T. (2014). Protecting our Great Lakes: assessing the effectiveness of wastewater treatments for the removal of chemicals of emerging concern. *Water Quality Research Journal of Canada*, *49*(1), 23-31.

Ashrafi, R., Westermark, A., Leppänen, M. T., & Vehniäinen, E. R. (2024). Female-biased sex ratios and delayed puberty in two fish species with different Ecologies in an Anthropogenically affected urban lake. *Environmental Research*, *262*, 119844.

Atasu, A. (2019). Operational perspectives on extended producer responsibility. *Journal of Industrial Ecology*, *23*(4), 744-750.

Atkinson, S. D., Bartholomew, J. L., & Lotan, T. (2018). Myxozoans: ancient metazoan parasites find a home in phylum Cnidaria. *Zoology*, *129*, 66-68.

Au-Yeung, N., Mandhana, R., & Horvath, C. M. (2013). Transcriptional regulation by STAT1 and STAT2 in the interferon JAK-STAT pathway. *Jak-stat*, *2*(3), e23931.

Bai, Y., Liu, X., Qi, X., Liu, X., Peng, F., Li, H., ... & Shao, S. (2019). PDIA6 modulates apoptosis and autophagy of non-small cell lung cancer cells via the MAP4K1/JNK signaling pathway. *EBioMedicine*, *42*, 311-325.

Bajard, L., Adamovsky, O., Audouze, K., Baken, K., Barouki, R., Beltman, J. B., ... & Blaha, L. (2023). Application of AOPs to assist regulatory assessment of chemical risks–Case studies, needs and recommendations. *Environmental Research*, *217*, 114650.

Baker, B. B., Haimbaugh, A. S., Sperone, F. G., Johnson, D. M., & Baker, T. R. (2022). Persistent contaminants of emerging concern in a great lakes urban-dominant watershed. *Journal of Great Lakes Research*, *48*(1), 171-182.

Bakker, R., Ellers, J., Roelofs, D., Vooijs, R., Dijkstra, T., van Gestel, C. A., & Hoedjes, K. M. (2023). Combining time-resolved transcriptomics and proteomics data for Adverse Outcome Pathway refinement in ecotoxicology. *Science of the Total Environment*, *869*, 161740.

Ball, S. C., Meador, J. P., James, C. A., & McIntyre, J. K. (2024). Exposure of juvenile Chinook salmon to effluent from a large urban wastewater treatment plant. Part 1. Physiological responses. *Aquaculture and Fisheries*, *9*(3), 355-366.

Balta, E., Kramer, J., & Samstag, Y. (2021). Redox regulation of the actin cytoskeleton in cell migration and adhesion: on the way to a spatiotemporal view. *Frontiers in cell and developmental biology*, *8*, 618261.

Bandyopadhyay, U., Das, D., & Banerjee, R. K. (1999). Reactive oxygen species: oxidative damage and pathogenesis. *Current science*, 658-666.

Bardaweel, S. K., Gul, M., Alzweiri, M., Ishaqat, A., ALSalamat, H. A., & Bashatwah, R. M. (2018). Reactive oxygen species: The dual role in physiological and pathological conditions of the human body. *The Eurasian journal of medicine*, *50*(3), 193.

Barreto, L. S., da Costa Souza, A. T., Martins, C. C., Araujo, S. B. L., & de Oliveira Ribeiro, C. A. (2020). Urban effluents affect the early development stages of Brazilian fish species with implications for their population dynamics. *Ecotoxicology and environmental safety*, *188*, 109907.

Barrett, D. E., & Bartholomew, J. L. (2021). A tale of two fish: Comparative transcriptomics of resistant and susceptible steelhead following exposure to *Ceratonova shasta* highlights differences in parasite recognition. *PLoS One*, *16*(2), e0234837.

Barton, B. A. (2002). Stress in fishes: a diversity of responses with particular reference to changes in circulating corticosteroids. *Integrative and comparative biology*, *42*(3), 517-525.

Baseler, W. A., Thapa, D., Jagannathan, R., Dabkowski, E. R., Croston, T. L., & Hollander, J. M. (2012). miR-141 as a regulator of the mitochondrial phosphate carrier (Slc25a3) in the type 1 diabetic heart. *American Journal of Physiology-Cell Physiology*, *303*(12), C1244-C1251.

Baud, O., Greene, A. E., Li, J., Wang, H., Volpe, J. J., & Rosenberg, P. A. (2004). Glutathione peroxidase-catalase cooperativity is required for resistance to hydrogen peroxide by mature rat oligodendrocytes. *Journal of Neuroscience*, *24*(7), 1531-1540.

Bearer, E. L., & Abraham, M. T. (1999). 2E4 (kaptin): a novel actin-associated protein from human blood platelets found in lamellipodia and the tips of the stereocilia of the inner ear. *European journal of cell biology*, *78*(2), 117-126.

Beghin, M., Paris-Palacios, S., Mandiki, S. N., Schmitz, M., Palluel, O., Gillet, E., ... & Kestemont, P. (2022). Integrative multi-biomarker approach on caged rainbow trout: A biomonitoring tool for wastewater treatment plant effluents toxicity assessment. *Science of the Total Environment*, *838*, 155912.

Benáková, Š., Holendová, B., & Plecitá-Hlavatá, L. (2021). Redox homeostasis in pancreatic β-cells: from development to failure. *Antioxidants*, *10*(4), 526.

Bentrop, D., Beyermann, M., Wissmann, R., & Fakler, B. (2001). NMR Structure of the "Ball-and-chain" Domain of KCNMB2, the β2-Subunit of Large Conductance Ca2+-and Voltage-activated Potassium Channels* 210. *Journal of Biological Chemistry*, *276*(45), 42116-42121.

Bernal, M. A., Schunter, C., Lehmann, R., Lightfoot, D. J., Allan, B. J., Veilleux, H. D., ... & Ravasi, T. (2020). Species-specific molecular responses of wild coral reef fishes during a marine heatwave. *Science Advances*, *6*(12).

Bertel-Sevilla, A., Alzate, J. F., & Olivero-Verbel, J. (2020). De novo assembly and characterization of the liver transcriptome of Mugil incilis (lisa) using next generation sequencing. *Scientific Reports*, *10*(1), 13957.

Best, C., Melnyk-Lamont, N., Gesto, M., & Vijayan, M. M. (2014). Environmental levels of the antidepressant venlafaxine impact the metabolic capacity of rainbow trout. *Aquatic Toxicology*, *155*, 190-198.

Bhatt, S., Nagappa, A. N., & Patil, C. R. (2020). Role of oxidative stress in depression. *Drug discovery today*, *25*(7), 1270-1276.

Bhattacharjee, S. (2014). Membrane lipid peroxidation and its conflict of interest: the two faces of oxidative stress. *Current science*, 1811-1823.

Bick, J. T., Zeng, S., Robinson, M. D., Ulbrich, S. E., & Bauersachs, S. (2019). Mammalian Annotation Database for improved annotation and functional classification of Omics datasets from less well-annotated organisms. *Database*, *2019*, baz086.

Biggs, K., Seidel, J. S., Wilson, A., & Martyniuk, C. J. (2013). γ-Amino-butyric acid (GABA) receptor subunit and transporter expression in the gonad and liver of the fathead minnow (*Pimephales promelas). Comparative Biochemistry and Physiology Part A: Molecular & Integrative Physiology*, *166*(1), 119-127.

Bisesi Jr, J. H., Bridges, W., & Klaine, S. J. (2014). Reprint of: Effects of the antidepressant venlafaxine on fish brain serotonin and predation behavior. *Aquatic toxicology*, *151*, 88-96.

Bisognin, R. P., Wolff, D. B., Carissimi, E., Prestes, O. D., Zanella, R., Storck, T. R., & Clasen, B. (2020). Potential environmental toxicity of sewage effluent with pharmaceuticals. *Ecotoxicology*, *29*, 1315-1326.

Black, J. L. (2003). The voltage-gated calcium channel γ subunits: a review of the literature. *Journal of bioenergetics and biomembranes*, *35*, 649-660.

Blanco, A. M., Bertucci, J. I., Hatef, A., & Unniappan, S. (2020). Feeding and food availability modulate brain-derived neurotrophic factor, an orexigen with metabolic roles in zebrafish. *Scientific Reports*, *10*(1), 10727.

Blonç, M., Lima, J., Balasch, J. C., Tort, L., Gravato, C., & Teles, M. (2023). Elucidating the effects of the lipids regulators fibrates and statins on the health status of finfish species: a review. *Animals*, *13*(5), 792.

Bolger, T., & Connolly, P. L. (1989). The selection of suitable indices for the measurement and analysis of fish condition. *Journal of Fish Biology*, *34*(2), 171-182.

Borowiec, B. G., Firth, B. L., & Craig, P. M. (2024). Oxygen consumption rate during recovery from loss of equilibrium induced by warming, hypoxia, or exhaustive exercise in rainbow darter (*Etheostoma caeruleum*). *Journal of Fish Biology*.

Bortolato, M., Chen, K., & Shih, J. C. (2008). Monoamine oxidase inactivation: from pathophysiology to therapeutics. *Advanced drug delivery reviews*, *60*(13-14), 1527-1533.

Bossu, C. M., & Near, T. J. (2013). Characterization of a contemporaneous hybrid zone between two darter species (*Etheostoma bison and E. caeruleum*) in the Buffalo River System. *Genetica*, *141*(1), 75-88.

Bottani, E., Cerutti, R., Harbour, M. E., Ravaglia, S., Dogan, S. A., Giordano, C., ... & Zeviani, M. (2017). TTC19 plays a husbandry role on UQCRFS1 turnover in the biogenesis of mitochondrial respiratory complex III. *Molecular cell*, *67*(1), 96-105.

Brinke, A., & Buchinger, S. (2017). Toxicogenomics in environmental science. *In vitro Environmental Toxicology-Concepts, Application and Assessment*, 159-186.

Britto, F. A., Cortade, F., Belloum, Y., Blaquière, M., Gallot, Y. S., Docquier, A., ... & Favier, F. B. (2018). Glucocorticoid-dependent REDD1 expression reduces muscle metabolism to enable adaptation under energetic stress. *BMC biology*, *16*, 1-17.

Brivio, P., Audano, M., Gallo, M. T., Miceli, E., Gruca, P., Lason, M., ... & Calabrese, F. (2023). Venlafaxine's effect on resilience to stress is associated with a shift in the balance between glucose and fatty acid utilization. *Neuropsychopharmacology*, *48*(10), 1475-1483.

Brockmeier, E. K., Hodges, G., Hutchinson, T. H., Butler, E., Hecker, M., Tollefsen, K. E., ... & Falciani, F. (2017). The role of omics in the application of adverse outcome pathways for chemical risk assessment. *Toxicological Sciences*, *158*(2), 252-262.

Brodin, T., Piovano, S., Fick, J., Klaminder, J., Heynen, M., & Jonsson, M. (2014). Ecological effects of pharmaceuticals in aquatic systems—impacts through behavioural alterations. *Philosophical Transactions of the Royal Society B: Biological Sciences*, *369*(1656), 20130580.

Brooks BW, Chambliss CK, Stanley JK, Ramirez A, Banks KE, Johnson RD, Lewis RJ. 2005. Determination of select antidepressants in fish from an effluent-dominated stream. *Environ Toxicol Chem* 24:464–469.

Brown, D., Snow, D., Hunt, G. A., & Bartelt‐Hunt, S. L. (2015). Persistence of pharmaceuticals in effluent‐dominated surface waters. *Journal of environmental quality*, *44*(1), 299-304.

Bryant, D. M., Johnson, K., DiTommaso, T., Tickle, T., Couger, M. B., Payzin-Dogru, D., ... & Whited, J. L. (2017). A tissue-mapped axolotl de novo transcriptome enables identification of limb regeneration factors. *Cell reports*, *18*(3), 762-776.

Bunker, R. D., Bulloch, E. M., Dickson, J. M., Loomes, K. M., & Baker, E. N. (2013). Structure and function of human xylulokinase, an enzyme with important roles in carbohydrate metabolism. *Journal of Biological Chemistry*, *288*(3), 1643-1652.

Burkina, V., Zlabek, V., & Zamaratskaia, G. (2015). Effects of pharmaceuticals present in aquatic environment on Phase I metabolism in fish. *Environmental toxicology and pharmacology*, *40*(2), 430-444.

Burnett, F. E., & Dinan, T. G. (1998). The clinical efficacy of venlafaxine in the treatment of depression. *Reviews in Contemporary Pharmacotherapy*, *9*(5), 303-320.

Byerly, M. S., Swanson, R. D., Semsarzadeh, N. N., McCulloh, P. S., Kwon, K., Aja, S., ... & Blackshaw, S. (2013). Identification of hypothalamic neuron-derived neurotrophic factor as a novel factor modulating appetite. *American Journal of Physiology-Regulatory, Integrative and Comparative Physiology*, *304*(12), R1085-R1095.

Byrne, A., McLaren, R. P., Mason, P., Chai, L., Dufault, M. R., Huang, Y., ... & Jiang, Y. (2010). Knockdown of human deubiquitinase PSMD14 induces cell cycle arrest and senescence. *Experimental cell research*, *316*(2), 258-271.

Caiaffo, V., Oliveira, B. D., de Sá, F. B., & Evêncio Neto, J. (2016). Anti−inflammatory, antiapoptotic, and antioxidant activity of fluoxetine. *Pharmacology research & perspectives*, *4*(3), e00231.

Candolin, U., & Wong, B. B. (2019). Mate choice in a polluted world: consequences for individuals, populations and communities. *Philosophical Transactions of the Royal Society B*, *374*(1781), 20180055.

Canosa, L. F., & Bertucci, J. I. (2023). The effect of environmental stressors on growth in fish and its endocrine control. *Frontiers in endocrinology*, *14*, 1109461.

Cargnello, M., & Roux, P. P. (2011). Activation and function of the MAPKs and their substrates, the MAPK-activated protein kinases. *Microbiology and molecular biology reviews*, *75*(1), 50-83.

Carruthers, M., Yurchenko, A. A., Augley, J. J., Adams, C. E., Herzyk, P., & Elmer, K. R. (2018). De novo transcriptome assembly, annotation and comparison of four ecological and evolutionary model salmonid fish species. *BMC genomics*, *19*, 1-17.

Colin, E., Cong, E. H., Mollet, G., Guichet, A., Gribouval, O., Arrondel, C., ... & Antignac, C. (2014). Loss-of-function mutations in WDR73 are responsible for microcephaly and steroid-resistant nephrotic syndrome: Galloway-Mowat syndrome. *The American Journal of Human Genetics*, *95*(6), 637-648.

Cech, J. N., & Peichel, C. L. (2015). Identification of the centromeric repeat in the threespine stickleback fish (Gasterosteus aculeatus). *Chromosome Research*, *23*, 767-779.

Celander, M. C. (2011). Cocktail effects on biomarker responses in fish. *Aquatic toxicology*, *105*(3-4), 72-77.

Chana-Muñoz, A., Jendroszek, A., Sønnichsen, M., Wang, T., Ploug, M., Jensen, J. K., ... & Panitz, F. (2019). Origin and diversification of the plasminogen activation system among chordates. *BMC evolutionary biology*, *19*, 1-17.

Chandel, N. S. (2010). Mitochondrial complex III: an essential component of universal oxygen sensing machinery?. *Respiratory physiology & neurobiology*, *174*(3), 175-181.

Chang, E. S., Neuhof, M., Rubinstein, N. D., Diamant, A., Philippe, H., Huchon, D., & Cartwright, P. (2015). Genomic insights into the evolutionary origin of Myxozoa within Cnidaria. *Proceedings of the National Academy of Sciences*, *112*(48), 14912-14917.

Chang, M. X. (2023). Emerging mechanisms and functions of inflammasome complexes in teleost fish. *Frontiers in Immunology*, *14*, 1065181.

Chang, M. X., Xiong, F., Wu, X. M., & Hu, Y. W. (2021). The expanding and function of NLRC3 or NLRC3-like in teleost fish: Recent advances and novel insights. *Developmental & Comparative Immunology*, *114*, 103859.

Chen, C. Y., Yeh, Y. W., Kuo, S. C., Liang, C. S., Ho, P. S., Huang, C. C., ... & Huang, S. Y. (2018). Differences in immunomodulatory properties between venlafaxine and paroxetine in patients with major depressive disorder. *Psychoneuroendocrinology*, *87*, 108-118.

Chen, H. W., Yang, Y. K., Xu, H., Yang, W. W., Zhai, Z. H., & Chen, D. Y. (2015). Ring finger protein 166 potentiates RNA virus-induced interferon-β production via enhancing the ubiquitination of TRAF3 and TRAF6. *Scientific reports*, *5*(1), 14770.

Chen, Q., Vazquez, E. J., Moghaddas, S., Hoppel, C. L., & Lesnefsky, E. J. (2003). Production of reactive oxygen species by mitochondria: central role of complex III. *Journal of Biological Chemistry*, *278*(38), 36027-36031.

Chen, Y., Wang, J., Xu, P., Xiang, J., Xu, D., Cheng, P., ... & Chen, Z. (2022). Antidepressants as emerging contaminants: Occurrence in wastewater treatment plants and surface waters in Hangzhou, China. *Frontiers in Public Health*, *10*, 963257.

Chiarugi, P., Pani, G., Giannoni, E., Taddei, L., Colavitti, R., Raugei, G., ... & Ramponi, G. (2003). Reactive oxygen species as essential mediators of cell adhesion: the oxidative inhibition of a FAK tyrosine phosphatase is required for cell adhesion. *The Journal of cell biology*, *161*(5), 933-944.

Chitwood, P. J., & Hegde, R. S. (2020). An intramembrane chaperone complex facilitates membrane protein biogenesis. *Nature*, *584*(7822), 630-634.

Chouhan, S., Sawant, M., Weimholt, C., Luo, J., Sprung, R. W., Terrado, M., ... & Mahajan, N. P. (2023). TNK2/ACK1-mediated phosphorylation of ATP5F1A (ATP synthase F1 subunit alpha) selectively augments survival of prostate cancer while engendering mitochondrial vulnerability. *Autophagy*, *19*(3), 1000-1025.

Chowdhury, S., & Saikia, S. K. (2020). Oxidative stress in fish: a review. *Journal of Scientific Research*, *12*(1), 145-160.

Chu, M. L., Pan, T. C., Conway, D., Kuo, H. J., Glanville, R. W., Timpl, R., ... & Deutzmann, R. (1989). Sequence analysis of alpha 1 (VI) and alpha 2 (VI) chains of human type VI collagen reveals internal triplication of globular domains similar to the A domains of von Willebrand factor and two alpha 2 (VI) chain variants that differ in the carboxy terminus. *The EMBO journal*, *8*(7), 1939-1946.

Chung, K. C., Gomes, I., Wang, D., Lau, L. F., & Rosner, M. R. (1998). Raf and fibroblast growth factor phosphorylate Elk1 and activate the serum response element of the immediate early gene pip92 by mitogen-activated protein kinase-independent as well as-dependent signaling pathways. *Molecular and cellular biology*, *18*(4), 2272-2281.

Chypre, M., Zaidi, N., & Smans, K. (2012). ATP-citrate lyase: a mini-review. *Biochemical and biophysical research communications*, *422*(1), 1-4.

Claudel, T., Staels, B., & Kuipers, F. (2005). The Farnesoid X receptor: a molecular link between bile acid and lipid and glucose metabolism. *Arteriosclerosis, thrombosis, and vascular biology*, *25*(10), 2020-2030.

Clinton, M., Król, E., Sepúlveda, D., Andersen, N. R., Brierley, A. S., Ferrier, D. E., ... & Martin, S. A. (2021). Gill transcriptomic responses to toxin-producing alga Prymnesium parvum in rainbow trout. *Frontiers in Immunology*, *12*, 794593.

Cocco, A., Rönnberg, A. C., Jin, Z., André, G. I., Vossen, L. E., Bhandage, A. K., ... & Winberg, S. (2017). Characterization of the γ-aminobutyric acid signaling system in the zebrafish (*Danio rerio Hamilton*) central nervous system by reverse transcription-quantitative polymerase chain reaction. *Neuroscience*, *343*, 300-321.

Cockcroft, S. (2012). The diverse functions of phosphatidylinositol transfer proteins. *Phosphoinositides and disease*, 185-208.

Colin, N., Porte, C., Fernandes, D., Barata, C., Padrós, F., Carrassón, M., ... & Maceda-Veiga, A. (2016). Ecological relevance of biomarkers in monitoring studies of macro-invertebrates and fish in Mediterranean rivers. *Science of the Total Environment*, *540*, 307-323.

Conesa, A., Madrigal, P., Tarazona, S., Gomez-Cabrero, D., Cervera, A., McPherson, A., ... & Mortazavi, A. (2016). A survey of best practices for RNA-seq data analysis. *Genome biology*, *17*, 1-19.

Connon, R. E., Hasenbein, S., Brander, S. M., Poynton, H. C., Holland, E. B., Schlenk, D., ... & Todgham, A. E. (2019). Review of and recommendations for monitoring contaminants and their effects in the San Francisco Bay– Delta. *San Francisco Estuary and Watershed Science*, *17*(4).

Connon, R. E., Jeffries, K. M., Komoroske, L. M., Todgham, A. E., & Fangue, N. A. (2018). The utility of transcriptomics in fish conservation. *Journal of Experimental Biology*, *221*(2), jeb148833.

Connors, K. A., Du, B., Fitzsimmons, P. N., Hoffman, A. D., Chambliss, C. K., Nichols, J. W., & Brooks, B. W. (2013). Comparative pharmaceutical metabolism by rainbow trout (*Oncorhynchus mykiss*) liver S9 fractions. *Environmental Toxicology and Chemistry*, *32*(8), 1810-1818.

Corcoran, J., Lange, A., Winter, M. J., & Tyler, C. R. (2012). Effects of pharmaceuticals on the expression of genes involved in detoxification in a carp primary hepatocyte model. *Environmental science & technology*, *46*(11), 6306-6314.

Correia, A. S., Cardoso, A., & Vale, N. (2023). Oxidative stress in depression: the link with the stress response, neuroinflammation, serotonin, neurogenesis and synaptic plasticity. *Antioxidants*, *12*(2), 470.

Costa, C., Semedo, M., Machado, S. P., Cunha, V., Ferreira, M., & Urbatzka, R. (2021). Transcriptional analyses reveal different mechanism of toxicity for a chronic exposure to fluoxetine and venlafaxine on the brain of the marine fish *Dicentrarchrus labrax*. *Comparative Biochemistry and Physiology Part C: Toxicology & Pharmacology*, *250*, 109170.

Coutens, B., Yrondi, A., Rampon, C., & Guiard, B. P. (2022). Psychopharmacological properties and therapeutic profile of the antidepressant venlafaxine. *Psychopharmacology*, *239*(9), 2735-2752.

Cowell, I. G., Casement, J. W., & Austin, C. A. (2023). To break or not to break: the role of TOP2B in transcription. *International Journal of Molecular Sciences*, *24*(19), 14806.

Curado, S., Ober, E. A., Walsh, S., Cortes-Hernandez, P., Verkade, H., Koehler, C. M., & Stainier, D. Y. (2010). The mitochondrial import gene tomm22 is specifically required for hepatocyte survival and provides a liver regeneration model. *Disease models & mechanisms*, *3*(7-8), 486-495.

Cvetkovic, M. A., Passaretti, P., Butryn, A., Reynolds-Winczura, A., Kingsley, G., Skagia, A., ... & Costa, A. (2023). The structural mechanism of dimeric DONSON in replicative helicase activation. *Molecular Cell*, *83*(22), 4017-4031.

Cvetkovic, M., Leake, B., Fromm, M. F., Wilkinson, G. R., & Kim, R. B. (1999). OATP and P-glycoprotein transporters mediate the cellular uptake and excretion of fexofenadine. *Drug metabolism and disposition*, *27*(8), 866-871.

da Silva, A. A. S., de Santi, F., Hinton, B. T., Cerri, P. S., & Sasso-Cerri, E. (2023). Venlafaxine increases aromatization, reduces apical V-ATPase in clear cells and induces increased number

of mast cells and smooth muscle cells death in rat cauda epididymis. *Life Sciences*, *315*, 121329.

Dai, C., Zheng, J., Qi, L., Deng, P., Wu, M., Li, L., & Yuan, J. (2023). Chronic stress boosts systemic inflammation and compromises antiviral innate immunity in *Carassius gibel*. *Frontiers in Immunology*, *14*, 1105156.

Danulat, E., & Mommsen, T. P. (1990). Norepinephrine: a potent activator of glycogenolysis and gluconeogenesis in rockfish hepatocytes. *General and comparative endocrinology*, *78*(1), 12-22.

Darnell Jr, J. E., Kerr, L. M., & Stark, G. R. (1994). Jak-STAT pathways and transcriptional activation in response to IFNs and other extracellular signaling proteins. *Science*, *264*(5164), 1415-1421.

Davalos, D., & Akassoglou, K. (2012). Fibrinogen as a key regulator of inflammation in disease. In *Seminars in immunopathology* (Vol. 34, pp. 43-62). Springer-Verlag.

David, A., Lange, A., Tyler, C. R., & Hill, E. M. (2018). Concentrating mixtures of neuroactive pharmaceuticals and altered neurotransmitter levels in the brain of fish exposed to a wastewater effluent. *Science of the Total Environment*, *621*, 782-790.

Dawkins, J. B., Wang, J., Maniati, E., Heward, J. A., Koniali, L., Kocher, H. M., ... & Grose, R. P. (2016). Reduced expression of histone methyltransferases KMT2C and KMT2D correlates with improved outcome in pancreatic ductal adenocarcinoma. *Cancer research*, *76*(16), 4861-4871.

De Caroli, M., Furini, A., DalCorso, G., Rojas, M., & Di Sansebastiano, G. P. (2020). Endomembrane reorganization induced by heavy metals. *Plants*, *9*(4), 482.

De Launoit, Y., & Adamski, J. (1999). Unique multifunctional HSD17B4 gene product: 17beta-hydroxysteroid dehydrogenase 4 and D-3-hydroxyacyl-coenzyme A dehydrogenase/hydratase involved in Zellweger syndrome. *J Mol Endocrinol*, *22*(3), 227-240.

De Prá, S. D., Ferreira, G. K., Carvalho-Silva, M., Vieira, J. S., Scaini, G., Leffa, D. D., ... & Streck, E. L. (2014). L-tyrosine induces DNA damage in brain and blood of rats. *Neurochemical research*, *39*, 202-207.

Demeter, A., Romero-Mulero, M. C., Csabai, L., Ölbei, M., Sudhakar, P., Haerty, W., & Korcsmáros, T. (2020). ULK1 and ULK2 are less redundant than previously thought: computational analysis uncovers distinct regulation and functions of these autophagy induction proteins. *Scientific reports*, *10*(1), 10940.

Dépatie, C., Houde, M., & Verreault, J. (2020). Environmental exposure of northern pike to a primary wastewater effluent: Impact on the lipidomic profile and lipid metabolism. *Aquatic Toxicology*, *221*, 105421.

Desmet, V. J. (1995). Histopathology of cholestasis. *Verhandlungen der Deutschen Gesellschaft fur Pathologie*, *79*, 233-240.

Deutekom, E. S., Snel, B., & van Dam, T. J. (2021). Benchmarking orthology methods using phylogenetic patterns defined at the base of Eukaryotes. *Briefings in bioinformatics*, *22*(3), bbaa206.

Di Prinzio, C. Y., Andrade-Muñoz, A. S., Assef, Y. A., Dromaz, W. M., Quinteros, P., & Miserendino, M. L. (2024). Impact of treated effluent discharges on fish communities: Evaluating the effects of pollution on fish distribution, abundance and environmental integrity. *Science of The Total Environment*, *917*, 170237.

Ding, F., Gao, F., Zhang, S., Lv, X., Chen, Y., & Liu, Q. (2021). A review of the mechanism of DDIT4 serve as a mitochondrial related protein in tumor regulation. *Science Progress*, *104*(1), 0036850421997273.

Dodds, P. F. (1995). Xenobiotic lipids: the inclusion of xenobiotic compounds in pathways of lipid biosynthesis. *Progress in lipid research*, *34*(3), 219-247.

Dogan, A., Płotka-Wasylka, J., Kempińska-Kupczyk, D., Namieśnik, J., & Kot-Wasik, A. (2020). Detection, identification and determination of chiral pharmaceutical residues in wastewater: Problems and challenges. *TrAC Trends in Analytical Chemistry*, *122*, 115710.

Doh, M. S., Oh, D. H., Kim, S. H., Choi, M. R., & Chai, Y. G. (2015). Profiling of proteins regulated by venlafaxine during neural differentiation of human cells. *Psychiatry Investigation*, *12*(1), 81.

Dong, J., Li, M., Peng, R., Zhang, Y., Qiao, Z., & Sun, N. (2024). ACACA reduces lipid accumulation through dual regulation of lipid metabolism and mitochondrial function via AMPK-PPARα-CPT1A axis. *Journal of Translational Medicine*, *22*(1), 196.

Dong, X., Li, J., He, J., Liu, W., Jiang, L., Ye, Y., & Wu, C. (2016). Anti-infective mannose receptor immune mechanism in large yellow croaker (*Larimichthys crocea*). *Fish & shellfish immunology*, *54*, 257-265.

Dringen, R., & Hamprecht, B. (1997). Involvement of glutathione peroxidase and catalase in the disposal of exogenous hydrogen peroxide by cultured astroglial cells. *Brain research*, *759*(1), 67-75.

Du, S. N., Choi, J. A., McCallum, E. S., McLean, A. R., Borowiec, B. G., Balshine, S., & Scott, G. R. (2019). Metabolic implications of exposure to wastewater effluent in bluegill sunfish. *Comparative Biochemistry and Physiology Part C: Toxicology & Pharmacology*, *224*, 108562.

Du, S. N., Mahalingam, S., Borowiec, B. G., & Scott, G. R. (2016). Mitochondrial physiology and reactive oxygen species production are altered by hypoxia acclimation in killifish (*Fundulus heteroclitus*). *Journal of Experimental Biology*, *219*(8), 1130-1138.

Du, S. N., McCallum, E. S., Vaseghi-Shanjani, M., Choi, J. A., Warriner, T. R., Balshine, S., & Scott, G. R. (2018). Metabolic costs of exposure to wastewater effluent lead to compensatory adjustments in respiratory physiology in bluegill sunfish. *Environmental science & technology*, *52*(2), 801-811.

Duarte, I. A., Reis-Santos, P., Fick, J., Cabral, H. N., Duarte, B., & Fonseca, V. F. (2023). Neuroactive pharmaceuticals in estuaries: occurrence and tissue-specific bioaccumulation in multiple fish species. *Environmental Pollution*, *316*, 120531.

Dumont, V., & Lehtonen, S. (2022). PACSIN proteins in vivo: Roles in development and physiology. *Acta Physiologica*, *234*(3), e13783.

Eakins, R.J. 2024. Ontario Freshwater Fishes Life History Database. Version 5.31. [Online].

Eberhardt, H. U., Buhlmann, D., Hortschansky, P., Chen, Q., Böhm, S., Kemper, M. J., ... & Skerka, C. (2013). Human factor H-related protein 2 (CFHR2) regulates complement activation. *PloS one*, *8*(11), e78617.

Echtay, K. S., Roussel, D., St-Pierre, J., Jekabsons, M. B., Cadenas, S., Stuart, J. A., ... & Brand, M. D. (2002). Superoxide activates mitochondrial uncoupling proteins. *Nature*, *415*(6867), 96-99.

Edmondson, D. E., Binda, C., Wang, J., Upadhyay, A. K., & Mattevi, A. (2009). Molecular and mechanistic properties of the membrane-bound mitochondrial monoamine oxidases. *Biochemistry*, *48*(20), 4220-4230.

Ehalt Macedo, H., Lehner, B., Nicell, J., Grill, G., Li, J., Limtong, A., & Shakya, R. (2022). Distribution and characteristics of wastewater treatment plants within the global river network. *Earth System Science Data*, *14*(2), 559-577.

Ehrman, A. (2022). *Potential ecological monitoring indicators and strategies for the Anguniaqvia niqiqyuam Marine Protected Area and a synopsis of available information*. DFO: Fisheries and Oceans Canada.

El-Saiy, K. A., Sayed, R. H., El-Sahar, A. E., & Kandil, E. A. (2022). Modulation of histone deacetylase, the ubiquitin proteasome system, and autophagy underlies the neuroprotective effects of venlafaxine in a rotenone-induced Parkinson's disease model in rats. *Chemico-Biological Interactions*, *354*, 109841.

Elenkov, I. J., Wilder, R. L., Chrousos, G. P., & Vizi, E. S. (2000). The sympathetic nerve—an integrative interface between two supersystems: the brain and the immune system. *Pharmacological reviews*, *52*(4), 595-638.

Ellis, E. M. (2007). Reactive carbonyls and oxidative stress: potential for therapeutic intervention. *Pharmacology & therapeutics*, *115*(1), 13-24.

Ellison, A. R., Webster, T. M. U., Rodriguez-Barreto, D., de Leaniz, C. G., Consuegra, S., Orozco-terWengel, P., & Cable, J. (2020). Comparative transcriptomics reveal conserved impacts of rearing density on immune response of two important aquaculture species. *Fish & Shellfish Immunology*, *104*, 192-201.

Elmer, K. R., Fan, S., Gunter, H. M., Jones, J. C., Boekhoff, S., Kuraku, S., & Meyer, A. (2010). Rapid evolution and selection inferred from the transcriptomes of sympatric crater lake cichlid fishes. *Molecular ecology*, *19*, 197-211.

Emms, D. M., & Kelly, S. (2019). OrthoFinder: phylogenetic orthology inference for comparative genomics. *Genome biology*, *20*, 1-14.

Eniola, J. O., Kumar, R., Barakat, M. A., & Rashid, J. (2022). A review on conventional and advanced hybrid technologies for pharmaceutical wastewater treatment. Journal of Cleaner Production, 356, 131826.

Environment Canada. (2010). Pulp and paper environmental effects monitoring (EEM) Technical Guidance Document. Ottawa, ON, Canada.

Environment Canada. (2012). Metal Mining Environmental Effects Monitoring (EEM) Technical Guidance Document. Ottawa, ON, Canada.

Escobar-Sierra, C., & Lampert, K. P. (2024). Field application of de novo transcriptomic analysis to evaluate the effects of sublethal freshwater salinization on Gasterosteus aculeatus in urban streams. *Plos one*, *19*(3), e0298213.

Esteban, F. J., Jiménez, A., Barroso, J. B., Pedrosa, J. A., Del Moral, M. L., Rodrigo, J., & Peinado, M. A. (1998). The innervation of rainbow trout (*Oncorhynchus mykiss*) liver: protein gene product 9.5 and neuronal nitric oxide synthase immunoreactivities. *The Journal of Anatomy*, *193*(2), 241-249.

Etit, D., Meramo, S., Ögmundarson, Ó., Jensen, M. K., & Sukumara, S. (2024). Can biotechnology lead the way toward a sustainable pharmaceutical industry?. *Current Opinion in Biotechnology*, *87*, 103100.

Evans, S. E., Davies, P., Lubben, A., & Kasprzyk-Hordern, B. (2015). Determination of chiral pharmaceuticals and illicit drugs in wastewater and sludge using microwave assisted extraction, solid-phase extraction and chiral liquid chromatography coupled with tandem mass spectrometry. *Analytica chimica acta*, *882*, 112-126.

Evans, S., Bagnall, J., & Kasprzyk-Hordern, B. (2017). Enantiomeric profiling of a chemically diverse mixture of chiral pharmaceuticals in urban water. *Environmental Pollution*, *230*, 368-377.

Evans, T. G., & Hofmann, G. E. (2012). Defining the limits of physiological plasticity: how gene expression can assess and predict the consequences of ocean change. *Philosophical Transactions of the Royal Society B: Biological Sciences*, *367*(1596), 1733-1745.

Ezeoyili, I. C., Mgbenka, B. O., Atama, C. I., Ngwu, G. I., Madu, J. C., & Nwani, C. D. (2019). Changes in brain acetylcholinesterase and oxidative stress biomarkers in African catfish exposed to carbendazim. *Journal of Aquatic Animal Health*, *31*(4), 371-379.

Farrell, A. P., Hinch, S. G., Cooke, S. J., Patterson, D. A., Crossin, G. T., Lapointe, M., & Mathes, M. T. (2008). Pacific salmon in hot water: applying aerobic scope models and biotelemetry to predict the success of spawning migrations. *Physiological and biochemical zoology*, *81*(6), 697-708.

Feder, M. E., & Hofmann, G. E. (1999). Heat-shock proteins, molecular chaperones, and the stress response: evolutionary and ecological physiology. *Annual review of physiology*, *61*(1), 243-282.

Feder, M. E., & Walser, J. C. (2005). The biological limitations of transcriptomics in elucidating stress and stress responses. *Journal of evolutionary biology*, *18*(4), 901-910.

Feijóo, C. G., Sarrazin, A. F., Allende, M. L., & Glavic, A. (2009). Cystein−Serine−Rich nuclear protein 1, Axud1/Csrnp1, is essential for cephalic neural progenitor proliferation and survival in zebrafish. *Developmental dynamics: an official publication of the American Association of Anatomists*, *238*(8), 2034-2043.

Fernandez-Fuente, G., Overmyer, K. A., Lawton, A. J., Kasza, I., Shapiro, S. L., Gallego-Muñoz, P., ... & Puglielli, L. (2023). The citrate transporters SLC13A5 and SLC25A1 elicit different metabolic responses and phenotypes in the mouse. *Communications Biology*, *6*(1), 926.

Ferro, E. S., Gewehr, M. C., & Navon, A. (2020). Thimet oligopeptidase biochemical and biological significances: past, present, and future directions. *Biomolecules*, *10*(9), 1229.

Filby, A. L., Neuparth, T., Thorpe, K. L., Owen, R., Galloway, T. S., & Tyler, C. R. (2007). Health impacts of estrogens in the environment, considering complex mixture effects. *Environmental health perspectives*, *115*(12), 1704-1710.

Finkel, T., & Holbrook, N. J. (2000). Oxidants, oxidative stress and the biology of ageing. *nature*, *408*(6809), 239-247.

Fiorucci, S., Cipriani, S., Mencarelli, A., Renga, B., Distrutti, E., & Baldelli, F. (2010). Counter-regulatory role of bile acid activated receptors in immunity and inflammation. *Current molecular medicine*, *10*(6), 579-595.

Fisheries Act, R.S.C. 1985, c. F-14 (2019). https://laws-lois.justice.gc.ca/eng/acts/f-14/ (Accessed December 2024).

Fletcher, D. A., & Mullins, R. D. (2010). Cell mechanics and the cytoskeleton. *Nature*, *463*(7280), 485-492.

Fogelman, S. M., Schmider, J., Venkatakrishnan, K., von Moltke, L. L., Harmatz, J. S., Shader, R. I., & Greenblatt, D. J. (1999). O-and N-demethylation of venlafaxine in vitro by human liver microsomes and by microsomes from cDNA-transfected cells: effect of metabolic inhibitors and SSRI antidepressants. *Neuropsychopharmacology*, *20*(5), 480-490.

Forrest, G. L., & Gonzalez, B. (2000). Carbonyl reductase. *Chemico-biological interactions*, *129*(1-2), 21-40.

Francis, W. R., Christianson, L. M., Kiko, R., Powers, M. L., Shaner, N. C., & D Haddock, S. H. (2013). A comparison across non-model animals suggests an optimal sequencing depth for de novo transcriptome assembly. *BMC genomics*, *14*, 1-12.

Franco, M. E., Hollender, J., & Schirmer, K. (2025). Differential biotransformation ability may alter fish biodiversity in polluted waters. *Environment International*, 109254.

Frank, S. R., Hatfield, J. C., & Casanova, J. E. (1998). Remodeling of the actin cytoskeleton is coordinately regulated by protein kinase C and the ADP-ribosylation factor nucleotide exchange factor ARNO. *Molecular biology of the cell*, *9*(11), 3133-3146.

Fridovich, I. (1981). Superoxide radical and superoxide dismutases. *Oxygen and Living Processes: An Interdisciplinary Approach*, 250-272.

Fritz, K. S., & Petersen, D. R. (2013). An overview of the chemistry and biology of reactive aldehydes. *Free Radical Biology and Medicine*, *59*, 85-91.

Fuiman, L. A., Cowan, Jr, J. H., Smith, M. E., & O'Neal, J. P. (2005). Behavior and recruitment success in fish larvae: variation with growth rate and the batch effect. *Canadian Journal of Fisheries and Aquatic Sciences*, *62*(6), 1337-1349.

Fukui M, Zhu BT. 2010. Mitochondrial superoxide dismutase SOD2, but not cytosolic SOD1, plays a critical role in protection against glutamate-induced oxidative stress and cell death in HT22 neuronal cells. *Free Radic Biol Med* 48:821–830.

Fuzzen, M. L., Bragg, L. M., Tetreault, G. R., Bahamonde, P. A., Tanna, R. N., Bennett, C. J., ... & Servos, M. R. (2016). An assessment of the spatial and temporal variability of biological

responses to municipal wastewater effluent in rainbow darter (*Etheostoma caeruleum*) collected along an urban gradient. *PLoS One*, *11*(10), e0164879.

Galus, M., Kirischian, N., Higgins, S., Purdy, J., Chow, J., Rangaranjan, S., ... & Wilson, J. Y. (2013). Chronic, low concentration exposure to pharmaceuticals impacts multiple organ systems in zebrafish. *Aquatic toxicology*, *132*, 200-211.

Garceau, N., Pichaud, N., & Couture, P. (2010). Inhibition of goldfish mitochondrial metabolism by in vitro exposure to Cd, Cu and Ni. *Aquatic Toxicology*, *98*(2), 107-112.

Gardea-Resendez, M., Coombes, B. J., Veldic, M., Tye, S. J., Romo-Nava, F., Ozerdem, A., ... & Frye, M. A. (2023). Antidepressants that increase mitochondrial energetics may elevate risk of treatment-emergent mania. *Molecular psychiatry*, *28*(3), 1020-1026.

Gaschler, M. M., & Stockwell, B. R. (2017). Lipid peroxidation in cell death. *Biochemical and biophysical research communications*, *482*(3), 419-425.

Gauthier, P. T., & Vijayan, M. M. (2020). Municipal wastewater effluent exposure disrupts early development, larval behavior, and stress response in zebrafish. *Environmental Pollution*, *259*, 113757.

Gauvreau, N. L., Bragg, L. M., Dhiyebi, H. A., Servos, M. R., & Craig, P. M. (2022). Impacts on antioxidative enzymes and transcripts in darter (*Etheostoma spp*.) brains in the Grand River exposed to wastewater effluent. *Comparative Biochemistry and Physiology Part C: Toxicology & Pharmacology*, *258*, 109381.

Geisler, C. E., Ghimire, S., Hepler, C., Miller, K. E., Bruggink, S. M., Kentch, K. P., ... & Renquist, B. J. (2021). Hepatocyte membrane potential regulates serum insulin and insulin sensitivity by altering hepatic GABA release. *Cell reports*, *35*(13).

Gentile, F., Arcaro, A., Pizzimenti, S., Daga, M., Cetrangolo, G. P., Dianzani, C., ... & Barrera, G. (2017). DNA damage by lipid peroxidation products: implications in cancer, inflammation and autoimmunity. *AIMS genetics*, *4*(02), 103-137.

Giannisis, A., Patra, K., Edlund, A. K., Nieto, L. A., Benedicto-Gras, J., Moussaud, S., ... & Nielsen, H. M. (2022). Brain integrity is altered by hepatic APOE ε4 in humanized-liver mice. *Molecular Psychiatry*, *27*(8), 3533-3543.

Gibson, D. I. (1996). *Guide to the parasites of fishes of Canada Part IV Trematoda*. NRC Research Press

Gies, E. A., LeNoble, J. L., Noël, M., Etemadifar, A., Bishay, F., Hall, E. R., & Ross, P. S. (2018). Retention of microplastics in a major secondary wastewater treatment plant in Vancouver, Canada. *Marine pollution bulletin*, *133*, 553-561.

Gijbels, E., Vilas-Boas, V., Deferm, N., Devisscher, L., Jaeschke, H., Annaert, P., & Vinken, M. (2019). Mechanisms and in vitro models of drug-induced cholestasis. *Archives of toxicology*, *93*, 1169-1186.

Go, G. W., & Mani, A. (2012). Low-density lipoprotein receptor (LDLR) family orchestrates cholesterol homeostasis. *The Yale journal of biology and medicine*, *85*(1), 19.

Gomes, T. B., Junior, S. F. S., Saint'Pierre, T. D., Correia, F. V., Hauser-Davis, R. A., & Saggioro, E. M. (2019). Sublethal psychotropic pharmaceutical effects on the model organism *Danio rerio*: Oxidative stress and metal dishomeostasis. *Ecotoxicology and Environmental Safety*, *171*, 781-789.

Gonçalves, A. M., Rocha, C. P., Marques, J. C., & Gonçalves, F. J. (2021). Fatty acids as suitable biomarkers to assess pesticide impacts in freshwater biological scales–A review. *Ecological indicators*, *122*, 107299.

González Peña, O. I., López Zavala, M. Á., & Cabral Ruelas, H. (2021). Pharmaceuticals market, consumption trends and disease incidence are not driving the pharmaceutical research on water and wastewater. *International journal of environmental research and public health*, *18*(5), 2532.

Goodwin, B., Jones, S. A., Price, R. R., Watson, M. A., McKee, D. D., Moore, L. B., ... & Kliewer, S. A. (2000). A regulatory cascade of the nuclear receptors FXR, SHP-1, and LRH-1 represses bile acid biosynthesis. *Molecular cell*, *6*(3), 517-526.

Government of Canada. (2018). *Pulp and Paper Effluent Regulations* (SOR/92-269) under the *Canadian Fisheries Act*. Ottawa, ON

Government of Canada. (2024a). *Wastewater Systems Effluent Regulations* (SOR/2012-139) under the *Canadian Fisheries Act*. Ottawa, ON

Government of Canada. (2024b). *Metal and Diamond Mining Effluent Regulations* (SOR/2002-222) under the *Canadian Fisheries Act*. Ottawa, ON

Grabherr, M. G., Haas, B. J., Yassour, M., Levin, J. Z., Thompson, D. A., Amit, I., ... & Regev, A. (2011). Trinity: reconstructing a full-length transcriptome without a genome from RNA-Seq data. *Nature biotechnology*, *29*(7), 644.

Gravel, A., & Vijayan, M. M. (2007). Non-steroidal anti-inflammatory drugs disrupt the heat shock response in rainbow trout. *Aquatic toxicology*, *81*(2), 197-206.

Grayfer, L., & Belosevic, M. (2009). Molecular characterization of novel interferon gamma receptor 1 isoforms in zebrafish (*Danio rerio*) and goldfish (*Carassius auratus L.*). *Molecular immunology*, *46*(15), 3050-3059.

Grbić, J., Helm, P., Athey, S., & Rochman, C. M. (2020). Microplastics entering northwestern Lake Ontario are diverse and linked to urban sources. *Water research*, *174*, 115623.

Griffis, E. R., Altan, N., Lippincott-Schwartz, J., & Powers, M. A. (2002). Nup98 is a mobile nucleoporin with transcription-dependent dynamics. *Molecular biology of the cell*, *13*(4), 1282-1297.

Guidi, S., Stagni, F., Bianchi, P., Ciani, E., Ragazzi, E., Trazzi, S., ... & Bartesaghi, R. (2013). Early Pharmacotherapy with Fluoxetine Rescues Dendritic Pathology in the Ts65Dn Mouse Model of D own Syndrome. *Brain pathology*, *23*(2), 129-143.

Guo, X., Stafford, L. J., Bryan, B., Xia, C., Ma, W., Wu, X., ... & Liu, M. (2003). A Rac/Cdc42-specific exchange factor, GEFT, induces cell proliferation, transformation, and migration. *Journal of Biological Chemistry*, *278*(15), 13207-13215.

Gusdon, A. M., Votyakova, T. V., Reynolds, I. J., & Mathews, C. E. (2007). Nuclear and mitochondrial interaction involving mt-Nd2 leads to increased mitochondrial reactive oxygen species production. *Journal of Biological Chemistry*, *282*(8), 5171-5179.

Haas, B. J., Papanicolaou, A., Yassour, M., Grabherr, M., Blood, P. D., Bowden, J., ... & Regev, A. (2013). De novo transcript sequence reconstruction from RNA-seq using the Trinity platform for reference generation and analysis. *Nature protocols*, *8*(8), 1494-1512.

Haase, M., & Fitze, G. (2016). HSP90AB1: Helping the good and the bad. *Gene*, *575*(2), 171-186.

Hagenbuch, B., & Gui, C. (2008). Xenobiotic transporters of the human organic anion transporting polypeptides (OATP) family. *Xenobiotica*, *38*(7-8), 778-801.

Haider, S., & Pal, R. (2013). Integrated analysis of transcriptomic and proteomic data. *Current genomics*, *14*(2), 91-110.

Hamid, N., Junaid, M., Wang, Y., Pu, S. Y., Jia, P. P., & Pei, D. S. (2021). Chronic exposure to PPCPs mixture at environmentally relevant concentrations (ERCs) altered carbohydrate and lipid metabolism through gut and liver toxicity in zebrafish. *Environmental Pollution*, *273*, 116494.

Han, C. Y., Rho, H. S., Kim, A., Kim, T. H., Jang, K., Jun, D. W., ... & Kim, S. G. (2018). FXR inhibits endoplasmic reticulum stress-induced NLRP3 inflammasome in hepatocytes and ameliorates liver injury. *Cell reports*, *24*(11), 2985-2999.

Hancu, G., Lupu, D., Milan, A., Budău, M., & Barabás−Hajdu, E. (2021). Enantioselective analysis of venlafaxine and its active metabolites: A review on the separation methodologies. *Biomedical Chromatography*, *35*(1), e4874.

Harduin-Lepers, A., Vallejo-Ruiz, V., Krzewinski-Recchi, M. A., Samyn-Petit, B., Julien, S., & Delannoy, P. (2001). The human sialyltransferase family. *Biochimie*, *83*(8), 727-737.

Hata, T., Rehman, F., Hori, T., & Nguyen, J. H. (2019). GABA, γ-aminobutyric acid, protects against severe liver injury. *journal of surgical research*, *236*, 172-183.

Haynes, C. M., Titus, E. A., & Cooper, A. A. (2004). Degradation of misfolded proteins prevents ER-derived oxidative stress and cell death. *Molecular cell*, *15*(5), 767-776.

He, X., & Zhang, J. (2006). Why do hubs tend to be essential in protein networks?. *PLoS genetics*, *2*(6), e88.

Head, J. A., Ewald, J. D., & Basu, N. (2024). The DIKW of Transcriptomics in Ecotoxicology: Extracting Information, Knowledge, and Wisdom From Big Data. *Environmental Toxicology and Chemistry*.

Hébert, N., Gagné, F., Cejka, P., Cyr, D., Marcogliese, D. J., Blaise, C., ... & Fournier, M. (2008). The effects of a primary-treated municipal effluent on the immune system of rainbow trout (*Oncorhynchus mykiss*): Exposure duration and contribution of suspended particles. *Comparative Biochemistry and Physiology Part C: Toxicology & Pharmacology*, *148*(3), 258-264.

Heintzman, N. D., Hon, G. C., Hawkins, R. D., Kheradpour, P., Stark, A., Harp, L. F., ... & Ren, B. (2009). Histone modifications at human enhancers reflect global cell-type-specific gene expression. *Nature*, *459*(7243), 108-112.

Hendry, A. P., Berg, O. K., & Quinn, T. P. (1999). Condition dependence and adaptation-by-time: breeding date, life history, and energy allocation within a population of salmon. *Oikos*, 499-514.

Hernandez, J. A., Castro, V. L., Reyes-Nava, N., Montes, L. P., & Quintana, A. M. (2019). Mutations in the zebrafish hmgcs1 gene reveal a novel function for isoprenoids during red blood cell development. *Blood Advances*, *3*(8), 1244-1254.

Hicks, K. A., & Servos, M. R. (2017). Site fidelity and movement of a small−bodied fish species, the rainbow darter (*Etheostoma caeruleum*): Implications for environmental effects assessment. *River Research and Applications*, *33*(7), 1016-1025.

Higashiguchi, Y., Katsuta, K., Minegishi, T., Yonemura, S., Urasaki, A., & Inagaki, N. (2016). Identification of a shootin1 isoform expressed in peripheral tissues. *Cell and tissue research*, *366*(1), 75-87.

Hipp, M. S., Kasturi, P., & Hartl, F. U. (2019). The proteostasis network and its decline in ageing. *Nature reviews Molecular cell biology*, *20*(7), 421-435.

Hirano, M., Hashimoto, S., Yonemura, S., Sabe, H., & Aizawa, S. (2008). EPB41L5 functions to post-transcriptionally regulate cadherin and integrin during epithelial–mesenchymal transition. *The Journal of cell biology*, *182*(6), 1217-1230.

Hirao, K., Hata, Y., Ide, N., Takeuchi, M., Irie, M., Yao, I., ... & Takai, Y. (1998). A Novel Multiple PDZ Domain-containing Molecule Interacting withN-Methyl-D-aspartateReceptors and Neuronal Cell Adhesion Proteins. *Journal of Biological Chemistry*, *273*(33), 21105-21110.

Hodgson, R., Bragg, L., Dhiyebi, H. A., Servos, M. R., & Craig, P. M. (2020). Impacts on metabolism and gill physiology of darter species (*Etheostoma spp*.) that are attributed to wastewater effluent in the grand river. *Applied Sciences*, *10*(23), 8364.

Hoeger, B., Köllner, B., Dietrich, D. R., & Hitzfeld, B. (2005). Water-borne diclofenac affects kidney and gill integrity and selected immune parameters in brown trout (*Salmo trutta f. fario*). *Aquatic toxicology*, *75*(1), 53-64.

Hoffmann, F., & Maser, E. (2007). Carbonyl reductases and pluripotent hydroxysteroid dehydrogenases of the short-chain dehydrogenase/reductase superfamily. *Drug metabolism reviews*, *39*(1), 87-144.

Holland, M. C. H., & Lambris, J. D. (2002). The complement system in teleosts. *Fish & shellfish immunology*, *12*(5), 399-420.

Hollingsworth Jr, P. R., & Near, T. J. (2009). Temporal patterns of diversification and microendemism in Eastern Highland endemic barcheek darters (*Percidae: Etheostomatinae*). *Evolution*, *63*(1), 228-243.

Holzer, A. S., Piazzon, M. C., Barrett, D., Bartholomew, J. L., & Sitjà-Bobadilla, A. (2021). To react or not to react: The dilemma of fish immune systems facing myxozoan infections. *Frontiers in Immunology*, *12*, 734238.

Hong, H., Zhou, Y., Wu, H., Luo, Y., & Shen, H. (2014). Lipid content and fatty acid profile of muscle, brain and eyes of seven freshwater fish: a comparative study. *Journal of the American Oil Chemists' Society*, *91*(5), 795-804.

Hook, S. E., Mondon, J., Revill, A. T., Greenfield, P. A., Smith, R. A., Turner, R. D., ... & Warne, M. S. J. (2018). Transcriptomic, lipid, and histological profiles suggest changes in health in fish from a pesticide hot spot. *Marine environmental research*, *140*, 299-321.

Horst, W. D., & Preskorn, S. H. (1998). Mechanisms of action and clinical characteristics of three atypical antidepressants: venlafaxine, nefazodone, bupropion. *Journal of affective disorders*, *51*(3), 237-254.

Hossain, M. S., Mawatari, S., & Fujino, T. (2020). Biological functions of plasmalogens. *Peroxisome biology: Experimental models, peroxisomal disorders and neurological diseases*, 171-193.

Howell, E. T., & Benoit, N. (2021). Nutrient footprints on the Toronto-Mississauga waterfront of Lake Ontario. *Journal of Great Lakes Research*, *47*(2), 343-365.

Hoyer, K. A., & Geheber, A. D. (2024). Impacts of Wastewater Effluent on Temperate Stream Fish Assemblage Structure. *Ichthyology & Herpetology*, *112*(2), 217-228.

Ontario Freshwater Fishes. (2025). Ontario Freshwater Fishes Life History Database. https://www.ontariofishes.ca

Hu, G., Wu, Z., Uversky, V. N., & Kurgan, L. (2017). Functional analysis of human hub proteins and their interactors involved in the intrinsic disorder-enriched interactions. *International journal of molecular sciences*, *18*(12), 2761.

Huang, W., Han, N., Du, L., Wang, M., Chen, L., & Tang, H. (2021). A narrative review of liver regeneration—from models to molecular basis. *Annals of Translational Medicine*, *9*(22).

Huerta, B., Rodriguez-Mozaz, S., Lazorchak, J., Barcelo, D., Batt, A., Wathen, J., & Stahl, L. (2018). Presence of pharmaceuticals in fish collected from urban rivers in the US EPA 2008–2009 National Rivers and Streams Assessment. *Science of The Total Environment*, *634*, 542-549.

Inserra, A., Campanale, A., Rezai, T., Romualdi, P., & Rubino, T. (2024). Epigenetic mechanisms of rapid-acting antidepressants. *Translational Psychiatry*, *14*(1), 359.

Ipson, B. R., Green, R. A., Wilson, J. T., Watson, J. N., Faull, K. F., & Fisher, A. L. (2019). Tyrosine aminotransferase is involved in the oxidative stress response by metabolizing meta-tyrosine in Caenorhabditis elegans. *Journal of Biological chemistry*, *294*(24), 9536-9554.

Irwin, D. M., & Tan, H. (2008). Molecular evolution of the vertebrate hexokinase gene family: Identification of a conserved fifth vertebrate hexokinase gene. *Comparative Biochemistry and Physiology Part D: Genomics and Proteomics*, *3*(1), 96-107.

Islas-Flores, H., Gómez-Oliván, L. M., Galar-Martínez, M., Colín-Cruz, A., Neri-Cruz, N., & García-Medina, S. (2013). Diclofenac-induced oxidative stress in brain, liver, gill and blood of common carp (*Cyprinus carpio*). *Ecotoxicology and environmental safety*, *92*, 32-38.

Ito, F., Sono, Y., & Ito, T. (2019). Measurement and clinical significance of lipid peroxidation as a biomarker of oxidative stress: oxidative stress in diabetes, atherosclerosis, and chronic inflammation. *Antioxidants*, *8*(3), 72.

Jackson, C. L., & McNiven, M. A. (2020). The hepatocellular secretory pathway. *The Liver: Biology and Pathobiology*, 75-85.

Jeffries, K. M., Fangue, N. A., & Connon, R. E. (2018). Multiple sub-lethal thresholds for cellular responses to thermal stressors in an estuarine fish. *Comparative Biochemistry and Physiology Part A: Molecular & Integrative Physiology*, *225*, 33-45.

Jeyachandran, S., Chellapandian, H., Park, K., & Kwak, I. S. (2023). A review on the involvement of heat shock proteins (extrinsic chaperones) in response to stress conditions in aquatic organisms. *Antioxidants*, *12*(7), 1444.

Jiang, X. S., Backlund, P. S., Wassif, C. A., Yergey, A. L., & Porter, F. D. (2010). Quantitative proteomics analysis of inborn errors of cholesterol synthesis: identification of altered metabolic pathways in DHCR7 and SC5D deficiency. *Molecular & Cellular Proteomics*, *9*(7), 1461-1475.

Jiao, Y., Lu, Y., & Li, X. Y. (2015). Farnesoid X receptor: a master regulator of hepatic triglyceride and glucose homeostasis. *Acta Pharmacologica Sinica*, *36*(1), 44-50.

Jin, G., Zhang, S., Zhang, X. S., & Chen, L. (2007). Hubs with network motifs organize modularity dynamically in the protein-protein interaction network of yeast. *PloS one*, *2*(11), e1207.

Jin, L., Wang, Q., Yan, M., Gu, J., Zhang, K., Lam, P. K., & Ruan, Y. (2023). Enantiospecific Uptake and Depuration Kinetics of Chiral Metoprolol and Venlafaxine in Marine Medaka (*Oryzias melastigma*): Tissue Distribution and Metabolite Formation. *Environmental Science & Technology*, *57*(11), 4471-4480.

Jones, E. R., Simning, D., Serafin, J., Sepúlveda, M. S., & Griffitt, R. J. (2020). Acute exposure to oil induces age and species-specific transcriptional responses in embryo-larval estuarine fish. *Environmental Pollution*, *263*, 114325.

Joshi, Y. B., & Praticò, D. (2014). Lipid peroxidation in psychiatric illness: overview of clinical evidence. *Oxidative medicine and cellular longevity*, *2014*(1), 828702.

Juan, C. A., Pérez de la Lastra, J. M., Plou, F. J., & Pérez-Lebeña, E. (2021). The chemistry of reactive oxygen species (ROS) revisited: outlining their role in biological macromolecules (DNA, lipids and proteins) and induced pathologies. *International journal of molecular sciences*, *22*(9), 4642.

Juin, A., Planus, E., Guillemot, F., Horakova, P., Albiges‐Rizo, C., Génot, E., ... & Saltel, F. (2013). Extracellular matrix rigidity controls podosome induction in microvascular endothelial cells. *Biology of the Cell*, *105*(1), 46-57.

Kabayama, M., Sakoori, K., Yamada, K., Ornthanalai, V. G., Ota, M., Morimura, N., ... & Aruga, J. (2013). Rines E3 ubiquitin ligase regulates MAO-A levels and emotional responses. *Journal of Neuroscience*, *33*(32), 12940-12953.

Kaboré, H. A., Goeury, K., Desrosiers, M., Vo Duy, S., Liu, J., Cabana, G., ... & Sauvé, S. (2022). Fish exhibit distinct fluorochemical and δ15N isotopic signatures in the St. Lawrence River impacted by municipal wastewater effluents. *Frontiers in Environmental Science*, *10*, 833164.

Kaiser, F., Krautwurst, S., Salentin, S., Haupt, V. J., Leberecht, C., Bittrich, S., ... & Schroeder, M. (2020). The structural basis of the genetic code: amino acid recognition by aminoacyl-tRNA synthetases. *Scientific Reports*, *10*(1), 12647.

Kalman, J., Palotas, A., Juhasz, A., Rimanoczy, A., Hugyecz, M., Kovacs, Z., ... & Puskás, L. G. (2005). Impact of venlafaxine on gene expression profile in lymphocytes of the elderly with major depression–evolution of antidepressants and the role of the "neuro-immune" system. *Neurochemical research*, *30*, 1429-1438.

Kaludercic, N., Deshwal, S., & Di Lisa, F. (2014). Reactive oxygen species and redox compartmentalization. *Frontiers in physiology*, *5*, 285.

Kang, J., Nagelkerken, I., Rummer, J. L., Rodolfo−Metalpa, R., Munday, P. L., Ravasi, T., & Schunter, C. (2022). Rapid evolution fuels transcriptional plasticity to ocean acidification. *Global Change Biology*, *28*(9), 3007-3022.

Karanth, S., Chaurasia, B., Bowman, F. M., Tippetts, T. S., Holland, W. L., Summers, S. A., & Schlegel, A. (2019). FOXN3 controls liver glucose metabolism by regulating gluconeogenic substrate selection. *Physiological reports*, *7*(18), e14238.

Karanth, S., Zinkhan, E. K., Hill, J. T., Yost, H. J., & Schlegel, A. (2016). FOXN3 regulates hepatic glucose utilization. *Cell reports*, *15*(12), 2745-2755.

Kårelid, V., Larsson, G., & Björlenius, B. (2017). Pilot-scale removal of pharmaceuticals in municipal wastewater: Comparison of granular and powdered activated carbon treatment at three wastewater treatment plants. *Journal of environmental management*, *193*, 491-502.

Kargapolova, Y., Rehimi, R., Kayserili, H., Brühl, J., Sofiadis, K., Zirkel, A., ... & Papantonis, A. (2021). Overarching control of autophagy and DNA damage response by CHD6 revealed by modeling a rare human pathology. *Nature Communications*, *12*(1), 3014.

Kasai, H., Crain, P. F., Kuchino, Y., Nishimura, S., Ootsuyama, A., & Tanooka, H. (1986). Formation of 8-hydroxyguanine moiety in cellular DNA by agents producing oxygen radicals and evidence for its repair. *Carcinogenesis*, *7*(11), 1849-1851.

Kashiwada, S., Hinton, D. E., & Kullman, S. W. (2005). Functional characterization of medaka CYP3A38 and CYP3A40: kinetics and catalysis by expression in a recombinant baculovirus system. *Comparative Biochemistry and Physiology Part C: Toxicology & Pharmacology*, *141*(4), 338-348.

Kasprzyk-Hordern, B., & Baker, D. R. (2012). Enantiomeric profiling of chiral drugs in wastewater and receiving waters. *Environmental science & technology*, *46*(3), 1681-1691.

Kaupmann, K., Huggel, K., Heid, J., Flor, P. J., Bischoff, S., Mickel, S. J., ... & Bettler, B. (1997). Expression cloning of GABAB receptors uncovers similarity to metabotropic glutamate receptors. *Nature*, *386*(6622), 239-246.

Kavembe, G. D., Franchini, P., Irisarri, I., Machado-Schiaffino, G., & Meyer, A. (2015). Genomics of adaptation to multiple concurrent stresses: insights from comparative transcriptomics of a Cichlid fish from one of earth's most extreme environments, the hypersaline soda Lake Magadi in Kenya, east Africa. *Journal of molecular evolution*, *81*, 90-109.

Keller, J. N., & Mattson, M. P. (1998). Roles of lipid peroxidation in modulation of cellular signaling pathways, cell dysfunction, and death in the nervous system. *Reviews in the Neurosciences*, *9*(2), 105-116.

Kelly, N. E., Guijarro-Sabaniel, J., & Zimmerman, R. (2021). Anthropogenic nitrogen loading and risk of eutrophication in the coastal zone of Atlantic Canada. *Estuarine, Coastal and Shelf Science*, *263*, 107630.

Khan, N. A., & Deschaux, P. (1997). Role of serotonin in fish immunomodulation. *Journal of experimental biology*, *200*(13), 1833-1838.

Khan, T. N., Khan, K., Sadeghpour, A., Reynolds, H., Perilla, Y., McDonald, M. T., ... & Wiener, J. (2019). Mutations in NCAPG2 cause a severe neurodevelopmental syndrome that expands the phenotypic spectrum of condensinopathies. *The American Journal of Human Genetics*, *104*(1), 94-111.

Khoriaty, R., Hesketh, G. G., Bernard, A., Weyand, A. C., Mellacheruvu, D., Zhu, G., ... & Ginsburg, D. (2018). Functions of the COPII gene paralogs SEC23A and SEC23B are interchangeable in vivo. *Proceedings of the National Academy of Sciences*, *115*(33), E7748-E7757.

Kim, K., & Yoon, H. (2023). Gamma-aminobutyric acid signaling in damage response, metabolism, and disease. *International Journal of Molecular Sciences*, *24*(5), 4584.

Kim, Y. J., Kim, K. S., Kim, S. H., Kim, C. H., Ko, J. H., Choe, I. S., ... & Lee, Y. C. (1996). Molecular cloning and expression of human Galβ1, 3GalNAc α2, 3-sialyltransferase (hST3Gal II). *Biochemical and biophysical research communications*, *228*(2), 324-327.

Kisielius, V., Kharel, S., Skaarup, J., Lauritzen, B. S., Lukas, M., Bogusz, A., ... & Bester, K. (2023). Process design for removal of pharmaceuticals in wastewater treatment plants based on predicted no effect concentration (PNEC). *Chemical Engineering Journal*, *476*, 146644.

Kitagawa, H., & Paulson, J. C. (1994). Cloning of a novel alpha 2, 3-sialyltransferase that sialylates glycoprotein and glycolipid carbohydrate groups. Journal of Biological Chemistry, 269(2), 1394-1401.

Kliewer, S. A., Goodwin, B., & Willson, T. M. (2002). The nuclear pregnane X receptor: a key regulator of xenobiotic metabolism. *Endocrine reviews*, *23*(5), 687-702.

Kondo, H., Morinaga, K., Misaki, R., Nakaya, M., & Watabe, S. (2005). Characterization of the pufferfish Takifugu rubripes apolipoprotein multigene family. *Gene*, *346*, 257-266.

Koné, M., Cologgi, D. L., Lu, W., Smith, D. W., & Ulrich, A. C. (2013). Pharmaceuticals in Canadian sewage treatment plant effluents and surface waters: occurrence and environmental risk assessment. *Environmental Technology Reviews*, *2*(1), 17-27.

Kono, T., Kusuda, R., Kawahara, E., & Sakai, M. (2003). The analysis of immune responses of a novel CC-chemokine gene from Japanese flounder Paralichthys olivaceus. *Vaccine*, *21*(5-6), 446-457.

Konovalova, S., Liu, X., Manjunath, P., Baral, S., Neupane, N., Hilander, T., ... & Tyynismaa, H. (2018). Redox regulation of GRPEL2 nucleotide exchange factor for mitochondrial HSP70 chaperone. *Redox Biology*, *19*, 37-45.

Korzekwa, K. R., & Jones, J. P. (1993). Predicting the cytochrome P450 mediated metabolism of xenobiotics. *Pharmacogenetics and Genomics*, *3*(1), 1-18.

Kot-Wasik, A., Jakimska, A., & Śliwka-Kaszyńska, M. (2016). Occurrence and seasonal variations of 25 pharmaceutical residues in wastewater and drinking water treatment plants. *Environmental monitoring and assessment*, *188*, 1-13.

Kotarba, G., Krzywinska, E., Grabowska, A. I., Taracha, A., & Wilanowski, T. (2018). TFCP2/TFCP2L1/UBP1 transcription factors in cancer. *Cancer letters*, *420*, 72-79.

Kozal, J. S., Jayasundara, N., Massarsky, A., Lindberg, C. D., Oliveri, A. N., Cooper, E. M., ... & Di Giulio, R. T. (2023). Mitochondrial dysfunction and oxidative stress contribute to cross-generational toxicity of benzo (a) pyrene in Danio rerio. *Aquatic Toxicology*, *263*, 106658.

Kožich, V., Morris, A. A., & Blom, H. J. (2022). Disorders of sulfur amino acid metabolism. In *Inborn metabolic diseases: diagnosis and treatment* (pp. 407-422). Berlin, Heidelberg: Springer Berlin Heidelberg.

Kumar, G., Abd-Elfattah, A., & El-Matbouli, M. (2015). Identification of differentially expressed genes of brown trout (*Salmo trutta*) and rainbow trout (*Oncorhynchus mykiss*) in response to Tetracapsuloides bryosalmonae (*Myxozoa*). *Parasitology Research*, *114*, 929-939.

Kuwata, H., & Hara, S. (2019). Role of acyl-CoA synthetase ACSL4 in arachidonic acid metabolism. *Prostaglandins & other lipid mediators*, *144*, 106363.

Kyjacova, L., Saup, R., Rönsch, K., Wallbaum, S., Dukowic-Schulze, S., Foss, A., ... & Sleeman, J. P. (2021). IER2-induced senescence drives melanoma invasion through osteopontin. *Oncogene*, *40*(47), 6494-6512.

Lalonde, B., & Garron, C. (2021). Nonylphenol, octylphenol, and nonylphenol ethoxylates dissemination in the Canadian freshwater environment. *Archives of environmental contamination and toxicology*, *80*(2), 319-330.

Lange A, Paull GC, Coe TS, Katsu Y, Urushitani H, Iguchi T, Tyler CR. 2009. Sexual reprogramming and estrogenic sensitization in wild fish exposed to ethinylestradiol. *Environ Sci Technol* 43:1219–1225.

Larivuo, I., Laukkala, H., Nevalainen, A., Arponen, O., & Nevalainen, O. P. (2023). Psychiatric medications and the risk of autoimmune and immune-mediated inflammatory diseases: A systematic review and meta-analysis of observational studies. *Plos one*, *18*(2), e0281979.

Lassègue, B., San Martín, A., & Griendling, K. K. (2012). Biochemistry, physiology, and pathophysiology of NADPH oxidases in the cardiovascular system. *Circulation research*, *110*(10), 1364-1390.

Lau, S. C., Mehdi, H., Bragg, L. M., Servos, M. R., Balshine, S., & Scott, G. R. (2021). Exposure to wastewater effluent disrupts hypoxia responses in killifish (*Fundulus heteroclitus*). *Environmental Pollution*, *284*, 117373.

Lavery, W. J., Barski, A., Wiley, S., Schorry, E. K., & Lindsley, A. W. (2020). KMT2C/D COMPASS complex-associated diseases [K CD COM-ADs]: an emerging class of congenital regulopathies. *Clinical epigenetics*, *12*, 1-20.

Leal Filho, W., Saari, U., Fedoruk, M., Iital, A., Moora, H., Klöga, M., & Voronova, V. (2019). An overview of the problems posed by plastic products and the role of extended producer responsibility in Europe. *Journal of cleaner production*, *214*, 550-558.

Lee, H. F. (1962). Life history of Heterobilharzia americana Price 1929, a schistosome of the raccoon and other mammals in southeastern United States. *The Journal of Parasitology*, 728-739.

Lee, J. E., Wang, C., Xu, S., Cho, Y. W., Wang, L., Feng, X., ... & Ge, K. (2013). H3K4 mono- and di-methyltransferase MLL4 is required for enhancer activation during cell differentiation. *elife*, *2*, e01503.

Lee, W. M. (2003). Drug-induced hepatotoxicity. *New England journal of medicine*, *349*(5), 474-485.

Lehmann, J. M., McKee, D. D., Watson, M. A., Willson, T. M., Moore, J. T., & Kliewer, S. A. (1998). The human orphan nuclear receptor PXR is activated by compounds that regulate CYP3A4 gene expression and cause drug interactions. *The Journal of clinical investigation*, *102*(5), 1016-1023.

Levine, T. (2004). Short-range intracellular trafficking of small molecules across endoplasmic reticulum junctions. *Trends in cell biology*, *14*(9), 483-490.

Li, C., Chen, Q., Zhang, X., Snyder, S. A., Gong, Z., & Lam, S. H. (2018). An integrated approach with the zebrafish model for biomonitoring of municipal wastewater effluent and receiving waters. *Water research*, *131*, 33-44.

Li, J. Y., Wang, Y. Y., Shao, T., Fan, D. D., Lin, A. F., Xiang, L. X., & Shao, J. Z. (2020). The zebrafish NLRP3 inflammasome has functional roles in ASC-dependent interleukin-1β maturation and gasdermin E–mediated pyroptosis. *Journal of Biological Chemistry*, *295*(4), 1120-1141.

Li, X., Xiong, D., Ju, Z., Xiong, Y., Ding, G., & Liao, G. (2021). Phenotypic and transcriptomic consequences in zebrafish early-life stages following exposure to crude oil and chemical dispersant at sublethal concentrations. *Science of The Total Environment*, *763*, 143053.

Li, Y., Chen, L., Huang, R., Yang, C., Gui, B., Li, Y., Liao, L., Zhu, Z., & Wang, Y. (2022). Grass carp SERPINA1 inhibits GCRV infection through degrading CF2. *Frontiers in Immunology, 13*, 969517.

Li, Z., Gomez, E., Fenet, H., & Chiron, S. (2013). Chiral signature of venlafaxine as a marker of biological attenuation processes. *Chemosphere*, *90*(6), 1933-1938.

Lin, S., Cheng, D., Liu, M. S., Chen, J., & Chang, T. Y. (1999). Human acyl-CoA: cholesterol acyltransferase-1 in the endoplasmic reticulum contains seven transmembrane domains. *Journal of Biological Chemistry*, *274*(33), 23276-23285.

Lin, T. Y., Wei, T. Y. W., Li, S., Wang, S. C., He, M., Martin, M., ... & Shyy, J. Y. J. (2016). TIFA as a crucial mediator for NLRP3 inflammasome. *Proceedings of the National Academy of Sciences*, *113*(52), 15078-15083.

Lindqvist, D., Jensen, S., & Asplund, L. (2014). Lipid-soluble conjugates of hydroxylated polybrominated diphenyl ethers in blue mussels from the Baltic Sea. *Environmental Science and Pollution Research*, *21*, 954-961.

Liney, K. E., Hagger, J. A., Tyler, C. R., Depledge, M. H., Galloway, T. S., & Jobling, S. (2006). Health effects in fish of long-term exposure to effluents from wastewater treatment works. *Environmental health perspectives*, *114*(Suppl 1), 81-89.

Little, C., Olinescu, R., Reid, K. G., & O'brien, P. J. (1970). Properties and regulation of glutathione peroxidase. *Journal of Biological Chemistry*, *245*(14), 3632-3636.

Liu, D., Lin, Y., Kang, T., Huang, B., Xu, W., Garcia-Barrio, M., ... & Thompson, W. E. (2012a). Mitochondrial dysfunction and adipogenic reduction by prohibitin silencing in 3T3-L1 cells. *PloS one*, *7*(3), e34315.

Liu, H., Fu, R., Zhang, Y., Mao, L., Zhu, L., Zhang, L., ... & Jiang, H. (2023). Integrate transcriptomic and metabolomic analysis reveals the underlying mechanisms of behavioral disorders in zebrafish (*Danio rerio*) induced by imidacloprid. *Science of The Total Environment*, *870*, 161541.

Liu, R., Long, Y., Liu, R., Song, G., Li, Q., Yan, H., & Cui, Z. (2022). Understanding the function and mechanism of zebrafish Tmem39b in regulating cold resistance. *International Journal of Molecular Sciences*, *23*(19), 11442.

Liu, S., Lai, J., Feng, Y., Zhuo, Y., Zhang, H., Chen, Y., ... & Zhong, W. (2023). Acetyl-CoA carboxylase 1 depletion suppresses de novo fatty acid synthesis and mitochondrial β-oxidation in castration-resistant prostate cancer cells. *Journal of Biological Chemistry*, *299*(1).

Liu, T., Daniels, C. K., & Cao, S. (2012b). Comprehensive review on the HSC70 functions, interactions with related molecules and involvement in clinical diseases and therapeutic potential. *Pharmacology & therapeutics*, *136*(3), 354-374.

Liu, Y., Zhou, J., & White, K. P. (2014). RNA-seq differential expression studies: more sequence or more replication?. *Bioinformatics*, *30*(3), 301-304.

Lopes-Ferreira, M., Magalhães, G. S., Fernandez, J. H., Inácio de Loiola, M., Le Ho, P., Lima, C., ... & Moura-da-Silva, A. M. (2011). Structural and biological characterization of Nattectin, a new C-type lectin from the venomous fish Thalassophryne nattereri. *Biochimie*, *93*(6), 971-980.

Lu, J., Meng, W., Poy, F., Maiti, S., Goode, B. L., & Eck, M. J. (2007). Structure of the FH2 domain of Daam1: implications for formin regulation of actin assembly. *Journal of molecular biology*, *369*(5), 1258-1269.

Lu, L., Horstmann, H., Ng, C., & Hong, W. (2001). Regulation of Golgi structure and function by ARF-like protein 1 (Arl1). *Journal of cell science*, *114*(24), 4543-4555.

Ludvik, A. E., Pusec, C. M., Priyadarshini, M., Angueira, A. R., Guo, C., Lo, A., ... & Layden, B. T. (2016). HKDC1 is a novel hexokinase involved in whole-body glucose use. *Endocrinology*, *157*(9), 3452-3461.

Luo, L. F., Xu, Z. S., Li, D. Y., Hu, Z., & Gao, Z. X. (2022). Comparative transcriptome profiles of four sexually size dimorphic fish. *Scientific Data*, *9*(1), 774.

Lupo, V., Van Vlierberghe, M., Vanderschuren, H., Kerff, F., Baurain, D., & Cornet, L. (2021). Contamination in reference sequence databases: time for divide-and-rule tactics. *Frontiers in Microbiology*, *12*, 755101.

Lushchak, V. I. (2016). Contaminant-induced oxidative stress in fish: a mechanistic approach. *Fish physiology and biochemistry*, *42*, 711-747.

Lutz, T., Stöger, R., & Nieto, A. (2006). CHD6 is a DNA-dependent ATPase and localizes at nuclear sites of mRNA synthesis. *FEBS letters*, *580*(25), 5851-5857.

Lv, C., Zhang, D., & Wang, Z. (2016). A novel C-type lectin, Nattectin-like protein, with a wide range of bacterial agglutination activity in large yellow croaker Larimichthys crocea. *Fish & Shellfish Immunology*, *50*, 231-241.

Ma, K., Saha, P. K., Chan, L., & Moore, D. D. (2006). Farnesoid X receptor is essential for normal glucose homeostasis. *The Journal of clinical investigation*, *116*(4), 1102-1109.

Ma, R., Qu, H., Wang, B., Wang, F., & Yu, G. (2020). Widespread monitoring of chiral pharmaceuticals in urban rivers reveals stereospecific occurrence and transformation. *Environment international*, *138*, 105657.

Ma, Z. R., Li, H. P., Cai, S. Z., Du, S. Y., Chen, X., Yao, J., ... & Wang, Q. (2023). The mitochondrial protein TIMM44 is required for angiogenesis in vitro and in vivo. *Cell Death & Disease*, *14*(5), 307.

Macêdo, L. G., Carvalho-Silva, M., Ferreira, G. K., Vieira, J. S., Olegário, N., Gonçalves, R. C., ... & Streck, E. L. (2013). Effect of acute administration of L-tyrosine on oxidative stress parameters in brain of young rats. *Neurochemical research*, *38*, 2625-2630.

Machuca-Sepúlveda, J., Miranda, J., Lefin, N., Pedroso, A., Beltrán, J. F., & Farias, J. G. (2023). Current Status of Omics in Biological Quality Elements for Freshwater Biomonitoring. *Biology*, *12*(7), 923.

MacLeod, S. L., & Wong, C. S. (2010). Loadings, trends, comparisons, and fate of achiral and chiral pharmaceuticals in wastewaters from urban tertiary and rural aerated lagoon treatments. *Water research*, *44*(2), 533-544.

Macqueen, D. J., & Johnston, I. A. (2009). Evolution of the multifaceted eukaryotic akirin gene family. *BMC evolutionary biology*, *9*, 1-20.

Madison, B. B. (2016). Srebp2: A master regulator of sterol and fatty acid synthesis1. *Journal of lipid research*, *57*(3), 333-335.

Madrigal-Bujaidar, E., Gómez-González, P., Camacho-Cantera, S., Morales-González, J. A., Madrigal-Santillán, E., & Álvarez-González, I. (2021). Genotoxic and cytotoxic evaluation of

venlafaxine in an acute and a subchronic assay in mouse. *Brazilian Journal of Biology*, *84*, e251289.

Mahlke, M. A., & Nechemia-Arbely, Y. (2020). Guarding the genome: CENP-A-chromatin in health and cancer. *Genes*, *11*(7), 810.

Mahoney, H., Ankley, P., Roberts, C., Lamb, A., Schultz, M., Zhou, Y., ... & Brinkmann, M. (2024). Unveiling the Molecular Effects of Replacement and Legacy PFASs: Transcriptomic Analysis of Zebrafish Embryos Reveals Surprising Similarities and Potencies. *Environmental Science & Technology*, *58*(42), 18554-18565.

Mandela, P., Yankova, M., Conti, L. H., Ma, X. M., Grady, J., Eipper, B. A., & Mains, R. E. (2012). Kalrn plays key roles within and outside of the nervous system. *BMC neuroscience*, *13*, 1-18.

Mao, Y., Zhang, J., Zhou, Q., He, X., Zheng, Z., Wei, Y., ... & Zhao, S. (2024). Hypoxia induces mitochondrial protein lactylation to limit oxidative phosphorylation. *Cell Research*, *34*(1), 13-30.

Marat, A. L., Ioannou, M. S., & McPherson, P. S. (2012). Connecdenn 3/DENND1C binds actin linking Rab35 activation to the actin cytoskeleton. Molecular biology of the cell, 23(1), 163-175.

Marisaldi, L., Basili, D., Gioacchini, G., Canapa, A., & Carnevali, O. (2021). De novo transcriptome assembly, functional annotation and characterization of the Atlantic bluefin tuna (*Thunnus thynnus*) larval stage. *Marine Genomics*, *58*, 100834.

Marnett, L. J. (1999). Lipid peroxidation—DNA damage by malondialdehyde. *Mutation Research/Fundamental and Molecular Mechanisms of Mutagenesis*, *424*(1-2), 83-95.

Marra, N. J., Richards, V. P., Early, A., Bogdanowicz, S. M., Pavinski Bitar, P. D., Stanhope, M. J., & Shivji, M. S. (2017). Comparative transcriptomics of elasmobranchs and teleosts highlight important processes in adaptive immunity and regional endothermy. *BMC genomics*, *18*, 1-18.

Martínez−Burguete, T., Peña−Marin, E. S., García−Gasca, A., Alvarez−González, C. A., & Llera−Herrera, R. (2021). Nutrigenomic marker discovery by de novo transcriptomic sequencing during early development of the tropical gar (*Atractosteus tropicus*). *Aquaculture Research*, *52*(8), 3829-3842.

Martins−de−Souza, D., Cassoli, J. S., Nascimento, J. M., Hensley, K., Guest, P. C., Pinzon−Velasco, A. M., & Turck, C. W. (2015). The protein interactome of collapsin response mediator protein−2 (CRMP2/DPYSL2) reveals novel partner proteins in brain tissue. *PROTEOMICS–Clinical Applications*, *9*(9-10), 817-831.

Massafra, V., Milona, A., Vos, H. R., Ramos, R. J., Gerrits, J., Willemsen, E. C., ... & van Mil, S. W. (2017). Farnesoid X receptor activation promotes hepatic amino acid catabolism and ammonium clearance in mice. *Gastroenterology*, *152*(6), 1462-1476.

Matés, J. M., & Sánchez-Jiménez, F. (1999). Antioxidant enzymes and their implications in pathophysiologic processes. *Front Biosci*, *4*(4), 339-345.

Matsui, A., Tran, M., Yoshida, A. C., Kikuchi, S. S., U, M., Ogawa, M., & Shimogori, T. (2013). BTBD3 controls dendrite orientation toward active axons in mammalian neocortex. *Science*, *342*(6162), 1114-1118.

Matt, T. (2002). Transcriptional control of the inflammatory response: a role for the CREB‐binding protein (CBP). *Acta Medica Austriaca*, *29*(3), 77-79.

Matthee, C., Brown, A. R., Lange, A., & Tyler, C. R. (2023). Factors determining the susceptibility of fish to effects of human pharmaceuticals. *Environmental science & technology*, *57*(24), 8845-8862.

Mattson, M. P. (1998). Modif ication of ion homeostasis by lipid peroxidation: roles in neuronal degeneration and adaptive plasticity. *Trends in neurosciences*, *21*(2), 53-57.

Maulvault, A. L., Camacho, C., Barbosa, V., Alves, R., Anacleto, P., Pousão-Ferreira, P., ... & Diniz, M. S. (2019). Living in a multi-stressors environment: An integrated biomarker approach to assess the ecotoxicological response of meagre (*Argyrosomus regius*) to venlafaxine, warming and acidification. *Environmental research*, *169*, 7-25.

Mauri, I., Romero, A., Acerete, L., MacKenzie, S., Roher, N., Callol, A., ... & Tort, L. (2011). Changes in complement responses in Gilthead seabream (*Sparus aurata*) and European seabass (*Dicentrarchus labrax*) under crowding stress, plus viral and bacterial challenges. *Fish & shellfish immunology*, *30*(1), 182-188.

Maxfield, F. R., & Tabas, I. (2005). Role of cholesterol and lipid organization in disease. *Nature*, *438*(7068), 612-621.

McCallum, E. S., Krutzelmann, E., Brodin, T., Fick, J., Sundelin, A., & Balshine, S. (2017). Exposure to wastewater effluent affects fish behaviour and tissue-specific uptake of pharmaceuticals. *Science of the Total Environment*, *605*, 578-588.

McCallum, E. S., Nikel, K. E., Mehdi, H., Du, S. N., Bowman, J. E., Midwood, J. D., ... & Balshine, S. (2019). Municipal wastewater effluent affects fish communities: A multi-year study involving two wastewater treatment plants. *Environmental Pollution*, *252*, 1730-1741.

Medkova, D., Lakdawala, P., Hodkovicova, N., Blahova, J., Faldyna, M., Mares, J., ... & Svobodova, Z. (2022). Effects of different pharmaceutical residues on embryos of fish species native to Central Europe. *Chemosphere*, *291*, 132915.

Mehdi, H., Dickson, F. H., Bragg, L. M., Servos, M. R., & Craig, P. M. (2018). Impacts of wastewater treatment plant effluent on energetics and stress response of rainbow darter (*Etheostoma caeruleum*) in the Grand River watershed. *Comparative Biochemistry and Physiology Part B: Biochemistry and Molecular Biology*, *224*, 270-279.

Mehdi, H., Bragg, L. M., Servos, M. R., & Craig, P. M. (2019). Multiple stressors in the environment: the effects of exposure to an antidepressant (venlafaxine) and increased temperature on zebrafish metabolism. *Frontiers in Physiology*, *10*, 1431.

Mehdi, H., Lau, S. C., Synyshyn, C., Salena, M. G., McCallum, E. S., Muzzatti, M. N., ... & Balshine, S. (2021). Municipal wastewater as an ecological trap: Effects on fish communities across seasons. *Science of The Total Environment*, *759*, 143430.

Mehdi, H., Morphet, M. E., Lau, S. C., Bragg, L. M., Servos, M. R., Parrott, J. L., ... & Balshine, S. (2022). Temperature modulates the impacts of wastewater exposure on the physiology and behaviour of fathead minnow. *Chemosphere*, *294*, 133738.

Melnyk-Lamont, N., Best, C., Gesto, M., & Vijayan, M. M. (2014). The antidepressant venlafaxine disrupts brain monoamine levels and neuroendocrine responses to stress in rainbow trout. *Environmental science & technology*, *48*(22), 13434-13442.

Mendelson, T. C. (2003). Evidence of intermediate and asymmetrical behavioral isolation between orangethroat and orangebelly darters (Teleostei: Percidae). *The American midland naturalist*, *150*(2), 343-347.

Mennigen JA, Stroud P, Zamora JM, Moon TW, Trudeau VL. 2011. Pharmaceuticals as neuroendocrine disruptors: lessons learned from fish on Prozac. *J Toxicol Environ Health B Crit Rev* 14:387–412.

Merino-Casallo, F., Gomez-Benito, M. J., Hervas-Raluy, S., & Garcia-Aznar, J. M. (2022). Unravelling cell migration: defining movement from the cell surface. *Cell adhesion & migration*, *16*(1), 25-64.

Mérour, E., Jami, R., Lamoureux, A., Bernard, J., Brémont, M., & Biacchesi, S. (2019). A20 (tnfaip3) is a negative feedback regulator of RIG-I-Mediated IFN induction in teleost. *Fish & Shellfish Immunology*, *84*, 857-864.

Metcalfe, C. D., Chu, S., Judt, C., Li, H., Oakes, K. D., Servos, M. R., & Andrews, D. M. (2010). Antidepressants and their metabolites in municipal wastewater, and downstream exposure in an urban watershed. *Environmental Toxicology and Chemistry*, *29*(1), 79-89.

Miksa, M., Das, P., Zhou, M., Wu, R., Dong, W., Ji, Y., ... & Wang, P. (2009). Pivotal role of the α2A-adrenoceptor in producing inflammation and organ injury in a rat model of sepsis. *PLoS One*, *4*(5), e5504.

Miller, B. M., & Goessling, W. (2024). Distribution and developmental timing of zebrafish liver innervation. *Biology Letters*, *20*(8), 20240288.

Miller, B. M., Oderberg, I. M., & Goessling, W. (2021). Hepatic nervous system in development, regeneration, and disease. *Hepatology*, *74*(6), 3513-3522.

Mimaki, M., Wang, X., McKenzie, M., Thorburn, D. R., & Ryan, M. T. (2012). Understanding mitochondrial complex I assembly in health and disease. *Biochimica et Biophysica Acta (BBA)-Bioenergetics*, *1817*(6), 851-862.

Minuk, G. Y. (1992). GABA and the liver: The first 40 years. *GABA outside the CNS*, 143-154.

Mishima, Y., Miyagi, S., Saraya, A., Negishi, M., Endoh, M., Endo, T. A., ... & Iwama, A. (2011). The Hbo1-Brd1/Brpf2 complex is responsible for global acetylation of H3K14 and required for fetal liver erythropoiesis. *Blood, The Journal of the American Society of Hematology*, *118*(9), 2443-2453.

Mittal, K., Ewald, J., Crump, D., Head, J., Hecker, M., Hogan, N., ... & Basu, N. (2023). Comparing Transcriptomic Responses to Chemicals Across Six Species Using the EcoToxChip RNASeq Database. *Environmental Toxicology and Chemistry*.

Mohamed, B. A., Hamid, H., Montoya-Bautista, C. V., & Li, L. Y. (2023). Circular economy in wastewater treatment plants: Treatment of contaminants of emerging concerns (CECs) in effluent using sludge-based activated carbon. *Journal of Cleaner Production*, *389*, 136095.

Mommsen, T. P., Vijayan, M. M., & Moon, T. W. (1999). Cortisol in teleosts: dynamics, mechanisms of action, and metabolic regulation. Reviews in fish biology and fisheries, 9, 211-268.

Montine, T. J., Neely, M. D., Quinn, J. F., Beal, M. F., Markesbery, W. R., Roberts II, L. J., & Morrow, J. D. (2002). Lipid peroxidation in aging brain and Alzheimer's disease. *Free Radical Biology and Medicine*, *33*(5), 620-626.

Moon, A., & Drubin, D. G. (1995). The ADF/cofilin proteins: stimulus-responsive modulators of actin dynamics. *Molecular biology of the cell*, *6*(11), 1423-1431.

Moore, S., Berger, N. D., Luijsterburg, M. S., Piett, C. G., Stanley, F. K., Schräder, C. U., ... & Goodarzi, A. A. (2019). The CHD6 chromatin remodeler is an oxidative DNA damage response factor. *Nature communications*, *10*(1), 241.

Moran, R. L., & Fuller, R. C. (2018a). Agonistic character displacement of genetically based male colour patterns across darters. *Proceedings of the Royal Society B*, *285*(1884), 20181248.

Moran, R. L., & Fuller, R. C. (2018b). Male-driven reproductive and agonistic character displacement in darters and its implications for speciation in allopatry. *Current Zoology*, *64*(1), 101-113.

Moran, R. L., Catchen, J. M., & Fuller, R. C. (2020). Genomic resources for darters (Percidae: Etheostominae) provide insight into postzygotic barriers implicated in speciation. *Molecular Biology and Evolution*, *37*(3), 711-729.

Moran, R. L., Zhou, M., Catchen, J. M., & Fuller, R. C. (2017). Male and female contributions to behavioral isolation in darters as a function of genetic distance and color distance. *Evolution*, *71*(10), 2428-2444.

Moran, R. L., Zhou, M., Catchen, J. M., & Fuller, R. C. (2018). Hybridization and postzygotic isolation promote reinforcement of male mating preferences in a diverse group of fishes with traditional sex roles. *Ecology and Evolution*, *8*(18), 9282-9294.

Moreira, P. I., Smith, M. A., Zhu, X., Nunomura, A., Castellani, R. J., & Perry, G. (2005). Oxidative stress and neurodegeneration. *Annals of the New York Academy of Sciences*, *1043*(1), 545-552.

Morimoto, N., Kono, T., Sakai, M., & Hikima, J. I. (2021). Inflammasomes in teleosts: structures and mechanisms that induce pyroptosis during bacterial infection. *International journal of molecular sciences*, *22*(9), 4389.

Moriya, S., Khel, N. B., & Parhar, I. S. (2015). Cloning and serotonergic regulation of RING finger protein38 (rnf38) in the brain of medaka (*Oryzias latipes)*. *Neuroscience*, *294*, 109-115.

Mostany, R., Valdizan, E. M., & Pazos, A. (2008). A role for nuclear β-catenin in SNRI antidepressant-induced hippocampal cell proliferation. *Neuropharmacology*, *55*(1), 18-26.

Moullan, N., Mouchiroud, L., Wang, X., Ryu, D., Williams, E. G., Mottis, A., ... & Auwerx, J. (2015). Tetracyclines disturb mitochondrial function across eukaryotic models: a call for caution in biomedical research. *Cell reports*, *10*(10), 1681-1691.

Mundahl, N. D., & Ingersoll, C. G. (1983). Early autumn movements and densities of Johnny (*Etheostoma nigrum*) and fantail (*E. flabellare*) darters in a southwestern Ohio stream.

Murphy, D. A., & Courtneidge, S. A. (2011). The'ins' and'outs' of podosomes and invadopodia: characteristics, formation and function. *Nature reviews Molecular cell biology*, *12*(7), 413-426.

Murphy, M. P. (2009). How mitochondria produce reactive oxygen species. *Biochemical journal*, *417*(1), 1-13.

Nagashima, S., Kodaka, M., Iwasa, H., & Hata, Y. (2015). Magi2/S-Scam Outside Brain. *The journal of biochemistry*, *157*(4), 177-184.

Nardocci, G., Navarro, C., Cortés, P. P., Imarai, M., Montoya, M., Valenzuela, B., ... & Fernández, R. (2014). Neuroendocrine mechanisms for immune system regulation during stress in fish. *Fish & shellfish immunology*, *40*(2), 531-538.

Ndong, D., Chen, Y. Y., Lin, Y. H., Vaseeharan, B., & Chen, J. C. (2007). The immune response of tilapia *Oreochromis mossambicus* and its susceptibility to *Streptococcus iniae* under stress in low and high temperatures. *Fish & Shellfish Immunology*, *22*(6), 686-694.

Near, T. J., & Benard, M. F. (2004). Rapid allopatric speciation in logperch darters (Percidae: Percina). *Evolution*, *58*(12), 2798-2808.

Near, T. J., Bossu, C. M., Bradburd, G. S., Carlson, R. L., Harrington, R. C., Hollingsworth Jr, P. R., ... & Etnier, D. A. (2011). Phylogeny and temporal diversification of darters (Percidae: Etheostomatinae). *Systematic Biology*, *60*(5), 565-595.

Neves, R. L., Marem, A., Carmona, B., Arata, J. G., Ramos, M. P. C., Justo, G. Z., ... & Icimoto, M. Y. (2023). Expression of thimet oligopeptidase (THOP) modulated by oxidative stress in human multidrug resistant (MDR) leukemia cells. *Biochimie*, *212*, 21-30.

Nie, Z., Hu, G., Wei, G., Cui, K., Yamane, A., Resch, W., ... & Levens, D. (2012). c-Myc is a universal amplifier of expressed genes in lymphocytes and embryonic stem cells. *Cell*, *151*(1), 68-79.

Nikel, K. E., McCallum, E. S., Mehdi, H., Du, S. N., Bowman, J. E., Midwood, J. D., ... & Balshine, S. (2021). Fish living near two wastewater treatment plants have unaltered thermal tolerance but show changes in organ and tissue traits. *Journal of Great Lakes Research*, *47*(2), 522-533.

Nikel, K. E., Tetreault, G. R., Marjan, P., Hicks, K. A., Fuzzen, M. L., Srikanthan, N., ... & Servos, M. R. (2023). Wild fish responses to wastewater treatment plant upgrades in the Grand River, Ontario. *Aquatic Toxicology*, *255*, 106375.

Niwa, R., Nagata-Ohashi, K., Takeichi, M., Mizuno, K., & Uemura, T. (2002). Control of actin reorganization by Slingshot, a family of phosphatases that dephosphorylate ADF/cofilin. *Cell*, *108*(2), 233-246.

Notch, E. G., & Mayer, G. D. (2009). Wastewater treatment effluent alters nucleotide excision repair in zebrafish (*Danio rerio*). *Comparative Biochemistry and Physiology Part C: Toxicology & Pharmacology*, *150*(2), 307-313.

Nowak, J., & Iovanna, J. (2009). TP53INP2 is the new guest at the table of self-eating. 573. *Autophagy*, *5*(383-384), 574.

Ock, C. Y., Kim, E. H., Choi, D. J., Lee, H. J., Hahm, K. B., & Chung, M. H. (2012). 8-Hydroxydeoxyguanosine: not mere biomarker for oxidative stress, but remedy for oxidative stress-implicated gastrointestinal diseases. *World journal of gastroenter*

Oliveira, D. R., Reid, B. N., & Fitzpatrick, S. W. (2021). Genome−wide diversity and habitat underlie fine−scale phenotypic differentiation in the rainbow darter (*Etheostoma caeruleum*). *Evolutionary Applications*, *14*(2), 498-512.

Oomen, R. A., & Hutchings, J. A. (2017). Transcriptomic responses to environmental change in fishes: insights from RNA sequencing. *Facets*, *2*(2), 610-641.

Orozco-Hernández, J. M., Gómez-Oliván, L. M., Elizalde-Velázquez, G. A., Rosales-Pérez, K. E., Cardoso-Vera, J. D., Heredia-García, G., ... & Galar-Martínez, M. (2022). Fluoxetine-induced neurotoxicity at environmentally relevant concentrations in adult zebrafish *Danio rerio*. *Neurotoxicology*, *90*, 121-129.

Ota, M., Gonja, H., Koike, R., and Fukuchi, S. (2016). Multiple-localization and hub proteins. PLoS ONE 11:e0156455. doi: 10.1371/journal.pone.0156455

Otsuka, T., & Matsui, H. (2023). Fish Models for Exploring Mitochondrial Dysfunction Affecting Neurodegenerative Disorders. *International Journal of Molecular Sciences*, *24*(8), 7079.

Ott, M., Gogvadze, V., Orrenius, S., & Zhivotovsky, B. (2007). Mitochondria, oxidative stress and cell death. *Apoptosis*, *12*, 913-922.

Otton, S. V., Ball, S. E., Cheung, S. W., Inaba, T., Rudolph, R. L., & Sellers, E. M. (1996). Venlafaxine oxidation in vitro is catalysed by CYP2D6. *British journal of clinical pharmacology*, *41*(2), 149-156.

Outram, S. V., Gordon, A. R., Hager-Theodorides, A. L., Metcalfe, J., Crompton, T., & Kemp, P. (2008). KLF13 influences multiple stages of both B and T cell development. *Cell Cycle*, *7*(13), 2047-2055.

Ozgun, H., Cicekalan, B., Akdag, Y., Koyuncu, I., & Ozturk, I. (2021). Comparative evaluation of cost for preliminary and tertiary municipal wastewater treatment plants in Istanbul. *Science of the Total Environment*, *778*, 146258.

Painter, M. M., Buerkley, M. A., Julius, M. L., Vajda, A. M., Norris, D. O., Barber, L. B., ... & Schoenfuss, H. L. (2009). Antidepressants at environmentally relevant concentrations affect predator avoidance behavior of larval fathead minnows (*Pimephales promelas*). *Environmental Toxicology and Chemistry*, *28*(12), 2677-2684.

Palmieri, F. (2013). The mitochondrial transporter family SLC25: identification, properties and physiopathology. *Molecular aspects of medicine*, *34*(2-3), 465-484.

Pamplona, R. (2008). Membrane phospholipids, lipoxidative damage and molecular integrity: a causal role in aging and longevity. *Biochimica et Biophysica Acta (BBA)-Bioenergetics*, *1777*(10), 1249-1262.

Pankhurst, N. W., & Van Der Kraak, G. (1997). Effects of stress on reproduction and growth of fish. *Fish stress and health in aquaculture*, *1*, 73-93.

Parekh, K., & Marlatt, V. L. (2023). Using Hepatic Gene Expression Assays in English Sole (*Parophrys vetulus*) to Investigate the Effects of Metro Vancouver Wastewater Effluents. *Toxics*, *11*(8), 657.

Parrott, J. L., & Metcalfe, C. D. (2018). Nest-defense behaviors in fathead minnows after lifecycle exposure to the antidepressant venlafaxine. *Environmental Pollution*, *234*, 223-230.

Pastor, F., Dumas, K., Barthélémy, M. A., Regazzetti, C., Druelle, N., Peraldi, P., ... & Giorgetti-Peraldi, S. (2017). Implication of REDD1 in the activation of inflammatory pathways. *Scientific reports*, *7*(1), 7023.

Patented Medicine Prices Review Board. (2021). *Annual report 2021*. Government of Canada. http://pmprb-cepmb.gc.ca/home

Pearce, G., Audzevich, T., & Jessberger, R. (2011). SYK regulates B-cell migration by phosphorylation of the F-actin interacting protein SWAP-70. *Blood, The Journal of the American Society of Hematology*, *117*(5), 1574-1584.

Pearl, L. H., & Prodromou, C. (2000). Structure and in vivo function of Hsp90. *Current opinion in structural biology*, *10*(1), 46-51.

Peña-Bautista, C., Vento, M., Baquero, M., & Cháfer-Pericás, C. (2019). Lipid peroxidation in neurodegeneration. *Clinica Chimica Acta*, *497*, 178-188.

Peng, X. Y., Wang, K. L., Li, L., Li, B., Wu, X. Y., Zhang, Z. W., ... & Chen, S. N. (2024). Transcription of NOD1 and NOD2 and their interaction with CARD9 and RIPK2 in IFN signaling in a perciform fish, the Chinese perch, Siniperca chuatsi. *Frontiers in Immunology*, *15*, 1374368.

Perez, A. S. C., Challis, J. K., Ji, X., Giesy, J. P., & Brinkmann, M. (2022). Impacts of wastewater effluents and seasonal trends on levels of antipsychotic pharmaceuticals in water and sediments from two cold-region rivers. *Science of the Total Environment*, *851*, 158247.

Pestka, S., Kotenko, S. V., Muthukumaran, G., Izotova, L. S., Cook, J. R., & Garotta, G. (1997). The interferon gamma (IFN-γ) receptor: a paradigm for the multichain cytokine receptor. *Cytokine & growth factor reviews*, *8*(3), 189-206.

Phrompanya, P., Panase, P., Saenphet, S., & Saenphet, K. (2021). Histopathology and oxidative stress responses of Nile tilapia *Oreochromis niloticus* exposed to temperature shocks. *Fisheries Science*, *87*(4), 491-502.

Pihlaja, T., Oksanen, T., Vinkvist, N., & Sikanen, T. (2024). Many human pharmaceuticals are weak inhibitors of the cytochrome P450 system in rainbow trout (*Oncorhynchus mykiss*) liver S9 fractions. *Frontiers in Toxicology*, *6*, 1406942.

Pirkkala, L., Alastalo, T. P., Zuo, X., Benjamin, I. J., & Sistonen, L. (2000). Disruption of heat shock factor 1 reveals an essential role in the ubiquitin proteolytic pathway. *Molecular and cellular biology*, *20*(8), 2670-2675.

Pizzinat, N., Copin, N., Vindis, C., Parini, A., & Cambon, C. (1999). Reactive oxygen species production by monoamine oxidases in intact cells. *Naunyn-Schmiedeberg's archives of pharmacology*, *359*, 428-431.

Plutner, H., Cox, A. D., Pind, S., Khosravi-Far, R., Bourne, J. R., Schwaninger, R., ... & Balch, W. E. (1991). Rab1b regulates vesicular transport between the endoplasmic reticulum and successive Golgi compartments. *The Journal of cell biology*, 115(1), 31-43.

Polakof, S., Míguez, J. M., & Soengas, J. L. (2009). A hepatic protein modulates glucokinase activity in fish and avian liver: a comparative study. *Journal of Comparative Physiology B*, *179*, 643-652.

Pomianowski, K., Burzyński, A., & Kulczykowska, E. (2021). A de novo transcriptome assembly of the European Flounder (*Platichthys flesus*): The preselection of transcripts encoding active forms of enzymes. *Frontiers in Marine Science*, *8*, 618779.

Pottinger, T. G., Henrys, P. A., Williams, R. J., & Matthiessen, P. (2013). The stress response of three-spined sticklebacks is modified in proportion to effluent exposure downstream of wastewater treatment works. *Aquatic toxicology*, *126*, 382-39

Prajapati, S., Beal, M., Maley, J., & Brinkmann, M. (2021). Qualitative and quantitative analysis of microplastics and microfiber contamination in effluents of the City of Saskatoon wastewater treatment plant. *Environmental Science and Pollution Research*, *28*, 32545-32553.

Preisner, M., Neverova-Dziopak, E., & Kowalewski, Z. (2020). Analysis of eutrophication potential of municipal wastewater. *Water Science and Technology*, *81*(9), 1994-2003.

Qiao, M., Jiang, Q. S., Liu, Y. J., Hu, X. Y., Wang, L. J., Zhou, Q. X., & Qiu, H. M. (2019). Antidepressant mechanisms of venlafaxine involving increasing histone acetylation and modulating tyrosine hydroxylase and tryptophan hydroxylase expression in hippocampus of depressive rats. *Neuroreport*, *30*(4), 255-261.

Qiu, Y., Li, Q., Lee, B. E., Ruecker, N. J., Neumann, N. F., Ashbolt, N. J., & Pang, X. (2018). UV inactivation of human infectious viruses at two full-scale wastewater treatment plants in Canada. *Water Research*, *147*, 73-81.

Qu, H., Ma, R., Wang, B., Yang, J., Duan, L., & Yu, G. (2019). Enantiospecific toxicity, distribution and bioaccumulation of chiral antidepressant venlafaxine and its metabolite in loach (*Misgurnus anguillicaudatus*) co-exposed to microplastic and the drugs. *Journal of hazardous materials*, *370*, 203-211.

Quéméneur, J. B., Danion, M., Cabon, J., Collet, S., Zambonino-Infante, J. L., & Salin, K. (2022). The relationships between growth rate and mitochondrial metabolism varies over time. *Scientific Reports*, *12*(1), 16066.

Buettner, G. (2011). Superoxide dismutase in redox biology: the roles of superoxide and hydrogen peroxide. *Anti-Cancer Agents in Medicinal Chemistry (Formerly Current Medicinal Chemistry-Anti-Cancer Agents)*, *11*(4), 341-346.

R Core Team (2021). R: A language and environment for statistical computing. R Foundation for Statistical Computing, Vienna, Austria. URL https://www.R-project.org/.

Ray, P. D., Huang, B. W., & Tsuji, Y. (2012). Reactive oxygen species (ROS) homeostasis and redox regulation in cellular signaling. *Cellular signalling*, *24*(5), 981-990.

Reed, N. P., Henderson, M. A., Oltz, E. M., & Aune, T. M. (2013). Reciprocal regulation of Rag expression in thymocytes by the zinc-finger proteins, Zfp608 and Zfp609. *Genes & Immunity*, *14*(1), 7-12.

Reinwald, H., Alvincz, J., Salinas, G., Schäfers, C., Hollert, H., & Eilebrecht, S. (2022). Toxicogenomic profiling after sublethal exposure to nerve-and muscle-targeting insecticides reveals cardiac and neuronal developmental effects in zebrafish embryos. *Chemosphere*, *291*, 132746.

Ribeiro, O., Félix, L., Ribeiro, C., Castro, B., Tiritan, M. E., Monteiro, S. M., & Carrola, J. S. (2022). Enantioselective ecotoxicity of venlafaxine in aquatic organisms: daphnia and zebrafish. *Environmental Toxicology and Chemistry*, *41*(8), 1851-1864.

Richards, D. J., Renaud, L., Agarwal, N., Starr Hazard, E., Hyde, J., & Hardiman, G. (2018). De Novo Hepatic Transcriptome Assembly and Systems Level Analysis of Three Species of Dietary Fish, Sardinops sagax, Scomber japonicus, and Pleuronichthys verticalis. *Genes*, *9*(11), 521.

Ricklin, D., Hajishengallis, G., Yang, K., & Lambris, J. D. (2010). Complement: a key system for immune surveillance and homeostasis. *Nature immunology*, *11*(9), 785-797.

Riesgo, A., Andrade, S. C., Sharma, P. P., Novo, M., Pérez-Porro, A. R., Vahtera, V., ... & Giribet, G. (2012). Comparative description of ten transcriptomes of newly sequenced invertebrates

and efficiency estimation of genomic sampling in non-model taxa. *Frontiers in zoology*, *9*, 1-24.

Robichaud, K., Bragg, L. M., Servos, M. R., & Craig, P. M. (2024). Venlafaxine exposure alters mitochondrial respiration and mitomiR abundance in zebrafish brains. *Environmental Toxicology and Chemistry*.

Rodriguez-Mozaz, S., Vaz-Moreira, I., Della Giustina, S. V., Llorca, M., Barceló, D., Schubert, S., ... & Manaia, C. M. (2020). Antibiotic residues in final effluents of European wastewater treatment plants and their impact on the aquatic environment. *Environment international*, *140*, 105733.

Rotondo, R., Moschini, R., Renzone, G., Tuccinardi, T., Balestri, F., Cappiello, M., ... & Del-Corso, A. (2016). Human carbonyl reductase 1 as efficient catalyst for the reduction of glutathionylated aldehydes derived from lipid peroxidation. *Free Radical Biology and Medicine*, *99*, 323-332.

Roubicek, D. A., & de Souza-Pinto, N. C. (2017). Mitochondria and mitochondrial DNA as relevant targets for environmental contaminants. *Toxicology*, *391*, 100-108.

Rui, L. (2014). Energy metabolism in the liver. *Comprehensive physiology*, *4*(1), 177.

Russell, S., Young, K. M., Smith, M., Hayes, M. A., & Lumsden, J. S. (2008). Cloning, binding properties, and tissue localization of rainbow trout (*Oncorhynchus mykiss*) ladderlectin. *Fish & shellfish immunology*, *24*(6), 669-683.

Saaristo, M., Brodin, T., Balshine, S., Bertram, M. G., Brooks, B. W., Ehlman, S. M., ... & Arnold, K. E. (2018). Direct and indirect effects of chemical contaminants on the behaviour, ecology and evolution of wildlife. *Proceedings of the Royal Society B*, *285*(1885), 20181297.

Safer, B. (1975). The metabolic significance of the malate-aspartate cycle in heart. *Circulation research*, *37*(5), 527-533.

Salahinejad, A., Attaran, A., Meuthen, D., Chivers, D. P., & Niyogi, S. (2022). Proximate causes and ultimate effects of common antidepressants, fluoxetine and venlafaxine, on fish behavior. *Science of the Total Environment*, *807*, 150846.

Salem, M., Paneru, B., Al-Tobasei, R., Abdouni, F., Thorgaard, G. H., Rexroad, C. E., & Yao, J. (2015). Transcriptome assembly, gene annotation and tissue gene expression atlas of the rainbow trout. *PloS one*, *10*(3), e0121778.

Salin, K., Auer, S. K., Rudolf, A. M., Anderson, G. J., Cairns, A. G., Mullen, W., ... & Metcalfe, N. B. (2015). Individuals with higher metabolic rates have lower levels of reactive oxygen species in vivo. *Biology Letters*, *11*(9), 20150538.

Salo, H. M., Hébert, N., Dautremepuits, C., Cejka, P., Cyr, D. G., & Fournier, M. (2007). Effects of Montreal municipal sewage effluents on immune responses of juvenile female rainbow trout (*Oncorhynchus mykiss*). *Aquatic toxicology*, *84*(4), 406-414.

Sameshima, S., Nakao, M., & Somamoto, T. (2012). Diversity of CD2 subfamily receptors in cyprinid fishes. *Results in Immunology*, *2*, 25-34.

Sandoval-Castillo, J., Gates, K., Brauer, C. J., Smith, S., Bernatchez, L., & Beheregaray, L. B. (2020). Adaptation of plasticity to projected maximum temperatures and across climatically defined bioregions. *Proceedings of the National Academy of Sciences*, *117*(29), 17112-17121.

Santos, L. H., Maulvault, A. L., Jaén-Gil, A., Marques, A., Barceló, D., & Rodríguez-Mozaz, S. (2020). Insights on the metabolization of the antidepressant venlafaxine by meagre (*Argyrosomus regis*) using a combined target and suspect screening approach. *Science of The Total Environment*, *737*, 140226.

Santos, L. H., Maulvault, A. L., Jaén-Gil, A., Marques, A., Barceló, D., & Rodríguez-Mozaz, S. (2023). Linking chemical exposure and fish metabolome: Discovering new biomarkers of environmental exposure of *Argyrosomus regius* to the antidepressant venlafaxine. *Environmental toxicology and pharmacology*, *98*, 104063.

Sarma, K., Pal, A. K., George, G., & Baruah, K. (2015). Effect of sub-lethal concentration of endosulfan on lipid and fatty acid metabolism of spotted murrel, *Channa punctatus*. *Journal of Environmental Biology*, *36*, 451-454.

Scaini, G., Maggi, D. D., De-Nês, B. T., Gonçalves, C. L., Ferreira, G. K., Teodorak, B. P., ... & Streck, E. L. (2011). Activity of mitochondrial respiratory chain is increased by chronic administration of antidepressants. *Acta neuropsychiatrica*, *23*(3), 112-118.

Schiöth, H. B., Roshanbin, S., Hägglund, M. G., & Fredriksson, R. (2013). Evolutionary origin of amino acid transporter families SLC32, SLC36 and SLC38 and physiological, pathological and therapeutic aspects. *Molecular aspects of medicine*, *34*(2-3), 571-585.

Schlüsener, M. P., Hardenbicker, P., Nilson, E., Schulz, M., Viergutz, C., & Ternes, T. A. (2015). Occurrence of venlafaxine, other antidepressants and selected metabolites in the Rhine catchment in the face of climate change. *Environmental pollution*, *196*, 247-256.

Schoch, C. L., Ciufo, S., Domrachev, M., Hotton, C. L., Kannan, S., Khovanskaya, R., ... & Karsch-Mizrachi, I. (2020). NCBI Taxonomy: a comprehensive update on curation, resources and tools. *Database*, *2020*, baaa062.

Schoenfuss, H. L., Wang, L. C., Korn, V. R., King, C. K., Kohno, S., & Hummel, S. L. (2020). Understanding the ecological consequences of ubiquitous contaminants of emerging concern in the Laurentian Great Lakes watershed: a continuum of evidence from the laboratory to the environment. *Contaminants of the Great Lakes*, 157-180.

Schreck, C. B., & Tort, L. (2016). The concept of stress in fish. In *Fish physiology* (Vol. 35, pp. 1-34). Academic Press.

Schultz, M. M., Furlong, E. T., Kolpin, D. W., Werner, S. L., Schoenfuss, H. L., Barber, L. B., ... & Vajda, A. M. (2010). Antidepressant pharmaceuticals in two US effluent-impacted streams: occurrence and fate in water and sediment, and selective uptake in fish neural tissue. *Environmental science & technology*, *44*(6), 1918-1925.

Schweiger, M., Schreiber, R., Haemmerle, G., Lass, A., Fledelius, C., Jacobsen, P., ... & Zimmermann, R. (2006). Adipose triglyceride lipase and hormone-sensitive lipase are the major enzymes in adipose tissue triacylglycerol catabolism. *Journal of biological chemistry*, *281*(52), 40236-40241.

Scott, K. L., & Plon, S. E. (2005). CHES1/FOXN3 interacts with Ski-interacting protein and acts as a transcriptional repressor. *Gene*, *359*, 119-126.

Seehawer, M., Li, Z., Nishida, J., Foidart, P., Reiter, A. H., Rojas-Jimenez, E., ... & Polyak, K. (2024). Loss of Kmt2c or Kmt2d drives brain metastasis via KDM6A-dependent upregulation of MMP3. *Nature Cell Biology*, *26*(7), 1165-1175.

Semeniuk, C. A. D., Jeffries, K. M., Li, T., Bettles, C. M., Cooke, S. J., Dufour, B. A., ... & Heath, D. D. (2022). Innovating transcriptomics for practitioners in freshwater fish management and conservation: best practices across diverse resource-sector users. *Reviews in Fish Biology and Fisheries*, *32*(3), 921-939.

Sena, L. A., & Chandel, N. S. (2012). Physiological roles of mitochondrial reactive oxygen species. *Molecular cell*, *48*(2), 158-167.

Sepp, T., Baines, C., Kreitsberg, R., Nogueira, P., Lang, T., Fort, J., ... & Meitern, R. (2024). Differences on the Level of Liver Transcriptome between Two Flatfish Species in Response to Liver Cancer and Environmental Pollution Levels. *Available at SSRN 4534480*.

Sgaravatti, Â. M., Magnusson, A. S., de Oliveira, A. S., Rosa, A. P., Mescka, C. P., Zanin, F. R., ... & Dutra-Filho, C. S. (2009). Tyrosine administration decreases glutathione and stimulates lipid and protein oxidation in rat cerebral cortex. *Metabolic brain disease*, *24*, 415-425.

Shan, J., Dudenhausen, E., & Kilberg, M. S. (2019). Induction of early growth response gene 1 (EGR1) by endoplasmic reticulum stress is mediated by the extracellular regulated kinase (ERK) arm of the MAPK pathways. *Biochimica et Biophysica Acta (BBA)-Molecular Cell Research*, *1866*(3), 371-381.

Shang, F., & Taylor, A. (2011). Ubiquitin–proteasome pathway and cellular responses to oxidative stress. *Free Radical Biology and Medicine*, *51*(1), 5-16.

Sharpe, L. J., & Brown, A. J. (2013). Controlling cholesterol synthesis beyond 3-hydroxy-3-methylglutaryl-CoA reductase (HMGCR). *Journal of Biological Chemistry*, *288*(26), 18707-18715.

Shi, C., Cheng, L., Yu, Y., Chen, S., Dai, Y., Yang, J., ... & Geng, N. (2024). Multi-omics integration analysis: tools and applications in environmental toxicology. *Environmental Pollution*, 124675.

Shinohara, H., Yamasaki, S., Maeda, S., Saito, T., & Kurosaki, T. (2009). Regulation of NF-κB-dependent T cell activation and development by MEKK3. *International immunology*, *21*(4), 393-401.

Shokolenko, I., Venediktova, N., Bochkareva, A., Wilson, G. L., & Alexeyev, M. F. (2009). Oxidative stress induces degradation of mitochondrial DNA. *Nucleic acids research*, *37*(8), 2539-2548.

Sies, H., & Cadenas, E. (1985). Oxidative stress: damage to intact cells and organs. *Philosophical Transactions of the Royal Society of London. B, Biological Sciences*, *311*(1152), 617-631.

Signorile, A., Sgaramella, G., Bellomo, F., & De Rasmo, D. (2019). Prohibitins: a critical role in mitochondrial functions and implication in diseases. *Cells*, *8*(1), 71.

Simão, F. A., Waterhouse, R. M., Ioannidis, P., Kriventseva, E. V., & Zdobnov, E. M. (2015). BUSCO: assessing genome assembly and annotation completeness with single-copy orthologs. *Bioinformatics*, *31*(19), 3210-3212.

Sims, D., Sudbery, I., Ilott, N. E., Heger, A., & Ponting, C. P. (2014). Sequencing depth and coverage: key considerations in genomic analyses. *Nature Reviews Genetics*, *15*(2), 121-132.

Singh, M., Singh, K. P., Shukla, S., & Dikshit, M. (2015). Assessment of in-utero venlafaxine induced, ROS-mediated, apoptotic neurodegeneration in fetal neocortex and neurobehavioral sequelae in rat offspring. *International Journal of Developmental Neuroscience*, *40*, 60-69.

Small, B. C., & Bilodeau, A. L. (2005). Effects of cortisol and stress on channel catfish (*Ictalurus punctatus*) pathogen susceptibility and lysozyme activity following exposure to *Edwardsiella ictaluri*. *General and comparative endocrinology*, *142*(1-2), 256-262.

Soengas, J. L., & Aldegunde, M. (2002). Energy metabolism of fish brain. *Comparative biochemistry and physiology part B: biochemistry and molecular biology*, *131*(3), 271-296.

Solcova, O., Dlaskova, M., & Kastanek, F. (2024). Challenges and Advances in Tertiary Waste Water Treatment for Municipal Treatment Plants. *Processes*, *12*(10), 2084.

Solomon, K. R., Baker, D. B., Richards, R. P., Dixon, K. R., Klaine, S. J., La Point, T. W., ... & Williams, W. M. (1996). Ecological risk assessment of atrazine in North American surface waters. *Environmental Toxicology and Chemistry: An International Journal*, *15*(1), 31-76.

Song, X., Wang, X., Li, X., Yan, X., Liang, Y., Huang, Y., ... & Zeng, H. (2021). Histopathology and transcriptome reveals the tissue-specific hepatotoxicity and gills injury in mosquitofish (*Gambusia affinis*) induced by sublethal concentration of triclosan. *Ecotoxicology and Environmental Safety*, *220*, 112325.

Song, Z., Xiong, H., Meng, X., Ma, Q., Wei, Y., Li, Y., ... & Xu, H. (2023). Dietary cholesterol supplementation inhibits the steroid biosynthesis but does not affect the cholesterol transport in two marine teleosts: a hepatic transcriptome study. *Aquaculture Nutrition*, *2023*(1), 2308669.

Sørhus, E., Incardona, J. P., Furmanek, T., Goetz, G. W., Scholz, N. L., Meier, S., ... & Jentoft, S. (2017). Novel adverse outcome pathways revealed by chemical genetics in a developing marine fish. *elife*, *6*, e20707.

Spurgeon, D., Lahive, E., Robinson, A., Short, S., & Kille, P. (2020). Species sensitivity to toxic substances: Evolution, ecology and applications. *Frontiers in Environmental Science*, *8*, 588380.

Srikanthan, N. (2019). *Analysis of temporal changes in estrogenic compounds released from municipal wastewater treatment plants* (Master's thesis, University of Waterloo).

Stadlmann, S., Portmann, S., Tschopp, S., & Terracciano, L. M. (2012). Venlafaxine-induced cholestatic hepatitis: case report and review of literature. *The American journal of surgical pathology*, *36*(11), 1724-1728.

Stamp, J. A., & Herbert, J. (1999). Multiple immediate-early gene expression during physiological and endocrine adaptation to repeated stress. *Neuroscience*, *94*(4), 1313-1322.

State of New York. (1927). *A biological survey of the Oswego River system: Supplemental to seventeenth annual report* (Plate 11, after p. 94). Albany, NY: New York Conservation Department.

Steinegger, M., & Salzberg, S. L. (2020). Terminating contamination: Large-scale search identifies more than 2,000,000 contaminated entries in GenBank. *Genome Biology, 21*(1), 115.

Stephenson, F. A. (2014). Revisiting the TRAK family of proteins as mediators of GABA A receptor trafficking. *Neurochemical Research*, *39*, 992-996.

Su, J., Lei, H., Xiao, T., & Cui, S. (2017). Ci-AMBP: a highly conserved member of the microglobulin superfamily of proteinase inhibitors in grass carp, Ctenopharyngodon idellus. *Genes & genetic systems*, *92*(5), 251-256.

Su, L. J., Zhang, J. H., Gomez, H., Murugan, R., Hong, X., Xu, D., ... & Peng, Z. Y. (2019). Reactive oxygen species−induced lipid peroxidation in apoptosis, autophagy, and ferroptosis. *Oxidative medicine and cellular longevity*, *2019*(1), 5080843.

Subramanya, S., Goswami, M. T., Miller, N., Weh, E., Chaudhury, S., Zhang, L., ... & Wubben, T. J. (2023). Rod photoreceptor-specific deletion of cytosolic aspartate aminotransferase, GOT1, causes retinal degeneration. *Frontiers in ophthalmology*, *3*, 1306019.

Sumoy, L., Pluvinet, R., Andreu, N., Estivill, X., & Escarceller, M. (2001). PACSIN 3 is a novel SH3 domain cytoplasmic adapter protein of the pacsin-syndapin-FAP52 gene family. *Gene*, *262*(1-2), 199-205.

Sun, W., Zhang, X., Qiao, Y., Griffin, N., Zhang, H., Wang, L., & Liu, H. (2023). Exposure to PFOA and its novel analogs disrupts lipid metabolism in zebrafish. *Ecotoxicology and Environmental Safety*, *259*, 115020.

Sun, Z., Tan, X., Xu, M., Liu, Q., Ye, H., Zou, C., & Ye, C. (2019). Liver transcriptome analysis and de novo annotation of the orange-spotted groupers (Epinephelus coioides) under cold stress. *Comparative Biochemistry and Physiology Part D: Genomics and Proteomics*, *29*, 264-273.

Swank, A., Wang, L., Ward, J., & Schoenfuss, H. (2021). Multigenerational effects of a complex urban contaminant mixture on the behavior of larval and adult fish in multiple fitness contexts. *Science of the Total Environment*, *791*, 148095.

Syed, M., Skonberg, C., & Hansen, S. H. (2016). Mitochondrial toxicity of diclofenac and its metabolites via inhibition of oxidative phosphorylation (ATP synthesis) in rat liver mitochondria: Possible role in drug induced liver injury (DILI). *Toxicology in vitro*, *31*, 93-102.

Tan, H., Polverino, G., Martin, J. M., Bertram, M. G., Wiles, S. C., Palacios, M. M., ... & Wong, B. B. (2020). Chronic exposure to a pervasive pharmaceutical pollutant erodes among-individual phenotypic variation in a fish. *Environmental Pollution*, *263*, 114450.

Tang, Y., Fan, Z., Yang, M., Zhang, S., Li, M., Fang, Y., ... & Feng, X. (2022). Low concentrations of the antidepressant venlafaxine affect courtship behaviour and alter serotonin and dopamine systems in zebrafish (*Danio rerio*). *Aquatic Toxicology*, *244*, 106082.

Tarazona, S., García-Alcalde, F., Dopazo, J., Ferrer, A., & Conesa, A. (2011). Differential expression in RNA-seq: a matter of depth. *Genome research*, *21*(12), 2213-2223.

Teles, M., Fierro-Castro, C., Na-Phatthalung, P., Tvarijonaviciute, A., Soares, A. M. V. M., Tort, L., & Oliveira, M. (2016). Evaluation of gemfibrozil effects on a marine fish (Sparus aurata) combining gene expression with conventional endocrine and biochemical endpoints. *Journal of hazardous materials*, *318*, 600-607.

Tetreault, G. R., Bennett, C. J., Cheng, C., Servos, M. R., & McMaster, M. E. (2012). Reproductive and histopathological effects in wild fish inhabiting an effluent-dominated stream, Wascana Creek, SK, Canada. *Aquatic Toxicology*, *110*, 149-161.

Tetreault, G. R., Bennett, C. J., Shires, K., Knight, B., Servos, M. R., & McMaster, M. E. (2011). Intersex and reproductive impairment of wild fish exposed to multiple municipal wastewater discharges. *Aquatic Toxicology*, *104*(3-4), 278-290.

Tetreault, G. R., Brown, C. J., Bennett, C. J., Oakes, K. D., McMaster, M. E., & Servos, M. R. (2013). Fish community responses to multiple municipal wastewater inputs in a watershed. *Integrated Environmental Assessment and Management*, *9*(3), 456-468.

Thibaut, R., Schnell, S., & Porte, C. (2006). The interference of pharmaceuticals with endogenous and xenobiotic metabolizing enzymes in carp liver: an in-vitro study. *Environmental science & technology*, *40*(16), 5154-5160.

Thompson, W. A., Arnold, V. I., & Vijayan, M. M. (2017). Venlafaxine in embryos stimulates neurogenesis and disrupts larval behavior in zebrafish. *Environmental science & technology*, *51*(21), 12889-12897.

Thompson, W. A., Shvartsburd, Z., & Vijayan, M. M. (2022). Sex-specific and long-term impacts of early-life venlafaxine exposure in zebrafish. *Biology*, *11*(2), 250.

Thompson, W. A., & Vijayan, M. M. (2020). Environmental levels of venlafaxine impact larval behavioural performance in fathead minnows. *Chemosphere*, *259*, 127437.

Thompson, W. A., & Vijayan, M. M. (2021). Venlafaxine deposition in the zygote disrupts the endocrine control of growth in juvenile zebrafish. *Environmental Research*, *202*, 111665.

Thompson, W. A., & Vijayan, M. M. (2022). Antidepressants as endocrine disrupting compounds in fish. *Frontiers in Endocrinology*, *13*, 895064.

Tiessen, A., Pérez-Rodríguez, P., & Delaye-Arredondo, L. J. (2012). Mathematical modeling and comparison of protein size distribution in different plant, animal, fungal and microbial species reveals a negative correlation between protein size and protein number, thus providing insight into the evolution of proteomes. *BMC research notes*, *5*, 1-23.

Tocher, D. R. (2003). Metabolism and functions of lipids and fatty acids in teleost fish. *Reviews in fisheries science*, *11*(2), 107-184.

Topić Popović, N., Čižmek, L., Babić, S., Strunjak-Perović, I., & Čož-Rakovac, R. (2023). Fish liver damage related to the wastewater treatment plant effluents. *Environmental science and pollution research*, *30*(17), 48739-48768.

Tort, L. (2011). Stress and immune modulation in fish. *Developmental & Comparative Immunology*, *35*(12), 1366-1375.

Trostchansky, A., & Alarcon, M. (2023). An Overview of Two Old Friends Associated with Platelet Redox Signaling, the Protein Disulfide Isomerase and NADPH Oxidase. *Biomolecules*, *13*(5), 848.

Tsuneki, K., & Ichihara, K. (1981). Electron microscope study of vertebrate liver innervation. *Archivum histologicum japonicum*, *44*(1), 1-13.

Tugasworo, D., Prasetyo, A., Kurnianto, A., Retnaningsih, R., Andhitara, Y., Ardhini, R., & Budiman, J. (2023). Malondialdehyde (MDA) and 8-hydroxy-2′-deoxyguanosine (8-OHdG) in ischemic stroke: a systematic review. *The Egyptian Journal of Neurology, Psychiatry and Neurosurgery*, *59*(1), 87.

Tune, C. E., Pilon, M., Saiki, Y., & Dosch, H. (2002). Sustained expression of the novel EBV-induced zinc finger gene, ZNFEB, is critical for the transition of B lymphocyte activation to oncogenic growth transformation. *The Journal of immunology*, *168*(2), 680-688.

Ueda, T., Kohama, Y., & Sakurai, H. (2019). IER family proteins are regulators of protein phosphatase PP2A and modulate the phosphorylation status of CDC25A. *Cellular Signalling*, *55*, 81-89.

Uno, T., Ishizuka, M., & Itakura, T. (2012). Cytochrome P450 (CYP) in fish. *Environmental toxicology and pharmacology*, *34*(1), 1-13.

Valdés ME, Huerta B, Wunderlin DA, Bistoni MA, Barceló D, Rodriguez-Mozaz S. Bioaccumulation and bioconcentration of carbamazepine and other pharmaceuticals in fish under field and controlled laboratory experiments. Evidences of carbamazepine metabolization by fish. *Sci Total Environ* 557-558: 58–67.

Vallabhajosyula, R. R., Chakravarti, D., Lutfeali, S., Ray, A., & Raval, A. (2009). Identifying hubs in protein interaction networks. *PloS one*, *4*(4), e5344.

Van De Sluis, B., Wijers, M., & Herz, J. (2017). News on the molecular regulation and function of hepatic low-density lipoprotein receptor and LDLR-related protein 1. *Current opinion in lipidology*, *28*(3), 241-247.

Van den Berg, D. L., Azzarelli, R., Oishi, K., Martynoga, B., Urban, N., Dekkers, D. H., ... & Guillemot, F. (2017). Nipbl interacts with Zfp609 and the integrator complex to regulate cortical neuron migration. *Neuron*, *93*(2), 348-361.

Van Niel, G., Carter, D. R., Clayton, A., Lambert, D. W., Raposo, G., & Vader, P. (2022). Challenges and directions in studying cell–cell communication by extracellular vesicles. *Nature Reviews Molecular Cell Biology*, *23*(5), 369-382.

Van Unen, J., Yin, T., Wu, Y. I., Mastop, M., Gadella Jr, T. W., & Goedhart, J. (2016). Kinetics of recruitment and allosteric activation of ARHGEF25 isoforms by the heterotrimeric G-protein Gαq. *Scientific Reports*, *6*(1), 36825.

Van Weerd, J. H., & Komen, J. (1998). The effects of chronic stress on growth in fish: a critical appraisal. *Comparative Biochemistry and Physiology Part A: Molecular & Integrative Physiology*, *120*(1), 107-112.

Van Wetering, S., van Buul, J. D., Quik, S., Mul, F. P., Anthony, E. C., Klooster, J. P. T., ... & Hordijk, P. L. (2002). Reactive oxygen species mediate Rac-induced loss of cell-cell adhesion in primary human endothelial cells. *Journal of cell science*, *115*(9), 1837-1846.

Vandereyken, K., Van Leene, J., De Coninck, B., & Cammue, B. P. (2018). Hub protein controversy: taking a closer look at plant stress response hubs. *Frontiers in plant science*, *9*, 694.

Varki, A. (2017). Biological roles of glycans. *Glycobiology*, *27*(1), 3-49.

Vaudreuil, M. A., Duy, S. V., Munoz, G., & Sauvé, S. (2022). Pharmaceutical pollution of hospital effluents and municipal wastewaters of Eastern Canada. *Science of the Total Environment*, *846*, 157353.

Vaudreuil, M. A., Munoz, G., Duy, S. V., & Sauvé, S. (2024). Tracking down pharmaceutical pollution in surface waters of the St. Lawrence River and its major tributaries. *Science of the Total Environment*, *912*, 168680.

Veith, A., & Moorthy, B. (2018). Role of cytochrome P450s in the generation and metabolism of reactive oxygen species. *Current opinion in toxicology*, *7*, 44-51.

Vercellino, I., & Sazanov, L. A. (2022). The assembly, regulation and function of the mitochondrial respiratory chain. *Nature reviews Molecular cell biology*, *23*(2), 141-161.

Vijayan, M. M., Aluru, N., & Leatherland, J. F. (2010). Stress response and the role of cortisol. In *Fish diseases and disorders, Volume 2* (pp. 182-201). Wallingford UK: CABI.

Vinken, M. (2019). Omics-based input and output in the development and use of adverse outcome pathways. *Current Opinion in Toxicology*, *18*, 8-12.

Vogel, P., Mägert, H. J., Cieslak, A., Adermann, K., & Forssmann, W. G. (1996). hDIP—a potential transcriptional regulator related to murine TSC-22 and Drosophila shortsighted (shs)—is expressed in a large number of human tissues. *Biochimica et Biophysica Acta (BBA)-Gene Structure and Expression*, *1309*(3), 200-204.

Voican, C. S., Corruble, E., Naveau, S., & Perlemuter, G. (2014). Antidepressant-induced liver injury: a review for clinicians. *American Journal of Psychiatry*, *171*(4), 404-415.

Vollmar, P., Haghikia, A., Dermietzel, R., & Faustmann, P. M. (2008). Venlafaxine exhibits an anti-inflammatory effect in an inflammatory co-culture model. *International Journal of Neuropsychopharmacology*, *11*(1), 111-117.

Waller, J. A., Tamm, J. A., Abdourahman, A., Pehrson, A. L., Li, Y., Cajina, M., & Sánchez, C. (2017). Chronic vortioxetine treatment in rodents modulates gene expression of neurodevelopmental and plasticity markers. *European Neuropsychopharmacology*, *27*(2), 192-203.

Wallner, M., Meera, P., & Toro, L. (1999). Molecular basis of fast inactivation in voltage and Ca2+-activated K+ channels: a transmembrane β-subunit homolog. *Proceedings of the National Academy of Sciences*, *96*(7), 4137-4142.

Wang, P., Tait, S. M., & Chaudry, I. H. (2000). Sustained elevation of norepinephrine depresses hepatocellular function. *Biochimica et Biophysica Acta (BBA)-Molecular Basis of Disease*, *1535*(1), 36-44.

Wang, P., Xia, P., Wang, Z., & Zhang, X. (2020). Evidence-based assessment on environmental mixture using a concentration-dependent transcriptomics approach. *Environmental Pollution*, *265*, 114839.

Wang, Q., Zhao, X., Liu, Y., Zheng, J., Cui, H., Wang, H., ... & Ding, Z. (2023). Characterization and Expression Analysis of Genes from Megalobrama amblycephala Encoding Hemoglobins with Extracellular Microbicidal Activity. *Genes*, *14*(10), 1972.

Wang, S., Zhang, L., Liu, C., & Lu, W. Y. (2017). Protective roles of hepatic GABA signaling in liver injury. *International Journal of Physiology, Pathophysiology and Pharmacology*, *9*(5), 153.

Wang, X., Shang, X., Luan, J., & Zhang, S. (2014). Identification, expression and function of apolipoprotein E in annual fish Nothobranchius guentheri: Implication for an aging marker. *Biogerontology*, *15*, 233-243.

Wang, Y., Ghaffari, N., Johnson, C. D., Braga-Neto, U. M., Wang, H., Chen, R., & Zhou, H. (2011). Evaluation of the coverage and depth of transcriptome by RNA-Seq in chickens. In *BMC bioinformatics* (Vol. 12, pp. 1-7). BioMed Central.

Watanabe, T. (1982). Lipid nutrition in fish. *Comparative Biochemistry and Physiology Part B: Comparative Biochemistry*, *73*(1), 3-15.

Waterhouse, R. M., Zdobnov, E. M., & Kriventseva, E. V. (2011). Correlating traits of gene retention, sequence divergence, duplicability and essentiality in vertebrates, arthropods, and fungi. *Genome biology and evolution*, *3*, 75-86.

Weber, A. V., Firth, B. L., Cadonic, I. G., & Craig, P. M. (2023). Interactive effects of venlafaxine and thermal stress on zebrafish (Danio rerio) inflammatory and heat shock responses. *Comparative Biochemistry and Physiology Part C: Toxicology & Pharmacology*, *269*, 109620.

Wei, X., Ai, K., Li, H., Zhang, Y., Li, K., & Yang, J. (2019). Ancestral T cells in fish require mTORC1-coupled immune signals and metabolic programming for proper activation and function. *The Journal of Immunology*, *203*(5), 1172-1188.

Wei, X., Zhang, Y., Li, C., Ai, K., Li, K., Li, H., & Yang, J. (2020). The evolutionarily conserved MAPK/Erk signaling promotes ancestral T-cell immunity in fish via c-Myc–mediated glycolysis. *Journal of Biological Chemistry*, *295*(10), 3000-3016.

Weil, C., Lefèvre, F., & Bugeon, J. (2013). Characteristics and metabolism of different adipose tissues in fish. *Reviews in Fish Biology and Fisheries*, *23*, 157-173.

Wendelaar Bonga, S. E. (1997). The stress response in fish. *Physiological reviews*, *77*(3), 591-625.

Weng, D., Lu, Y., Wei, Y., Liu, Y., & Shen, P. (2007). The role of ROS in microcystin-LR-induced hepatocyte apoptosis and liver injury in mice. *Toxicology*, *232*(1-2), 15-23.

Whitehead, A., Triant, D. A., Champlin, D., & Nacci, D. (2010). Comparative transcriptomics implicates mechanisms of evolved pollution tolerance in a killifish population. *Molecular Ecology*, *19*(23), 5186-5203.

Widmer, C. C., Pereira, C. P., Gehrig, P., Vallelian, F., Schoedon, G., Buehler, P. W., & Schaer, D. J. (2010). Hemoglobin can attenuate hydrogen peroxide–induced oxidative stress by acting as an antioxidative peroxidase. *Antioxidants & redox signaling*, *12*(2), 185-198.

Wigner, P., Synowiec, E., Czarny, P., Bijak, M., Jóźwiak, P., Szemraj, J., ... & Śliwiński, T. (2020). Effects of venlafaxine on the expression level and methylation status of genes involved in oxidative stress in rats exposed to a chronic mild stress. *Journal of Cellular and Molecular Medicine*, *24*(10), 5675-5694.

Wiles, S. C., Bertram, M. G., Martin, J. M., Tan, H., Lehtonen, T. K., & Wong, B. B. (2020). Long-term pharmaceutical contamination and temperature stress disrupt fish behavior. *Environmental Science & Technology*, *54*(13), 8072-8082.

Wilhelm, S., Jacob, S., Ziegler, M., Köhler, H. R., & Triebskorn, R. (2018). Influence of different wastewater treatment technologies on genotoxicity and dioxin-like toxicity in effluent-exposed fish. *Environmental Sciences Europe*, *30*, 1-11.

Wilkinson, J. L., Boxall, A. B., Kolpin, D. W., Leung, K. M., Lai, R. W., Galbán-Malagón, C., ... & Teta, C. (2022). Pharmaceutical pollution of the world's rivers. *Proceedings of the National Academy of Sciences*, *119*(8), e2113947119.

Williams, M. J., Almén, M. S., Fredriksson, R., & Schiöth, H. B. (2012). What model organisms and interactomics can reveal about the genetics of human obesity. *Cellular and Molecular Life Sciences*, *69*, 3819-3834.

Wood, J. D., Yuan, J., Margolis, R. L., Colomer, V., Duan, K., Kushi, J., ... & Ross, C. A. (1998). Atrophin-1, the DRPLA gene product, interacts with two families of WW domain-containing proteins. *Molecular and Cellular Neuroscience*, *11*(3), 149-160.

Writer, J. H., Ferrer, I., Barber, L. B., & Thurman, E. M. (2013). Widespread occurrence of neuro-active pharmaceuticals and metabolites in 24 Minnesota rivers and wastewaters. *Science of the total environment*, *461*, 519-527.

Wu, J., Choi, T. Y., & Shin, D. (2017). tomm22 knockdown-mediated hepatocyte damages elicit both the formation of hybrid hepatocytes and biliary conversion to hepatocytes in zebrafish larvae. *Gene expression*, *17*(3), 237.

Wu, N., Song, Y. L., Wang, B., Zhang, X. Y., Zhang, X. J., Wang, Y. L., ... & Zhang, Y. A. (2016). Fish gut-liver immunity during homeostasis or inflammation revealed by integrative transcriptome and proteome studies. *Scientific reports*, *6*(1), 36048.

Wu, S., Liu, M., Zhang, M., Ye, X., Gu, H., Jiang, C., ... & Cao, M. (2024). The gene expression of CALD1, CDH2, and POSTN in fibroblast are related to idiopathic pulmonary fibrosis. *Frontiers in Immunology*, *15*, 1275064.

Xiao, B., Kuruvilla, J., & Tan, E. K. (2022). Mitophagy and reactive oxygen species interplay in Parkinson's disease. *npj Parkinson's Disease*, *8*(1), 135.

Xin, Y., Li, C., Guo, Y., Xiao, R., Zhang, H., & Zhou, G. (2019). RNA-Seq analysis reveals a negative role of MSMO1 with a synergized NSDHL expression during adipogenesis of 3T3-L1. *Bioscience, biotechnology, and biochemistry*, *83*(4), 641-652.

Xu, C., Evensen, Ø., & Munang'andu, H. M. (2015). De novo assembly and transcriptome analysis of Atlantic salmon macrophage/dendritic-like TO cells following type I IFN treatment and Salmonid alphavirus subtype-3 infection. *BMC genomics*, *16*, 1-16.

Xu, Z., Cao, J., Qin, X., Qiu, W., Mei, J., & Xie, J. (2021). Toxic effects on bioaccumulation, hematological parameters, oxidative stress, immune responses and tissue structure in fish exposed to ammonia nitrogen: a review. *Animals*, *11*(11), 3304.

Yan, J., Liao, K., Wang, T., Mai, K., Xu, W., & Ai, Q. (2015). Dietary lipid levels influence lipid deposition in the liver of large yellow croaker (*Larimichthys crocea*) by regulating lipoprotein receptors, fatty acid uptake and triacylglycerol synthesis and catabolism at the transcriptional level. *PloS one*, *10*(6)

Yang, T., Espenshade, P. J., Wright, M. E., Yabe, D., Gong, Y., Aebersold, R., ... & Brown, M. S. (2002). Crucial step in cholesterol homeostasis: sterols promote binding of SCAP to INSIG-1, a membrane protein that facilitates retention of SREBPs in ER. *Cell*, *110*(4), 489-500.

Yarden, Y., & Sliwkowski, M. X. (2001). Untangling the ErbB signalling network. *Nature reviews Molecular cell biology*, *2*(2), 127-137.

Yeh, A., Marcinek, D. J., Meador, J. P., & Gallagher, E. P. (2017). Effect of contaminants of emerging concern on liver mitochondrial function in Chinook salmon. *Aquatic toxicology*, *190*, 21-31.

Yeh, Y. C., Lee, C. W., Pan, Y. W., Hsu, Y. J., Hung, H. Y., Chen, Y. M., ... & Wang, H. C. (2012). Identification and characterization of DSCAM isoforms isolated from orange-spotted grouper Epinephelus coioides. *Developmental & Comparative Immunology*, *38*(1), 148-159.

Young, M. D., Wakefield, M. J., Smyth, G. K., & Oshlack, A. (2010). Gene ontology analysis for RNA-seq: accounting for selection bias. *Genome biology*, *11*, 1-12.

Zagklis, D. P., & Bampos, G. (2022). Tertiary wastewater treatment technologies: a review of technical, economic, and life cycle aspects. *Processes*, *10*(11), 2304.

Zeisberg, M., & Neilson, E. G. (2009). Biomarkers for epithelial-mesenchymal transitions. *The Journal of clinical investigation*, *119*(6), 1429-1437.

Zera, A. J., & Harshman, L. G. (2001). The physiology of life history trade-offs in animals. *Annual review of Ecology and Systematics*, *32*(1), 95-126.

Zhang, A. (2009). *Protein interaction networks: computational analysis*. Cambridge University Press.

Zhang, Y., & Wong, H. S. (2021). Are mitochondria the main contributor of reactive oxygen species in cells?. *Journal of Experimental Biology*, *224*(5), jeb221606.

Zhang, Y., Zhang, J., Gao, K., Lu, R., Cao, X., Yang, L., & Nie, G. (2023). Genome‐wide comparative identification and analysis of membrane‐FADS‐like superfamily genes in freshwater economic fishes. *FEBS Open bio*, *13*(6), 1067-1085.

Zhang, Z., Zhang, S., Jiang, X., Wu, D., Du, Y., & Yang, X. D. (2022). Spata2L suppresses TLR4 signaling by promoting CYLD-Mediated deubiquitination of TRAF6 and TAK1. *Biochemistry (Moscow)*, *87*(9), 957-964.

Zhao, F., Jiang, G., Wei, P., Wang, H., & Ru, S. (2018). Bisphenol S exposure impairs glucose homeostasis in male zebrafish (Danio rerio). *Ecotoxicology and environmental safety*, *147*, 794-802.

Zhao, Y., & Zhao, B. (2013). Oxidative stress and the pathogenesis of Alzheimer′ s disease. *Oxidative medicine and cellular longevity*, *2013*(1), 316523.

Zheng, F., Asim, M., Lan, J., Zhao, L., Wei, S., Chen, N., ... & Lin, L. (2015). Molecular cloning and functional characterization of mannose receptor in zebra fish (Danio rerio) during infection with Aeromonas sobria. *International journal of molecular sciences*, *16*(5), 10997-11012.

Zhou, Y., Wu, S., Zhou, H., Huang, H., Zhao, J., Deng, Y., ... & Luo, L. (2018). Chiral pharmaceuticals: environment sources, potential human health impacts, remediation technologies and future perspective. *Environment international*, *121*, 523-537.

Ziegler, M., Eckstein, H., Ottmann, S., Reinelt, L., Stepinski, S., Köhler, H. R., & Triebskorn, R. (2020). Biochemical and cellular biomarkers in brown trout (*Salmo trutta f. fario*) in response to the antidepressants citalopram and venlafaxine. *Environmental Sciences Europe*, *32*, 1-15.

Zimmermann, R., Strauss, J. G., Haemmerle, G., Schoiswohl, G., Birner-Gruenberger, R., Riederer, M., ... & Zechner, R. (2004). Fat mobilization in adipose tissue is promoted by adipose triglyceride lipase. *Science*, *306*(5700), 1383-1386.

Zorov, D. B., Juhaszova, M., & Sollott, S. J. (2014). Mitochondrial reactive oxygen species (ROS) and ROS-induced ROS release. *Physiological reviews*, *94*(3), 909-950.

Zou, J., & Secombes, C. J. (2011). Teleost fish interferons and their role in immunity. *Developmental & Comparative Immunology*, *35*(12), 1376-1387.

Appendix A

Table A1.1: Summary of RNA sequencing quality metrics for liver samples collected from rainbow (*Etheostoma caeruleum*), fantail (*E. flabellare*), johnny (*E. nigrum*), and greenside darter (*E. blennioides*). Metrics include RNA Integrity Number (RIN), total raw paired-end reads, filtered reads post-quality control, percentage of preserved reads post-trimming, and overall alignment rate to the respective assembled transcriptome. Three samples (JK4, FE7, GK5) underwent a second sequencing run, with reads concatenated for downstream processing. Sample identifiers beginning with F, G, J, and R correspond to fantail, greenside, johnny, and rainbow darter, respectively. Identifiers containing K and E denote upstream (KIW) and downstream (EIT) sampling sites respectively.

Sample	RIN	Raw Reads	Filtered Reads	Preserved reads (%)	Overall Alignment (%)
FE1	10	56,426,960	54,734,611	96.81	87.95
FE2	10	57,208,244	55,417,511	96.87	87.83
FE5	10	65,312,270	63,310,181	96.93	84.90
FE6	10	60,498,261	58,552,687	96.78	86.81
FE10	8.9	61,332,800	59,465,993	96.96	84.29
FE7	9.8	65,378,201	63,237,950	96.73	68.08
FK1	9.9	59,183,517	57,250,793	96.73	87.82
FK3	10	63,028,951	60,829,932	96.51	89.81
FK4	10	50,268,679	48,733,701	96.95	87.80
FK5	10	63,109,958	60,987,491	96.64	88.34
FK6	10	60,630,910	58,663,412	96.75	87.55
FK7	9.8	58,707,219	56,864,811	96.86	88.02
GE1	10	55,845,501	54,045,871	96.89	84.29
GE2	10	83,649,753	80,829,656	96.63	87.95
GE3	10	63,677,217	61,810,154	97.07	87.83
GE4	10	62,106,772	60,014,886	96.63	84.90
GE5	10	63,578,265	61,800,306	97.20	86.81
GE6	9.7	72,930,041	70,731,102	96.98	88.48
GK2	10	58,887,282	57,046,993	96.87	88.26
GK3	10	63,677,217	61,810,154	97.07	87.81
GK4	10	53,421,910	51,712,092	96.80	87.46

GK5	10	54,807,251	53,199,339	97.07	86.59
GK6	10	58,748,117	56,793,854	96.67	88.34
GK7	9.9	63,956,833	61,977,745	96.91	88.37
JE1	10	61,709,847	55,296,409	97.01	89.08
JE2	10	96,714,993	93,556,510	96.73	88.99
JE3	10	63,027,716	59,801,515	94.88	88.44
JE4	10	65,145,405	61,336,981	94.15	88.45
JE5	10	69,323,498	63,194,991	91.16	88.82
JE6	10	72,334,820	67,390,791	93.17	88.21
JK1	10	70,140,014	57,051,863	81.34	88.74
JK2	10	65,517,579	63,613,329	97.09	88.51
JK3	10	55,962,770	54,206,202	96.86	89.33
JK4	10	62,489,344	60,672,115	97.09	88.34
JK5	10	59,151,220	57,362,107	96.98	88.90
JK6	9.9	64,847,391	62,969,615	97.10	88.70
RE1	10	63,053,334	69,866,893	96.98	89.15
RE11	10	66,944,159	61,269,549	91.52	89.15
RE12	9.9	75,406,694	64,957,081	86.14	89.39
RE2	10	73,222,064	61,159,071	83.53	89.69
RE5	10	69,377,923	59,266,183	85.43	89.56
RE6	9.7	73,178,651	67,181,040	91.80	89.16
RK10	9.9	73,824,403	70,870,101	96.00	89.09
RK11	9.9	78,773,155	71,745,243	91.08	88.33
RK12	10	76,267,324	70,362,557	92.26	89.05
RK3	10	72,133,333	68,361,755	94.77	89.36
RK4	9.9	68,567,358	66,454,155	96.92	88.92
RK5	10	63,463,390	61,550,245	96.99	89.30

Table A1.2: List of all annotated significantly differentially expressed genes (log2FC <-1, >1; FDR < 0.05) in rainbow (*Etheostoma caeruleum*), fantail (*E. flabellare*), johnny (*E. nigrum*), and greenside darter (*E. blennioides*) following exposure to MWWTP effluent. Ordered alphabetically.

Species	UniProt ID	Gene Symbol	Trinity gene ID	log2FC	FDR
Rainbow Darter (*Etheostoma caeruleum*)					
	ABCA7_HUMAN	*abca7*	TRINITY_DN9975_c0_g1	4.614	9.72e-04
	ALBU1_SALSA	*alb*	TRINITY_DN6517_c1_g1	8.581	9.33e-03
	AMBP_HUMAN	*ambp*	TRINITY_DN69806_c0_g1	5.354	2.32e-02
	APOA4_HUMAN	*apoa4*	TRINITY_DN1014_c0_g2	-1.152	3.32e-02
	APOE_HUMAN	*apoe*	TRINITY_DN9649_c0_g2	-1.103	3.03e-02
	ARF4_HUMAN	*arf4*	TRINITY_DN58_c0_g2	-2.037	5.85e-03
	B3GN9_HUMAN	*b3gnt9*	TRINITY_DN69511_c0_g6	10.436	2.03e-06
	BT2A2_HUMAN	*btn2a2*	TRINITY_DN6142_c1_g1	8.389	4.28e-02
	CACP_HUMAN	*crat*	TRINITY_DN26282_c0_g2	-9.413	3.16e-03
	CADH2_RAT	*cdh2*	TRINITY_DN21288_c1_g1	8.682	3.10e-06
	CCG4_HUMAN	*cacng4*	TRINITY_DN2109_c7_g1	-8.194	3.70e-02
	CENPA_HUMAN	*cenpa*	TRINITY_DN29803_c2_g1	-8.494	3.11e-04
	CP2K1_ONCMY	*cyp2k1*	TRINITY_DN1525_c4_g1	1.527	3.56e-02
	DI3L1_HUMAN	*dis3l*	TRINITY_DN5780_c0_g2	1.592	9.33e-03
	DIK1B_HUMAN	*dipk1b*	TRINITY_DN42860_c0_g1	11.527	4.80e-02
	DRC7_XENTR	*drc7*	TRINITY_DN773_c0_g2	10.025	3.96e-02
	GAS7_HUMAN	*gas7*	TRINITY_DN30707_c0_g1	3.024	4.47e-02
	HEPC_MORCS	*hamp*	TRINITY_DN5094_c0_g1	4.873	3.01e-02
	HXK1_HUMAN	*hk1*	TRINITY_DN1092_c0_g2	9.473	2.75e-06
	HKDC1_HUMAN	*hkdc1*	TRINITY_DN8633_c2_g1	2.466	3.56e-02
	HOOK1_HUMAN	*hook1*	TRINITY_DN1246_c0_g1	2.695	1.26e-02
	HXK4_HUMAN	*gck*	TRINITY_DN10630_c0_g1	3.623	1.50e-02
	KCNKD_HUMAN	*kcnk13*	TRINITY_DN12959_c0_g2	1.767	2.40e-02
	LAYN_HUMAN	*layn*	TRINITY_DN14069_c0_g1	1.062	7.23e-03
	LIPL_HUMAN	*lpl*	TRINITY_DN61572_c3_g1	8.682	2.03e-04
	NAL12_HUMAN	*nlrp12*	TRINITY_DN107694_c0_g1	-10.122	2.88e-13

	NCAPD3	*ncapd3*	TRINITY_DN14571_c2_g2	9.544	2.97e-04
	NLRP1_HUMAN	*nlrp1*	TRINITY_DN173546_c0_g1	-8.346	4.41e-02
	Q13747_HUMAN	*serpina1*	TRINITY_DN24874_c1_g1	10.238	2.03e-03
	Q6LCH2_HUMAN	*ldlr*	TRINITY_DN6821_c5_g1	8.460	3.01e-02
	RN180_HUMAN	*rnf180*	TRINITY_DN26746_c0_g1	-9.819	6.57e-05
	SC6A8_HUMAN	*slc6a8*	TRINITY_DN22044_c0_g1	1.456	3.19e-02
	SMR8A_DANRE	*smcr8a*	TRINITY_DN2395_c18_g1	-8.291	4.41e-02
	SMYD1_HUMAN	*smyd1*	TRINITY_DN2480_c0_g2	1.870	2.14e-03
	STPG1_HUMAN	*stpg1*	TRINITY_DN985_c3_g1	1.152	4.23e-02
	ZG7_XENLA	*ZG7_XENLA*	TRINITY_DN901_c1_g3	1.008	4.63e-05
Fantail Darter (*Etheostoma flabellare*)					
	ABCF3_HUMAN	*abcf3*	TRINITY_DN6285_c0_g1	-1.301	1.78e-02
	ACLY_BOVIN	*acly*	TRINITY_DN9868_c0_g3	-1.205	1.02e-02
	ACOD_CYPCA	*ACOD_CYPCA*	TRINITY_DN3978_c0_g2	-1.813	6.84e-03
	ACSL4_RAT	*acsl4*	TRINITY_DN1360_c0_g2	-1.242	1.22e-02
	ADRM1_DANRE	*adgre1*	TRINITY_DN27838_c0_g1	-1.007	1.08e-02
	AGRE1_MOUSE	*adrm1*	TRINITY_DN8600_c0_g2	1.653	4.12e-02
	ALG13_RAT	*alg13*	TRINITY_DN88_c1_g1	-1.026	1.60e-02
	ANXA3_HUMAN	*anxa3*	TRINITY_DN907_c0_g1	1.369	4.28e-02
	AP4M1_BOVIN	*ap4m1*	TRINITY_DN10274_c0_g1	-1.017	5.22e-03
	ARF1_RAT	*arf1*	TRINITY_DN15485_c0_g1	-1.062	1.46e-02
	ARF6_RAT	*arf6*	TRINITY_DN7919_c0_g1	-1.030	5.88e-03
	ARP2A_DANRE	*actr2a*	TRINITY_DN12811_c0_g3	-1.047	6.78e-03
	AT2A2_CHICK	*atp2a2*	TRINITY_DN1907_c0_g2	-1.043	2.88e-02
	AT2B2_RAT	*atp2b2*	TRINITY_DN14816_c0_g1	1.864	3.77e-02
	ATL5_HUMAN	*atp5f1a*	TRINITY_DN2781_c2_g1	1.434	4.65e-02
	ATP5H_HUMAN	*atp5pd*	TRINITY_DN9583_c0_g1	-1.055	1.95e-02
	BBS5_DANRE	*bbs5*	TRINITY_DN4913_c0_g1	1.458	3.64e-02
	BHMT1_DANRE	*bhmt*	TRINITY_DN1241_c0_g1	-1.028	1.66e-02
	BLCAP_DANRE	*blcap*	TRINITY_DN18306_c0_g2	-1.090	2.09e-02
	BLMH_CHICK	*blmh*	TRINITY_DN14267_c0_g1	-1.024	1.67e-02

BTBD3_MUSPF	*btbd3*	TRINITY_DN1498_c1_g1	-1.204	8.47e-03
BTD_TAKRU	*btd*	TRINITY_DN7459_c0_g2	-1.713	3.51e-02
BUB3_XENLA	*bub3*	TRINITY_DN65440_c0_g1	-1.054	4.43e-02
C1QB_MOUSE	*c1qb*	TRINITY_DN12705_c1_g1	-1.108	3.60e-02
C1QBP_RAT	*c1qbp*	TRINITY_DN580_c0_g2	-1.006	4.27e-02
C1QC_RAT	*c1qc*	TRINITY_DN18788_c1_g1	-1.300	3.91e-02
C340_ORYLA	*cyp3a40*	TRINITY_DN20768_c7_g1	-1.785	3.65e-04
CA050_DANRE	*c1orf50*	TRINITY_DN1563_c10_g1	-1.224	6.44e-03
CAF17_DANRE	*c8b*	TRINITY_DN14184_c0_g1	-1.131	3.32e-02
CALX_RAT	*canx*	TRINITY_DN54502_c3_g1	-1.329	4.76e-02
CAN3_PIG	*capn3*	TRINITY_DN10322_c0_g1	1.588	1.23e-02
CCD47_DANRE	*ccdc47*	TRINITY_DN8537_c0_g1	-1.038	9.54e-03
CD63_HUMAN	*cd63*	TRINITY_DN1216_c0_g2	-1.021	3.11e-02
CD9_MOUSE	*cd9*	TRINITY_DN31396_c0_g1	-1.071	2.57e-02
CHCH1_MOUSE	*chchd1*	TRINITY_DN900_c0_g3	-1.198	1.56e-02
CHIA_HUMAN	*chia*	TRINITY_DN35250_c0_g1	11.018	2.44e-03
CHM2A_DANRE	*chmp2a*	TRINITY_DN8193_c1_g1	-1.002	4.13e-03
CHM4C_DANRE	*chmp4c*	TRINITY_DN33705_c1_g5	-1.019	2.70e-02
CIRBP_LITCT	*cirbp*	TRINITY_DN11312_c0_g1	-1.263	3.50e-03
CLCN2_CAVPO	*clcn2*	TRINITY_DN199_c0_g2	1.103	2.71e-02
CNOT8_HUMAN	*cnot8*	TRINITY_DN4038_c0_g1	-1.016	2.58e-02
CO3_ONCMY	*c3*	TRINITY_DN2551_c0_g1	8.589	8.40e-07
CRBG1_HUMAN	*crybg1*	TRINITY_DN47595_c0_g1	2.064	3.24e-02
CRIP2_BOVIN	*crip2*	TRINITY_DN1457_c0_g2	-1.075	2.02e-02
CRNL1_RAT	*crnkl1*	TRINITY_DN289_c1_g1	-1.032	1.40e-02
CRY1_CHICK	*cry1*	TRINITY_DN178_c0_g1	-1.182	5.33e-04
CSTF2_BOVIN	*cstf2*	TRINITY_DN12032_c0_g1	-1.015	3.96e-02
CUBN_HUMAN	*cubn*	TRINITY_DN918_c6_g3	8.195	1.14e-02
CXCR2_MOUSE	*cxcr2*	TRINITY_DN802_c0_g1	1.333	1.23e-02
CYP51_DANRE	*cyp51*	TRINITY_DN1007_c0_g1	-1.171	2.89e-04
DAD1_RAT	*dad1*	TRINITY_DN1069_c2_g2	-1.079	8.30e-03
DCUP_DANRE	*urod*	TRINITY_DN15569_c0_g2	-1.067	4.18e-03

DD19A_MOUSE	*ddx17*	TRINITY_DN29608_c0_g2	-1.128	1.95e-02
DDX17_MOUSE	*ddx19a*	TRINITY_DN33230_c0_g3	1.473	9.03e-04
DEGS1_CHICK	*degs1*	TRINITY_DN7174_c1_g2	-1.340	5.08e-03
DHB4_RAT	*hsd17b4*	TRINITY_DN14270_c0_g1	-1.434	2.53e-02
DHB7_RAT	*hsd17b7*	TRINITY_DN705_c0_g1	-1.119	1.09e-02
DPM3_BOVIN	*dpm3*	TRINITY_DN2994_c0_g1	-1.001	1.89e-02
DPY30_HUMAN	*dpy30*	TRINITY_DN1213_c1_g1	-1.019	1.25e-02
DPYL2_RAT	*dpysl2*	TRINITY_DN53215_c0_g1	2.532	3.27e-02
ECHM_MOUSE	*echs1*	TRINITY_DN29126_c0_g1	-1.023	2.69e-02
ECSIT_DANRE	*ecsit*	TRINITY_DN91970_c0_g1	-1.159	3.14e-02
EF1A_AJECG	*eftud2*	TRINITY_DN2274_c1_g1	-1.037	2.85e-02
EIF3B_HUMAN	*eif3b*	TRINITY_DN6522_c0_g1	-1.223	3.97e-02
EIF3I_DANRE	*eif3i*	TRINITY_DN4560_c0_g2	-1.176	4.48e-02
EKI1_MOUSE	*etnk1*	TRINITY_DN3077_c0_g3	1.003	4.19e-02
EPD2_CARAU	*epd2*	TRINITY_DN4470_c0_g1	-1.070	2.34e-03
EXOS3_HUMAN	*exosc3*	TRINITY_DN22625_c0_g1	-1.272	1.91e-02
FBX9_DANRE	*fbxo9*	TRINITY_DN98111_c0_g1	-1.036	5.13e-03
FDFT_PONAB	*fdft1*	TRINITY_DN18738_c0_g1	-1.159	8.22e-03
FETUA_BOVIN	*ahsg*	TRINITY_DN8466_c0_g1	-1.151	5.23e-03
FETUB_HUMAN	*fetub*	TRINITY_DN2737_c0_g1	-1.035	5.40e-03
FHI1A_MOUSE	*fh*	TRINITY_DN33621_c0_g2	2.410	2.21e-02
FHIT_BOVIN	*fhit*	TRINITY_DN22951_c0_g1	-1.095	3.78e-02
G6PI_PIG	*gpi*	TRINITY_DN5043_c1_g1	-1.110	3.70e-03
GAL3A_DANRE	*gatd3*	TRINITY_DN10611_c0_g1	6.321	2.36e-02
GEMI6_HUMAN	*gemin6*	TRINITY_DN157234_c0_g1	-1.470	3.80e-03
GLMP_SALSA	*glmp*	TRINITY_DN51377_c0_g2	-1.029	2.27e-02
GLT10_RAT	*galnt10*	TRINITY_DN12605_c0_g2	-1.077	1.89e-02
GLU2B_HUMAN	*glud1*	TRINITY_DN6287_c0_g1	-1.021	5.25e-03
GMPPB_DANRE	*gmppb*	TRINITY_DN1530_c2_g2	-1.086	3.32e-03
GOGA4_RAT	*golga4*	TRINITY_DN12209_c0_g2	1.097	4.00e-02
GOT1B_MOUSE	*golt1b*	TRINITY_DN24261_c0_g1	-1.060	2.53e-02
GPAT4_PONAB	*gpat4*	TRINITY_DN6667_c0_g1	-1.065	2.83e-02

GRPE1_PONAB	*grpel1*	TRINITY_DN24252_c1_g1	-1.000	4.13e-02
GSTT3_MOUSE	*gstt3*	TRINITY_DN8999_c0_g1	-1.090	1.08e-02
GT251_DANRE	*colgalt1*	TRINITY_DN120_c2_g1	1.275	1.31e-02
HERP1_HUMAN	*herpud1*	TRINITY_DN3090_c0_g2	-1.002	9.24e-03
HGF_CANLF	*hgf*	TRINITY_DN4576_c0_g1	-1.016	1.44e-02
HIG1A_MOUSE	*higd1a*	TRINITY_DN11130_c0_g1	-1.188	3.02e-03
HIPL1_MOUSE	*hhipl1*	TRINITY_DN64176_c1_g1	-1.357	3.63e-02
HMCS1_CHICK	*hmgcs1*	TRINITY_DN2919_c1_g6	-1.254	1.74e-03
HNMT_TETNG	*hnmt*	TRINITY_DN2298_c1_g3	1.118	2.00e-02
HNRPD_MOUSE	*hnrnpd*	TRINITY_DN30994_c0_g1	1.437	1.31e-02
HS90A_RABIT	*hsp90ab1*	TRINITY_DN2058_c0_g2	-2.271	2.40e-03
HS90B_XENLA	*hsp90aa1*	TRINITY_DN14402_c0_g1	-2.489	3.14e-02
HSP74_CANLF	*hspa8*	TRINITY_DN26273_c0_g3	-1.081	2.09e-02
IDHC_MICOH	*idh1*	TRINITY_DN1849_c0_g2	-1.216	6.27e-03
IF4E3_DANRE	*eif4e3*	TRINITY_DN4632_c4_g1	-1.199	2.97e-02
IFI44_HUMAN	*ifi44*	TRINITY_DN25907_c0_g2	-2.219	9.48e-03
IFIT1_MACFA	*ifit1*	TRINITY_DN2578_c0_g2	-2.956	3.78e-03
ILF2_DANRE	*ilf2*	TRINITY_DN2362_c0_g1	-1.171	4.37e-03
IMA1_HUMAN	*kpna2*	TRINITY_DN12101_c0_g1	-1.104	2.76e-02
INT10_DANRE	*ints10*	TRINITY_DN6493_c0_g1	1.031	2.78e-02
IPO7_HUMAN	*ipo7*	TRINITY_DN23629_c0_g6	-1.426	2.76e-02
ITIH3_RABIT	*itih3*	TRINITY_DN12351_c1_g1	1.529	1.58e-03
ITSN1_HUMAN	*itsn1*	TRINITY_DN3772_c0_g1	1.167	4.25e-02
KCJ10_HUMAN	*kcnj10*	TRINITY_DN28399_c0_g2	1.517	6.32e-03
KCRT_ONCMY	*tck1*	TRINITY_DN3868_c0_g3	-1.556	4.56e-02
KDM6B_HUMAN	*kdm6b*	TRINITY_DN4462_c0_g1	1.313	1.78e-02
KLH31_DANRE	*klhl31*	TRINITY_DN17027_c0_g1	1.184	2.95e-02
KV5A1_MOUSE	*igkv6-17*	TRINITY_DN3598_c0_g1	-1.949	4.50e-02
L3BPA_DANRE	*lgals3bpa*	TRINITY_DN51668_c2_g1	-1.912	9.50e-03
LEG8_HUMAN	*lgals8*	TRINITY_DN314215_c0_g1	-1.216	2.02e-02
LEG9_RAT	*lgals9*	TRINITY_DN37203_c1_g2	-1.180	1.43e-02
LGMN_BOVIN	*lgmn*	TRINITY_DN4765_c0_g1	-1.005	1.48e-02

LRC17_HUMAN	*lrrc17*	TRINITY_DN1527_c0_g2	-1.028	2.88e-02
LSM4_HUMAN	*lsm4*	TRINITY_DN5236_c2_g2	-1.062	6.32e-03
LSM8_PONAB	*lsm8*	TRINITY_DN11493_c0_g1	-1.008	3.63e-02
LSS_RAT	*lss*	TRINITY_DN7369_c0_g1	-1.462	6.23e-03
MAP7_HUMAN	*map7*	TRINITY_DN2343_c0_g1	-1.128	4.21e-02
MED31_DANRE	*med31*	TRINITY_DN28037_c0_g1	-1.067	2.86e-02
MPV17_DANRE	*mpv17*	TRINITY_DN1163_c0_g3	-1.059	2.69e-02
MSMO1_CHICK	*msmo1*	TRINITY_DN11011_c1_g1	-1.300	3.87e-02
MTCH1_HUMAN	*mtch1*	TRINITY_DN2081_c0_g1	1.142	4.37e-02
MYL9_BOVIN	*myl9*	TRINITY_DN34806_c1_g3	-1.205	7.25e-03
MYO1B_HUMAN	*myo1b*	TRINITY_DN596_c0_g1	1.747	8.29e-03
NAMPT_RAT	*nampt*	TRINITY_DN1490_c0_g2	-1.138	2.73e-02
NCK1_MOUSE	*nck1*	TRINITY_DN7800_c1_g3	1.052	1.31e-02
NDE1_RAT	*nde1*	TRINITY_DN562_c2_g2	-1.065	1.96e-02
NDUA9_RAT	*ndufa9*	TRINITY_DN58785_c0_g2	-1.063	2.41e-02
NDUAD_BOVIN	*ndufa13*	TRINITY_DN36919_c0_g1	-1.031	1.76e-02
NDUB6_PONAB	*ndufb6*	TRINITY_DN9433_c0_g1	-1.006	2.69e-02
NDUC2_MOUSE	*ndufc2*	TRINITY_DN23393_c0_g1	-1.054	9.67e-03
NDUS5_PANTR	*ndufs5*	TRINITY_DN21353_c0_g2	-1.028	4.36e-03
NEUR3_BOVIN	*neu3*	TRINITY_DN1189_c0_g1	1.885	1.02e-03
NGBR_DANRE	*nus1*	TRINITY_DN34167_c0_g1	-1.310	1.63e-03
NHLC3_PONAB	*nhlrc3*	TRINITY_DN1651_c1_g1	-1.256	3.79e-03
NIPA2_PONAB	*nipa2*	TRINITY_DN11463_c0_g1	-1.019	3.91e-03
NKTR_MOUSE	*nktr*	TRINITY_DN9554_c0_g1	1.140	2.04e-02
NOD1_MOUSE	*nod1*	TRINITY_DN14020_c0_g1	1.516	2.84e-02
NRK2_HUMAN	*nmrk2*	TRINITY_DN9367_c0_g1	-1.031	3.65e-02
NSF1C_CHICK	*nsfl1c*	TRINITY_DN31772_c0_g2	-1.397	2.94e-03
NU2M_TETNG	*mt-nd2*	TRINITY_DN21590_c0_g1	-9.257	1.50e-02
ODP2_HUMAN	*dlat*	TRINITY_DN5526_c0_g1	-1.037	7.71e-03
OTOG_HUMAN	*otog*	TRINITY_DN6489_c3_g1	1.208	1.76e-02
PABPA_XENLA	*parp14*	TRINITY_DN5202_c0_g3	-1.540	2.73e-02
PDIA6_MOUSE	*pdia6*	TRINITY_DN35471_c1_g2	-1.269	2.04e-02

PEF1_DANRE	*pef1*	TRINITY_DN362_c4_g1	-1.147	4.53e-02
PELO_DANRE	*pelo*	TRINITY_DN333_c1_g1	-1.026	9.82e-04
PEPA_CANLF	*per2*	TRINITY_DN283874_c0_g1	12.498	8.92e-03
PER2_CHICK	*per2*	TRINITY_DN8577_c0_g1	-1.252	3.90e-03
PGAM1_BOVIN	*pgam1*	TRINITY_DN16353_c0_g2	-1.624	4.68e-02
PGAM1_HUMAN	*pgam1*	TRINITY_DN16353_c0_g1	-1.284	7.22e-03
PGAP1_MOUSE	*pgap1*	TRINITY_DN801_c4_g2	1.127	2.14e-02
PGM2L_MOUSE	*pgm2l1*	TRINITY_DN2250_c0_g1	1.479	4.02e-03
PGP_MOUSE	*pgp*	TRINITY_DN158322_c0_g1	-1.248	1.33e-02
PHB1_CHICK	*phb1*	TRINITY_DN2320_c3_g2	-1.192	1.70e-02
PHB2_XENTR	*phb2*	TRINITY_DN12901_c0_g2	-1.096	2.43e-02
PHF5A_RAT	*phf5a*	TRINITY_DN14604_c1_g2	-1.363	7.71e-03
PIGC_MOUSE	*pigc*	TRINITY_DN148556_c0_g1	-1.229	6.38e-03
PPCE_MOUSE	*prep*	TRINITY_DN537_c0_g4	-1.052	2.12e-02
PSA1_HUMAN	*psma1*	TRINITY_DN9819_c0_g1	-1.017	5.22e-03
PSB2_BOVIN	*psmb2*	TRINITY_DN3739_c0_g1	-1.115	5.67e-03
PSB4_XENLA	*psmb4*	TRINITY_DN937_c0_g1	-1.079	3.70e-03
PSB5_MOUSE	*psmb5*	TRINITY_DN7570_c2_g1	-1.090	3.79e-03
PSB8_RAT	*psmb8*	TRINITY_DN6800_c0_g1	-1.205	4.56e-02
PSD11_RAT	*psmd11*	TRINITY_DN24115_c1_g1	-1.526	3.47e-02
PSDE_MOUSE	*psmd14*	TRINITY_DN11468_c0_g2	-1.107	1.66e-03
PSMD1_CHICK	*psmd1*	TRINITY_DN7223_c0_g2	-1.030	1.19e-02
PSMD2_MOUSE	*psmd2*	TRINITY_DN4005_c1_g2	-1.162	1.20e-02
PSMD6_HUMAN	*psmd6*	TRINITY_DN8810_c0_g1	-1.039	4.37e-03
PSMD7_MOUSE	*psmd7*	TRINITY_DN21578_c0_g2	-1.047	1.88e-03
PSMD8_BOVIN	*psmd8*	TRINITY_DN24789_c1_g1	-1.043	8.08e-03
PTH2_BOVIN	*ptrh2*	TRINITY_DN159_c1_g2	-1.050	2.24e-03
PTRD1_BOVIN	*ptrhd1*	TRINITY_DN8587_c0_g1	-1.116	3.77e-02
QPCT_HUMAN	*qpct*	TRINITY_DN8931_c1_g1	-1.033	1.31e-02
RAN_CARAU	*ran*	TRINITY_DN8103_c0_g1	-1.109	2.03e-02
RCC2_DANRE	*rcc2*	TRINITY_DN15745_c1_g1	-1.032	3.01e-03
RDH10_HUMAN	*rdh10*	TRINITY_DN45875_c0_g1	-1.302	1.42e-02

RDH13_HUMAN	*rdh13*	TRINITY_DN12658_c0_g1	9.032	4.14e-02
RHOAB_DANRE	*rhoab*	TRINITY_DN12941_c1_g1	-1.058	3.97e-02
RN146_AILME	*rnf146*	TRINITY_DN13927_c0_g1	-1.175	1.31e-02
RNF24_MOUSE	*rnf24*	TRINITY_DN2965_c0_g2	1.200	4.08e-03
RPGP2_CHICK	*rap1gap2*	TRINITY_DN6229_c0_g1	1.374	5.07e-03
RSBNL_HUMAN	*rsbn1l*	TRINITY_DN9521_c0_g3	1.532	3.49e-02
RSMB_CHICK	*snrpb*	TRINITY_DN5796_c0_g1	-1.208	1.63e-02
RXRAA_DANRE	*rxraa*	TRINITY_DN44062_c1_g1	8.126	3.64e-02
S25A3_MOUSE	*slc25a3*	TRINITY_DN3308_c0_g1	-1.044	2.33e-02
S39A9_RAT	*slc39a9*	TRINITY_DN6410_c1_g2	2.783	1.87e-02
SC5D_MOUSE	*sc5d*	TRINITY_DN48444_c0_g1	-1.257	1.96e-02
SDF2_MOUSE	*sdf2*	TRINITY_DN10747_c0_g1	-1.082	8.20e-03
SEC13_BOVIN	*sec13*	TRINITY_DN10828_c0_g1	-1.081	1.19e-02
SELK_DANRE	*selenok*	TRINITY_DN11496_c0_g2	-1.069	1.25e-02
SERB_PONAB	*psph*	TRINITY_DN22889_c0_g1	-1.249	4.63e-03
SF3B4_HUMAN	*sf3b4*	TRINITY_DN11321_c1_g1	-1.066	3.77e-02
SHLB2_HUMAN	*sh3glb2*	TRINITY_DN5475_c0_g2	1.116	1.09e-02
SIAS_HUMAN	*nans*	TRINITY_DN8667_c1_g2	-1.042	1.09e-02
SNF5_TETFL	*smarcb1*	TRINITY_DN1253_c0_g5	-1.007	1.62e-02
SNG2_BOVIN	*syngr2*	TRINITY_DN1086_c0_g2	-1.138	2.71e-02
SNPC1_MACFA	*snapc1*	TRINITY_DN11106_c2_g1	-1.035	4.46e-02
SPA31_BOVIN	*serpina3*	TRINITY_DN7178_c0_g2	-1.765	4.06e-03
SQSTM_RAT	*sqstm1*	TRINITY_DN3641_c0_g1	-1.273	1.29e-02
SRBP2_DANRE	*srebf2*	TRINITY_DN2476_c3_g2	-1.421	4.69e-05
STAB2_HUMAN	*stab2*	TRINITY_DN1855_c3_g1	-1.076	2.82e-02
STAT1_PIG	*stat1*	TRINITY_DN751_c7_g1	-1.606	8.87e-03
STAT3_PIG	*stat3*	TRINITY_DN4916_c0_g1	-1.145	8.46e-03
STT3B_CANLF	*stt3b*	TRINITY_DN953_c0_g2	-1.106	3.42e-02
SUCA_COLLI	*suclg1*	TRINITY_DN107_c2_g3	-1.006	1.24e-02
SYYM_MOUSE	*yars2*	TRINITY_DN20380_c1_g2	-1.025	2.88e-02
TCB1_CAEBR	*tbc1d23*	TRINITY_DN24216_c0_g1	1.292	4.06e-02
TECR_HUMAN	*tecr*	TRINITY_DN562_c3_g1	-1.072	6.40e-03

THOP1_MOUSE	*thop1*	TRINITY_DN11495_c0_g2	-1.123	1.15e-02
TI17A_HUMAN	*timm17a*	TRINITY_DN11081_c0_g2	-1.246	1.40e-03
TIM44_HUMAN	*timm44*	TRINITY_DN96700_c0_g4	-1.354	1.89e-02
TM101_BOVIN	*tmem101*	TRINITY_DN316638_c0_g1	-1.087	3.71e-02
TM165_HUMAN	*tmem165*	TRINITY_DN25_c2_g2	-1.092	2.32e-02
TM230_MOUSE	*tmem230*	TRINITY_DN879_c5_g1	-1.006	4.76e-02
TMM82_XENLA	*tmem82*	TRINITY_DN1149_c1_g1	-1.015	4.18e-02
TNR14_MOUSE	*tnfsf14*	TRINITY_DN90_c2_g2	-1.803	2.28e-02
TOM22_MACFA	*tomm22*	TRINITY_DN7828_c0_g1	-1.050	8.47e-03
TOM40_XENTR	*tomm40*	TRINITY_DN7429_c0_g1	-1.201	5.65e-03
TPST1_DANRE	*tp53inp2*	TRINITY_DN566_c0_g1	-1.150	6.38e-03
TRI25_HUMAN	*trim25*	TRINITY_DN31159_c0_g1	1.095	2.76e-02
TYSY_HUMAN	*tyms*	TRINITY_DN1151_c2_g1	1.452	8.08e-03
U2AF1_BOVIN	*u2af1*	TRINITY_DN479_c0_g4	-1.173	5.13e-03
UB2L3_MOUSE	*ube2l3*	TRINITY_DN3902_c0_g2	-1.050	7.14e-03
UBIQP_XENLA	*ubb*	TRINITY_DN3737_c0_g1	-2.537	7.06e-03
UBP2_CHICK	*usp2*	TRINITY_DN1783_c1_g1	-1.457	3.47e-02
UBP5_HUMAN	*usp5*	TRINITY_DN15811_c0_g1	-1.108	3.01e-03
UCRI_COLPO	*uqcrfs1*	TRINITY_DN40305_c0_g2	-1.435	7.88e-03
UNC50_DANRE	*unc50*	TRINITY_DN10779_c0_g1	-1.052	1.72e-02
VA0D1_DANRE	*serpina3*	TRINITY_DN19654_c0_g2	-1.049	7.74e-03
VMP1_DANRE	*vmp1*	TRINITY_DN32903_c0_g1	-1.084	1.50e-02
WBP11_DANRE	*wbp11*	TRINITY_DN39451_c0_g1	-1.056	2.86e-03
WDR55_ORYLA	*wdr55*	TRINITY_DN16995_c0_g1	1.930	5.49e-04
WDR74_HUMAN	*wdr74*	TRINITY_DN2625_c0_g1	-1.090	1.10e-02
XBP1_RAT	*xbp1*	TRINITY_DN51054_c0_g1	-1.112	1.19e-02
YIPF6_DANRE	*yipf6*	TRINITY_DN2577_c6_g1	-1.099	1.10e-02
ZFY21_HUMAN	*zfyve21*	TRINITY_DN3405_c0_g1	-1.051	2.93e-02
ZN326_BOVIN	*znf326*	TRINITY_DN7826_c0_g3	1.376	3.11e-03
ZP3_PIG	*zp3*	TRINITY_DN26367_c0_g1	-1.199	1.78e-02

ACAC_CHICK	*acac*	TRINITY_DN9002_c0_g1	2.226	5.58e-03
AVR2B_CHICK	*acvr2b*	TRINITY_DN3016_c1_g1	-1.103	6.64e-03
CO3_ONCMY	*c3*	TRINITY_DN40028_c0_g1	-11.033	1.69e-04
CO7_BOVIN	*c7*	TRINITY_DN32197_c0_g1	-12.452	1.14e-02
FHR2_HUMAN	*cfhr2*	TRINITY_DN82698_c0_g1	8.786	7.44e-08
CHAC2_DANRE	*chac2*	TRINITY_DN8258_c1_g1	1.260	4.58e-02
CPT1A_HORSE	*cpt1a*	TRINITY_DN3855_c4_g2	-2.124	2.57e-02
GPT_BOVIN	*dpagt1*	TRINITY_DN1345_c0_g2	1.445	8.74e-03
DUS1_HUMAN	*dusp1*	TRINITY_DN2318_c0_g1	-2.428	1.16e-02
EGLN2_HUMAN	*egln2*	TRINITY_DN7012_c6_g1	1.289	4.06e-04
EGR1_DANRE	*egr1*	TRINITY_DN176_c2_g1	-2.441	5.16e-03
FADS6_BOVIN	*fads6*	TRINITY_DN232_c1_g2	2.786	5.89e-03
FAAA_HUMAN	*fah*	TRINITY_DN63386_c0_g1	1.449	4.21e-02
FIBA2_PETMA	*fga*	TRINITY_DN386_c20_g1	7.540	5.89e-03
GCSP_HUMAN	*gldc*	TRINITY_DN2437_c0_g1	2.354	2.95e-03
3HAO_DANRE	*haao*	TRINITY_DN5042_c2_g2	2.039	2.80e-03
HEXA_ANOGA	*hexa*	TRINITY_DN24850_c0_g1	14.115	6.30e-03
IER2_DANRE	*ier2*	TRINITY_DN65175_c0_g1	-3.119	1.33e-04
OXLA_SIGCA	*il4i1*	TRINITY_DN10043_c1_g1	1.718	2.97e-02
ITIH2_MOUSE	*itih2*	TRINITY_DN19293_c0_g1	-2.657	1.70e-02
JUNB_CYPCA	*junb*	TRINITY_DN3320_c0_g1	-2.464	2.13e-03
KLF13_MOUSE	*klf13*	TRINITY_DN1_c0_g1	1.960	1.46e-03
LRCH3_MOUSE	*lrch3*	TRINITY_DN429_c3_g1	1.292	5.29e-04
METK2_HUMAN	*mat2a*	TRINITY_DN26128_c2_g1	2.292	3.53e-02
TRI18_HUMAN	*mid1*	TRINITY_DN965_c0_g1	-1.471	7.56e-03
MIOX_DANRE	*miox*	TRINITY_DN2201_c0_g1	2.329	1.55e-03
ATP6_SALSA	*mt-atp6*	TRINITY_DN19254_c0_g1	4.752	9.15e-05
COX1_ONCMY	*mt-co1*	TRINITY_DN19012_c0_g2	9.555	5.55e-04
COX3_CARAU	*mt-co3*	TRINITY_DN38705_c0_g2	5.102	1.31e-06
CYB_DACPE	*mt-cyb*	TRINITY_DN7369_c0_g6	5.891	2.15e-05

	NF7B_XENLA	*nf7b*	TRINITY_DN2940_c0_g1	4.297	3.36e-02
	NHRF1_RAT	*nherf1*	TRINITY_DN21587_c1_g1	2.273	8.48e-07
	NHRF3_PONAB	*pdzk1*	TRINITY_DN1688_c0_g1	1.287	1.14e-03
	PGBD4_HUMAN	*pgbd4*	TRINITY_DN7563_c0_g2	1.233	3.50e-02
	PHLA2_SALSA	*phlda2*	TRINITY_DN28575_c1_g1	-1.985	8.57e-03
	PLCG1_BOVIN	*plcg1*	TRINITY_DN34264_c0_g1	-7.279	3.84e-02
	PKHA6_HUMAN	*plekha6*	TRINITY_DN7326_c3_g1	1.570	2.37e-02
	PTN4_MOUSE	*ptpn4*	TRINITY_DN50197_c0_g2	-9.227	6.73e-04
	RNPC3_DANRE	*rnpc3*	TRINITY_DN78070_c1_g1	8.713	3.69e-03
	RL12_BOVIN	*rpl12*	TRINITY_DN43556_c0_g1	2.198	1.06e-03
	SAMD3_HUMAN	*samd3*	TRINITY_DN4626_c0_g1	-6.069	1.15e-02
	S13A5_HUMAN	*slc13a5*	TRINITY_DN23648_c0_g2	2.382	1.29e-03
	S238B_DANRE	*slc25a38b*	TRINITY_DN4770_c0_g1	2.437	2.05e-03
	S38A4_HUMAN	*slc38a4*	TRINITY_DN67931_c0_g1	1.794	3.33e-02
	SO1A2_HUMAN	*slco1a2*	TRINITY_DN20913_c1_g1	-1.626	4.94e-02
	TC1A_CAEEL	*tc1a*	TRINITY_DN86861_c0_g1	-9.237	5.84e-04
	TCB1_CAEBR	*tcb1*	TRINITY_DN18421_c1_g3	4.424	3.18e-02
	TCTP_LATJA	*tpt1*	TRINITY_DN18921_c1_g1	9.861	2.26e-05
	TRAK1_HUMAN	*trak1*	TRINITY_DN2500_c0_g1	1.067	3.37e-02
	TRM2B_DANRE	*trmt2b*	TRINITY_DN2284_c0_g1	1.452	4.94e-02
Greenside Darter (*Etheostoma blennioides*)					
	LECH_CHICK	*asgr2*	TRINITY_DN7604_c0_g1	-1.044	2.40e-02
	ANGL5_HUMAN	*angptl5*	TRINITY_DN6770_c0_g1	1.736	9.28e-03
	BHMT1_DANRE	*bhmt*	TRINITY_DN21362_c0_g5	1.770	1.15e-02
	BIN2_MOUSE	*bin2*	TRINITY_DN18201_c0_g1	-1.259	8.31e-03
	C1S_RAT	*c1s*	TRINITY_DN85628_c1_g1	-8.966	1.46e-03
	CARD9_RAT	*card9*	TRINITY_DN5321_c1_g1	-1.357	5.12e-04
	PEBB_HUMAN	*cbfb*	TRINITY_DN3558_c2_g2	-1.197	4.73e-02
	CBP_HUMAN	*crebbp*	TRINITY_DN522_c0_g2	1.389	2.78e-03
	CSRN1_HUMAN	*csrnp1*	TRINITY_DN5535_c0_g1	1.683	2.38e-03

CATL1_CANLF	*ctsl*	TRINITY_DN1670_c0_g1	1.224	5.12e-04
CYH2_CHLAE	*cyth2*	TRINITY_DN8602_c0_g1	-1.357	4.17e-03
DDIT4_DANRE	*ddit4*	TRINITY_DN346_c0_g1	3.071	4.73e-02
DOK2_MOUSE	*dok2*	TRINITY_DN642_c2_g1	-1.155	1.43e-03
DONS_XENLA	*donson*	TRINITY_DN14100_c0_g1	2.177	4.26e-03
ZG57_XENLA	*zg57_xenl*	TRINITY_DN2271_c4_g1	9.394	1.73e-04
DSCAM_CHICK	*dscam*	TRINITY_DN7751_c0_g1	-1.213	3.77e-02
ERRFI_MOUSE	*errfi1*	TRINITY_DN1599_c0_g1	1.527	4.42e-03
FRIM_SALSA	*frim*	TRINITY_DN20004_c0_g1	-1.629	1.07e-02
GIMA8_HUMAN	*gimap8*	TRINITY_DN8184_c0_g1	-1.284	2.37e-02
GNPAT_BOVIN	*gnpat*	TRINITY_DN10270_c0_g2	-1.374	9.58e-03
GOT1A_BOVIN	*golt1a*	TRINITY_DN7423_c0_g1	1.178	1.92e-02
GPCP1_RAT	*gpcpd1*	TRINITY_DN99261_c0_g2	2.470	5.68e-03
G6PI_HUMAN	*gpi*	TRINITY_DN5592_c0_g2	1.377	2.40e-02
GRK6_MOUSE	*grk6*	TRINITY_DN10979_c0_g1	-1.151	3.05e-02
HBA_TREBE	*hba*	TRINITY_DN2884_c0_g1	1.225	4.44e-02
HBA1_ANAMI	*hba1*	TRINITY_DN27657_c0_g1	1.213	7.85e-03
HBB1_ELEMC	*hbb1*	TRINITY_DN60694_c0_g1	1.306	4.40e-02
HBB2_ANAMI	*hbb2*	TRINITY_DN3033_c0_g1	1.303	5.51e-03
HS3SB_HUMAN	*hs3st3b1*	TRINITY_DN27_c0_g3	1.700	3.35e-02
HSP7C_HUMAN	*hspa8*	TRINITY_DN52432_c0_g1	-1.903	5.49e-03
INSI1_DANRE	*insig1*	TRINITY_DN4297_c0_g1	1.287	1.17e-03
IRS2_MOUSE	*irs2*	TRINITY_DN272_c3_g2	1.670	2.30e-02
ITAL_MOUSE	*itgal*	TRINITY_DN837_c5_g1	-1.001	3.49e-02
KLF13_MOUSE	*klf13*	TRINITY_DN5646_c0_g1	1.557	3.53e-03
KPTN_MOUSE	*kptn*	TRINITY_DN13936_c0_g2	-9.184	3.48e-03
LCE_ORYLA	*lce*	TRINITY_DN247_c0_g2	3.605	2.40e-02
LDLR_RAT	*ldlr*	TRINITY_DN1358_c0_g1	1.255	1.21e-03
LONF3_MACFA	*lonrf3*	TRINITY_DN7805_c1_g1	1.439	1.75e-02
HMR1_RAT	*mr1*	TRINITY_DN2732_c0_g1	-1.230	4.58e-02
MRC1_HUMAN	*mrc1*	TRINITY_DN13672_c10_g1	-8.045	2.50e-02
MYC_ONCMY	*myc*	TRINITY_DN1020_c1_g1	1.998	1.06e-02

NLRC3_MOUSE	*nlrc3*	TRINITY_DN72266_c0_g2	-1.248	5.59e-04
NAL12_MOUSE	*nlrp12*	TRINITY_DN18318_c0_g1	-1.676	7.39e-03
NLRP3_BOVIN	*nlrp3*	TRINITY_DN6613_c1_g1	9.069	4.73e-02
CRCM1_DANRE	*orai1*	TRINITY_DN80107_c0_g1	1.620	1.77e-04
PLMN_PONAB	*plg*	TRINITY_DN36602_c0_g2	3.109	2.96e-02
ARY1_CHICK	*pnat10*	TRINITY_DN1033_c0_g2	1.460	5.12e-04
PLPL2_BOVIN	*pnpla2*	TRINITY_DN6564_c0_g1	1.834	7.85e-03
PTPRH_MOUSE	*ptprh*	TRINITY_DN4212_c1_g1	-1.466	2.51e-02
RAB44_MOUSE	*rab44*	TRINITY_DN175_c1_g1	-1.202	3.26e-02
RPGF1_HUMAN	*rapgef1*	TRINITY_DN3319_c1_g1	-1.039	3.35e-03
SAR1B_MOUSE	*sar1b*	TRINITY_DN31848_c0_g1	1.045	2.41e-02
SHOT1_MOUSE	*shtn1*	TRINITY_DN36854_c0_g1	-1.254	3.87e-02
SLAF6_HUMAN	*slamf6*	TRINITY_DN2329_c0_g1	-1.623	2.93e-03
S2533_DANRE	*slc25a33*	TRINITY_DN517_c2_g2	1.092	2.40e-02
CTR3_RAT	*slc7a3*	TRINITY_DN24515_c0_g1	1.059	3.67e-02
SMR8A_DANRE	*smcr8a*	TRINITY_DN9595_c0_g2	-2.936	2.78e-03
SOAT1_CHLAE	*soat1*	TRINITY_DN160721_c0_g1	3.300	2.78e-03
SSH2_HUMAN	*ssh2*	TRINITY_DN1006_c0_g1	1.520	1.63e-02
STAB2_HUMAN	*stab2*	TRINITY_DN1108_c1_g1	-1.555	1.63e-02
TFCP2_CHICK	*tfcp2*	TRINITY_DN42690_c1_g1	-1.620	2.11e-02
TIFA_RAT	*tifa*	TRINITY_DN6255_c0_g2	1.397	3.67e-02
TNAP3_MOUSE	*tnfaip3*	TRINITY_DN9172_c3_g2	1.356	3.67e-02
TOP2B_CRILO	*top2b*	TRINITY_DN117255_c0_g1	-8.400	1.51e-02
T53I2_RAT	*tp53inp2*	TRINITY_DN2594_c0_g1	1.016	8.50e-03
T22D3_PIG	*tsc22d3*	TRINITY_DN2492_c0_g1	1.363	3.02e-02
UB2R2_HUMAN	*ube2r2*	TRINITY_DN42992_c0_g1	1.019	9.58e-03
ULK2_HUMAN	*ulk2*	TRINITY_DN9944_c0_g1	1.380	1.12e-02

Table A1.3: Significantly enriched (Fisher's exact P and weight W test $p < 0.05$) gene ontologies identified in species-specific orthogroups of four darter species: rainbow darter (*Etheostoma caeruleum*), fantail darter (*E. flabellare*), johnny darter (*E. nigrum*), and greenside darter (*E. blennioides*) based on 707, 1005, 657, 824 species-specific genes and 19,427, 20,376, 19,912, 21,454 background genes respectively.

Species	GO Category	GO ID	Term	p-value
Rainbow Darter (*Etheostoma caeruleum*)				
	CC	GO:0043005	neuron projection	9.84e-11
	BP	GO:0050789	regulation of biological process	1.11e-05
	BP	GO:0034330	cell junction organization	3.95e-05
	BP	GO:0007275	multicellular organism development	6.73e-05
	MF	GO:0005515	protein binding	9.30e-05
	CC	GO:0005911	cell-cell junction	2.32e-03
	MF	GO:0015267	channel activity	3.91e-03
	CC	GO:0034702	monoatomic ion channel complex	9.96e-03
	MF	GO:0046030	inositol trisphosphate phosphatase activity	2.78e-02
	BP	GO:0098609	cell-cell adhesion	4.67e-02
Fantail Darter (*Etheostoma flabellare*)				
	CC	GO:0071944	cell periphery	1.71e-13
	BP	GO:0006810	transport	1.73e-12
	BP	GO:0007275	multicellular organism development	3.80e-10
	MF	GO:0022857	transmembrane transporter activity	1.56e-08
	BP	GO:0003012	muscle system process	1.69e-04
	MF	GO:0005515	protein binding	5.32e-04
	CC	GO:0042995	cell projection	7.01e-04
	CC	GO:0012505	endomembrane system	1.35e-03

	BP	GO:0034330	cell junction organization	1.37e-03
	BP	GO:0141124	intracellular signalling cassette	6.03e-03
Johnny Darter (*Etheostoma nigrum*)				
	CC	GO:0005737	cytoplasm	8.07e-05
	BP	GO:0051179	localization	5.84e-04
	CC	GO:1903561	extracellular vesicle	1.88e-03
	BP	GO:0006996	organelle organization	1.92e-03
	CC	GO:0016020	membrane	2.32e-03
	MF	GO:0005515	protein binding	2.69e-03
Greenside Darter (*Etheostoma blennioides*)				
	CC	GO:0071944	cell periphery	5.74e-18
	BP	GO:0007275	multicellular organism development	4.56e-14
	MF	GO:0005515	protein binding	1.15e-11
	CC	GO:0043005	neuron projection	1.96e-10
	BP	GO:0007155	cell adhesion	2.97e-05
	CC	GO:0005737	cytoplasm	3.65e-05
	CC	GO:0030027	lamellipodium	7.31e-04
	CC	GO:0012505	endomembrane system	2.23e-03
	BP	GO:0097435	supramolecular fiber organization	2.53e-03
	MF	GO:0005201	extracellular matrix structural constituent	6.49e-03
	BP	GO:1902414	protein localization to cell junction	2.08e-02
	CC	GO:0098588	bounding membrane of organelle	2.40e-02
	BP	GO:0006810	transport	2.78e-02
	MF	GO:0015276	ligand-gated monoatomic ion channel activity	3.69e-02
	BP	GO:0030198	extracellular matrix organization	4.05e-02
	BP	GO:0006915	apoptotic process	4.05e-02

Table A1.4: Significantly enriched (FDR < 0.05) gene ontologies within the biological process category identified in differentially expressed genes from rainbow darter (*Etheostoma caeruleum*), fantail darter (*E. flabellare*), johnny darter (*E. nigrum*), and greenside darter (*E. blennioides*) exposed to WWTP effluent, based on 47,944, 58,452, 57, 292, and 62,204 background unigenes and 36, 239, 50, 68 differentially expressed genes respectively.

Species	GO Term Name	GO ID	FDR	Gene Count
Rainbow Darter (*Etheostoma caeruleum*)				
	Plasma lipoprotein particle organization	GO:0071827	4.79e-06	5
	Protein-lipid complex subunit organization	GO:0071825	4.06e-06	5
	Regulation of plasma lipoprotein particle levels	GO:0097006	1.85e-05	5
	Regulation of plasma lipoprotein remodelling	GO:0034369	5.00e-06	5
	Positive regulation of interleukin-1 beta production	GO:0032731	9.81e-05	4
	Plasma lipoprotein remodelling	GO:0034369	1.07e-05	4
	Protein-containing complex remodelling	GO:0034367	1.07e-05	4
	Cholesterol efflux	GO:0033344	8.23e-04	3
	Glucose 6-phosphate metabolic process	GO:0051156	8.47e-04	3
	Phospholipid efflux	GO:0033700	7.5e-04	3
	Chylomicron remodelling	GO:0034371	3.662e-04	3
	Very-low-density lipoprotein particle remodelling	GO:0034372	3.662e-04	3
	High-density lipoprotein particle assembly	GO:0034380	1.18e-04	3
	Positive regulation of phospholipid efflux	GO:1902995	8.60e-04	2
	Regulation of phospholipid efflux	GO:1902994	8.60e-04	2
Fantail Darter (*Etheostoma flabellare*)				
	Catabolic process	GO:0009056	1.75e-08	75
	Immune system process	GO:0002376	1.63e-07	71
	Gene expression	GO:0010467	2.66e-07	70
	Small molecule metabolic process	GO:0044281	1.50e-08	66
	Cellular catabolic process	GO:0044248	3.71e-08	66
	Organic substance catabolic process	GO:1901575	3.71e-08	66
	Establishment of localization in cell	GO:0051649	1.69e-06	54
	Interspecies interaction between organisms	GO:0044419	1.13e-07	53
	Organonitrogen compound biosynthetic process	GO:1901566	4.76e-08	53

	Cellular nitrogen compound biosynthetic process	GO:0044271	9.16e-07	45
	Immune response	GO:0006955	1.15e-07	
	Organonitrogen compound catabolic process	GO:1901565	2.35e-08	45
	Macromolecule catabolic process	GO:0009057	2.09e-08	39
	Positive regulation of immune system process	GO:0002684	1.69e-06	37
	protein catabolic process	GO:0030163	3.45e-08	36
	Cellular protein catabolic process	GO:0044257	1.79e-06	29
	amide metabolic process	GO:0043603	5.32e-07	29
	Proteolysis involved in cellular protein catabolic process	GO:0051603	4.55e-05	29
	Immune effector process	GO:0002252	1.37e-06	27
	mitochondrion organization	GO:0007005	1.89e-06	26
Johnny Darter (*Etheostoma nigrum*)				
	Small molecule metabolic process	GO:0044281	3.74e-03	14
	Ion transport	GO:0006811	3.62e-03	13
	Transmembrane transport	GO:0055085	5.5e-03	13
	Cation transport	GO:0006812	4.48e-03	12
	Ion transmembrane transport	GO:0034220	4.16e-03	10
	Oxidation-reduction process	GO:0055114	9.1e-03	10
	Small molecule catabolic process	GO:0044282	4.70e-03	7
	Monovalent inorganic cation transport	GO:0015672	4.70e-03	7
	Organic acid catabolic process	GO:0044282	4.74e-03	6
	Electron transport chain	GO:0022900	4.34e-03	5
	Carboxylic acid transmembrane transport	GO:1905039	4.45e-03	5
	Alpha-amino acid catabolic process	GO:0009063	5.77e-03	4
	Oxidative phosphorylation	GO:0006119	9.1e-03	4
	Cellular amino acid catabolic process	GO:0009063	1.52e-02	4
	Aromatic amino acid family catabolic process	GO:0009074	4.13e-03	3
	Energy coupled proton transport, down electrochemical gradient	GO:0015988	4.74e-03	2
	Electron transport coupled proton transport	GO:0015990	4.74e-03	2
Greenside Darter (*Etheostoma blennioides*)				
	Regulation of immune system process	GO:0002682	6.73e-03	16

Interspecies interaction between organisms	GO:0044419	2.06e-02	16
Regulation of response to stress	GO:0080134	1.76e-02	14
Regulation of immune response	GO:0050776	3.78e-02	12
Negative regulation of intracellular signal transduction	GO:1902532	2.75e-02	10
Negative regulation of phosphorylation	GO:0042326	2.83e-02	10
Negative regulation of phosphate metabolic process	GO:0019220	4.115e-02	6
Negative regulation of protein phosphorylation	GO:0001933	4.115e-02	6
Negative regulation of immune system process	GO:0002683	4.129e-02	6
Negative regulation of inflammatory response	GO:0050728	2.453e-02	6
Lipid homeostasis	GO:0055088	2.925e-02	6
Negative regulation of interleukin-1 production	GO:0032692	6.34e-03	4
Negative regulation of NF-kappaB transcription factor activity	GO:0032088	2.925e-02	4
Regulation of interleukin-1 beta production	GO:0032691	3.16e-02	3
Negative regulation of NIK/NF-kappaB signalling	GO:1901223	3.16e-02	3
Negative regulation of interleukin-1 beta production	GO:0032691	3.438e-02	2
Regulation of keratinocyte differentiation	GO:0045616	3.724e-02	2
Negative regulation of interleukin-6 production	GO:0032715	3.724e-02	2

Table A1.5: Network characteristics of differentially expressed genes in the live of rainbow (*Etheostoma caeruleum*), fantail (*E. flabellare*), johnny (*E. nigrum*), and greenside (*E. blennioides*) darters, exposed to WWTP effluent, based on STRING-derived protein-protein interaction (PPI) networks. Metrics include the number of nodes (transcripts) and edges (interactions), PPI enrichment p-value, average node degree (SD), local clustering coefficient, number of Markov Cluster Algorithm (MCL) clusters, and average betweenness centrality (SD). Values in parentheses under notes indicate the total number of differentially expressed genes used in the network construction.

Species	Nodes	Edges	p-value	Avg. Degree	Avg. local clustering coefficient	MCL clusters	Avg. Betweenness
Rainbow darter (*Etheostoma caeruleum*)	18 (33)	27	9.97e-08	3 (±2.37)	0.461	4	0.07 (±0.13)
Fantail darter (*Etheostoma flabellare*)	188 (224)	783	1.00e-16	8.5 (±8.2)	0.43	30	0.01 (±0.02)
Johnny darter (*Etheostoma nigrum*)	25 (45)	23	5.61e-04	2 (±1.1)	0.45	8	0.1 (±0.2)
Greenside darter (*Etheostoma blennioides*)	30 (64)	36	2.19e-02	2.26 (± 1.5)	0.255	9	0.09 (±0.13)

Table A1.6: Summary of hub and bottleneck transcripts identified in STRING-derived protein-protein interaction (PPI) networks for differentially expressed genes in the live of rainbow (*Etheostoma caeruleum*), fantail (*E. flabellare*), johnny (*E. nigrum*), and greenside (*E. blennioides*) darters, exposed to WWTP effluent. The degree cutoff used to define hub proteins is listed for each species, rounded to the neared whole number. Hubs represent highly connected proteins with degree in parentheses, while bottleneck proteins act as key intermediates with high betweenness centrality, potentially influencing multiple functional pathways.

Rainbow darter (*Etheostoma caeruleum*)		
	Cutoff	6.74 ≈ 7
	Hubs (degree)	*apoe (8)*
	Bottlenecks	*lpl, gck*
Fantail darter (*Etheostoma flabellare*)		
	Cutoff	24.75 ≈ 25
	Hubs	*hsp90aa1 (45), hsp90ab1 (43), hspa8 (40), atp5f1a (33), psmd14 (30), phb (26), eftud2 (25)*
	Bottlenecks	*canx, stat3, gpi, acly, idh1, ran, atp2a2, stat1, sqstm1, psmd11, c1qbp, sec13, ddx17, pdia6, cd63, tomm40, eif3b, hnrnpd, tomm22, uqcrfs1, u2af1, ndufa9, phb2, kdm6b, ilf2 fh, psmb2, xbp1, slc25a3, atp5pd*
Johnny darter (*Etheostoma nigrum*)		
	Cutoff	4.24 ≈ 4
	Hubs	*c3 (4), mt-co3 (4), mt-atp6 (4)*
	Bottlenecks	*il4i1*
Greenside darter (*Etheostoma blennioides*)		
	Cutoff	5.46 ≈ 5
	Hubs	*myc (6), crebbp (6), hspa8 (6)*
	Bottlenecks	*tnfaip3, nlrp3, cbfb*

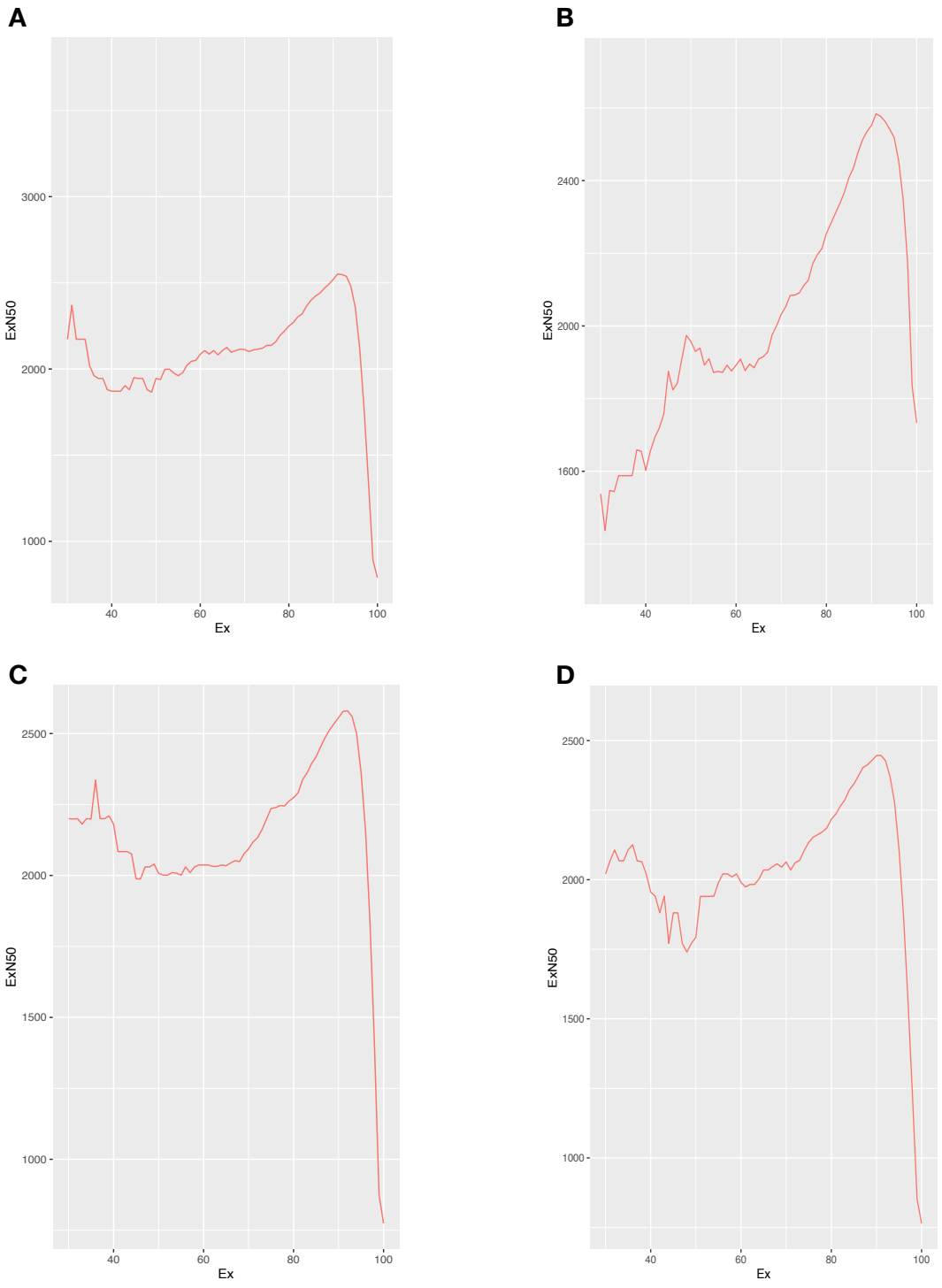


Figure A1.1: ExN50 plot illustrating the relationship between the N50 contig length and the percentage of total normalized expression (Ex) for the assembled hepatic transcriptomes of four darter species. Panels represent data for (A) rainbow darter, (B) fantail darter, (C) johnny darter, and (D) greenside darter. Higher ExN50 values indicate longer contigs among the most highly expressed transcripts, reflecting improved assembly quality and completeness.

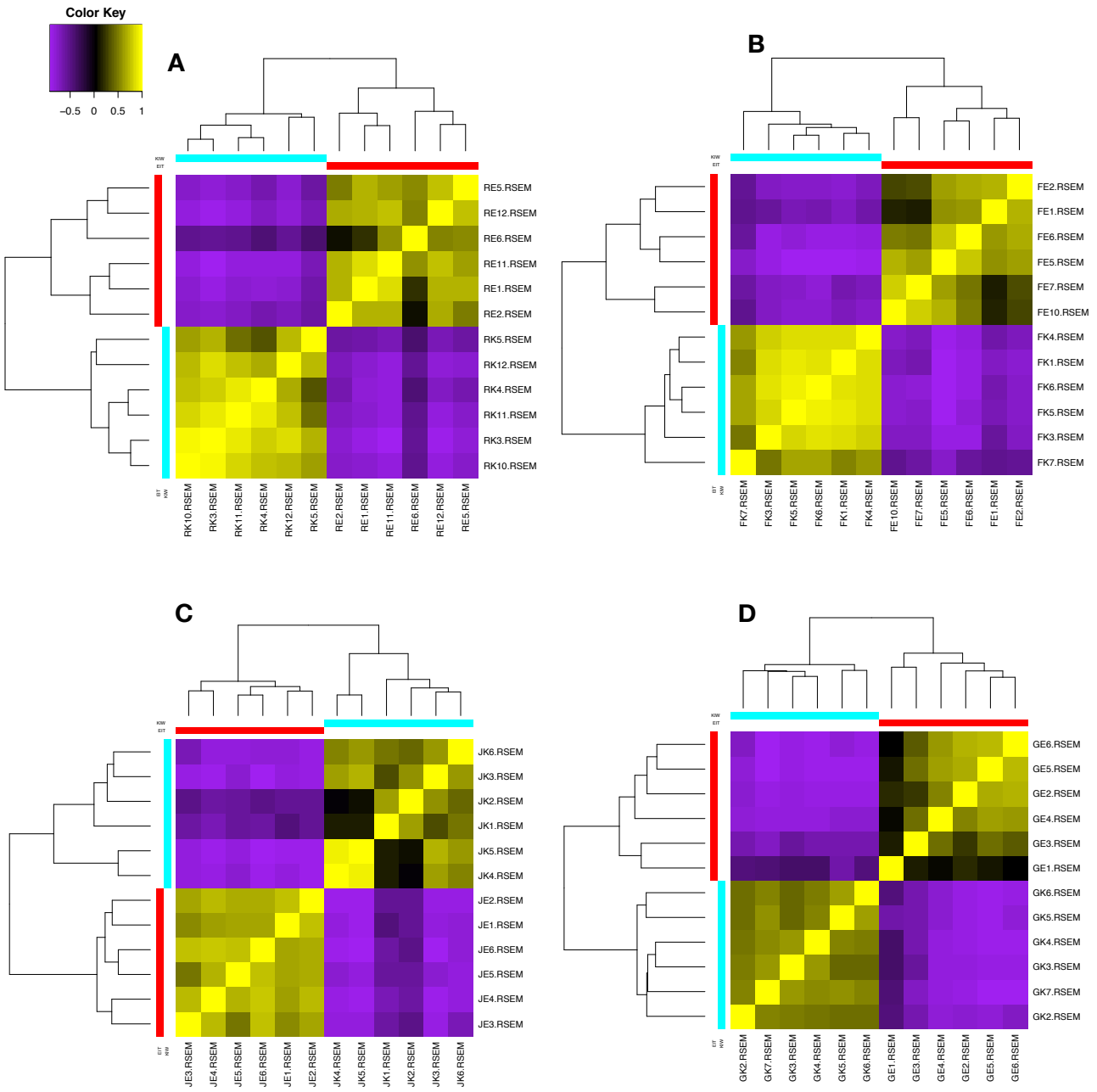


Figure A1.2: A correlation heat map matrix presented with pairwise correlations between each sample used for transcriptome assembly, based on the liver gene expression profiles for (A) rainbow darter (*Etheostoma caeruleum*), (B) fantail darter (*E. flabellare*), (C) johnny darter (*E. nigrum*), and (D) greenside darter (*E. blennioides*) exposed to WWTP effluent. Each cell in the matrix represents the correlation coefficient between the respective samples on the x-axis and y-axis. A correlation coefficient close to 1 (yellow) suggests a very strong positive correlation, meaning as the gene expression in one sample increases, the expression in the correlated sample also increases. A coefficient close to -1 indicates a strong negative correlation. A coefficient near 0 suggests no correlation. Each row and column is labeled with corresponding sample identifiers. The same colour scale applies to all panels.

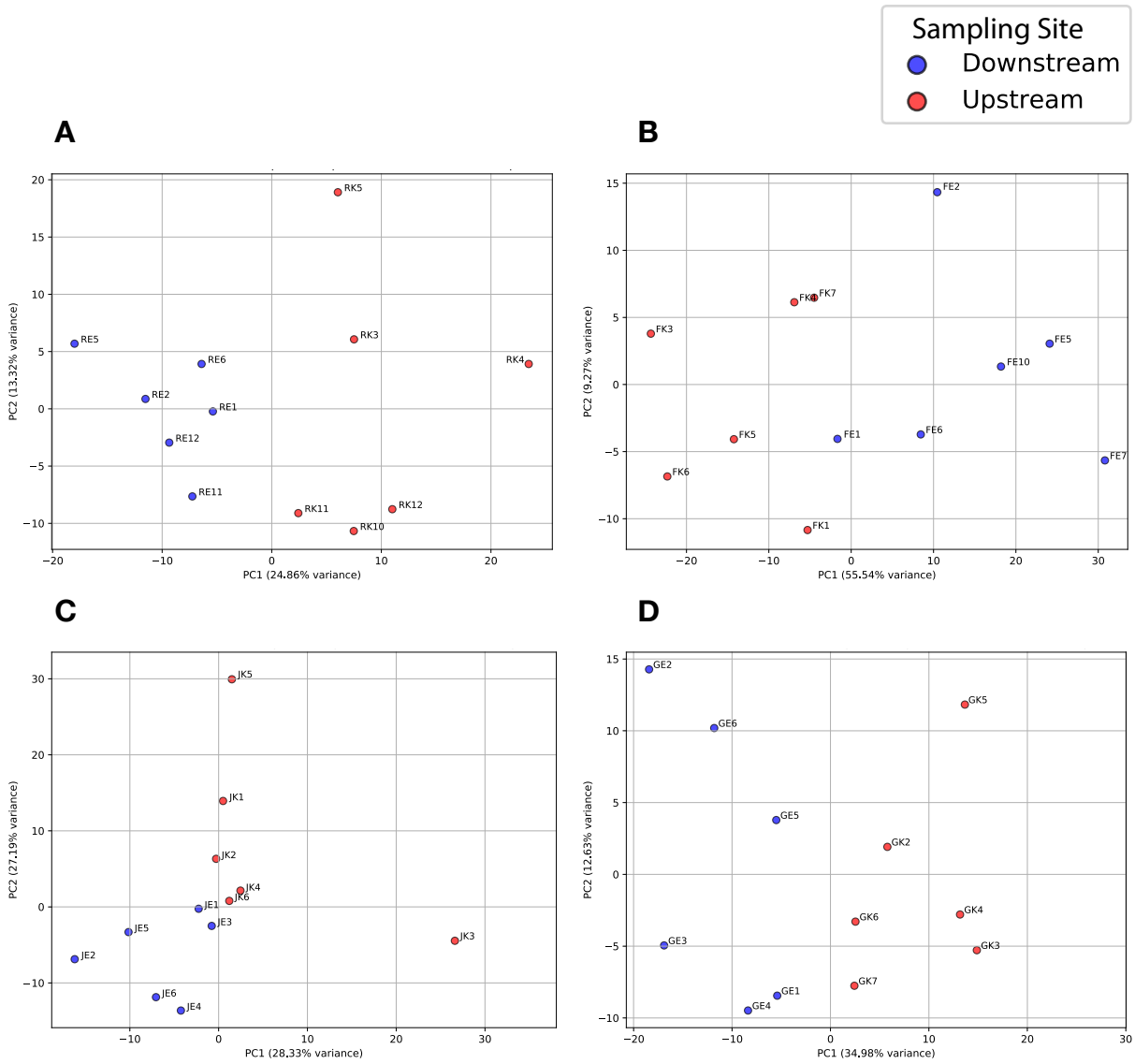
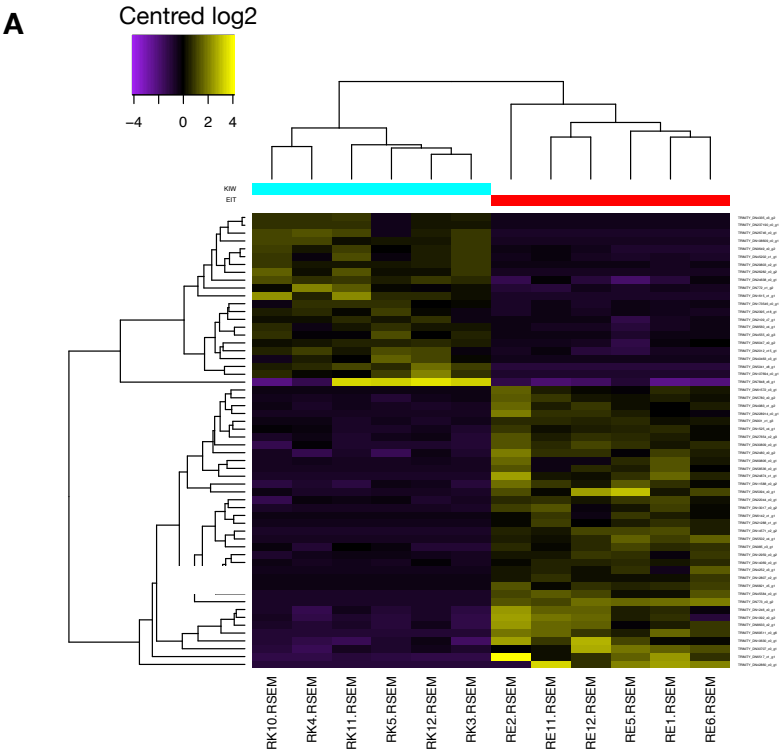
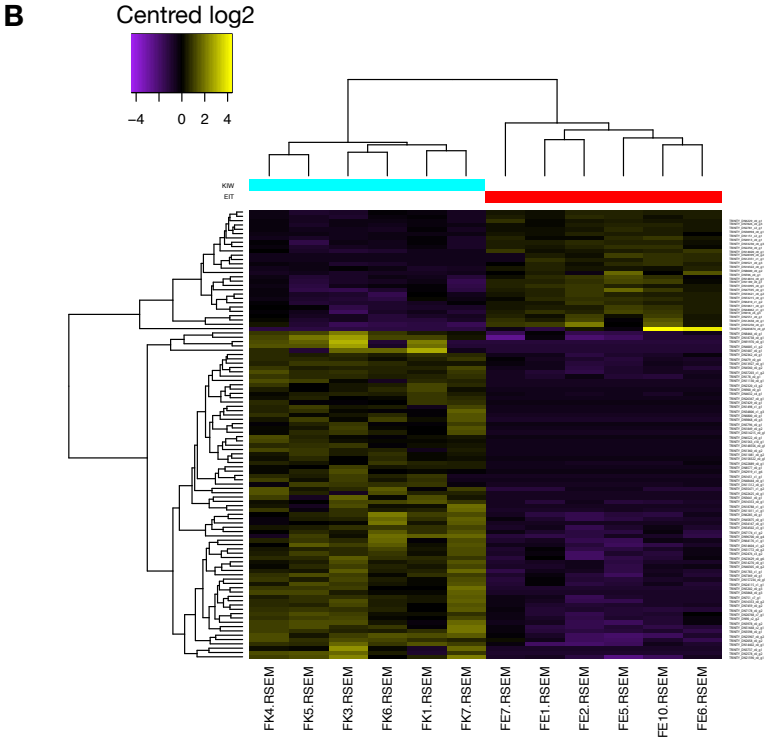
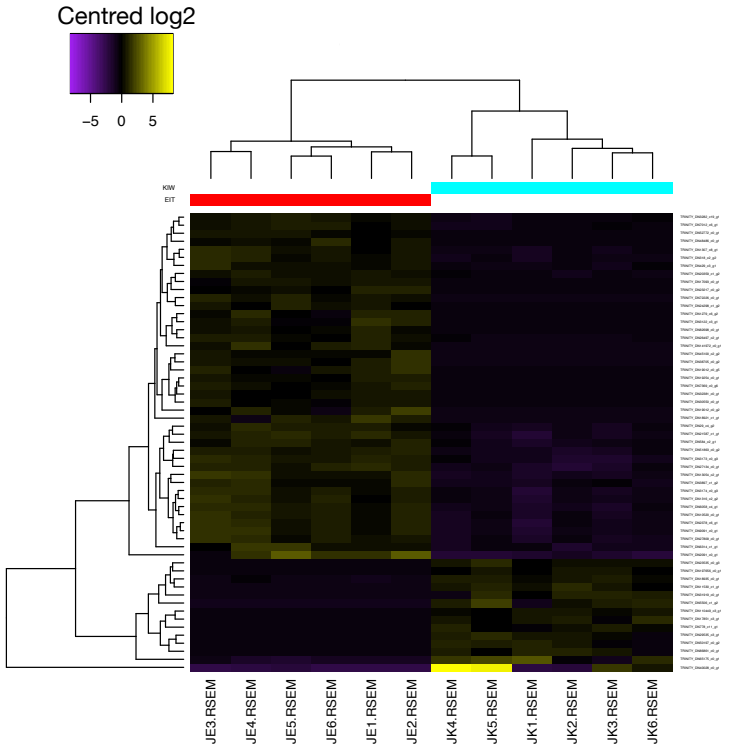


Figure A1.3: Principal component analysis (PCA) of the top 500 most variable transcripts in liver tissue from (A) rainbow darter (*Etheostoma caeruleum*), (B) fantail darter (*E. flabellare*), (C) johnny darter (*E. nigrum*), and (D) greenside darter (*E. blennioides*) from Upstream (red) and Downstream (blue) sampling sites. Each point represents a biological replicate. PCA was performed on $\log_2$-transformed transcript counts using the "PCA" function in the scikit-learn package in Python. The first two principal components (PC1, PC2) can explain more than (A) 38%,(B) 64%,(C) 55%, and (D) 47% of the variability among the samples.


A
Centred log2
−4
0
2
4
KIW
EIT
RK10.RSEM
RK4.RSEM
RK11.RSEM
RK5.RSEM
RK12.RSEM
RK3.RSEM
RE2.RSEM
RE11.RSEM
RE12.RSEM
RE5.RSEM
RE1.RSEM
RE6.RSEM


B
Centred log2
−4
0
2
4
KIW
EIT
FK4.RSEM
FK5.RSEM
FK3.RSEM
FK6.RSEM
FK1.RSEM
FK7.RSEM
FE7.RSEM
FE1.RSEM
FE2.RSEM
FE5.RSEM
FE10.RSEM
FE6.RSEM

C


Centred log2
−5 0 5
KIW
EIT
JE3.RSEM
JE4.RSEM
JE5.RSEM
JE6.RSEM
JE1.RSEM
JE2.RSEM
JK4.RSEM
JK5.RSEM
JK1.RSEM
JK2.RSEM
JK3.RSEM
JK6.RSEM

D

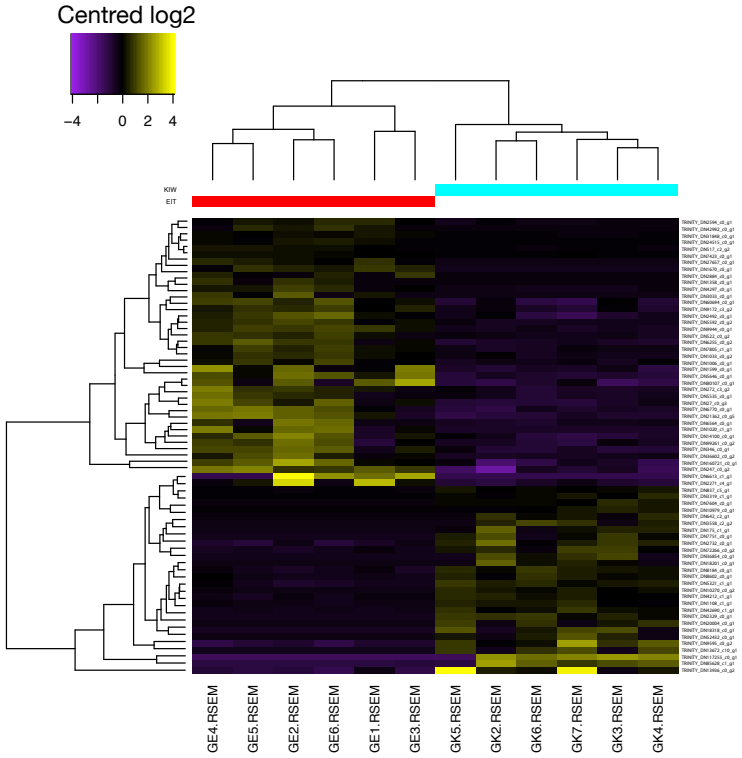

Centred log2
−4 0 2 4
KIW
EIT
GE4.RSEM
GE5.RSEM
GE2.RSEM
GE6.RSEM
GE1.RSEM
GE3.RSEM
GK5.RSEM
GK2.RSEM
GK6.RSEM
GK7.RSEM
GK3.RSEM
GK4.RSEM

Figure A1.3: Heat maps showing expression levels of differentially expressed transcripts in four darter species exposed to WWTP effluent: (A) 36 transcripts in rainbow darter, (B) the 105 most significant of 292 differentially expressed transcripts in fantail darter, (C) 50 transcripts in johnny darter, and (D) 68 transcripts in greenside darter (log2FC<-1, > 1; FDR < 0.05, n = 6). Expression values represent log2-transformed, median-centered FPKM. Yellow and purple intensities indicate transcript upregulation and downregulation, respectively. Dendrogram clustering on the X-axis reflects sample similarity, while clustering on the Y-axis groups transcripts with similar expression patterns.

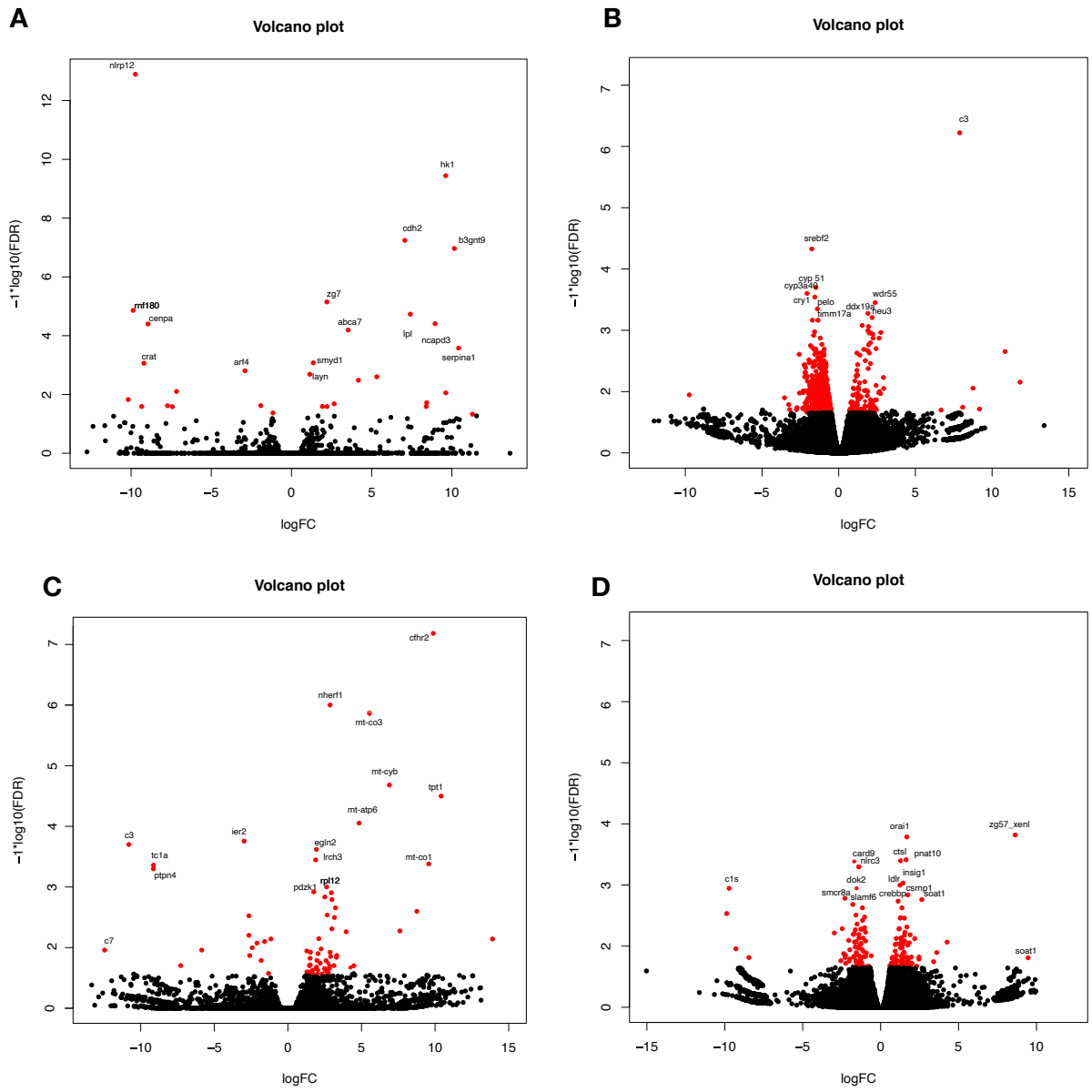


Figure A1.4: Volcano plots displaying differentially expressed transcripts identified in the liver of four darter species exposed to WWTP effluent. Each plot represents annotated differentially expressed transcripts detected in (A) rainbow darter, (B) fantail darter, (C) johnny darter, and (D) greenside darter. The x-axis represents log2 fold change (log2FC), while the y-axis represents the $-\log_{10}$(FDR), highlighting statistical significance. Red points indicate significantly differentially expressed transcripts (log2FC <-1, > 1, FDR < 0.05). Labeled points correspond to the 15 most significantly differentially expressed transcripts.

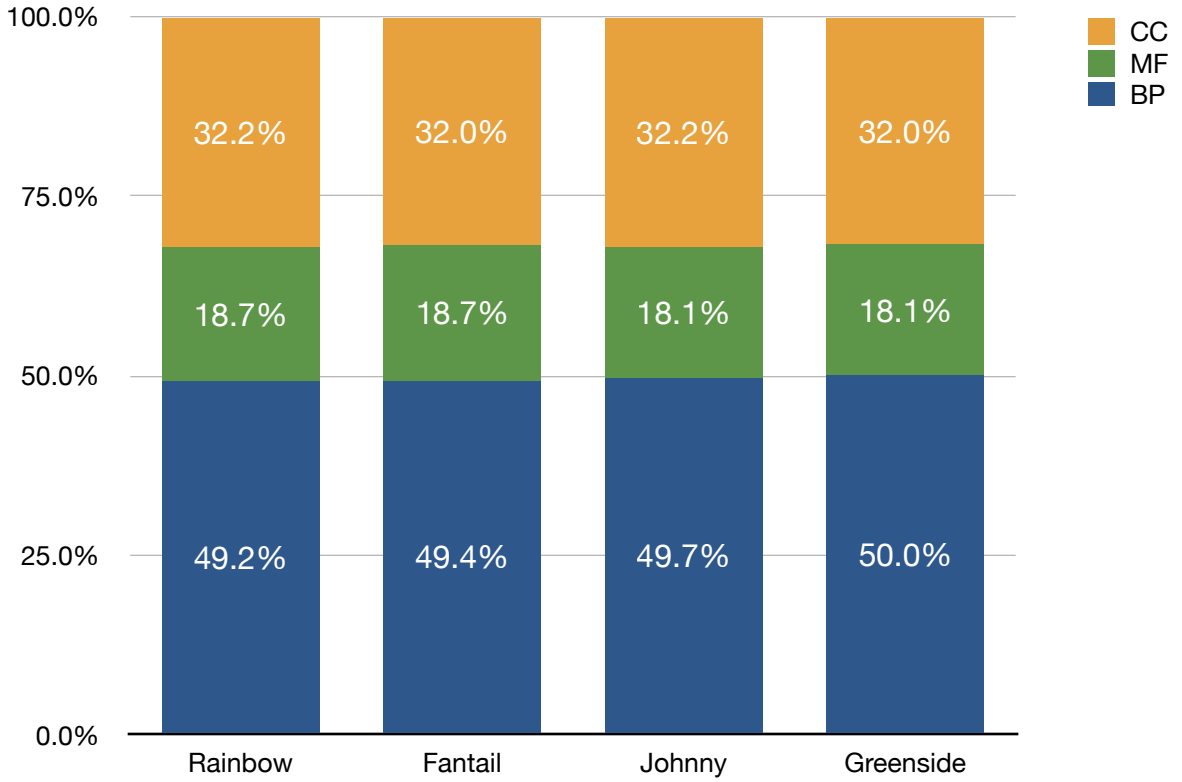


Figure A1.5: Distribution of gene ontology terms assigned to unigenes from each of the four darter liver transcriptomes (rainbow, fantail, johnny, and greenside darter), represented as a percentage distribution of the top-level ontology terms; Biological Process (BP; blue), Molecular Function (MF; green), and Cellular Component (CC; yellow), relative the the total number of GO terms assigned to unigenes in that transcriptome.

Appendix B

Table A2.1: Summary of RNA sequencing quality metrics for liver samples collected from rainbow darter (*Etheostoma caeruleum*) exposed to each enantiomer of venlafaxine (VEN). Metrics include RNA Integrity Number (RIN), total raw paired-end reads, filtered reads post-quality control, percentage of preserved reads post-trimming, and overall alignment rate to the assembled transcriptome. Sample identifiers beginning with C, R, and S correspond to Control, R-VEN, and S-VEN treatments, respectively. Identifiers also indicate exposure duration (Day 14) and the tank from which each fish was collected (A, B, or C).

Sample	RIN	Raw Reads	Filtered Reads	Preserved reads (%)	Overall Alignment (%)
C14A5	9.6	75654376	73200855	96.76	89.76%
C14A6	9.4	51044270	48897076	95.79	89.74%
C14B2	9.6	70093986	67156376	95.81	89.34%
C14B5	9.4	51150471	49332610	96.45	89.24%
C14C1	10	70333063	67929500	96.58	90.39%
C14C2	10	61735693	59658960	96.64	89.46%
R14A2	10	64199328	61864980	96.36	89.58%
R14A5	10	60727552	58479019	96.30	89.73%
R14B3	10	69306855	66713512	96.26	90.22%
R14B6	10	59772090	57473360	96.15	90.06%
R14C5	8.5	61593621	59517072	96.63	89.84%
R14C6	10	72020290	69457742	96.44	89.96%
S14A4	9.5	59493583	57118806	96.01	89.22%
S14A6	10	58575173	56774916	96.93	90.07%
S14B2	7.4	55107635	53111530	96.38	89.42%
S14B4	8.6	59284664	57089029	96.30	89.78%
S14C3	6.2	55282011	53598444	96.95	90.09%
S14C4	8.1	59389346	57229616	96.36	90.10%

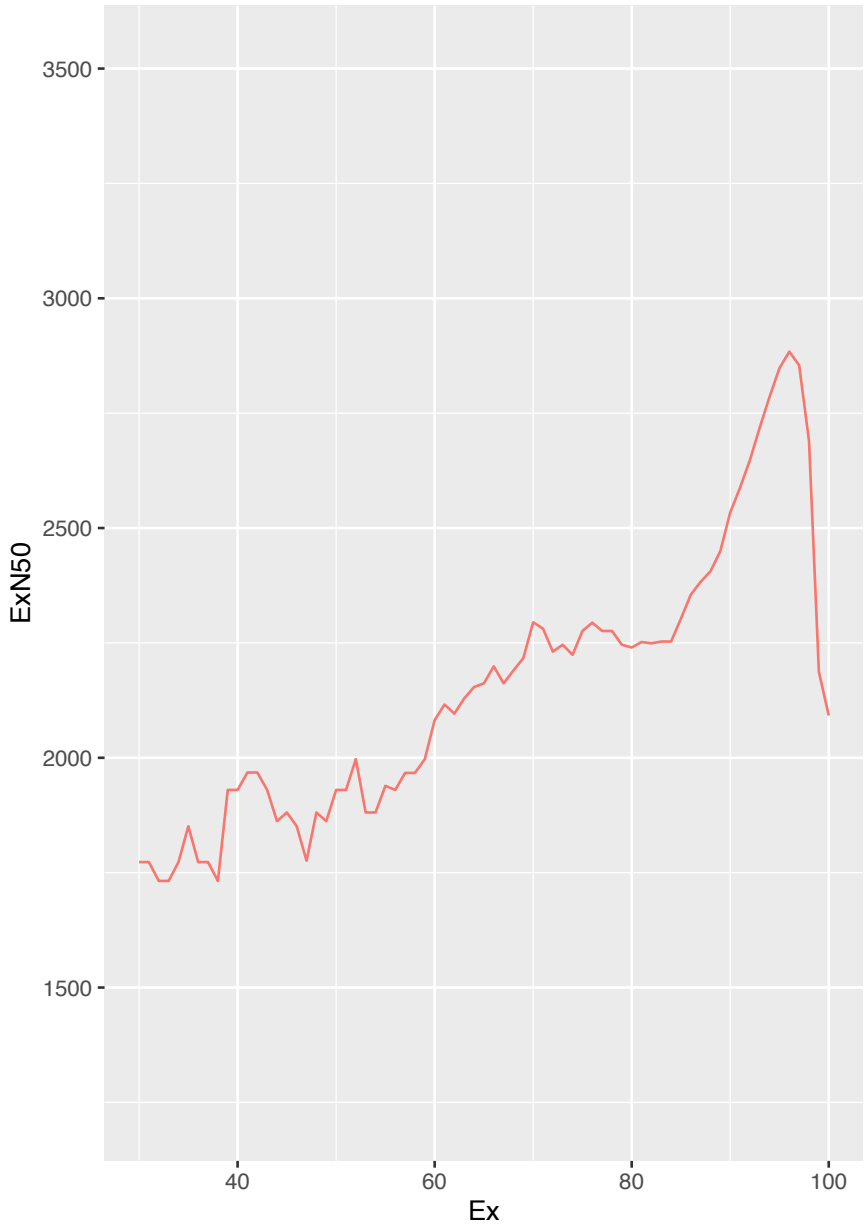


Figure A2.1: ExN50 plot showing the relationship between N50 contig length and the percentage of total normalized expression (Ex) in the assembled transcriptomes of rainbow darter liver following fourteen day venlafaxine exposure. Higher ExN50 values indicate longer contigs among the most highly expressed transcripts, reflecting improved assembly quality and completeness.

Table A2.2: Annotated differentially expressed genes (DEGs) in rainbow darter (*Etheostoma caeruleum*) following R- and S-venlafaxine exposure. List of significantly differentially expressed genes (log2FC < -1 or >1; FDR < 0.05) in rainbow darters exposed to R- and S-venlafaxine (R-VEN, S-VEN) for 14 days, including DEGs identified between treatments. Genes are ordered by log2FC.

Treatment	UniProt ID	Gene Symbol	Trinity gene ID	log2FC	FDR
R-VEN					
	GABR2_HUMAN	*gabbr2*	TRINITY_DN2417_c0_g2	10.63	2.82e-02
	LADD_ONCMY	*ll*	TRINITY_DN7029_c0_g1	10.33	1.16e-02
	APLP2_RAT	*aplp2*	TRINITY_DN12811_c1_g1	10.25	2.91e-02
	MRC2_RAT	*mrc2*	TRINITY_DN3512_c0_g11	10.11	7.49e-05
	LECG_THANI	*galig*	TRINITY_DN3512_c0_g1	10.14	2.37e-04
	DAAM1_HUMAN	*daam1*	TRINITY_DN7364_c0_g1	9.53	1.35e-03
	CHP1_BOVIN	*chp1*	TRINITY_DN61178_c0_g1	9.09	1.80e-03
	FRPD1_HUMAN	*frmpd1*	TRINITY_DN3262_c0_g1	8.91	2.66e-03
	M3K2_MOUSE	*map3k2*	TRINITY_DN11064_c0_g1	8.76	3.54e-03
	INR1L_CARAU	*ifngr1*	TRINITY_DN2069_c0_g2	2.18	3.90e-02
	ATTY_RAT	*tat*	TRINITY_DN185_c20_g1	-1.59	1.87e-02
	NUP98_MOUSE	*nup98*	TRINITY_DN4621_c2_g2	-1.60	3.82e-02
	RN166_RAT	*rnf166*	TRINITY_DN809_c5_g2	-1.60	1.87e-02
	SC23A_HUMAN	*sec23a*	TRINITY_DN6234_c1_g1	-3.27	1.64e-02
	AATC_CHICK	*got1*	TRINITY_DN1845_c0_g1	-5.99	4.63e-03
	SPA2L_HUMAN	*spata2l*	TRINITY_DN638_c0_g1	-8.16	4.50e-02
	NR1H4_BOVIN	*nr1h4*	TRINITY_DN2_c2_g1	-8.37	2.52e-02
	A0A8M3AVQ1_DANRE	*kalrna*	TRINITY_DN1402_c4_g2	-8.48	7.02e-08
	PACN3_MOUSE	*pacsin3*	TRINITY_DN2181_c1_g1	-8.54	3.35e-02
	KCMB2_HUMAN	*kcnmb2*	TRINITY_DN16301_c0_g1	-8.56	3.06e-02
	FOXN3_XENTR	*foxn3*	TRINITY_DN1181_c1_g1	-9.99	9.16e-05
	BRD1_MOUSE	*brd1*	TRINITY_DN1114_c0_g1	-9.99	8.80e-03

	HYKK_DANRE	*hykk*	TRINITY_DN8821_c0_g1	-10.55	1.35e-03
	ARL1_BOVIN	*arl1*	TRINITY_DN1299_c2_g1	-10.96	3.06e-02
	STAT1_HUMAN	*stat1*	TRINITY_DN2694_c0_g1	-11.31	8.90e-03
	SIA4B_RAT	*st3gal2*	TRINITY_DN103_c2_g1	-12.70	3.35e-02
S-VEN					
	ZN608_MOUSE	*znf608*	TRINITY_DN118_c0_g1	14.10	6.66e-07
	ARHGP_MOUSE	*arhgef25*	TRINITY_DN8463_c0_g1	12.67	4.77e-02
	CBR1_MOUSE	*cbr1*	TRINITY_DN2446_c0_g3	11.86	4.04e-04
	GABR2_HUMAN	*gabbr2*	TRINITY_DN2417_c0_g2	10.46	2.48e-03
	SYAM_RAT	*aars2*	TRINITY_DN118_c1_g2	10.29	2.89e-02
	NENF_BOVIN	*nenf*	TRINITY_DN4570_c0_g1	9.67	4.84e-04
	H2LAI8_ORYLA	*sh3pxd2a*	TRINITY_DN1911_c0_g1	9.47	4.04e-04
	SWP70_BOVIN	*swap70*	TRINITY_DN418_c13_g1	8.91	2.75e-04
	CHD6_MOUSE	*chd6*	TRINITY_DN1386_c1_g1	8.81	4.95e-03
	MAGI2_RAT	*magi2*	TRINITY_DN5537_c0_g1	8.57	6.50e-04
	THOP1_MOUSE	*thop1*	TRINITY_DN1784_c0_g4	8.55	3.15e-03
	K1C9_MOUSE	*krt9*	TRINITY_DN12710_c0_g2	6.52	2.03e-03
	SESD1_DANRE	*sestd1*	TRINITY_DN900_c1_g1	5.20	4.04e-04
	ZN271_MOUSE	*zn271*	TRINITY_DN4357_c3_g1	5.79	4.62e-04
	LADD_ONCMY	*ll*	TRINITY_DN2914_c0_g1	2.70	7.15e-04
	CADH2_DANRE	*cdh2*	TRINITY_DN856_c0_g2	1.16	1.22e-03
	XYLB_BOVIN	*xylb*	TRINITY_DN1022_c1_g1	-2.76	2.48e-03
	CO6A2_CHICK	*col6a2*	TRINITY_DN4413_c0_g1	-5.41	4.50e-02
	WDR73_DANRE	*wdr73*	TRINITY_DN2776_c0_g2	-5.84	3.38e-04
	PITM2_HUMAN	*pitpnm2*	TRINITY_DN6492_c0_g1	-8.34	5.38e-03
	LRC3B_DANRE	*lrrc3b*	TRINITY_DN5439_c0_g2	-9.02	9.34e-03
	CENPA_CHICK	*cenpa*	TRINITY_DN5538_c0_g1	-10.03	1.34e-04
	E41L5_BOVIN	*epb41l5*	TRINITY_DN865_c2_g1	-10.29	4.04e-04

	KMT2C_MOUSE	*kmt2c*	TRINITY_DN310_c0_g1	-10.69	4.77e-02
	KMT2D_HUMAN	*kmt2d*	TRINITY_DN751_c4_g1	-12.44	1.01e-03
RlS-VEN					
	ZN608_MOUSE	*znf608*	TRINITY_DN118_c0_g1	-13.54	7.30e-06
	SIA4C_PANTR	*st3gal4*	TRINITY_DN876_c0_g1	-11.38	3.95e-03
	SYAM_RAT	*aars2*	TRINITY_DN118_c0_g2	-10.32	2.00e-02
	FOXN3_XENTR	*foxn3*	TRINITY_DN1181_c1_g1	-9.85	1.28e-04
	RAB1B_RAT	*rab1b*	TRINITY_DN2484_c0_g1	-9.43	1.59e-03
	PACN3_MOUSE	*pacsin3*	TRINITY_DN2181_c1_g1	-9.16	7.12e-04
	CLC10_HUMAN	*clec10a*	TRINITY_DN2078_c0_g1	-8.87	1.28e-04
	DEN1C_MOUSE	*dennd1c*	TRINITY_DN8535_c1_g1	-8.84	7.91e-03
	ZN384_RAT	*znf384*	TRINITY_DN10218_c0_g1	-8.64	1.92e-03
	STAR9_HUMAN	*stard9*	TRINITY_DN6002_c0_g1	-8.52	9.12e-03
	ARRD3_BOVIN	*arrdc3*	TRINITY_DN9601_c0_g1	-8.40	3.08e-03
	A0A0B4J1A8_DANRE	*ubash3bb*	TRINITY_DN1636_c0_g2	-7.54	1.94e-03
	PGRC1_BOVIN	*pgrmc1*	TRINITY_DN3562_c0_g1	-6.55	3.66e-02
	MDHC_CHICK	*mdh2*	TRINITY_DN19817_c1_g1	-6.25	2.46e-04
	IOD3_PIG	*dio3*	TRINITY_DN821_c11_g1	-4.68	3.95e-03
	GHR_CANLF	*ghr*	TRINITY_DN1006_c0_g1	-1.28	4.03e-02
	NR5A2_CHICK	*nr5a2*	TRINITY_DN634_c2_g1	1.01	4.08e-02
	MOCS1_MOUSE	*mocs1*	TRINITY_DN4064_c0_g1	1.26	3.00e-02
	INR1L_CARAU	*ifngr1*	TRINITY_DN2069_c0_g2	2.65	1.92e-03
	FBN1_BOVIN	*fbn1*	TRINITY_DN206_c0_g1	3.89	4.08e-02
	ATL3_HUMAN	*adamtsl3*	TRINITY_DN5490_c1_g1	8.35	3.95e-03
	HMBX1_HUMAN	*hmbox1*	TRINITY_DN979_c0_g1	8.63	5.10e-03
	GBGT1_CHICK	*gbgt1*	TRINITY_DN7641_c0_g1	8.72	2.46e-04
	DNS2A_PIG	*dnase2*	TRINITY_DN21009_c0_g2	9.65	2.42e-03
	VP13B_HUMAN	*vps13b*	TRINITY_DN1796_c0_g2	10.21	3.06e-03

DUS16_HUMAN	*dusp16*	TRINITY_DN433_c0_g1	10.27	2.59e-02
TSN8_MOUSE	*tspan8*	TRINITY_DN16816_c1_g1	10.29	1.56e-03
SRXN1_MOUSE	*srxn1*	TRINITY_DN969_c1_g1	10.45	3.80e-05
NAL12_MOUSE	*nlrp12*	TRINITY_DN2165_c0_g2	10.53	2.34e-02
PLAK_BOVIN	*jup*	TRINITY_DN3442_c0_g1	10.54	3.95e-03
FBX7_RAT	*fbxo7*	TRINITY_DN7312_c2_g1	10.94	2.61e-03
AIFM3_HUMAN	*aifm3*	TRINITY_DN1685_c0_g2	11.70	9.36e-04
S35B1_DANRE	*slc35b1*	TRINITY_DN5693_c0_g2	12.78	5.16e-04

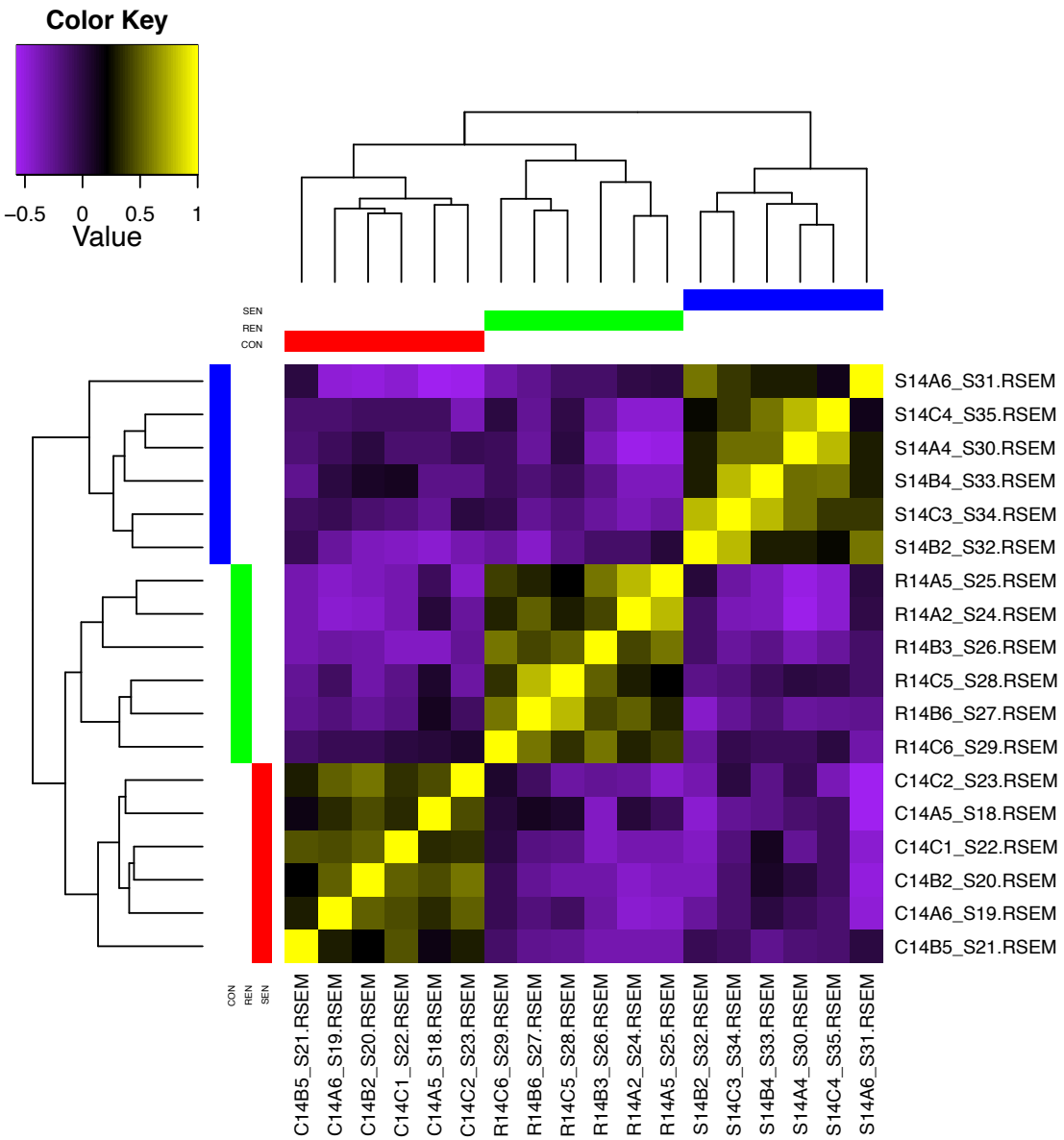


Figure A2.2: A clustered Pearson correlation heat map matrix presented with pairwise correlations between each sample used for transcriptome assembly, based on the liver gene expression profiles for rainbow darter (*Etheostoma caeruleum*) exposed to R-venlafaxine(REN) and S-venlafaxine (SEN). Each cell in the matrix represents the correlation coefficient between the respective samples on the x-axis and y-axis. A correlation coefficient close to 1 (yellow) suggests a very strong positive correlation. A coefficient close to -1 indicates a strong negative correlation. A coefficient near 0 suggests no correlation.

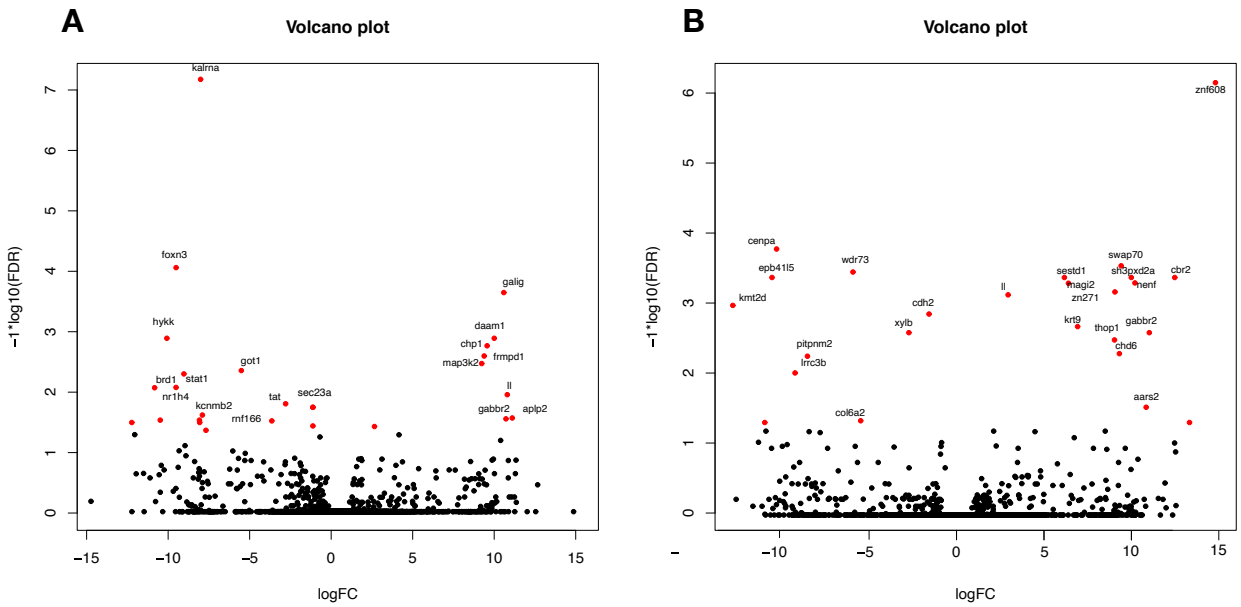


Figure A2.3: Volcano plots displaying differentially expressed transcripts in the liver of rainbow darter following a 14-day exposure to each enantiomer of venlafaxine. Each plot represents annotated differentially expressed transcripts detected in response to (A) R-venlafaxine and (B) S-venlafaxine. The x-axis represents log fold change (log2FC), while the y-axis represents $-\log_{10}$(FDR), indicating statistical significance. Red points denote significantly differentially expressed transcripts ($\text{log2FC} > 1, \text{FDR} < 0.05$). Labeled points correspond to the 15 most significant differentially expressed transcripts.

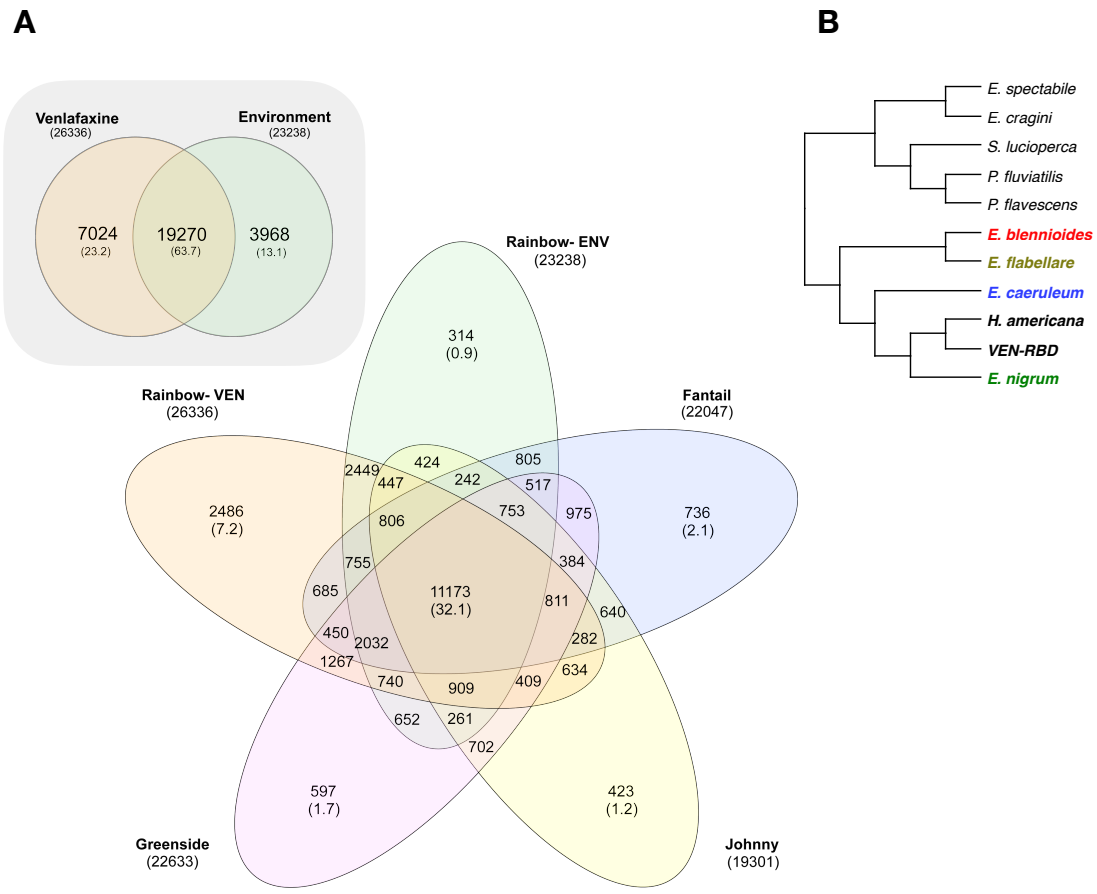


Figure A2.4: (A) Venn diagrams showing shared and unique orthogroups identified in rainbow darter exposed to venlafaxine (Rainbow-VEN), rainbow darter (Rainbow-ENV), fantail darter, greenside darter, and johnny darter based on OrthoFinder analysis before presumed parasite transcript removal. Numbers represent the count of orthogroups unique to or shared among species, with percentages indicating their relative proportion. The upper left Venn diagram compares orthogroups between venlafaxine-exposed and effluent exposed rainbow darters. (B) Phylogenetic tree of Percidae species based on OrthoFinder results. VEN-RBD represents the transcriptome of rainbow darters exposed to venlafaxine, while other species include sequenced proteomes from NCBI. Darter species are color-coded (*Etheostoma caeruleum* in blue, *E. flabellare* in yellow, *E. blennioides* in red, and *E. nigrum* in green) to distinguish among taxa. This phylogenetic tree includes *H. americana*.

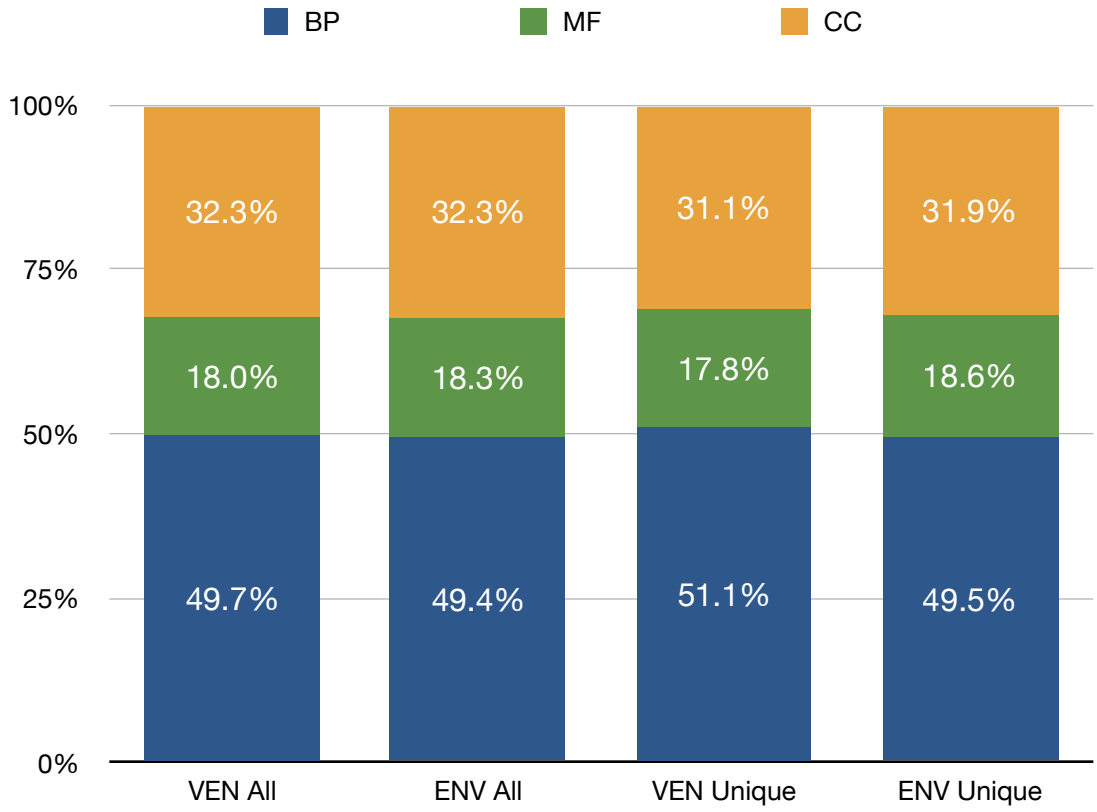


Figure A2.5: Distribution of gene ontology terms assigned to all unigenes (All) from venlafaxine (VEN) and WWTPE (ENV) exposed rainbow darter in comparison to assembly specific unigenes (Unique) within these transcriptomes, represented as a percentage distribution of the top-level ontology terms; Biological Process (BP; blue), Molecular Function (MF; green), and Cellular Component (CC; yellow), relative to the total number of GO terms assigned to unigenes in that transcriptome.

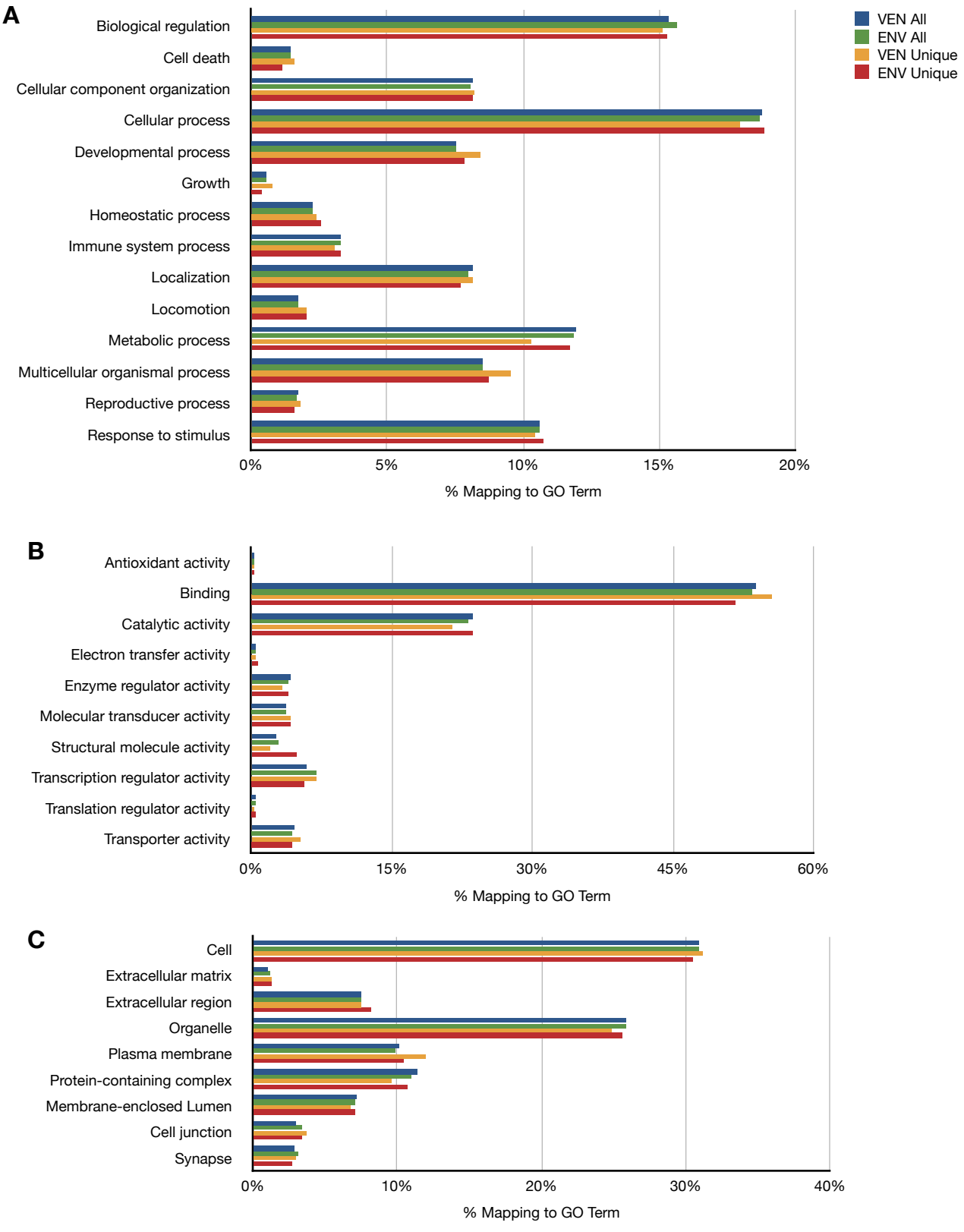

A
Biological regulation
Cell death
Cellular component organization
Cellular process
Developmental process
Growth
Homeostatic process
Immune system process
Localization
Locomotion
Metabolic process
Multicellular organismal process
Reproductive process
Response to stimulus
0%
5%
10%
15%
20%
% Mapping to GO Term
VEN All
ENV All
VEN Unique
ENV Unique
B
Antioxidant activity
Binding
Catalytic activity
Electron transfer activity
Enzyme regulator activity
Molecular transducer activity
Structural molecule activity
Transcription regulator activity
Translation regulator activity
Transporter activity
0%
15%
30%
45%
60%
% Mapping to GO Term
C
Cell
Extracellular matrix
Extracellular region
Organelle
Plasma membrane
Protein-containing complex
Membrane-enclosed Lumen
Cell junction
Synapse
0%
10%
20%
30%
40%
% Mapping to GO Term

Figure A2.6: Proportion of Level 2 Gene Ontology (GO) term classifications mapped to unigenes in rainbow darter transcriptomes. GO term classifications were assigned to unigenes from rainbow darters exposed to venlafaxine (blue) and wastewater treatment plant effluent (WWTPE) (green), as well as assembly-specific unigenes in venlafaxine-exposed (yellow) and WWTPE-exposed (red) rainbow darters. GO terms are categorized into the three primary ontologies: (A) Biological Process, (B) Molecular Function, and (C) Cellular Component. Percentages indicate the proportion of unigenes assigned to each GO term.

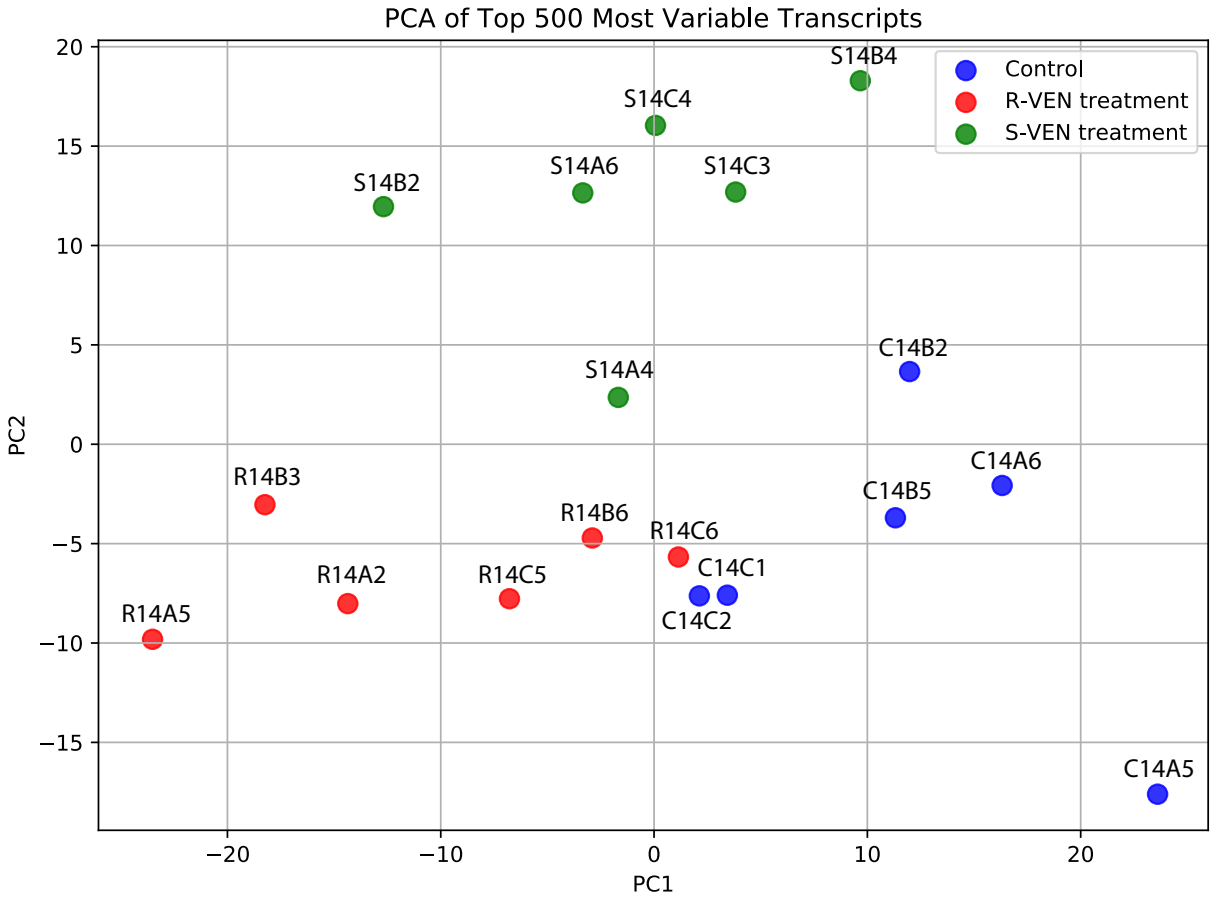


Figure A2.7: Principal component analysis (PCA) of the top 500 most variable transcripts in liver tissue from Rainbow Darter (Etheostoma caeruleum) exposed to control conditions, R-enantiomer venlafaxine (R-VEN), or S-enantiomer venlafaxine (S-VEN). Each point represents a biological replicate, with colours indicating treatment groups (blue = control, red = R-VEN, green = S-VEN). PCA was performed on $\log_2$-transformed transcript counts using the "PCA" function in the scikit-learn package in Python. Principal component 1 (PC1) and principal component 2 (PC2) explain 17.91% and 12.70% of the variance, respectively.

Table A2.4: Significantly enriched biological process gene ontologies (FDR < 0.05) identified in differentially expressed genes from rainbow darter (*Etheostoma caeruleum*) exposed to R-venlafaxine (R-VEN) or S-venlafaxine (S-VEN). Enrichment analysis was conducted using 46,149 background unigenes, with 26 differentially expressed genes in the R-VEN group and 25 in the S-VEN group.

Treatment	GO Term Name	GO ID	FDR	Gene Count
R-VEN				
	Alpha amino acid metabolic process	GO:1901605	2.1e-02	4
	Cellular amino acid metabolic process	GO:0009063	4.5e-02	4
	Glutamate metabolic process	GO:0006536	6.3e-03	3
	Positive regulation of cation transmembrane transport	GO:1904062	4.7e-02	3
	Glutamine family amino acid metabolic process	GO:0009064	2.1e-02	3
	Dicarboxylic acid metabolic process	GO:0043648	2.1e-02	3
	Cellular amino acid catabolic process	GO:0009063	2.9e-02	3
	Alpha-amino acid catabolic process	GO:1901606	2.1e-02	3
	Positive regulation of phospholipid biosynthetic process	GO:1903725	2.1e-02	2
	Regulation of response to interferon-gamma	GO:0060330	3.0e-02	2
	Response to immobilization stress	GO:0035902	3.0e-02	2
	Positive regulation of erythrocyte differentiation	GO:0045648	4.7e-02	2
	2-oxoglutarate metabolic process	GO:0006103	2.1e-02	2
	Positive regulation of phospholipid biosynthetic process	GO:0071073	2.1e-02	2
	Positive regulation of phospholipid metabolic process	GO:1903727	2.1e-02	2
	Aspartate family amino acid catabolic process	GO:0009068	2.6e-02	2
	Regulation of interferon-gamma-mediated signalling pathway	GO:0060334	3.0e-02	2
	Regulation of phospholipid metabolic process	GO:1903725	4.7e-02	2
S-VEN				
	oxoacid metabolic process	GO:0043436	2.2e-02	3
	carboxylic acid metabolic process	GO:0019752	2.2e-02	3

organic acid metabolic process	GO:0006082	2.2e-02	3
Lipid biosynthetic process	GO:0008610	4.3e-02	2
Monocarboxylic acid metabolic process	GO:0032787	4.5e-02	2
epithelial cell development	GO:0002064	4.9e-02	2
Planar cell polarity pathway involved in axis elongation	GO:0090179	4.9e-02	1
Neural plate development	GO:0001840	4.9e-02	1
Regulation of calcium ion transmembrane transport via high voltage-gated calcium channel	GO:1902514	4.3e-02	1
Nerve growth factor signalling pathway	GO:0038180	4.9e-02	1
Prostaglandin biosynthetic process	GO:0001516	4.4e-02	1
unsaturated fatty acid biosynthetic process	GO:0006636	4.4e-02	1
unidimensional cell growth	GO:0009826	4.9e-02	1
apical constriction	GO:0003383	4.9e-02	1

Identification and Exclusion of Parasitic Transcripts in Darter Transcriptomes

Orthogroup analysis revealed a subset of sequences with high homology to genes from *Heterobilharzia americana*, a trematode parasite, and from various Cnidaria species. Given that fishes are not part of the life cycle of *H. americana* (Lee, 1962), it is unlikely that these sequences originate from incidental host contamination. Instead, they may derive from another trematode or a myxozoan parasite, organisms that due to recent reclassification are now considered part of the phylum Cnidaria (Atkinson & Bartholomew, 2018; Chang et al., 2015). Anecdotal evidence from previous fieldwork in our laboratory noted the presence of small (≤1mm) off-white cysts within the body cavities of various darter species, although such cysts were not observed in the present study. A reference guide by Gibson (1996) outlines several trematode parasites infecting darters, including *Ichthyocotylurus platycephalus*, which is characterized by thick-walled encysted metacercariae on serous membranes and the liver. While the possibility of *I. platycephalus* infection remains speculative, the observed sequence homology also supports a potential myxozoan origin, as myxozoans are known to primarily associate with teleosts and can exhibit host-specific pathogenicity (Kumar et al., 2015; Holzer et al., 2021). The relatively poor annotation of myxozoan sequences in the NCBI database may have lead to the alignment of other Cnidaria taxa, reflecting their close phylogenetic relationship (Chang et al., 2015). Although the absence of cysts might argue against active infection, the high sequence homology suggests that trematode infection is a likely source, though concurrent parasitism with myxozoans cannot be entirely excluded.